

Biodegradable Materials Created by the Controlled
Ring Opening Polymerisation of α -Amino Acid
N-Carboxyanhydrides and *O*-Carboxyanhydrides

Mthulisi Khuphe

Supervised by Dr Paul Thornton
Co-Supervisor: Prof James Guthrie

Submitted in accordance with the requirements for the degree of
Doctor of Philosophy

School of Chemistry, University of Leeds

June 2017

The candidate confirms that the work submitted is his own, except where work which has formed part of jointly-authored publications has been included. The contribution of the candidate and the other authors to this work has been explicitly indicated below. The candidate confirms that appropriate credit has been given within the thesis where reference has been made to the work of others.

In Chapter 6, Bethan McAvan and Mthulisi Khuphe jointly carried out the synthesis of the NCA monomer and the ring opening polymerisation reactions. With the exception of thermal (DSC and TGA) characterisations, additional SEM imaging and advanced polymer chromatographic analyses, which were carried out by Mthulisi, all the other material characterisations were a joint effort. In addition, Mthulisi provided project direction.

This copy has been supplied on the understanding that it is copyright material and that no quotation from the thesis may be published without proper acknowledgement.

© 2017 the University of Leeds and Mthulisi Khuphe

Abstract

Polymeric materials are excellent candidates for use as biomaterials. They are often employed as drug carriers to provide protection to encapsulated therapeutic molecules against premature metabolism, inactivation and clearance, and to reduce drug leakage and burst release, *in vivo*. Although significant progress in the medical sector has been registered, challenges still abound for the delivery of therapeutics. As such, the development of requisite nanocarriers and improvement of existing ones is crucial. NCA ROP and OCA ROP provide an alternative to solid phase peptide synthesis for the syntheses of polymeric biomaterials that have targeted applicability in drug delivery, in pharmaceuticals and in tissue engineering.

This thesis demonstrates the use of controlled NCA ROPs and OCA ROPs to generate a range of novel poly(amino acid)s, poly(ester)s and hybrid materials through novel combinations of both techniques. Innovative routes to contemporary biomaterials that are presented include; employing a model therapeutic molecule, dopamine, to initiate NCA ROP, to yield amphiphilic dopamine-(peptide)-(peptoid) conjugates that self-assembled into biodegradable particles. Steglich esterification being used to graft alkyl groups from the OH-side groups of an oligo(L-serine) to yield a polymer capable of immobilising large quantities of edible vegetable oil, thus forming biodegradable organogels. NCA ROP initiated from a PEG star polymer that resulted in the generation of star-shaped hybrid polymers, which upon modification by thiol-ene click crosslinking, yielded polymers capable of forming disulphide-crosslinked hydrogels. Employing glucosamine to initiate sequential NCA ROP and OCA ROP reactions, to generate amphiphilic polymers that self-aggregated into monodisperse, glucose-presenting NPs. Oligo(L-serine), which was created by NCA ROP, being used to initiate the ROP of Phe OCA, yielding graft copolymers which self-aggregated into NPs that could be used for the controlled release of doxorubicin. The synthesis of diblock homopoly(ester)s, which could be used for the controlled release of hydrophobic chemotherapeutics, by the sequential ROP of Phe OCA and Glu(Bz) OCA, Phe OCA and Lys(Cbz) OCA, and Glu(Bz) OCA and Lys(Cbz) OCA. Collaborative initiatives led to the creation of prospective poly(amino acid)-metal-based anticancer therapeutics. *In vitro* biological studies and payload release studies were conducted on the materials created, to demonstrate their suitability as biomaterials. Proteolytic enzymes were used to trigger the degradation of poly(amino acid)-based materials, reduced environmental pH conditions were used to trigger the hydrolysis of poly(ester)-based materials and reductive environments were used to trigger the dissociation of disulfide-crosslinked hydrogels.

Acknowledgements

I am hugely indebted to my supervisor, Dr Paul Thornton, for the direction that you provided in this research work, for the long hours that you always put in to ensure my success, for being patient with me and of course for putting your trust in me by gifting me the opportunity to pursue a PhD training program. Your passion inspires my own, thank you! To my co-supervisor, Prof James Guthrie, I am grateful to you for having always been there to offer timely and valuable feedback. Notably, I am grateful to the fact that, despite your retirement towards the end of my PhD training, you continued to show unparalleled dedication to this cause, by committing your resources to driving a long way from your home to come and meet me on campus. I will be grateful forever to my generous sponsors, the Beit Trust and the University of Leeds for providing the funding which was necessary for me to carry out this research.

To Dr Algy Kazlaucius and Mr Martin Huscroft, who put in tremendous shifts in assisting me with the analytical and technical aspects of the research, thank you! I am also thankful to my dedicated friend, Dr Blessing Mukonoweshuro, for all the time that you spent training me in the culturing of mammalian cells and in biological studies, and to Prof Eileen Ingham for kindly allowing me to use her research facilities to carry out biological analyses. I appreciate the intellectual inputs and physical inputs of my research collaborators, especially Dr Heba Abdelgawad and Dr Charlotte Willans. This includes the various masters students that I am privileged to have mentored and learnt a lot from, some of whom went on to become my great research co-workers; Mr Daniel Price and Ms Bethan McAvan, I wish you all the best in your PhDs. Special mentions to Dr Clare Mahon, Dr Saminu Magami, Dr Nicola Ingram, Mr Thomas Howell and Dr Robert Davies, who helped me, one way or another, during my research journey, and all members of the Polymer and Colour Science Group, past and present, for camaraderie.

To my aunt and uncle; you greatly aided this journey two decades ago, but I wonder if you ever imagined that it would turn out like this? I hope that at the very least, you are proud of yourselves; thank you! I will always be grateful to the Higherlife Foundation and its patrons for the undergraduate scholarship and the leadership training. To the two lovely women in my life, my mum and my fiancée, you are my world. Mum, I hope that I can count on you to be the proudest of me. Joanna, this is no place for love lyrics, but still, you are the most amazing human being, with the most beautiful character. Thank you for your most unwavering and reliable support throughout this my turbulent journey. And to the only wise God our Saviour, be glory and majesty, dominion and power, both now and ever. Amen!

List of Contents

Abstract.....	ii
Acknowledgements.....	iii
Chapter 1 . Introduction.....	1
1.1. Amino Acids.....	1
1.2. Ring Opening Polymerisation of α -Amino Acid <i>N</i> -Carboxyanhydrides (NCA ROP)	3
1.3. Poly(Amino Acid) Materials: Creation and Architecture.....	10
1.4. Poly(Amino Acid) Materials: Biological Relevance.....	17
1.5. Peptidomimetic Materials: Peptoids.....	25
1.6. ROP of <i>O</i> -Carboxyanhydrides, Created from α -Hydroxy Acids of α -Amino Acids (OCA ROP).....	27
1.7. Research Aims and Thesis Outline.....	29
1.8. References	31
Chapter 2 . Instrumentations, General Methods and Materials	37
2.1. Nuclear Magnetic Resonance (NMR) Spectroscopy.....	37
2.2. Fourier Transform Infrared (FTIR) Spectroscopy.....	37
2.3. Melting Point Determination	37
2.4. Centrifugation, Sample-Drying and Lyophilisation	37
2.5. pH Measurements.....	38
2.6. Mass Spectrometry (MS).....	38
2.7. High Performance Liquid Chromatography (HPLC)	38
2.8. Circular Dichroism (CD) Spectrometry	38
2.9. Differential Scanning Colorimetry (DSC) and Thermogravimetry (TGA).....	38
2.10. Ultraviolet-Visible (UV-Vis) Spectrophotometry.....	39
2.11. Fluorescence Microscopy.....	39
2.12. Preparation of Phosphate Buffered Saline (PBS) Solutions	39
2.13. Preparation of Sodium Acetate Buffers.....	39
2.14. Preparation of Nanoparticles (Nanoprecipitation).....	40
2.15. Dynamic Light Scattering (DLS) and Zeta Potential Studies.....	41

2.16.	Determination of Critical Aggregation Concentration (CAC).....	41
2.17.	Sample Preparation, Sputter-Coating and Scanning Electron Microscopy (SEM)	42
2.18.	Transmission Electron Microscopy (TEM)	42
2.19.	Mammalian Cell Culturing and Passaging	42
2.20.	ATPlite-M® Assay.....	43
2.21.	Advanced Polymer Chromatography (APC).....	44
2.22.	The Korsemeayar-Peppas (KP) model	44
2.23.	Drug Encapsulation Efficiency and Drug Loading Content	45
2.25.	References	48
Chapter 3 . Cyclic Monomers Created from α -Amino Acids.....		49
3.1.	Creation of α -Amino Acid NCA Monomers	49
3.2.	Creation of α -Amino Acid OCA Monomers	53
3.3.	Experimental Details	54
3.3.1.	Synthesis of <i>O</i> -benzyl-L-serine (Ser(OBz)) NCA	54
3.3.2.	Synthesis of L-Alanine (Ala) NCA	55
3.3.3.	Synthesis of N ϵ -Carbobenzyloxy-L-Lysine (Lys(Cbz)) NCA.....	55
3.3.4.	Synthesis of γ -Benzyl-L-Glutamate (Glu(Bz)) NCA	56
3.3.5.	Synthesis of L-Phenylalanine (Phe) NCA.....	56
3.3.6.	Synthesis of L-Valine (Val) NCA	57
3.3.7.	Synthesis of <i>S</i> - <i>tert</i> Butylmercapto-L-Cysteine (STM-Cys) NCA	57
3.3.8.	Synthesis of L-Aspartic acid β -benzyl ester (Asp(Bz)) NCA	57
3.3.9.	Synthesis of Sarcosine (Sar) <i>N</i> -NCA.....	58
3.3.10.	Synthesis of Phe OCA	59
3.3.11.	Synthesis of Glu(Bz) OCA.....	60
3.3.12.	Synthesis of Lys(Cbz) OCA	62
3.4.	References	63
Chapter 4 . The Formation of Biodegradable Particles from a Therapeutic Initiator for Enzyme-Mediated Drug Delivery		65
	Preamble.....	65

Abstract.....	65
4.1. Introduction	65
4.2. Experimental Details	67
4.3. Results and Discussion	71
4.4. Conclusions	81
4.5. References	82
Chapter 5 . A Vegetable Oil-Based Organogel for Use In pH-Mediated Drug Delivery.....	84
Preamble.....	84
Abstract.....	84
5.1. Introduction	84
5.2. Experimental	89
5.3. Results and Discussion	92
5.4. Conclusions	107
5.5. References	108
Chapter 6 . Polymer Hydrogels for Glutathione-Mediated Protein Release	111
Preamble.....	111
Abstract.....	111
6.1. Introduction	111
6.2. Experimental Details	113
6.3. Results and Discussion	116
6.4. Conclusions	125
6.5. References	126
Chapter 7 . Glucose-Bearing Biodegradable Poly(Amino Acid) and Poly(Amino Acid)-Poly(Ester) Conjugates for Controlled Payload Release	127
Preamble.....	127
Abstract.....	127
7.1. Introduction	127
7.2. Experimental Details	130
7.3. Results and Discussion	132

7.4.	Conclusion.....	143
7.5.	References	144
Chapter 8 . Poly[(Amino Acid)-(Ester)] Graft Copolymer Nanoparticles for the Acid-Mediated Release of Doxorubicin.....		
	Abstract.....	146
8.1.	Introduction	146
8.2.	Experimental Procedures	147
8.3.	Results and Discussion	149
8.4.	Conclusions	157
8.5.	References	158
Chapter 9 . Biodegradable Poly(Ester) Nanoparticles Created by Sequential ROP of α -Amino Acid OCAs for the Controlled Release of Chemotherapeutics.....		
	Abstract.....	159
9.1.	Introduction	159
9.2.	Experimental Details	160
9.3.	Results and Discussion	162
9.4.	Conclusion.....	171
9.5.	References	172
Chapter 10 . A Diblock Poly(Ester) for the Controlled Release of Hydrophobic Chemotherapeutics and for the pH-Induced Reversible Assembly in Nanobiotechnological Applications.....		
	Abstract.....	173
10.1.	Introduction	173
10.2.	Experimental Details	175
10.3.	Results and Discussion	177
10.4.	Conclusion.....	189
10.5.	References	190
Chapter 11 . Proof-of-Concept Studies in the Development of Poly(Amino Acid)-Silver(I)-N-Heterocyclic Carbene Anticancer Therapeutics		
	Abstract.....	192
11.1.	Introduction	192

11.2.	Experimental Details	196
11.3.	Results and Discussions.....	203
11.3.1.	Poly(Amino Acid) Syntheses	203
11.3.2.	Silver(I)- <i>N</i> -Heterocyclic Carbene (NHC) Complexes	206
11.3.3.	Physical Encapsulation of Complexes in an Amphiphilic Polymer	208
11.3.4.	Charge-Driven (Electrostatic) Coordination of Complexes with Polymers	212
11.3.5.	Covalent Conjugation of Silver(I)-NHC Complexes to Poly(Amino Acid)s	215
11.4.	Conclusion.....	218
11.5.	References	220
	Concluding Remarks and Future Work.....	223
	List of Publications	224
	Appendix.....	218

List of Figures

Figure 1.1.	Generic illustration of random coil, α -helix and β -sheet conformations.....	2
Figure 1.2.	Generalised route to the creation of poly(amino acid)s by NCA ROP.	3
Figure 1.3.	Schematic presentation of poly(amino acid)-based material architectures.....	11
Figure 1.4.	Pathway for a typical example of a hybrid poly(amino acid)-based macromolecule.	13
Figure 1.5.	Illustration of the grafting-to approach and grafting-from approach	13
Figure 1.6.	Representation of potential approaches to obtaining core crosslinked peptide-based star polymers; core-first (grafting-from), grafting-to and arm first approach.....	15
Figure 1.7.	Stealth properties of PEG are exploited in the creation of amphiphilic macromolecules. ..	16
Figure 1.8.	Self-aggregation of amphiphilic poly(amino acid)-based block copolymers	18
Figure 1.9.	Schematic view of the self-assembled poly(Arg ₆₀)- <i>b</i> -poly(Leu ₂₀) vesicle.....	19
Figure 1.10.	Schematic representation of the di-block amphiphilic PEG-Poly[(Asp)-Dox].. ..	20
Figure 1.11.	Schematic representation of poly(amino acid)-based hybrid hydrogels:.....	21
Figure 1.12.	Schematic representation of a pH-responsive peptide hybrid material.....	22
Figure 1.13.	Schematic classification of ERMs, according to their structural design.....	22
Figure 1.14.	Illustration of the concepts of payload delivery by ERMs.....	23
Figure 1.15.	Some of the extensively documented aliphatic poly(ester)s.....	28

Figure 1.16. Schematic illustration of the route to the creation of poly(ester)s using OCA ROP.	28
Figure 2.1. Generation of (nano)particles from poly(amino acid)s using the 'dropping-in' method.....	40
Figure 3.1. Generic illustration of NCA monomers and OCA monomers.	49
Figure 4.1. Cell-seeding plan for the determination of the cytotoxicity of Dop-(Ala) ₅ -(Sar) ₁₅ and of Dop-(Phe) ₄ -(Sar) ₁₈ , against C3H mouse dermal fibroblasts.....	70
Figure 4.2. Scheme for dopamine acting as a model therapeutic molecule.	71
Figure 4.3. ¹ H NMR spectrum of Dop-(Ala) ₅ -(Sar) ₁₅ and The ESI-MS spectrum of Dop-(Ala) ₅ -(Sar) ₁₅	73
Figure 4.4. ¹ H NMR spectrum of Dop-(Phe) ₄ -(Sar) ₁₅ and The ESI-MS spectrum of Dop-(Phe) ₄ -(Sar) ₁₅ ..	74
Figure 4.5. SEM images of Dop-(Ala) ₅ -(Sar) ₁₅ particles and Dop-(Phe) ₄ -(Sar) ₁₈ particles. DLS charts revealing the size distribution of Dop-(Ala) ₅ -(Sar) ₁₅ particles and Dop-(Phe) ₄ -(Sar) ₁₈ particles.....	75
Figure 4.6. Chart detailing the stability of Dop-(Ala) ₅ -(Sar) ₁₅ and Dop-(Phe) ₄ -(Sar) ₁₈ particles.....	76
Figure 4.7. CD spectra obtained from Dop-(Ala) ₅ -(Sar) ₁₅ particles and Dop-(Phe) ₄ -(Sar) ₁₅ particles.....	77
Figure 4.8. Enzymatic degradation of Dop-(Peptide)-(Peptoid) particles.....	78
Figure 4.9. ESI-MS-verification of dopamine released from particles.	79
Figure 4.10. Determination of the cytotoxicity of Dop-(Ala) ₅ -(Sar) ₁₅ and Dop-(Phe) ₅ -(Sar) ₁₅	81
Figure 5.1. Classification of gels, in particular, organogels.....	85
Figure 5.2. General illustration of the plate-coating and cell-seeding layout plan.....	91
Figure 5.3. ¹ H NMR spectra of Oligo(Ser) and of Oligo(Ser(OBz)).....	93
Figure 5.4. FTIR spectra of Oligo(Ser(OBz)) and Oligo(Ser), DSC thermograms of octadecanoic acid, Oligo(Ser), and the PSOA gelator.	94
Figure 5.5. GPC trace of Oligo(Ser).....	95
Figure 5.6. ESI-MS fragmentation pattern obtained from Oligo(Ser).....	95
Figure 5.7. ¹ H NMR of PSOA gelator.....	96
Figure 5.8. Formation of organogels from an PSOA gelator in safflower oil	97
Figure 5.9. Representative DSC thermogram obtained from PSOA-safflower oil organogels.	98
Figure 5.10. DSC thermogram obtained from six heating-cooling cycles of the organogels.....	98
Figure 5.11. SEM micrographs showing the morphology of the 2 wt. % organogel.....	99
Figure 5.12. Rheological assessments of the PSOA-safflower oil organogel	100
Figure 5.13. Determination of suitability of PSOA gel in supporting cell growth and proliferation.	102
Figure 5.14. Plate seeding plan showing the appearance of the culture medium after 120 hours.....	103
Figure 5.15. The release of rhodamine B from a 2 wt. % and 4 wt. % PSOA-safflower oil organogel .	104
Figure 5.16. Fluorescence images obtained from a 2 wt. % PSOA-safflower oil organogel	105

Figure 5.17. KP model plots for payload release from 2 wt.% and 4 wt. % organogels.....	106
Figure 6.1. ¹ H NMR spectra of STBM-L-Cys NCA and poly[(STBM-L-cys _n) ₄ -b-(StarPEG _{10k})] polymers..	117
Figure 6.2. FTIR spectra of the PEG star polymer, STBM-L-Cyst NCA (b) and hybrid macromolecules. APC chromatograms of the macromolecules .	118
Figure 6.3. DSC and TGA thermograms of PEG star polymer initiator, poly[(STMB-L-cys ₁₀) ₄ -b-(StarPEG _{10k})], poly[(L-cys ₁₀) ₄ -b-(StarPEG _{10k})] (c) and the crosslinked xerogel.....	120
Figure 6.4. Self-aggregation of STBM-protected macromolecules in aqueous medium.....	121
Figure 6.5. Graphical illustration of the generation of disulfide crosslinked chemical hydrogels.	122
Figure 6.6. SEM micrographs of a poly((L-cys ₁₀) ₄ -b-(starPEG _{10k})) hydrogel	123
Figure 6.7. Variation of PBS solution uptake by hydrogel scaffolds in relation to crosslink density....	123
Figure 6.8. The release of FITC-albumin from hydrogels.....	124
Figure 7.1. ¹ H NMR spectra of Glu-poly[(Sar) _m -b-(Phe) _n] and Glu-poly[(Sar) _m -b-(PheLA) _n] polymers .	133
Figure 7.2. FTIR spectra of Glu-poly[(Sar) _m -b-(Phe) _n] and Glu-poly[(Sar) _m -b-(PheLA) _n] polymers	134
Figure 7.3. APC traces of Glu-poly[(Sar) _m -b-(PheLA) _n] and of Glu-poly[(Sar) _m -b-(Phe) _n].	135
Figure 7.4. TEM images of NPs of Glu-poly[(Sar) _m -b-(PheLA) _n] and Glu-poly[(Sar) _m -b-(Phe) _n].	136
Figure 7.5. The stability of Glu-poly[(Sar) _m -b-(Phe) _n] NPs and of Glu-poly[(Sar) _m -b-(PheLA) _n] NPs.	137
Figure 7.6. Assessment of binding of Con A and RCA ₁₂₀ lectins to glucose-bearing NPs.	138
Figure 7.7. Release of rhodamine from Glu-poly[(Sar) _m -b-(PheLA) _n], Glu-poly[(Sar) _m -b-(Phe) _n] NPs..	139
Figure 7.8. Enzymatic-mediated release of rhodamine B from glucose-bearing NPs.	140
Figure 7.9. K-P model plots for the release of molecular cargo from NPs.	142
Figure 8.1. FTIR spectra for oligo(Ser(OBz)), oligo(Ser) and poly[(Ser)- <i>graft</i> -(Phe AHA)].	151
Figure 8.2. ¹ H NMR spectra for oligo(Ser(OBz)), Phe OCA, oligo(Ser) and poly[(Ser)- <i>g</i> -(Phe AHA)]. ...	152
Figure 8.3. DLS trace and SEM microphotograph obtained from poly[(Ser) _{19.6} - <i>g</i> -(Phe AHA) _{6.0}] NPs...	153
Figure 8.4. Dox-loading in poly[(Ser) _{19.6} - <i>g</i> -(Phe AHA) _{6.0}] NPs	154
Figure 8.5. The release of dox from poly[(Ser) _{19.6} - <i>g</i> -(Phe AHA) _{6.0}] NPs.	155
Figure 8.6. MTT assay assessment of poly[(Ser) _{19.6} - <i>g</i> -(Phe AHA) _{6.0}] against T47D cells.	156
Figure 9.1. ¹ H NMR kinetics for the ROP of Phe OCA	163
Figure 9.2. Charts detailing the conversion of OCA monomers into poly(ester)s..	163
Figure 9.3. ¹ H NMR spectra for the progress of the poly(PheLA)-mediated ROP of Lys(Cbz) OCA,.....	164
Figure 9.4. ¹ H NMR spectra for the progress of poly(PheLA)-mediated ROP of Glu(bz) OCA.....	165
Figure 9.5. GPC traces and FTIR spectroscopy spectra for the poly(ester)s	166
Figure 9.6. DLS traces for poly[(PheLA) _{10.4} - <i>b</i> -(Glu(Bz)LA) _{30.2}], poly[(PheLA) _{10.4} - <i>b</i> -(Lys(Cbz)LA) _{31.4}] NP.	167

Figure 9.7. The encapsulation efficiency of dox into poly(ester) NPs and PDIs of dox-loaded NPs.....	169
Figure 9.8. Acidic pH-mediated release of dox from poly(ester) NPs.....	169
Figure 9.9. KP model plots of dox-release from poly(ester) NPs.....	170
Figure 10.1. ¹ H NMR spectra for reaction fractions extracted from the ROP of Lys(Cbz) OCA.....	178
Figure 10.2. ¹ H NMR spectrum, FTIR spectra and GPC chromatograms for poly[(Lys(Cbz)LA) _{26.6} - <i>b</i> -(Glu(Bz)LA) _{28.3}], before after deprotection, respectively.....	179
Figure 10.3. DLS assessment of assembly of poly[(Lys(Cbz)LA) _{26.6} - <i>b</i> -(Glu(Bz)LA) _{28.3}].....	181
Figure 10.4. SEM microphotograph and DLS chart revealing the size-distribution of dox-loaded poly[(Lys(Cbz)LA) _{26.6} - <i>b</i> -(Glu(Bz)LA) _{28.3}] NPs..	181
Figure 10.5. pH-mediated release of dox from poly[(Lys(Cbz)LA) _{26.6} - <i>b</i> -(Glu(Bz)LA) _{28.3}] NPs.....	182
Figure 10.6. MTT assay of poly[(Lys(Cbz)LA) _{26.6} - <i>b</i> -(Glu(Bz)LA) _{28.3}] against T47D and MCF-7 cells.....	183
Figure 10.7. ¹ H NMR spectra of poly[(Lys(Cbz)LA) _m - <i>b</i> -(Glu(Bz)LA) _n], before and after deprotection..	185
Figure 10.8. SEM and DLS analyses of the zwitterionic behaviour of poly[(LysLA) _{26.6} - <i>b</i> -(GluLA) _{28.3}]..	186
Figure 10.9. Zeta potential assessment of zwitterionic behaviour of poly[(LysLA) _{26.6} - <i>b</i> -(GluLA) _{28.3}] ...	187
Figure 10.10. Aggregation of poly[(LysLA) _{26.6} - <i>b</i> -(GluLA) _{28.3}] in acidic and alkali pH.	188
Figure 11.1. ¹ H NMR spectra of Lys(Cbz) NCA, mPEG ₅₀₀₀ - <i>b</i> -poly(Lys(Cbz)), mPEG ₅₀₀₀ - <i>b</i> -poly(Lys)	204
Figure 11.2. ¹ H NMR spectra of Glu(Bz) NCA, poly(Glu(Bz)) and poly(Glu).....	204
Figure 11.3. ¹ H NMR spectra of Phe NCA and mPEG ₅₀₀₀ - <i>b</i> -poly(Phe).....	205
Figure 11.4. Evaluation of anticancer potencies of silver(I)-NHC complexes and cisplatin, against Panc. 10.05 cells and against ARPE-19 cells.....	208
Figure 11.5. DLS charts revealing C01-loaded particles, C02-loaded particles . SEM images of C01-loaded particles and C02-loaded particles	209
Figure 11.6. SEM microphotograph of the C02-loaded mPEG ₅₀₀₀ - <i>b</i> -poly(Phe) ₂₄ particles, EDX map of a C02-loaded particle and EDX spectrum of a C02-loaded particle.....	210
Figure 11.7. Confocal microscopy images from C02-loaded mPEG ₅₀₀₀ - <i>b</i> -poly(Phe) ₂₄ particles.....	211
Figure 11.8. Charge-driven coordination of metal complexes with poly(amino acids) in solution	212
Figure 11.9. DLS charts for mPEG ₅₀₀₀ - <i>b</i> -Poly(L-lys) _n -C03 particles.....	214
Figure 11.10. DLS traces obtained from mPEG ₅₀₀₀ - <i>b</i> -Poly(L-lys) ₃₉ -C04 particles (a), mPEG ₅₀₀₀ - <i>b</i> -Poly(L-lys) ₅₀ -C04 particles (b) and mPEG ₅₀₀₀ - <i>b</i> -Poly(L-lys) ₁₄₀ -C04 particles (c).	214
Figure 11.11. DLS traces obtained from mPEG ₅₀₀₀ - <i>b</i> -Poly(L-lys) ₃₉ -C05 particles (a), mPEG ₅₀₀₀ - <i>b</i> -Poly(L-lys) ₅₀ -C05 particles (b) and mPEG ₅₀₀₀ - <i>b</i> -Poly(L-lys) ₁₄₀ -C05 particles (c).	214
Figure 11.12. The anticancer potencies of C03-loaded mPEG- <i>b</i> -poly(Lys) _n particles.....	215
Figure 11.13. ¹ H NMR spectra of poly(Glu) ₂₄ , C01 and poly[(Glu) ₂₄ -silver(I)-NHC] (PGC01)	216
Figure 11.14. FTIR spectra of poly(Glu) ₂₄ , C01 and poly[(Glu) ₂₄ -silver(I)-C01] (PGC01).	217

Figure 11.15. Comparison of the anticancer potency of PGC01 and C01, against Panc. 10.05 cells .. 217

List of Tables

Table 1.1. Proteinogenic Amino Acids	1
Table 1.2. Properties of Peptoids.	26
Table 2.1 Chemicals that were used during the research program.	46
Table 2.2. Chemicals that were used during the research program (continued).	47
Table 4.1. HPLC instrumentation settings and experimental conditions.....	69
Table 4.2. The theoretical composition and molecular weights of dop-conjugated macromolecules..	72
Table 5.1. Atomic composition of Oligo(Ser) and the PSOA gelator.....	94
Table 5.2. Release exponents and correlation coefficients computed from the KP model.....	106
Table 6.1. Composition of the copolymers obtained from StarPEG _{10k} -initiated NCA ROPs.....	119
Table 7.1. The molecular weight of the polymers produced.....	135
Table 7.2. The release exponents that were determined using the KP model.....	141
Table 8.1. Composition of variants of oligo(Ser), computed by ¹ H NMR and APC	152
Table 8.2. Hybrid macromolecules produced by sequential NCA ROP and OCA ROP	153
Table 8.3. Mean particle size and PDI values obtained from DLS analyses	154
Table 9.1. Polymer molecular weights and critical aggregation concentrations (CAC)s.....	165
Table 9.2. The critical aggregation concentrations, hydrodynamic sizes and PDIs of poly(ester) NP..	168
Table 11.1. Silver-NHC anticancer complexes bearing different xylyl spacers [49].	195
Table 11.2. Silver acetate-NHC complexes that exhibit anticancer potency against breast cancer.	195
Table 11.3. The various poly(amino acids) that were synthesised by NCA ROP	205
Table 11.4. Structure of NHC ligands and their respective silver(I)-NHC complexes.....	207
Table 11.5. Electrostatic coordination of silver complexes to mPEG-b-poly(Lys) _n polymers.....	213

List of Schemes

Scheme 1.1. The normal amine mechanism for the ROP of α -amino acid NCAs	4
Scheme 1.2. The activated monomer mechanism for the ROP of α -amino acid NCAs	5
Scheme 1.3. Organo-metal initiated NCA ROP:.....	6
Scheme 1.4. Chain transfer of a poly(amino acid) to the NCA anion during NCA ROP	9
Scheme 1.5. The primary amine hydrochloride-mediated NCA ROP.	10
Scheme 1.6. Imidazole-initiated NCA ROP generation of cyclic poly(amino acid)s [4].	14

Scheme 3.1. Leuchs' method for the synthesis of NCA synthesis.	50
Scheme 3.2. The Fuchs-Farthing method for NCA synthesis.....	51
Scheme 3.3. The creation of α -amino acid OCAs	53
Scheme 5.1. The synthesis route to the PSOA organogelator	92
Scheme 6.1. The route to the generation of thiol-ene cross-linkable macromolecules.....	116
Scheme 7.1. The syntheses of biodegradable poly[(sar)- <i>b</i> -(ester)] and poly[(sar)- <i>b</i> -(amino acid)]	133
Scheme 8.1. The benz-initiated ROP of Ser(<i>Obz</i>) NCA to produce oligo(Ser(<i>Obz</i>)) macromolecules; deprotection of oligo(Ser(<i>Obz</i>)) to yield oligo(Ser). Oligo(Ser)-initiated ROP of Phe OCA (c).....	150
Scheme 9.1. The syntheses of diblock poly(ester) macromolecules by isobutanol-mediated sequential OCA ROP and deprotection of poly(ester) macromolecules by catalytic Pd/C.....	162
Scheme 10.1. The sequential ROP of lys(CBZ) OCA and Glu(Bz) OCA, and the deprotection of the lys(Cbz) and Glu(Bz) repeat units, using catalytic Pd/C hydrogenolysis.....	178
Scheme 11.1. Synthesis of mPEG ₅₀₀₀ - <i>b</i> -Poly(Lys(Cbz)), (b) deprotection of mPEG ₅₀₀₀ - <i>b</i> -Poly(Lys(Cbz)), synthesis of poly(Glu(Bz)) _n , deprotection of poly(Glu(Bz)) _n , synthesis of poly(Phe) _n	203
Scheme 11.2. The formation of a poly[(Glu) ₂₄ -silver(I)-C01] (PGC01) anticancer conjugate.....	216

List of Abbreviations

3D - Three dimensional

AAM - Activated monomer mechanism

AHA - α -Hydroxy Acid

Ala - L-alanine

ANOVA - Analysis of variance

APC - Advanced Polymer Chromatography

Ar - Aromatic

Asp - L-Aspartic Acid

Chapter 1 Asp(Bz): - β -benzyl-L-Aspartate

ATR - Attenuated total reflectance

ATR: - Attenuated total reflection

Benz - Benzylamine

Bz - Benzyl ester

ca. - Approximately

Calcd - Calculated

Cbz - Carbobenzyloxy

CD - Circular dichroism

Cps - Counts per second

Cys - L-Cysteine

DCC:- Dicyclohexylcarbodiimide

DLS - Dynamic light scattering

DMAP: - 4-dimethylaminopyridine

DMEM - Dulbecco's Modified Eagle Medium

DMF - N,N-Dimethylformamide

DMSO - Dimethylsulfoxide

Dop - Dopamine

DSC - Differential scanning calorimetry

EDTA - Ethylenediamine tetra-acetic acid

EPR: - Enhanced permeability and retention

ESI - Electron spray ionisation

Fmoc - Fluorenylmethyloxycarbonyl

G' - Loss or Viscous modulus

G'' - Elastic or Storage modulus

Glu - L-Glutamic acid

GPC - Gel permeation chromatography

His - L-Histidine

HRMS: - High resolution mass spectrometry

HVT - High vacuum techniques

IC₅₀ - Half maximal inhibitory concentration

KP - Korsmeyer-Peppas

LMWOG - Low molecular weight organogelator

LVER - linear viscoelastic region

Lys - Lysine

M/I - Monomer-to-initiator ratio

\bar{M}_n - Number average molecular weight

MSD - Mean Square Deviation

MTT: - 3-(4, 5-dimethylthiazolyl-2)-2,5-diphenyltetrazoliumbromide

\dot{M}_w - Weight average molecular weight

MWCO - Molecular weight cut-off

MWD - Molecular weight distribution

NAM - Normal amine mechanism

NAMI-A: - New Anti-tumour Metastasis Inhibitor

NCA - N-carboxyanhydride

NHC: - *N*-Heterocyclic Carbene

NPs: - Nanoparticles

OBz - *O*-benzyl

PDI - Polydispersity index

Phe - L-Phenylalanine

PS - Poly(styrene)

PSOA - Poly(L-serine)-*graft*-Octadecanoic Acid

Rad- Radians

ROP - Ring opening polymerisation

Sar - Sarcosine

SEM - Scanning electron microscopy

Ser - Serine

STBM - S-tertbutylmercapto

Tan δ - Loss factor

t-Boc - Tert-butyloxycarbonyl

TEM - Transmission electron microscopy

TFA - Trifluoroacetic acid

TFA- $_d$ - Deuterated trifluoroacetic acid

TGA - Thermogravimetric analysis

Tgel - Temperature of gelation

THF - Tetrahydrofuran

Tyr - L-Tyrosine

U - Units

UV/Vis - Ultraviolet-visible

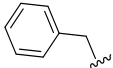
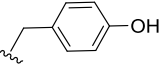
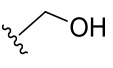
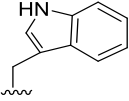
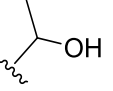
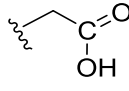
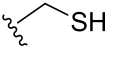
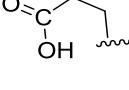
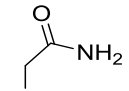
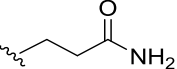
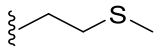
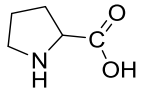
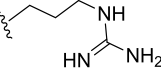
λ_{max} - Wavelength of maximum absorbance

Chapter 1. Introduction

1.1. Amino Acids

Amino acids are the molecular building blocks of two important components of organisms; peptides and proteins [1]. Proteins are naturally-occurring and consist of one or more amino acids that are combined in unique, specific sequences. Although there are more than 250 types of amino acids in nature, only 20 are proteinogenic amino acids (Table 1.1).

Table 1.1. Proteinogenic Amino Acids [2].

Amino Acid		R-Group	Amino Acid		R-Group
Glycine	Gly	H	Phenylalanine	Phe	
Alanine	Ala	CH ₃	Tyrosine	Tyr	
Serine	Ser		Tryptophan	Trp	
Threonine	Thr		Aspartic acid	Asp	
Cysteine	Csy		Glutamic acid	Glu	
Valine	Val		Asparagine	Asn	
Leucine	Leu		Glutamine	Gln	
Isoleucine	Ile		Histidine	His	
Methionine	Met		Lysine	Lys	
Proline	Pro		Arginine	Arg	

Each of the 20 proteinogenic amino acids has a unique side group functionality (R-group). The side group can be one of the following: hydrophobic, hydrophilic, acidic, basic, polar or non-

polar. Also, the side groups influence the physicochemical properties of the amino acid and subsequently the peptide or poly(amino acid) that is obtainable from them [2].

Cyclic monomers obtained from amino acids may undergo ring-opening polymerisation (ROP) to yield amino acids *via* chain-growth polymerisation from a functional initiator [3]. Cyclic monomers that are of key interest to this research are *N*-carboxyanhydrides (NCAs) and the *O*-carboxyanhydrides (OCA)s of α -amino acids (Chapter 3). Both NCA ROP [4] and OCA ROP [5] offer an alternative to the conventional solid phase peptide synthesis route (SPPS) [6] for the production of polymers from amino acids. Poly(amino acid)-based materials may readily form discrete structures through polymeric self-assembly that is maintained by hydrophobic interactions, hydrogen bonding, aromatic (π - π) stacking and electrostatic interactions. Significantly, poly(amino acid)s can form stable secondary and tertiary conformations [7-10] including random coils, β -sheets and α -helices (Figure 1.1) [1, 8].

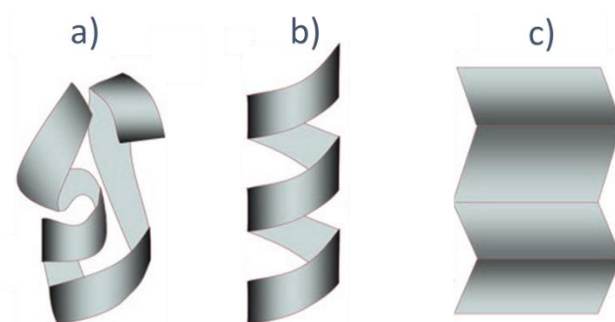
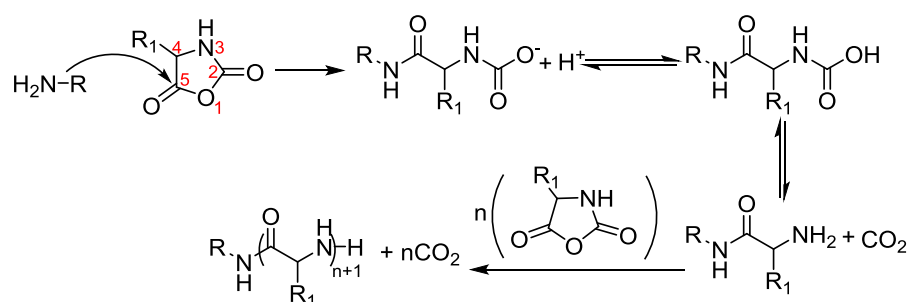


Figure 1.1. Generic illustration of a) random coil, b) α -helix and c) β -sheet conformations.

The ability of poly(amino acid)s to self-assemble into ordered and stable conformations, that give rise to useful biomimetic structures, distinguishes poly(amino acid)s from most synthetic polymers. Furthermore, the biomimeticism, biocompatibility and biodegradability that poly(amino acid)s commonly exhibit renders them particularly appealing for employment in biomedicine, pharmaceuticals, personal care product formulation, as biomaterials such as scaffolds for tissue engineering and vehicles for controlled drug delivery [11-14]. Poly(amino acid)-based nanomaterials may be in the form of gels, nanofilms, nanofibres, nanorods, nanotubes, micelles and vesicles [15-18]. The possibility of combining poly(amino acid)s with either natural non-poly(amino acid) macromolecules or synthetic non-poly(amino acid) macromolecules can afford the creation of hybrid materials, which boast functional versatility and other desirable physicochemical attributes [7, 8].

pathway [22]. These compounds are mostly more nucleophilic than basic. As such, in the NAM pathway (Scheme 1.1), the nucleophilic initiator attacks the NCA ring at the electrophilic 5-CO position. The NCA ring can then open to generate an unstable carbamic acid upon proton transfer. The subsequent loss of a CO₂ molecule results in the generation of a primary amino terminal group. This *N*-terminal becomes the active species for the subsequent addition of another NCA molecule. The cycle continues, thereby generating an oligomer or polymer whose chain length is governed by the monomer-to-initiator molar feed ratio.



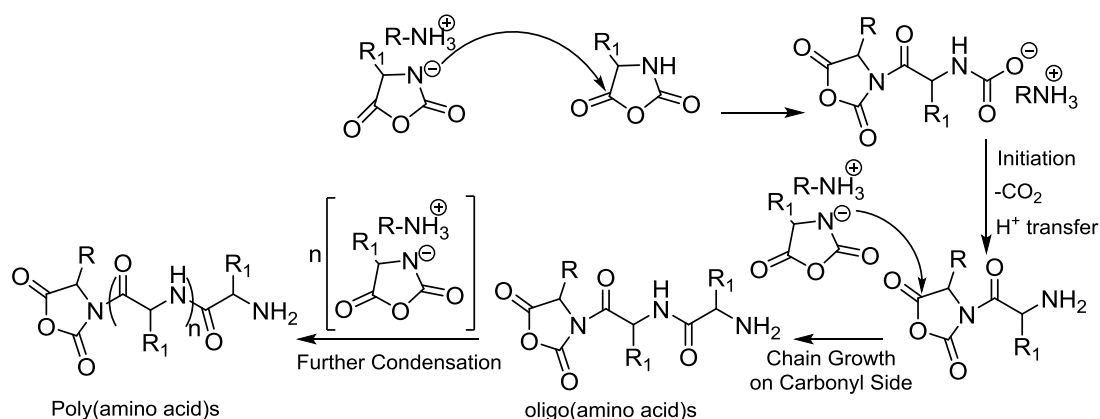
Scheme 1.1. The normal amine mechanism for the ROP of α -amino acid NCAs [3, 10, 23, 24].

It has been reported that in NCA ROP, the efficiency of an initiator is dependent on its nucleophilic strength [23]. Primary amines, being strong nucleophiles (i.e., high nucleophilicity / basicity ratio), can be strong initiators for NCA ROP. Consequently, the NAM is characterised by a very high initiation rate (that is greater than the propagation rate). High molecular weight poly(amino acid)s are difficult to obtain using this mechanism. Consequently, the NAM is utilised when there is need for control over both the chain length (molecular weight) and the chain end group [21, 25].

1.2.2. Activated Monomer Mechanism

In contrast to the NAM, polymerisations of NCAs that propagate *via* the AMM are initiated by bases. Typical initiators include tertiary amines and metal alkoxides. It is actually more accurate to state that in the AMM (Scheme 1.2), the tertiary amine catalyses the reaction rather than initiates it [10, 23, 26]. This is because the amine serves to deprotonate the NCA at the 3-N position to generate an NCA anion (i.e., ROP by deprotonation). The resultant NCA anion initiates chain propagation by attacking an NCA monomer at the 5-CO unit to generate another NCA anion. The amine is recovered upon decarboxylation (to form CO_2) and proton transfer. Hence there is the assertion that the agent acts as a catalyst rather than as an initiator [10, 23].

Due to the nature of this mechanism, NCA ROP *via* the AMM is only possible for *N*-unsubstituted NCAs that possess a pendant proton that is bonded to the '3N' position.



Scheme 1.2. The activated monomer mechanism for the ROP of α -amino acid NCAs [10, 23].

Secondary amines (with bulky substituent groups) can be used to initiate NCA ROP by the AMM. However, their intermediate nature (nucleophilicity-to-basicity) renders the synthesis more susceptible to side reactions. This is because secondary amine-mediated reactions tend to switch back-and-forth between the AMM and the NAM [25]. Due to the diminished reactivity (nucleophilicity) of the tertiary amine group, the activated amine mechanism is characterised by a relatively slow initiation rate and a faster propagation rate. Consequently, this mechanism is used when higher molecular weight poly(amino acid)s are desired [23, 25, 27]. However, it should be noted that due to the slow initiation rate, poly(amino acid)s obtained *via* the AMM are characterised by broader polydispersity indices compared to those obtained *via* the NAM.

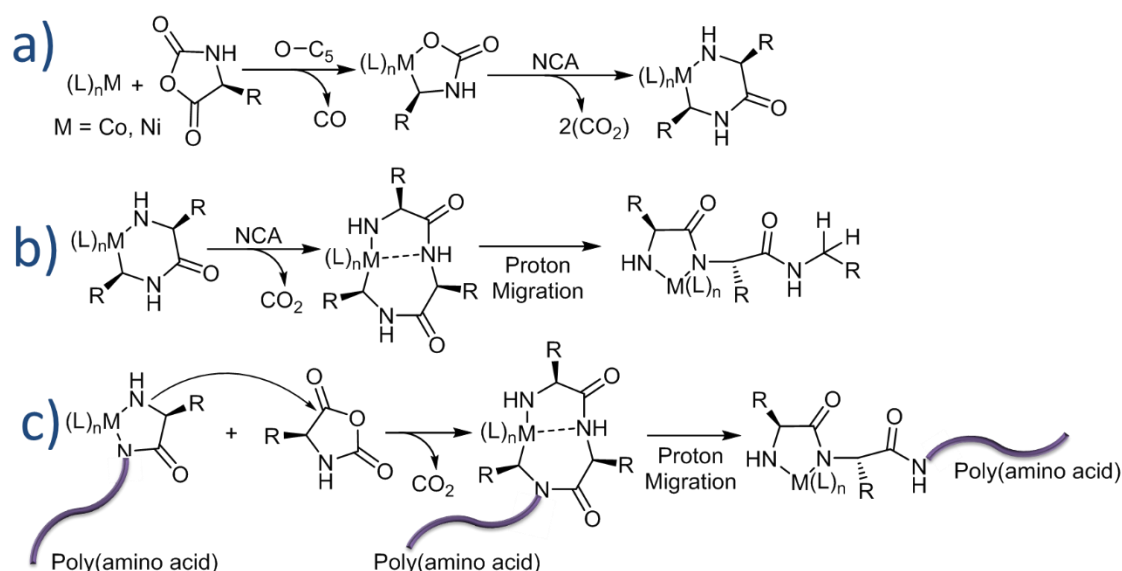
1.2.3. Recent Advances in NCA ROP

The ever-increasing interest in materials that have been created by NCA ROP has led to several attempts at improving the NAM and AMM pathways in order to achieve a living NCA ROP. Some of the documented attempts include performing NCA ROP under high vacuum [26], the use of ammonium salt catalysts [10, 28], synthesis at low temperatures [10, 29], the use of zero-valent nickel and cobalt organometallic catalysts [10, 23] and hexamethyldisilazane-mediated NCA ROP [21, 25, 30].

1.2.3.1. Transition Metal Complex-Catalysed NCA ROP

Transition metal-based compounds have extensively been deployed to catalyse polymerisations [31]. As such, the use of metal complex catalysts in NCA ROP was inspired partly by the fact that transition metals have previously been used to catalyse vinyl polymerisations [10, 23, 32, 33]. Transition metal complex-catalysed NCA ROPs have been achieved using zero-valent nickel complexes and cobalt complexes (i.e., $\text{bipyNi}(\text{COD})$ and $(\text{PMe}_3)_4\text{Co}$) [4, 10, 21, 23, 32, 34-36] ($\text{bipy} = 2,2'$ -bipyridyl and $\text{COD} = 1,5$ -cyclooctadiene).

The mechanism involves the continuous formation and the subsequent contraction of a chelating metallacycle intermediate through a stepwise oxidative addition of the nickel/cobalt metal complex across the anhydride bond (5C carbonyl bond) of the NCA monomers (Scheme 1.3). The six-membered amido-alkyl metallacycle can add across an NCA monomer to form a much larger, but short-lived, metallacycle that contracts into a relatively small, five-membered amido-amidate metallacycle. Ring contraction occurs through the migration of an amide-bound proton to the metal bound carbon atom, thereby terminating the metal-carbon bond and freeing the chain end. The five-membered amido-amidate metallacycle ring becomes the active chain-initiating species in a ROP cycle. This involves the migration of the metal to the newly added NCA, followed by contraction (proton transfer), then loss of CO_2 and reformation of the active species [10, 23].



Scheme 1.3. Steps in organo-metal initiated NCA ROP: a) oxidative addition of NCAs to CO and to Ni complexes, b) metallacycle ring contraction c) chain propagation. *Adapted from* [10].

It is reported that this transition metal complex-catalysed pathway can yield poly(amino acid)s that are characterised by narrow PDIs (<1.2) and controlled molecular weights. These claims supersede those reported for products of primary amine-initiated syntheses in terms of the polymer molecular weights that may be achieved, but not the mono-dispersity of the polymers produced [10, 26].

The disadvantages of using these zero-valent catalysts include, the *in-situ* generation of the active species within the polymer produced. As such, it becomes impossible to achieve end-chain functionalisation of the C-terminal of the poly(amino acid). In addition, metal-based impurities often need to be removed from the final product, which calls for an extra processing step. Furthermore, the requirement for a proton at the 3-N position means that N-substituted NCAs cannot be successfully polymerised using this method [26]. To facilitate functional versatility at the C-terminal chain-end, Deming *et al.* [10] developed allyloxy-carboxyl-amino-amides that act as precursors to the amido-amidate nickelacycles. There have been reports of transition metal complexes, which are based on platinum, being used to initiate NCA ROP. This ROP follows a mechanism which is similar to the one that was proposed for the nickel-based complexes [21, 37].

1.2.3.2. The High Vacuum Techniques (HVTs)

HVTs have frequently been used in the anionic polymerisation of vinyl polymers, with much success [38]. This technique has been extended to NCA ROP, by Hadjichristidis and his group, who reported widely on primary amine-initiated NCA ROP carried out using high vacuum conditions [38, 39]. The controlled living NCA ROP, using high vacuum conditions, has been attributed to the ease at which impurities and/or by-products are eliminated from the polymerisation reagents, especially from the solvent and the amine initiator. It is highly likely that such impurities act to catalyse side reactions, and cause premature chain termination. As such, under high vacuum, impurities such as CO₂ and carbamic groups, are eliminated rapidly from the reaction medium, before they could otherwise promote side reactions [3, 10].

The controls over chain growth and chain architecture that are achieved with HVTs enable the formation of block copoly(amino acid)s. Homopoly(amino acid)s of γ -benzyl-L-glutamate (Glu(Bz)), with PDI values of 1.18, have been synthesised using this technique [35]. Hybrid

poly(amino acid)-based materials are also possible through the use of amine-functionalised non-poly(amino acid) polymers as macroinitiators [40, 41]. For instance, poly(styrene)-amino macroinitiators have been used in the ROP of Glu(Bz) NCA and Lys(Z) NCA monomers, using high vacuum conditions. Structural versatility can also be achieved by varying the location of the amine initiating sites on the backbone of the macroinitiator. 100% yields, and narrow PDI values (1.11), have been achieved using HVTs [40, 41].

1.2.3.3. The Temperature Factor

The exploitation of thermal conditions to improve the yields of reactions is not new in polymer synthesis [42]. The temperature used has been reported to have an effect on the PDI and molecular weight values of poly(amino acid)s produced by primary amine-initiated NCA ROP. The controlled living ROP of *N*-trifluoroacetyl-L-lysine (Lys(TFA) NCA) has been achieved at 0 °C [29]. The efficacy of this polymerisation deteriorated upon an increase in reaction temperature, suggesting the prevalence of side reactions at temperatures greater than 0 °C. Yang *et al.* [43] attempted the syntheses of homopolymers and block copolymers of Glu(Bz) and β -benzyl-L-aspartate [Asp(Bz)], at reduced temperatures. They reported the successful ROP of Glu(Bz) NCA at -30 °C, at -10 °C and at 0 °C. The degree of polymerisation of the monomer decreased when the temperature of the reaction medium was increased. This observation could suggest the prevalence of side reactions, such as the chain-transfer reactions, at greater temperatures. In contrast, they reported that the ROP of Asp(Bz) NCA did not occur at the low temperatures which were studied (0 °C and -10 °C). Instead, it occurred at 25 °C.

The effect of temperature on NCA ROP may be explained by the fact that chain propagation and the side reactions are antagonistic in NCA ROP. As such, lowering the reaction temperature effectively reduces the activation energy barrier for chain propagation, increasing the activation energy barrier that must be overcome for side reactions to occur [10, 41, 43, 44]. Habraken *et al.* [27] were able to combine and to manipulate the temperature whilst using HVTs to achieve the controlled ROP of a range of NCA monomers.

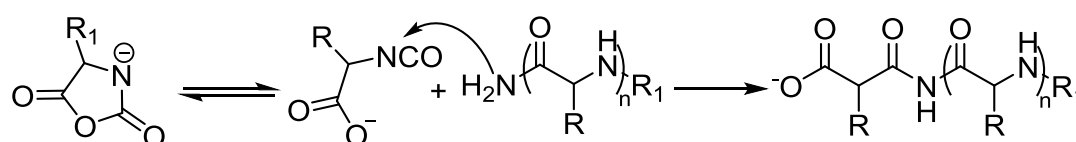
1.2.3.4. Organosilicon Amine-Mediated NCA ROP

Lu and Cheng [21, 30] pioneered the use of a specialised secondary amine, the hexamethyldisilazane (HMDS), to mediate NCA ROP. Homopoly(amino acid)s and block

copoly(amino acid)s derived from the NCAs of Glu(Bz), Lys(Z) and L-Leucine (Leu), were synthesised using this technique. The polymers produced possessed PDI values of less than 1.2. The behaviour of trimethylsiloxane (TMS) carbamate during the initiation step and the chain propagation step prompted the authors to conclude that the TMS carbamate is central to the initiation and the progression of this polymerisation technique. As is the case with the NAM, nucleophilic attack by HMDS occurs at the NCA's 5-CO position. However, the polymerisation is slow and monomer conversion rates are low due to the diminished reactivity of the organosilicon amines [10, 30]. As such, only low molecular weight polymers can be produced. Obtaining greater yields from the ROP of less reactive NCAs, such as L-proline (Pro), is challenging. An alternative synthesis route has been suggested. This involves the HMDS, acting as a base, mimicking the AMM by deprotonating the amino group of the NCA. However, this route has not gained much popularity [26]. Other authors have expanded the HMDS-mediated NCA ROP concept to include other organosilicon amines, in order to ease the difficulties associated with the functionalisation of the C-terminal group of the poly(amino acid)s [10, 21].

1.2.3.5. Primary Amine-Hydrochlorides as Substitutes for Primary Amines

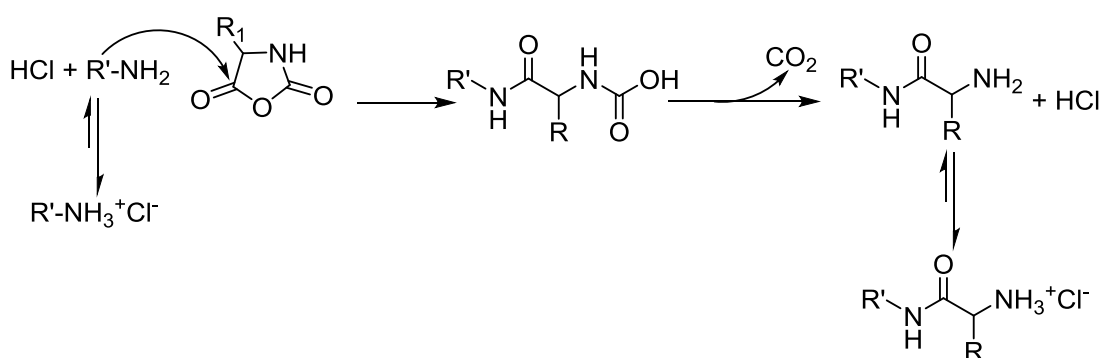
NCA anions that are generated in amine-mediated NCA ROPs are partially responsible for chain transfer side reactions, especially in the AMM [10, 23]. One such undesirable side reaction is the termination of the propagating poly(amino acid) chain by the addition of the NCA anion to the active N-terminal unit of the poly(amino acid) chain (Scheme 1.4).



Scheme 1.4. Chain transfer of a poly(amino acid) to the NCA anion during NCA ROP [10]

Schlaad *et al.* [10, 28] reported a synthesis method that was designed to minimise the effect of NCA anions that are generated *in situ* during chain propagation. This method promotes the scavenging of the NCA anions that are formed during polymerisation. Primary amine initiators are substituted with an initiator that has a diminished reactivity, such as a primary amine hydrochloride salt, which have been found to offer better control of the initiation step. The equilibrium between the primary amine and its corresponding hydrochloride salt lies towards

primary amine-hydrochloride formation. As such, any free amino groups that are present during the initiation step are protonated quickly to prevent them reacting. At elevated temperatures the equilibrium lies more towards the free amine, and so increasing the reaction temperature promotes chain propagation, and the rapid protonation of any free NCA anions, which minimises chain transfer side reactions. This results in an NCA ROP that preferentially propagates *via* the normal amine mechanism (Scheme 1.5), but avoids the generation of the chain-terminating NCA anions.



Scheme 1.5. The primary amine hydrochloride-mediated NCA ROP [28].

Consequently, the inherent problem of side reactions, emanating from a reaction that switches back and forth between the normal amine mechanism and the activated monomer mechanism, is eliminated. A positive feature of this method is that the prevailing acidic conditions will enhance the elimination of the CO₂ by-product from the reaction medium, further driving the polymerisation equilibrium [27, 28].

1.3. Poly(Amino Acid) Materials: Creation and Architecture

Poly(amino acid)-based materials may present various architectural forms. These can be classified further on the basis of their composition or microstructure, topology and functionality (Figure 1.3) [45, 46]. Some of the documented architectures include linear homopolypeptides, cyclic polypeptides, block copolypeptides, random copolypeptides, hybrid block copolymers, star-shaped polypeptides and complex polypeptide materials [45-47]. Some of these materials have been shown to self-assemble into secondary structures and to possess biological, mechanical and environmental significance [21, 48]. Some of the common architectures are discussed briefly in the following sections.

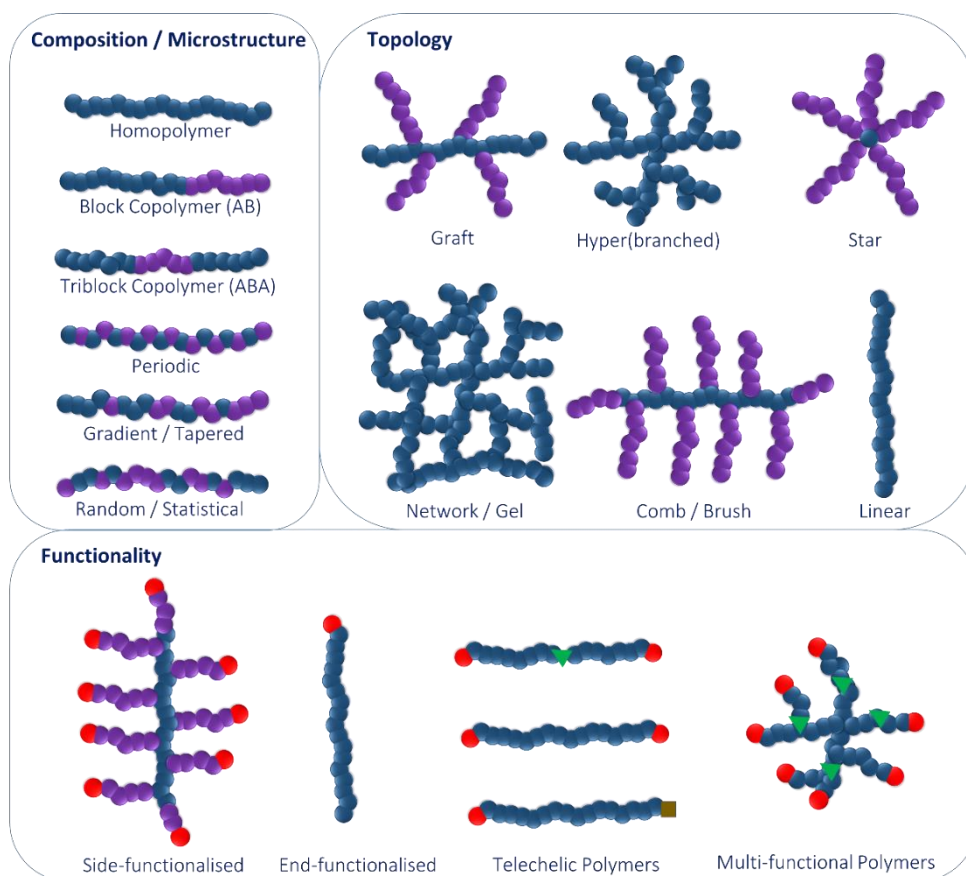


Figure 1.3. Schematic presentation of poly(amino acid)-based material architectures that can be created, affording both the structural and the functional versatility needed in pharmaceuticals, drug delivery and personal care applications. *Adapted from* [45, 46].

1.3.1. Random coPoly(Amino Acid)s

This class of polypeptides is widely created by amine-mediated NCA ROP and transition metal-catalysed NCA ROP. Hadjichristidis [26] described how random copoly(amino acid) materials can be produced by the simultaneous copolymerisation of two or more different NCAs to yield random blocks of peptides on the poly(amino acid) backbone. The deprotection of labile side groups of the copoly(amino acid) chain can also be carried out to furnish the polymer with additional functionalities [4, 26]. The possibilities of harnessing desirable properties from many relevant amino acids affords the creation of random copoly(amino acid)s that are functionally more appealing [49].

Some of the amino acids that have been used widely in various combinations, to produce random copoly(amino acid)s by random copolymerisation of their NCAs, include β -benzyl-L-

aspartate, *O*-acetyl L-tyrosine, L-alanine, sarcosine, L-leucine, L-valine, glycine, L-alanine, γ -benzyl-L-glutamate, L-methionine, D,L-leucine, D,L-valine and Lys(Cbz). For example, amphiphilic copoly(amino acid)s have been reported, which were synthesised using the random copolymerisation of hydrophilic amino acids and hydrophobic amino acids, such as the combination of Lys(Z) and Phe, respectively [4, 10, 23, 26, 49]. Wamsley [50] has reported the creation and characterisation of L-leucine (Leu), L-valine (Val) and Asp(Bz) terpolymers, dioxane being the solvent. The random copolymerisation of several poly(amino acid)s that have labile protective groups, which include TFA, Fmoc, tBoc, Benzyl (Bz) and carbobenzyloxy (Cbz), has been reported. The selective deprotection of these side groups has been shown to be a good strategy for generating complex and functionally versatile poly(amino acid)s. Using this approach, Hernandez and Klok [51] synthesised random poly(amino acid)s that had potential use as scaffolds for antigen binding. Zhao *et al.* [47], carried out the random ROP copolymerisation of propargyl-Glu NCA and Glu(Bz) NCA, and produced random poly(amino acid)s that boast alkyne side chain functionalities, which could be exploited in post-polymerisation modifications.

1.3.2. Block coPoly(Amino Acid)s and Hybrid Materials

Block copolypeptides can be created by the sequential ROP of different NCA monomers using amine initiators or transitional metal complex catalysts [52, 53]. The first NCA monomer should be polymerised to exhaustion, thereby yielding a macroinitiator for the grafting of a subsequent poly(amino acid) block [3]. Additional blocks are then created following the exhaustion of the NCA monomer of the preceding block. This cycle can be repeated and yields precisely defined peptide blocks within the polymer chain. It is possible for block copolymers to consist entirely of poly(amino acid) blocks or have blocks which are composed of other non-poly(amino acid) macromolecules, e.g. a vinyl polymer. The latter may be termed a hybrid block copolymer and harnesses the independent, desirable properties of the peptide and non-peptide polymers into one polymeric material [54]. The creation of diblock (AB) and triblock (ABA) copolypeptides using NCA ROP has been reported [21, 26, 47]. Highly functional AB diblock poly(amino acid) hybrid materials and ABA triblock poly(amino acid) hybrid materials have been created from macroinitiated NCA ROP, whereby A is the poly(amino acid) block. Linear hybrid terpolymers have also been reported. For example, hybrid pentablock

terpolymers, were created from the ROP of Glu(Bz) NCA and Lys(Cbz) NCA, initiated from an amino-difunctionalised poly(styrene) macroinitiator (Figure 1.4) [41]. Linear macroinitiators can be functionalised on one end or both ends (difunctional), to create different polymeric architectures. As such, variations from simple linear architectures to complex architectures are possible through the careful selection of initiators for NCA ROP. For example, star-shaped multifunctional macroinitiators can be created (Figure 1.6) [4, 19, 26, 40].

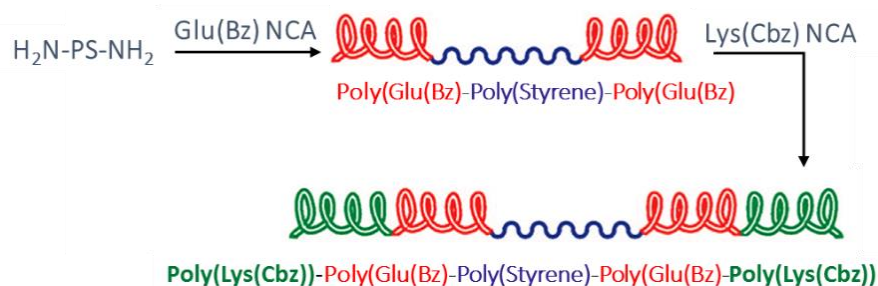


Figure 1.4. Pathway for a typical example of a hybrid poly(amino acid)-based macromolecule: A pentablock; poly(Lys(Cbz)-poly(Glu(Bz)-poly(Styrene)-poly(Glu(Bz)-poly(Lys(Cbz) terpolymer, created by NCA ROP from a difunctional polystyrene macroinitiator [26, 41].

NCA ROP allows for the creation of surface-grafted poly(amino acid)-based materials, to create useful films and interfaces. The ‘grafting-to’ a functionalised surface approach and the ‘grafting-from’ a functionalised surface approach or the surface-initiated NCA ROP approach, are the common strategies (Figure 1.5) [18, 55].

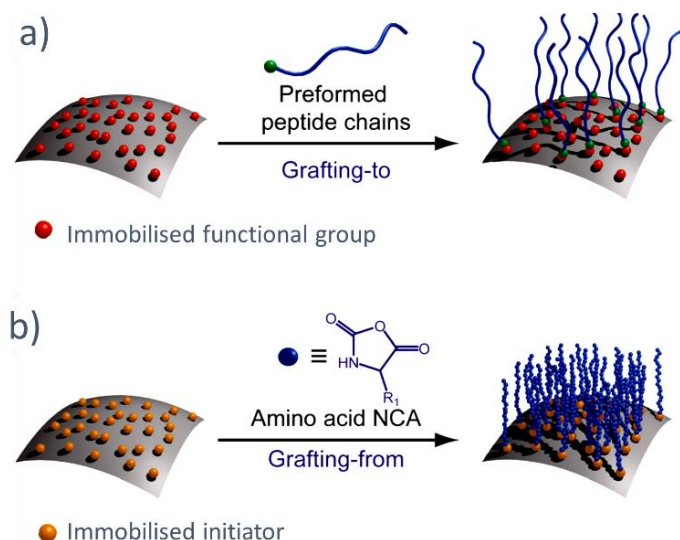
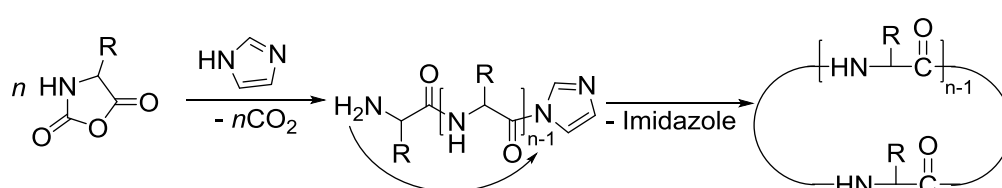


Figure 1.5. Illustration of the (a) grafting-to approach and (b) grafting-from approach for the production of surface-grafted poly(amino acid)s. *Image reproduced from [55].*

Some of the surfaces that have been used in the production of surface-grafted poly(amino acid)s include, non-porous and mesoporous silica NPs [56, 57], gold substrates [58, 59], magnetic NPs [60, 61], cellulose and cotton fabrics [62] and microporous polymer membranes [63, 64]. Surface-grafted poly(amino acid)-based materials have many prospective applications, including in tissue engineering, bionanocoatings, biosensing and drug delivery [18, 56].

1.3.3. Cyclic Poly(Amino Acid)s

Cyclic poly(amino acid)-based materials have been reported by several authors, including Hadjichristidis *et al.* [26], Kricheldorf *et al.* [65] and Guo *et al.* [66]. Although it can be claimed that these materials originally resulted from the effects of unfortunate side reactions in NCA ROP, their occurrence cannot be ignored. The use of secondary and tertiary amine initiators introduces a number of factors that alter chain propagation *via* the NAM. These key factors include the extent of steric hindrance arising from the initiator's bulky side groups, and the strength of the initiator's nucleophilicity-basicity. Deviation from NAM kinetics can lead to end-to-end chain cyclisation *via* controlled polycondensation reactions. The synthesis of various cyclic polypeptides has been reported [4, 38]. Imidazole (Scheme 1.6) and pyridines (*via* a zwitterionic monomer mechanism) and trialkylamines (NCA deprotonation to generate the nucleophile) have been used successfully to initiate the ROP of N-unsubstituted NCAs to create cyclic poly(amino acid)s, at high temperatures [26].



Scheme 1.6. Imidazole-initiated NCA ROP generation of cyclic poly(amino acid)s [4].

The thermal polymerisation of N-unsubstituted NCAs has also been reported, whereby the NCAs are heated above their melting point to yield cyclic polypeptides *via* either a step-growth or a chain-growth polycondensation [26]. Kricheldorf *et al.* [67] hypothesised that cyclic poly(amino acid)s, formed during NCA ROP, are a result of a solvent-induced polymerisation which is possibly initiated by the zwitterions that are generated in the reaction medium. This

hypothesis followed from the observation that the generation of cyclic poly(amino acid)s was prevalent in those reactions that were conducted in solvents with a greater nucleophilicity and basicity, such as DMF and NMP, respectively.

1.3.4. Star-Shaped Hybrid Materials and Complex Architectures

Star-shaped poly(amino acid)-based materials can be created using multifunctional star initiators (*grafting from*) or multifunctional linking agents (*grafting to*) [19, 68, 69] (Figure 1.6). Thus, three, four, six, or up to nine amino-functionalised initiators can be used for the NCA ROP-grafting of poly(amino acid)s. As such, in the *grafting from* approach, the poly(amino acid) arms are grafted outwards to create a complex macromolecule that has the initiator as its core (Figure 1.6 a).

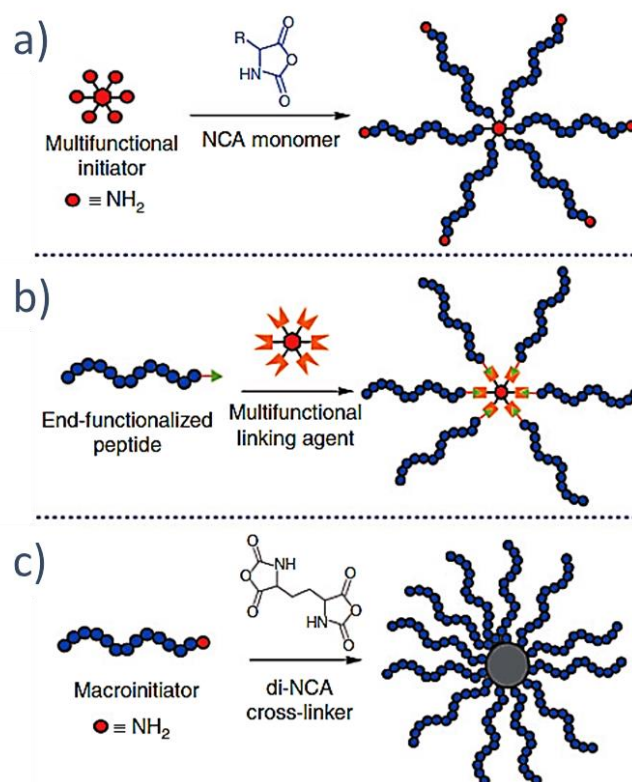


Figure 1.6. Representation of potential approaches to obtaining core crosslinked peptide-based star polymers; (a) core-first (*grafting-from*), (b) *grafting-to* and (c) arm first approach [19, 70]

It is important for the rate of initiation to be greater than the rate of polymer chain propagation, and that the initiating sites on the multifunctional initiator should offer the same reactivity, in order to achieve uniform polymer chain propagation. This enhances the chances of obtaining polymers with narrow PDIs. However, materials created this way are difficult to

characterise, due to the difficulty of determining the molecular weight of each individual polymer arm [26]. The use of the *grafting from* strategy, to create useful star poly(amino acid) materials, has been reported by several other authors [68, 69, 71-74].

Complex hybrid materials can also be created by connecting end-functionalised poly(amino acid)s to a multifunctional molecules using techniques such as click chemistry (Figure 1.6 b). The *arm first* method incorporates a separate synthesis step to create the living mono-functional polymer chains (amine-terminated arms) that are then crosslinked by NCA ROP from a di-NCA monomer. Therefore, unlike in the core first approach, the arms are ROP-synthesised first. The arms may then be linked to the core during an independent step. Well-defined polymers are possible, but the characterisation of the resultant hybrid macromolecule may only be possible by characterising the isolated arms, prior to grafting onto the crosslinker. Polymerisation techniques, such as reversible addition-fragmentation transfer (RAFT), may also be used to create stars of varying molecular weights [75-77].

1.3.5. 'PEGylation' and Other Synthetic Polymers

Poly(ethylene glycol) (PEG) macromolecules are among a class of non-poly(amino acid) synthetic macromolecules that are extensively used to create hybrid poly(amino acid)-based materials. Apart from its biocompatibility and commercial availability in different amine end-functionalised architectures, other desirable properties of PEG include its desired hydrophilicity, protein resistance and the enhanced pharmacokinetics that it imparts to drugs, *in vivo* [10, 78, 79]. PEGylation can be used to create crosslinked hybrid materials [80, 81], poly(amino acid)-based brushes [82] and amphiphilic hybrid materials (Figure 1.7) [83], which may self-assemble in aqueous media to generate versatile nanocarriers which include polymer micelles, vesicles and hydrogels.

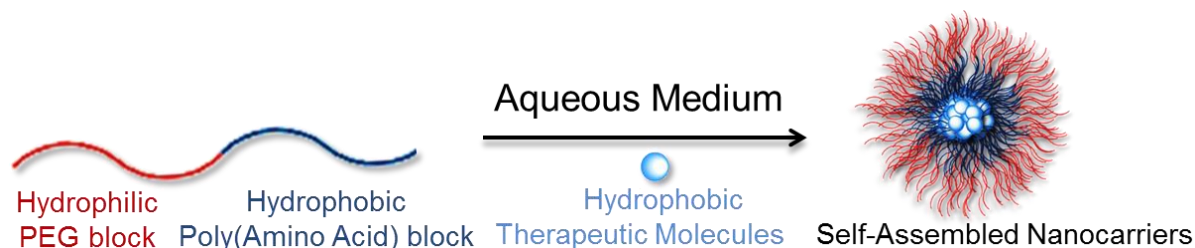


Figure 1.7. PEG possesses stealth properties which are exploited extensively in the creation of amphiphilic macromolecules.

PEGylated poly(amino acid)s can self-assemble in aqueous media into nanostructures that adopt α -helix conformations and β -sheet conformations, thus enabling the creation of nanostructures which can be exploited for drug delivery [84, 85]. PEGylated, pH-responsive poly(amino acid)-based drug delivery vehicles are extensive, and include those which have been created from Lys [86], Glu [87], Phe [88] and Ser [89]. Iijima *et al.* [90] have generated particles and hydrogels from a range of ABCBA pentablock hybrid poly(amino acid)s, which were produced by initiating the ROPs of a various NCA monomers from amine-functionalised PEG macroinitiators. Other non-poly(amino acid) polymers, i.e. synthetic polymers and also naturally-occurring polymers, have been used to create hybrid poly(amino acid)-based nanomaterials [10]. These include, poly(styrene) [41], poly(lactic acid) [91], monosaccharide and polysaccharides (which can afford the creation of glycosylated hybrid materials) [10, 49].

1.4. Poly(Amino Acid) Materials: Biological Relevance

Poly(amino acid)-based materials have many applications and potential applications in the biomedicine, pharmaceuticals and biotechnology fields. Poly(amino acid)s have been used widely as drug delivery agents, scaffolds in tissue engineering, therapeutics, sensors and bioelectronics [22, 92]. The popularity of these materials frequently stems from their adoption of secondary ordered conformations such as the α -helices, random coils and β -sheets (Section 1.1), and their subsequent self-assembly, to yield useful nanostructures which can be designed to mimic biological agents. Furthermore, their ability to respond to various stimuli (temperature, pH, light, electrical, magnetic, enzymatic/biological etc.) in a programmed manner dictates that they are functionally versatile materials [14, 22, 93]. Some of the useful nanostructures obtained through self-assembly include organogels and hydrogels, particles (vesicles, micelles), tubes and fibres [22, 92]. These nanostructures can be obtained from wholly poly(amino acid) materials and from composites that contain other (macro)molecules.

1.4.1. Poly(amino acid)-Based Micelles and Vesicles

Micelles are self-assembled spherical, cylindrical or ellipsoidal aggregates of amphipathic molecules in an aqueous matrix solvent, that is common only to one of the polymer's segments [94]. In water, polymer micelles form as a response to the hydrophilic segments of the macromolecules spreading out into the aqueous medium to form a single outer shell while the

hydrophobic segments are shielded to form a hydrophobic core. This behaviour is generally true of vesicles. However, unlike micelles, vesicles consist of a bilayer in which hydrophilic segments are exposed to the aqueous medium while sequestering the hydrophobic segments. The resultant bilayer forms a highly-selective membrane that encloses a hollow compartment (Figure 1.8) [95].

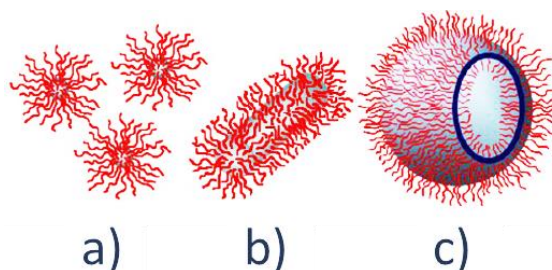


Figure 1.8. Representative illustration that amphiphilic poly(amino acid)-based block copolymers which possess various architectures can self-aggregate to yield nanomaterials such a) spherical micelles, b) cylindrical micelles, c) vesicles (polymersomes) [96].

Nanoparticles (NPs) that are obtained from poly(amino acid)-based macromolecules have many current applications and potential biomedical applications, as delivery vehicles for drug molecules [97, 98]. Several benefits that arise from the use of these materials as delivery agents include enhancing the blood circulation of therapeutic molecules, targeted delivery and subsequent controlled release of the therapeutic cargo [99]. Diblock and triblock copoly(amino acid)s of varying molecular weights, that incorporate hydrophobic segments and hydrophilic segments, have been synthesised by NCA ROP and shown to hierarchically self-assemble into either vesicles or micelles in water and in other solvents [3, 98, 100, 101].

By employing an amine-initiated living NCA ROP in a sequential order, Sun *et al.* [102] were able to synthesise poly(Lys)-*block*-poly(Phe) diblock copoly(amino acid)s. The polymers were able to self-assemble when dispersed in water, into vesicles. The resulting vesicles were able to form complexes with DNA, suggesting that this polymer composition has potential applications in gene delivery. Arginine (Arg) and leucine (Leu)-based block copoly(amino acid)s were reported by Holowka *et al* [103]. The polymers, which were created by varying the molar feeds of NCA monomers in order to tune the compositions and molecular weights, self-assembled into vesicles. One such poly(amino acid), poly(Arg₆₀)-*b*-poly(Leu₂₀) (Figure 1.9) self-

assembled in the presence of an aqueous medium. The vesicles that were formed exhibited potential endosomal intercellular activity [3, 8, 103, 104].

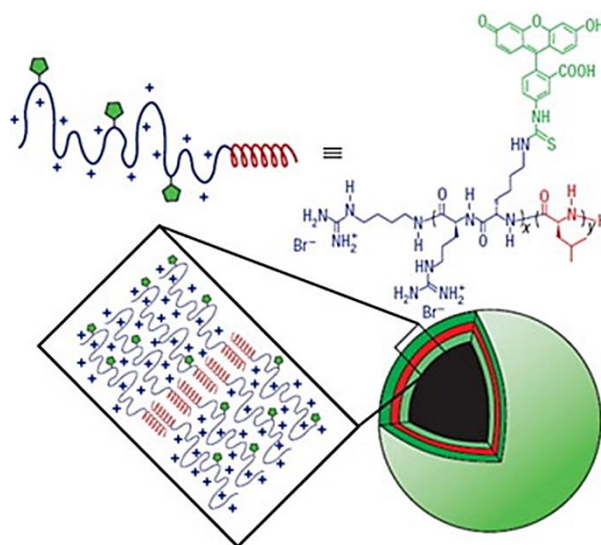


Figure 1.9. Schematic view of the self-assembled poly(Arg₆₀)-*b*-poly(Leu₂₀) vesicle [8].

Checot *et al.* [105] have reported Lys-based and Glu-based block copolypeptides, which exhibited zwitterionic behaviour. Their pH-dependent self-assembly enabled the formation of vesicles and micelle particles. The same authors also reported on the creation of poly(butadiene)-*b*-poly(Glu) and poly(isoprene)-*b*-poly(Lsy) block copolymers. The polymers self-assembled in aqueous media. The formation of either vesicular structures or micellar structures was dictated by the monomer molar feed ratios that were applied in the creation of the macromolecules. Iatrou *et al* [79] used NCA ROP to synthesise the ABA triblock polymer, poly(Lys)-*b*-poly(Glu)-*b*-poly(Lsy), which self-assembled into vesicles in aqueous solution. pH responsive vesicles were also reported by Deming *et al.* [106], from the self-assembly of poly(2-[2-(methoxyethoxy) ethoxy] acetyl-Lys)₁₆₀-*b*-poly(Leu_{0.3}-CO-Lys_{0.7})₄₀.

Micelles, which are obtainable from peptide-based hybrid diblock copolymers, have been reported [107-109]. For example, PEGylated poly(amino acid)-drug conjugates were reported by Katoka *et al.* [110], in which the chemotherapeutic doxorubicin (dox) molecules were covalently linked to the repeat units of the hydrophobic poly(Asp) block (Figure 1.10). These polymer-drug conjugates self-assembled into micelles, which achieved prolonged circulation in the blood and significant accumulation in the tumours. The subsequent controlled release of dox from the micelles caused complete tumour regression. The properties of poly(amino

acid)-based micelles can also be tuned by selecting macroinitiators which possess properties that are sought. For example, thermo-responsive micelles have been reported, which were created by employing amine-functionalised macroinitiators that are both hydrophilic and thermosensitive, e.g. poly(*N*-isopropylacrylamide) [111] and poly(propylene oxide) [112].

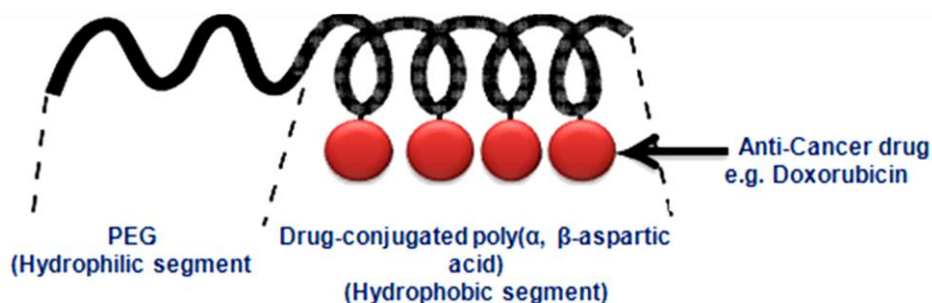


Figure 1.10. Schematic representation of the di-block amphiphilic PEG-Poly[(Asp)-Dox]. The macromolecule self-assembled in aqueous to form dox-loaded micelles [110].

1.4.2. Polymer Hydrogels

Hydrogels are crosslinked, three-dimensional polymer networks that can immobilise a large volume of water. They are rendered insoluble because of the numerous crosslinks between the polymer chains [113]. The crosslinks can be achieved chemically, e.g. covalent crosslinking, or they can be achieved physically, e.g. hydrogen bonding, ionic interactions, hydrophobic interactions or simple chain entanglements. The ‘smart’ behaviour of hydrogels, in that they are able to simulate natural biological soft tissues and respond to different stimuli e.g. by swelling and collapsing, makes them useful biomaterials. Furthermore, their great water-holding capacity and possible biocompatibility are the basis of the huge interest in hydrogels for applications in biomedical and pharmaceutical sectors [114]. Hydrogels have been reported for use in drug delivery [115], contact lenses [113], tissue engineering [113], wound dressings and implants [116] and cell therapy [117].

Amphiphilic block copoly(amino acid)s can exhibit gelation properties as a result of hydrophobic interactions, π - π stacking and by hydrogen bonding [80]. Injectable hydrogels are a unique class of biomaterials that can gel *in vivo* upon injection and exposure to a gelation stimulus, such as a change in environmental temperature. These gels offer versatility in the design of injectable scaffolds and drug delivery systems [118]. Chen *et al.* [119] reported the creation and characterisation of non-ionic poly(amino acid) hybrid materials. These materials,

which were based on diethylene-glycol-monomethyl-ether and Glu, self-assembled by adopting α -helix conformations and β -sheet conformations, to yield hydrogels, which have potential biomedical applications as non-ionic, injectable hydrogels (Figure 1.11) [119]. Their findings revealed that the shear-thinning properties of the gels were dependent on the length of the substituent alkyl chain.

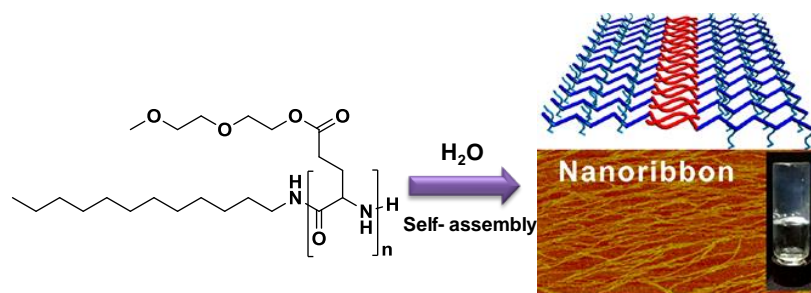


Figure 1.11. Schematic representation of poly(amino acid)-based hybrid hydrogels: Poly-L-diethylene-glycol-monomethyl-ether-glutamic acid polymers self-assembling into nanofibres to give injectable hydrogels [119].

Thermosensitive, biocompatible hydrogels derived from the oligo(Ala-co-Phe-co- β -benzyl-Asp)-poloxamer-oligo(β -benzyl-Asp-co-Phe-co-Ala) copolymer were reported by Chiang *et al.* [120]. Their investigations revealed that the conformation adopted by the hydrogels could be altered from α -helix confirmation to β -sheet conformation by deprotecting the Asp groups. Such hydrogels, which exhibit temperature dependent sol-gel properties, are useful candidates for sustained drug release [80]. pH-responsive hydrogels are another class of nanomaterials that have useful applications in therapeutics. Due to the presence of specific pH conditions in different parts of the human body, particularly in disease-affected cells, pH-responsive hydrogels can be used for targeted payload delivery. For example, the normal physiological pH is 7.4, but the extracellular pH of disease-affected cells or tumour cells may decrease to around pH 5. As such, carrier systems such as hydrogels, micelles and vesicles, can be fabricated, that undergo reversible conformational or self-assembly transitions, or degradation when subjected to a change in environmental pH, resulting in payload release. A pH-responsive hybrid nanogel, consisting of a poly(His-co-Phe) hydrophobic core that is surrounded by a hydrophilic sheath of PEG and bovine serum albumin, was reported by Lee *et al.* [121]. This gel was able to swell on exposure to a solution of pH of 6.4 due to the protonation of His residues, which resulted in the release of encapsulated doxorubicin. A poly(Glu)-based hydrogel

consisting of PEG crosslinks was reported, that can contract at neutral pH, thereby encapsulating the molecular cargo, and subsequently de-swell rapidly at acidic pH to release the molecular cargo (Figure 1.12) [115]. Several other peptide-based hydrogel materials have been reported [85, 114, 119, 122-126].

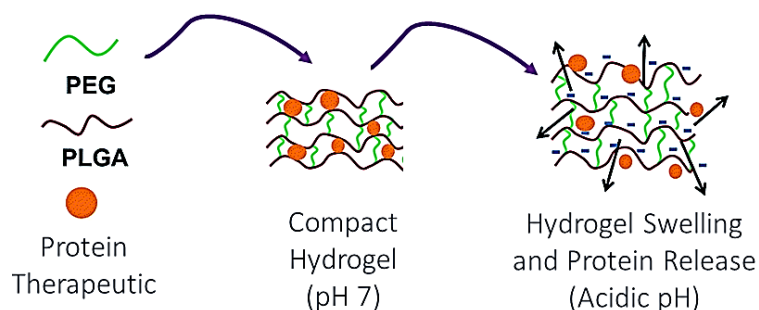


Figure 1.12. Schematic representation of a pH-responsive peptide hybrid material, exhibiting hydrogel properties that can be used for drug delivery [115].

1.4.3. Enzyme-Responsive Materials (ERMs)

Enzymes are central to the normal functioning of biological processes in organisms. Also crucial is the fact that specific enzymes play key roles in disease pathways [80]. For example, cancer, acquired immune deficiency syndrome, diabetes, Alzheimer’s and vascular diseases have each been shown to be associated with an over-expression of specific proteases [127, 128]. The abundance of enzymes in the physiological system can be exploited to create artificial biomimetic peptide-based materials (Figure 1.13), whose chemical properties or physical properties are modified by the selective and specific action of targeted enzymes. Protease substrates consist of specific amino acid sequences, and so most ERMs are designed to incorporate peptide blocks to confer enzyme responsiveness [118].

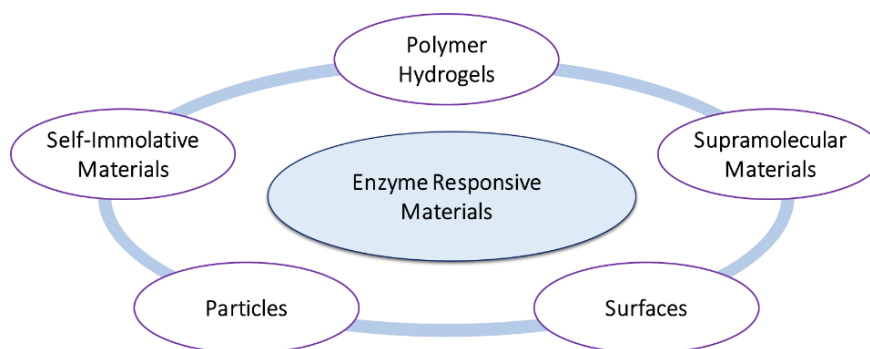


Figure 1.13. Schematic classification of ERMs, according to their structural design [118].

In cancer therapy, cancer-associated proteases (CAPs) are widely used stimuli [129]. Enzyme-responsive peptide materials are based on supramolecular assemblies, nanoparticle surfaces (e.g. mesoporous silica) and gels bearing enzyme-susceptible moieties or crosslinks [130]. Peptide-based nanocarriers (e.g., vesicles, micelles and hydrogels) that contain enzyme labile bridges such as peptide bonds, ester bonds and disulfide bonds can be used for targeted delivery at sites where targeted enzymes are over-expressed. ERMs have gained popularity in controlled targeted drug deliveries [80] and in regenerative medicine [130].

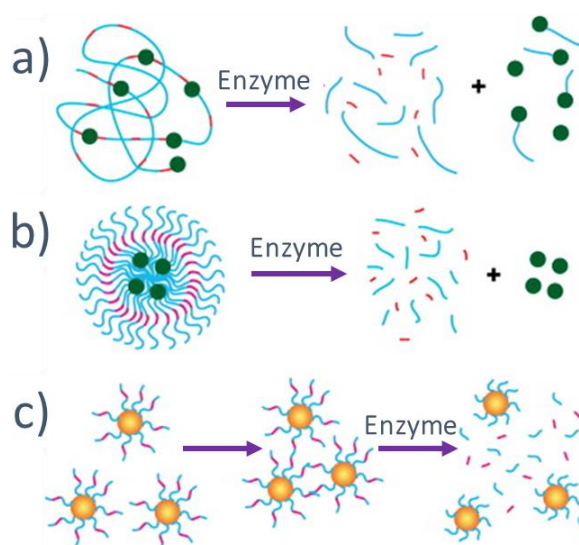


Figure 1.14. Illustration of the concept of payload delivery by ERMs: a) cleavage and targeted release of covalently-bound drugs from polymeric NPs e.g. by proteases in peptide carriers or glycosidases in polysaccharide carriers, b) enzyme-induced drug release from liposomes e.g. by proteases in peptide carriers or lipases in phospholipids, c) diagnostics using inorganic particles and hydrolase-induced disassembly [131].

The enzyme-induced self-assembly of poly(amino acid) materials has also been reported. Toledano *et al.* [132] reported the self-assembly of poly(amino acid)s occurring through the π - π stacking of the pendant Fmoc groups, caused by the 'reverse hydrolysis' of peptide bonds. Figure 1.14 illustrates some of the possible mechanisms of cargo release that are pertinent selected enzyme-responsive NPs.

1.4.4. Glucopeptides / Glycopeptides

Synthetic peptide-based materials consisting of carbohydrate moieties are termed glycopeptides or glycopoly(amino acid)s because of their resemblance to the naturally-

occurring glycoproteins [133-136]. They are an important class of biomaterials that exploit the desirable properties of glycans and peptides. They can be synthesised by NCA ROP and tuned to respond to different stimuli conditions, and thus are appropriate drug delivery vehicles. pH-responsive poly(amino acid)s [137], thermo-responsive poly(amino acid)s [138] and oxidation-responsive glucopeptides have been reported [139].

Glucopeptides are excellent candidates for use as scaffolds in tissue engineering [140]. Aliphatic synthetic polyesters, based on lactic acid and glycolide have long been used to develop temporary scaffolds for tissue engineering. However, their cell affinity is relatively low, compromising their role as temporary support structures. Ideally, to function as scaffolds for cell growth and proliferation, they should fully mimic the native extracellular matrix. In reality, they fall short of this. In contrast, polysaccharides offer good surface interaction to cells due to their enhanced hydrophilicity and the presence of surface-binding sites. Furthermore, the mutual affinity is enhanced by the fact that some of the carbohydrate groups found in polysaccharides are also present in cellular matrix glycoproteins. Glucopeptide scaffolds that are based on block copolymers of chitin and Leu have been created by NCA ROP [140].

Glucopeptides are used in providing protection against proteases and in drug delivery [138]. Tian *et al.* [141] reported the synthesis of a D-gluconolactone-functionalised macromolecule which is based on poly(Lys₃₀)-*b*-poly(THF)-*b*-poly(Lys₃₀) triblock copolymer. These copolymers self-assembled in water into spherical morphologies and possess the potential to be used in controlled drug delivery and in biomimetic mineralisation. The syntheses of glucopeptides was also reported from the ROP of *O*-tetra-*O*-acetyl- β -D-glucofuranosyl-functionalised Ser NCA and from the ROP of *N*-acetyl-D-glucosamine-functionalised Ser NCA [133]. Other authors have also reported their work on the syntheses of glucopeptide materials from the ROP of NCA monomers to generate useful carbohydrate-functionalised poly(amino acid)s [142-146].

1.4.5. Biomimetic Mineralisation

Peptide-based materials have been reported for their use in biomineralisation. Living organisms produce essential minerals such as CaCO₃, required to harden the structural and defensive tissues, e.g. bones in vertebrates [147-149]. Naturally, this process is regulated by proteins. However, materials scientists have long been interested in findings ways to mimic

this natural process (biomimetic mineralisation) [148]. The biocompatibility and biodegradability of peptide materials make them suitable candidates for aiding biomimetic mineralisation. By making use of controlled NCA ROP, high molecular weight polymers with narrow PDIs can be created. In nature, acidic proteins play a key role in the biomineralisation process. Other important factors that have been cited include hydrogen bonding, the polymer's net charge and its hydrophobicity/hydrophilicity balance. Peptides also play a vital role in the creation of a new class of amphiphilic materials, double hydrophilic block copolymers, that are widely used in biomineralisation [150]. Copolymers based on amino acids, such as Lys (which assumes positive charge at acidic pH), Ala (hydrophobic) and Glu (which assumes negative charge at alkaline pH), have all been reported for use in the mineralisation of CaCO_3 [148].

1.5. Peptidomimetic Materials: Peptoids

Amphiphilic poly(amino acid)-based macromolecules can self-assemble when present above their critical aggregation concentration in aqueous media, driven by the minimisation of hydrophobic interactions and optimisation of intermolecular attractions between the chains [151]. This ability to self-organise into useful polymeric nano-carriers makes amphiphilic polymers excellent candidates for use in pharmaceuticals and in drug delivery. However, few polymers possess the biologically-imperative properties that are required of the hydrophilic block in a nano-carrier. Polymers created from polar amino acids and from charged amino acids can be used as hydrophilic segments of amphiphilic polymers, which could interact with the aqueous physiological system *in vivo*. Some of the candidates include Glu, Ser, Lys, Tyr, Cys and Asp, [2]. Although they are used extensively in pharmaceutical applications and in biomedical applications, poly(amino acid)-based therapeutic products also have drawbacks that emanate from their lack of 'stealthiness', *in vivo*. For example, they are highly susceptible to proteolytic cleavage [152]. As such, they have a relatively short half-life *in vivo*. This leads to low oral bioavailability and tissue bioavailability of therapeutics [153, 154]. Furthermore, some of the hydrophilic poly(amino acid)s, such as poly(Lys), are cytotoxic polycations that exhibit significant cytotoxicity *in vivo* [155].

PEGylation of poly(amino acid)s is widely used to achieve the desired hydrophilicity, protein resistance and pharmacokinetic behaviour. However, PEG can present long-term demerits,

such as the macromolecular syndrome. This arises because the human body lacks the ability to biodegrade ether bonds and subsequently excrete PEG macromolecules [156]. As such, these rapidly accumulate in the liver and other storage organs including the spleen and kidneys. Furthermore, it has also been reported that the physiological system generates anti-PEG immunoglobulins in response to some PEGylated therapeutics, further limiting their therapeutic efficacy due to accelerated blood clearance [154, 157].

Table 1.2. The biologically-imperative properties of peptoids, that are required of the hydrophilic block in a polymeric nanocarrier [158, 159].

Properties of Peptoids that are Desirable in Drug Delivery

- Slow degradability due to stability against proteolysis
 - Comparable protein resistance to that of PEG
 - Extensive solubility in aqueous media
 - Non-ionic nature
 - Weak hydrogen bond acceptor profiles
 - Non-immunogenic
 - Naturally occurring raw materials, e.g. sarcosine
 - Polymerise by ROP following the NAM only (no need for special reaction conditions or catalysis)
-

Peptoids or poly(*N*-substituted glycine)s are peptidomimetic compounds that offer an exciting prospects as the hydrophilic component of amphiphilic poly(amino acid)s. They have no known adverse effects [158, 160]. Their lack of the proteolytically-susceptible peptide bond means that they possess some of the desirable properties that are required in drug delivery (Table

1.2). Sarcosine (Sar)-based polymers are particularly appealing due to their biodegradable and biocompatible nature [161, 162].

1.6. ROP of *O*-Carboxyanhydrides, Created from α -Hydroxy Acids of α -Amino Acids (OCA ROP)

Poly(ester)-based materials are an exciting prospect, as functional materials, in the biomedical applications, in pharmaceuticals, and in personal care products. This is because they are responsive to pH stimuli and enzymatic stimuli. Furthermore, the wide availability of starting materials means that biocompatible materials are accessible [163-165]. Consequently, poly(ester)s are suitable candidates for use in drug delivery, scaffolds for tissue engineering, as dental composites for dental fillings, and surgery (as surgical sutures) [164, 166-168].

Conventionally, biologically-relevant poly(ester)s have been created by the step-growth polymerisation of diesters and diols [42, 169]. The large number of diesters and diols that are available dictates that functionally-versatile materials may be created using step-growth polymerisation. Synthesis is conducted at very high temperatures, usually above 250 °C. Furthermore, this method is reliant on high vacuum conditions for the *in situ* removal of impurities in order to achieve high molecular weight poly(ester)s [170]. The ROP of cyclic esters is another method that has been used to create poly(ester)s. Some of the cyclic esters that can be used include lactides, β -lactones and ϵ -caprolactone [171-173]. The ROP of cyclic esters can be performed at low temperatures and offers control over the molecular weight and the molecular weight distribution of the poly(ester)s. However, many poly(ester)s obtained by ROP lack the desired functional versatility. This is because of the limited functionality in the cyclic esters utilised (Figure 1.15). Furthermore, the reactions are very slow in their achievement of high molecular products weight products compared to conventional poly(ester) synthesis. The use of metal catalysis can improve reaction rates and yields but introduces the risk of cytotoxicity in products that have *in vivo* applications [174].

Poly(ester)s with considerable functional versatility can be created by the copolymerisation of epoxides with cyclic anhydrides. However, this method is not economically viable, and lacks environmental friendliness as it requires the use of metal-complex catalysis to achieve reasonably viable yields of high molecular weight poly(ester)s [175-178].

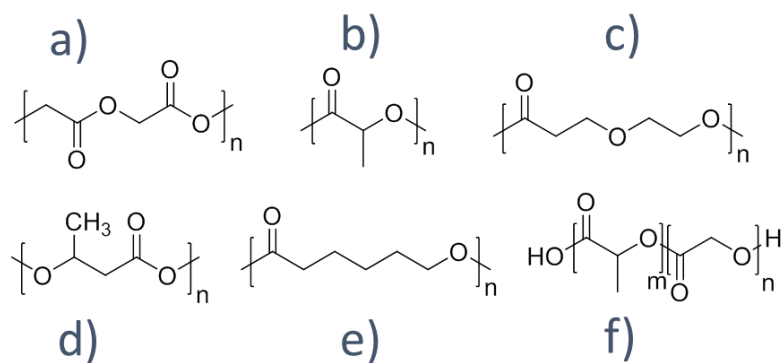


Figure 1.15. Some of the extensively documented aliphatic poly(ester)s: a) PGA, b) PLA, c) PDXO, d) P(β -BL), e) P(ϵ -CL) and f) PLGA. This class of poly(ester)s lacks side chain functionality.

Biologically-relevant poly(ester)s may be created by the ROP of the O-carboxyanhydrides of amino acids (OCA ROP) (Figure 1.16) [179]. Similar to NCA ROP, living polymerisations can be achieved using OCA ROP if this is performed under the optimal reaction conditions. Historically, metal catalysts, e.g., zinc [5] have been used, but there is a growing tendency for the use of the relatively safer option of organo-catalysis, such as 4-dimethylaminopyridine (DMAP) [180].

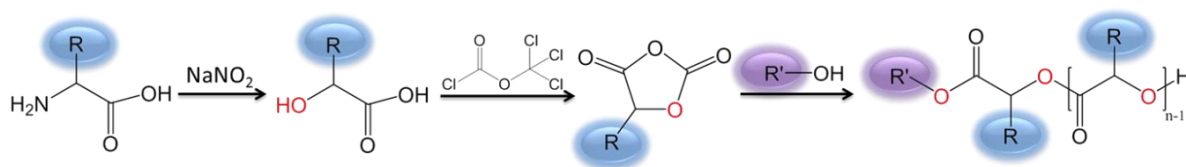


Figure 1.16. Schematic illustration of the route to the creation of poly(ester)s using OCA ROP.

A by-product of this reaction is gaseous carbon dioxide, which is easily eliminated from the poly(ester) product. Furthermore, this method benefits from the wide availability of side-chain functionalised amino acids which can be used to generate functionally-versatile and biocompatible poly(ester)s, that may be degraded hydrolytically and/or enzymatically. Utilising this method, poly(ester)s have been synthesised from the ROP of cyclic monomers of Glu [180], Ser [181] and Lys [179]. These materials possess excellent biocompatibility, rendering them promising candidates that could be used in drug delivery, in gene delivery and in tissue engineering [182, 183].

1.7. Research Aims and Thesis Outline

This research programme involved the use of controlled NCA ROPs and OCA ROPs to generate a range of novel poly(amino acid)-based materials and poly(ester)-based materials, respectively, that possessed bio-applicability. In addition, the combination of both techniques, which is a novel initiative, led to creation of poly(amino acid)-poly(ester) hybrid materials. The materials created were characterised, including by carrying out biological studies and payload release studies to demonstrate their suitability as biomaterials. Collaborative initiatives led to the acquisition of additional knowledge in research fields that are independent of NCA ROP and OCA ROP, including the synthesis of silver compounds for use in the development of poly(amino acid)-metal-based anticancer therapeutics.

The initial emphasis of the research, given in Chapter 3, was placed on the use of the Fuchs-Farthing method to create a library of α -amino acid NCA monomers, and the sarcosine *N*-NCA monomer, that are suitable for use in ROPs. Furthermore, selected α -amino acids were derivatised to their corresponding α -hydroxy acids. The α -hydroxy acids were subsequently cyclised to create OCA monomers that could be used in OCA ROPs. In Chapter 4 to Chapter 6, NCA ROPs were used for the creation of a range of poly(amino acid)-based materials. In Chapter 4, a model therapeutic molecule, dopamine, was used to initiate the sequential ROP of hydrophobic NCAs (of Phe and Ala) and the hydrophilic *N*-NCA of Sar. The resulting amphiphilic macromolecules self-assembled in aqueous media, to form monodisperse particles. The particles exhibited biocompatibility to mammalian cells and demonstrated the controlled release of the covalently encapsulated molecular cargo, upon peptide degradation by targeted protease enzymes. Chapter 5 details the creation of oligo(Ser) by NCA ROP and the subsequent post-polymerisation modification of the oligo(amino acid), yielding a graft copolymer that is able to gel large quantities of edible vegetable oil. The resultant organogel supported the growth of mammalian mouse dermal fibroblasts. The gel encapsulated a model molecular cargo and subsequently released it in a controlled and sustained manner, in response to incubation in an acidic environment. In Chapter 6, NCA ROP was initiated from a amine terminated PEG star macromolecule, to generate star-shaped, hybrid macromolecules. The polymers self-aggregated in aqueous medium, into particles. Post-polymerisation modification, by thiol-ene click crosslinking, yielded chemical hydrogels, which encapsulated

significant amounts of protein cargo, and subsequently released this payload upon glutathione-mediated reduction of the disulfide crosslinks.

In Chapter 7 and Chapter 8, OCA ROP and NCA ROP were combined to create dual stimuli-responsive hybrid poly(amino acid-ester) materials. In Chapter 7, a glucosamine molecule was used as the initiator, in the sequential NCA ROP and OCA ROP, to generate amphiphilic macromolecules that self-aggregated into monodisperse NPs. The glucose-presenting NPs were susceptible to enzymatic-induced polymer degradation and to pH-induced polymer degradation. The NPs selectively bound concanavalin A. In Chapter 8, the hydroxyl side groups of an oligo(Ser) were used as multiple initiating sites for the ROP of Phe OCA. The resultant graft copolymers self-aggregated in aqueous solution to form monodisperse NPs. The NPs were able to encapsulate the chemotherapeutic doxorubicin (dox) and then released it, in a controlled manner, in response to an acidic pH stimulus. In addition, the dox-loaded NPs particles exhibited anticancer potency against T47D human breast cancer cells.

Research evolution led to the generation of homopoly(ester) functional materials, in Chapter 9 and Chapter 10, from the ROP of OCAs. Chapter 9 details the creation of diblock, amphiphilic poly(ester)s, from the sequential ROP of Phe OCA and Lys(Cbz) OCA, and from the sequential ROP of Phe OCA and Glu(Bz) OCA. The resulting poly(ester)s self-aggregated in aqueous solution, into NPs which encapsulated dox and subsequently released it in a controlled manner, in response to acidic pH-induced poly(ester) degradation. OCA ROP was exploited further in Chapter 10, in the creation of a diblock poly(ester), by the sequential ROP of Lys(Cbz) OCA and Glu(Bz) OCA. The poly(ester) self-aggregated in aqueous medium, yielding monodisperse, spherical particles, which encapsulated dox and then selectively released it in response to acidic pH stimulus. The dox-loaded particles demonstrated significant anticancer potency against T47D and MCF-7 breast cancer cells. Poly(ester) deprotection furnished a zwitterionic polymer, that exhibited a pH-dependent reversible-assembly. Lastly, Chapter 11 details the proof-of-concept studies in the creation of poly(amino acid)-silver(I)-*N*-heterocyclic carbene anticancer therapeutics. Five silver-based compounds, which were synthesised as part of a collaborative-initiative, were encapsulated in poly(amino acid)s, using three strategies. The resulting polymer-metal complex compounds were characterised using DLS and SEM and were subsequently assessed for their anticancer potency against the pancreatic adenocarcinoma.

1.8. References

1. de la Rica, R. and Matsui, H. *Chem. Soc. Revs.*, **2010**, 39, 3499-3509.
2. Chow, D., Nunalee, M.L., Lim, D.W., Simnick, A.J. and Chilkoti, A. *ater. Sci. Eng. R-Rep.*, **2008**, 62, 125-155.
3. Habraken, G.J.M., Heise, A. and Thornton, P.D. *Macromol. Rapid Commun.*, **2012**, 33, 272-286.
4. Kricheldorf, H.R. *Angew. Chem. Int. Ed.*, **2006**, 45, 5752-5784.
5. Martin Vaca, B. and Bourissou, D. *ACS Macro Lett.* **2015**, 4, 792-798.
6. Merrifield, R.B. Solid-Phase Peptide Synthesis. In: Katsoyannis, P.G. ed. *The Chemistry of Polypeptides*. Springer US, **1973**, 335-361.
7. Lowik, D.W.P.M., Leunissen, E.H.P., van den Heuvel, M., Hansen, M.B. and van Hest, J.C.M. *Chem. Soc. Revs.*, **2010**, 39, 3394-3412.
8. Carlsen, A. and Lecommandoux, S. *Curr. Opin. Colloid Interface Sci.*, **2009**, 14, 329-339.
9. Rao, J., Luo, Z., Ge, Z., Liu, H. and Liu, S. *Biomacromolecules*. **2007**, 8, 3871-3878.
10. Cheng, J. and Deming, T. Synthesis of Polypeptides by Ring-Opening Polymerization of α -Amino Acid N-Carboxyanhydrides. In: Deming, T. ed. *Peptide-Based Materials*. Springer Berlin Heidelberg, **2012**, 1-26.
11. Wang, K., Luo, G.-F., Liu, Y., Li, C., Cheng, S.-X., Zhuo, R.-X. and Zhang, X.-Z. *Polym. Chem.*, **2012**, 3, 1084-1090.
12. Deming, T.J. *Nature*. **1997**, 390, 386-389.
13. Yu, S., Wu, G., Gu, X., Wang, J., Wang, Y., Gao, H. and Ma, J. *Colloids and Surfaces B: Biointerfaces*. **2013**, 103, 15-22.
14. Shen, Y., Fu, X., Fu, W. and Li, Z. *Chem. Soc. Revs.*, **2015**, 44, 612-622.
15. Altunbas, A. and Pochan, D. Peptide-Based and Polypeptide-Based Hydrogels for Drug Delivery and Tissue Engineering. In: Deming, T. ed. *Peptide-Based Materials*. Springer Berlin Heidelberg, **2012**, 135-167.
16. Huesmann, D., Klinker, K. and Barz, M. *Polym. Chem.*, **2017**, 8, 957-971.
17. Song, A., Rane, A.A. and Christman, K.L. *Acta Biomater.*, **2012**, 8, 41-50.
18. Borase, T. and Heise, A. *Advanced Materials*. **2016**, 28, 5725-5731.
19. Sulistio, A., Gurr, P.A., Blencowe, A. and Qiao, G.G. *Aust. J. Chem.*, **2012**, 65, 978-984.
20. Habraken, G.J., Wilsens, K.H., Koning, C.E. and Heise, A. *Polym. Chem.*, **2011**, 2, 1322-1330.
21. Lu, H., Wang, J., Song, Z., Yin, L., Zhang, Y., Tang, H., Tu, C., Lin, Y. and Cheng, J. *Chem. Commun.*, **2014**, 50, 139-155.
22. Huang, J. and Heise, A. *Chem. Soc. Revs.*, **2013**, 42, 7373-7390.
23. Deming, T.J. *J. Polym. Sci. A Polym. Chem.*, **2000**, 38, 3011-3018.
24. Kramer, J.R. and Deming, T.J. *Biomacromolecules*. **2010**, 11, 3668-3672.
25. Johnson, R.P., John, J.V. and Kim, I. *Eur. Poly. J.*, **2013**, 49, 2925-2948.
26. Hadjichristidis, N., Iatrou, H., Pitsikalis, M. and Sakellariou, G. *Chem. revs.*, **2009**, 109, 5528-5578.
27. Habraken, G.J.M., Wilsens, K.H.R.M., Koning, C.E. and Heise, A. *Polym. Chem.*, **2011**, 2, 1322-1330.
28. Dimitrov, I. and Schlaad, H. *Chem. Commun.*, **2003**, 2944-2945.
29. Vayaboury, W., Giani, O., Cottet, H., Deratani, A. and Schué, F. *Macromol. Rapid Commun.*, **2004**, 25, 1221-1224.
30. Lu, H. and Cheng, J. *J. Am. Chem. Soc.*, **2007**, 129, 14114-14115.
31. Kamigaito, M., Ando, T. and Sawamoto, M. *Chem. revs.*, **2001**, 101, 3689-3746.
32. Deming, T.J. *Adv. Mater.*, **1997**, 9, 299-311.
33. Asandei, A.D. and Moran, I.W. *J. Am. Chem. Soc.*, **2004**, 126, 15932-15933.
34. Pattabiraman, V.R. and Bode, J.W. *Nature*. **2011**, 480, 471-479.

35. Klok, H.-A. Polypeptide Synthesis, Ring-Opening Polymerization of α -Amino Acid N-Carboxyanhydrides. In: *Encyclopedia of Polymer Science and Technology*. John Wiley & Sons, Inc., **2002**.
36. Deming, T.J. *Macromolecules*. **1999**, 32, 4500-4502.
37. Peng, Y.-L., Lai, S.-L. and Lin, C.-C. *Macromolecules*. **2008**, 41, 3455-3459.
38. Hadjichristidis, N., Iatrou, H., Pispas, S. and Pitsikalis, M. *J. Polym. Sci. A Polym. Chem.*, **2000**, 38, 3211-3234.
39. Aliferis, T., Iatrou, H. and Hadjichristidis, N. *Biomacromolecules*. **2004**, 5, 1653-1656.
40. Karatzas, A., Iatrou, H., Hadjichristidis, N., Inoue, K., Sugiyama, K. and Hirao, A. *Biomacromolecules*. **2008**, 9, 2072-2080.
41. Robson Marsden, H. and Kros, A. *Macromol. Biosci.*, **2009**, 9, 939-951.
42. Odian, G. *Principles of polymerization*. John Wiley & Sons, **2004**.
43. Yang, W.-t., Xu, R.-w., Wu, G.-y., Wu, Y.-x. and Wang, L.-l. *hin. J. Polym. Sci.*, **2008**, 26, 381-391.
44. Cha, R.-t., Du, T., Li, J.-h. and Yuan, Z. *Polym. Int.*, **2006**, 55, 1057-1062.
45. Matyjaszewski, K. and Tsarevsky, N.V. *Nat Chem*. **2009**, 1, 276-288.
46. Matyjaszewski, K. *Science*. **2011**, 333, 1104-1105.
47. Zhao, W., Gnanou, Y. and Hadjichristidis, N. *Polym. Chem.*, **2016**, 7, 3487-3491.
48. Rinkenauer, A.C., Schubert, S., Traeger, A. and Schubert, U.S. *J. Mater. Chem. B.*, **2015**, 3, 7477-7493.
49. Deming, T. Polypeptide and Polypeptide Hybrid Copolymer Synthesis via NCA Polymerization. In: Klok, H.-A. and Schlaad, H. eds. *Peptide Hybrid Polymers*. Springer Berlin Heidelberg, **2006**, 1-18.
50. Wamsley, A., Jasti, B., Phiasivongsa, P. and Li, X. *J. Polym. Sci. A Polym. Chem.*, **2004**, 42, 317-325.
51. Hernández, J.R. and Klok, H.A. *J. Polym. Sci. A Polym. Chem.*, **2003**, 41, 1167-1187.
52. Gaspard, J., Silas, J.A., Shantz, D.F. and Jan, J.-S. *Supramol. Chem.*, **2010**, 22, 178-185.
53. Fan, J., Li, R., He, X., Seetho, K., Zhang, F., Zou, J. and Wooley, K.L. *Polym. Chem.*, **2014**, 5, 3977-3981.
54. Murphy, R., Borase, T., Payne, C., O'Dwyer, J., Cryan, S.A. and Heise, A. *RSC Adv.*, **2016**, 6, 23370-23376.
55. Wibowo, S.H., Sulistio, A., Wong, E.H.H., Blencowe, A. and Qiao, G.G. *Chem. Commun.*, **2014**, 50, 4971-4988.
56. Borase, T., Iacono, M., Ali, S.I., Thornton, P.D. and Heise, A. *Polym. Chem.*, **2012**, 3, 1267-1275.
57. Fong, B. and Russo, P.S. *Langmuir*. **1999**, 15, 4421-4426.
58. Niwa, M., Kuwagaki, Y., Yamaguchi, S. and Higashi, N. *Angew. Chem. Int. Ed.*, **2003**, 42, 1839-1841.
59. Higashi, N., Koga, T. and Niwa, M. *Langmuir*. **2000**, 16, 3482-3486.
60. Marcelo, G., Muñoz-Bonilla, A. and Fernández-García, M. *J. Phys. Chem. C.*, **2012**, 116, 24717-24725.
61. Marcelo, G., Muñoz-Bonilla, A., Rodríguez-Hernández, J. and Fernández-García, M. *Polym. Chem.*, **2013**, 4, 558-567.
62. Wibowo, S.H., Sulistio, A., Wong, E.H.H., Blencowe, A. and Qiao, G.G. *Aust. J. Chem.*, **2014**, 67, 598-602.
63. Liu, Z.-M., Xu, Z.-K., Wang, J.-Q., Yang, Q., Wu, J. and Seta, P. *Eur. Polym. J.*, **2003**, 39, 2291-2299.
64. Ito, Y., Ochiai, Y., Park, Y.S. and Imanishi, Y. *J. Am. Chem. Soc.*, **1997**, 119, 1619-1623.
65. Kricheldorf, H.R., v. Lossow, C., Schwarz, G. and Fritsch, D. *Macromol. Chem. Phys.*, **2005**, 206, 1165-1170.
66. Guo, L., Li, J., Brown, Z., Ghale, K. and Zhang, D. *Peptide Science*. **2011**, 96, 596-603.
67. Kricheldorf, H.R., v. Lossow, C. and Schwarz, G. *Macromol. Chem. Phys.*, **2005**, 206, 282-290.

68. Junnila, S., Houbenov, N., Hanski, S., Iatrou, H., Hirao, A., Hadjichristidis, N. and Ikkala, O. *Macromolecules*. **2010**, 43, 9071-9076.
69. Sánchez-Ferrer, A. and Mezzenga, R. *Macromolecules*. **2009**, 43, 1093-1100.
70. Blencowe, A., Tan, J.F., Goh, T.K. and Qiao, G.G. *Polymer*. **2009**, 50, 5-32.
71. Klok, H.-A., Hernández, J.R., Becker, S. and Müllen, K. *J. Polym. Sci. A Polym. Chem.*, **2001**, 39, 1572-1583.
72. Aoi, K., Tsutsumiuchi, K., Yamamoto, A. and Okada, M. *Tetrahedron*. **1997**, 53, 15415-15427.
73. Aoi, K., Hatanaka, T., Tsutsumiuchi, K., Okada, M. and Imae, T. *Macromol. Rapid Commun.*, **1999**, 20, 378-382.
74. Appelhans, D., Komber, H., Kirchner, R., Seidel, J., Huang, C.-F., Voigt, D., Kuckling, D., Chang, F.-C. and Voit, B. *Macromol. Rapid Commun.*, **2005**, 26, 586-591.
75. Sulistio, A., Widjaya, A., Blencowe, A., Zhang, X. and Qiao, G. *Chem. Commun.*, **2011**, 47, 1151-1153.
76. Audouin, F., Knoop, R.J.I., Huang, J. and Heise, A. *J. Polym. Sci. A Polym. Chem.*, **2010**, 48, 4602-4610.
77. Sulistio, A., Lowenthal, J., Blencowe, A., Bongiovanni, M.N., Ong, L., Gras, S.L., Zhang, X. and Qiao, G.G. *Biomacromolecules*. **2011**, 12, 3469-3477.
78. Li, Y., Shen, Y., Wang, S., Zhu, D., Du, B. and Jiang, J. *RSC Adv.*, **2015**, 5, 30380-30388.
79. Iatrou, H., Frielinghaus, H., Hanski, S., Ferderigos, N., Ruokolainen, J., Ikkala, O., Richter, D., Mays, J. and Hadjichristidis, N. *Biomacromolecules*. **2007**, 8, 2173-2181.
80. Wong, S., Shim, M.S. and Kwon, Y.J. *J. Mater. Chem. B.*, **2014**, 2, 595-615.
81. DeForest, C.A., Polizzotti, B.D. and Anseth, K.S. *Nat Mater*. **2009**, 8, 659-664.
82. Zhang, Y., Yin, Q., Lu, H., Xia, H., Lin, Y. and Cheng, J. *ACS Macro Lett.*, **2013**, 2, 809-813.
83. Qadir, M.A., Morton, S.W., Deng, Z.J., Shopsowitz, K.E., Murphy, R.P., Epps, T.H. and Hammond, P.T. *Mol. Pharm.*, **2014**, 11, 2420-2430.
84. Zhang, J., Chen, X.-F., Wei, H.-B. and Wan, X.-H. *Chem. Soc. Revs.*, **2013**, 42, 9127-9154.
85. Kopeček, J. and Yang, J. *Acta Biomater.*, **2009**, 5, 805-816.
86. Yang, B., Lv, Y., Zhu, J.-y., Han, Y.-t., Jia, H.-z., Chen, W.-h., Feng, J., Zhang, X.-z. and Zhuo, R.-x. *Acta Biomater.*, **2014**, 10, 3686-3695.
87. Li, Y., Wang, S., Zhu, D., Shen, Y., Du, B., Liu, X. and Zheng, Y. *RSC Adv.*, **2015**, 5, 20025-20034.
88. Wen, H., Dong, H., Liu, J., Shen, A., Li, Y. and Shi, D. *J. Mater. Chem. B.*, **2016**, 4, 7859-7869.
89. Cai, C., Lin, J., Lu, Y., Zhang, Q. and Wang, L. *Chem. Soc. Revs.*, **2016**, 45, 5985-6012.
90. Iijima, M., Ulkoski, D., Sakuma, S., Matsukuma, D., Nishiyama, N., Otsuka, H. and Scholz, C. *Polym. Int.*, **2016**, 65, 1132-1141.
91. Yin, Q., Tong, R., Xu, Y., Baek, K., Dobrucki, L.W., Fan, T.M. and Cheng, J. *Biomacromolecules*. **2013**, 14, 920-929.
92. Castillo-León, J.S.L.S.W.E. *Self-assembled peptide nanostructures : advances and applications in nanobiotechnology*. Singapore: Pan Stanford Pub., **2013**.
93. Fan, J., Zou, J., He, X., Zhang, F., Zhang, S., Raymond, J.E. and Wooley, K.L. *Chem. Sci.*, **2014**, 5, 141-150.
94. Dill, K.A. and Flory, P.J. *PNAS*. **1981**, 78, 676-680.
95. Li, M.-H. and Keller, P. *Soft Matter*. **2009**, 5, 927-937.
96. Blanazs, A., Armes, S.P. and Ryan, A.J. *Macromol. Rapid Commun.*, **2009**, 30, 267-277.
97. Panda, J.J. and Chauhan, V.S. *Polym. Chem.*, **2014**, 5, 4418-4436.
98. Chécot, F., Brûlet, A., Oberdisse, J., Gnanou, Y., Mondain-Monval, O. and Lecommandoux, S. *Langmuir*. **2005**, 21, 4308-4315.
99. Choe, U.-J., Sun, V., Tan, J.-K. and Kamei, D. Self-Assembled Polypeptide and Polypeptide Hybrid Vesicles: From Synthesis to Application. In: Deming, T. ed. *Peptide-Based Materials*. Springer Berlin Heidelberg, **2012**, 117-134.
100. Zhang, X., Yang, Y., Tian, J. and Zhao, H. *Chem. Commun.*, **2009**, 3807-3809.

101. Takae, S., Miyata, K., Oba, M., Ishii, T., Nishiyama, N., Itaka, K., Yamasaki, Y., Koyama, H. and Kataoka, K. *J. Am. Chem. Soc.*, **2008**, 130, 6001-6009.
102. Sun, J., Chen, X., Deng, C., Yu, H., Xie, Z. and Jing, X. *Langmuir*. **2007**, 23, 8308-8315.
103. Eric, P.H., Victor, Z.S., Daniel, T.K. and Timothy, J.D. *Nat. Mater.*, **2006**, 6, 52-57.
104. Sun, V.Z., Li, Z., Deming, T.J. and Kamei, D.T. *Biomacromolecules*. **2010**, 12, 10-13.
105. Chécot, F., Rodríguez-Hernández, J., Gnanou, Y. and Lecommandoux, S. *Biomol. Eng.*, **2007**, 24, 81-85.
106. Bellomo, E.G., Wyrsta, M.D., Pakstis, L., Pochan, D.J. and Deming, T.J. *Nat. Mater.* **2004**, 3, 244-248.
107. Kwon, G.S., Naito, M., Kataoka, K., Yokoyama, M., Sakurai, Y. and Okano, T. *Colloids Surf B Biointerfaces*. **1994**, 2, 429-434.
108. Kwon, G.S. and Kataoka, K. *Adv. Drug Deliv. Rev.*, **1995**, 16, 295-309.
109. Kwon, G., Naito, M., Yokoyama, M., Okano, T., Sakurai, Y. and Kataoka, K. *J. Control. Release*. **1997**, 48, 195-201.
110. Kataoka, K., Harada, A. and Nagasaki, Y. *Adv. Drug Deliv. Rev.*, **2001**, 47, 113-131.
111. He, C., Zhao, C., Chen, X., Guo, Z., Zhuang, X. and Jing, X. *Macromol. Rapid Commun.*, **2008**, 29, 490-497.
112. Cai, C., Zhang, L., Lin, J. and Wang, L. *J. Phys. Chem. B.*, **2008**, 112, 12666-12673.
113. Kopecek, J. *J. Polym. Sci. A Polym. Chem.*, **2009**, 47, 5929-5946.
114. Lowik, D.W.P.M. and van Hest, J.C.M. *Chem. Soc. Revs.*, **2004**, 33, 234-245.
115. Markland, P., Zhang, Y., Amidon, G.L. and Yang, V.C. *J. Biomed. Mater. Res.*, **1999**, 47, 595-602.
116. Corkhill, P.H., Hamilton, C.J. and Tighe, B.J. *Biomaterials*. **1989**, 10, 3-10.
117. Wang, C., Varshney, R.R. and Wang, D.-A. *Adv. Drug Deliv. Rev.*, **2010**, 62, 699-710.
118. Zelzer, M., Todd, S.J., Hirst, A.R., McDonald, T.O. and Ulijn, R.V. *Biomater. Sci.*, **2013**, 1, 11-39.
119. Chen, C., Wu, D., Fu, W. and Li, Z. *Biomacromolecules*. **2013**, 14, 2494-2498.
120. Chiang, P.-R., Lin, T.-Y., Tsai, H.-C., Chen, H.-L., Liu, S.-Y., Chen, F.-R., Hwang, Y.-S. and Chu, I.M. *Langmuir*. **2013**, 29, 15981-15991.
121. Lee, E.S., Kim, D., Youn, Y.S., Oh, K.T. and Bae, Y.H. *Angew. Chem. Int. Ed.*, **2008**, 47, 2418-2421.
122. Zhang, X., Chu, X., Wang, L., Wang, H., Liang, G., Zhang, J., Long, J. and Yang, Z. *Angew. Chem. Int. Ed.*, **2012**, 51, 4388-4392.
123. Nowak, A.P., Breedveld, V., Pakstis, L., Ozbas, B., Pine, D.J., Pochan, D. and Deming, T.J. *Nature*. **2002**, 417, 424-428.
124. Huang, J., Hastings, C.L., Duffy, G.P., Kelly, H.M., Raeburn, J., Adams, D.J. and Heise, A. *Biomacromolecules*. **2012**, 14, 200-206.
125. Park, M.H., Joo, M.K., Choi, B.G. and Jeong, B. *Acc. Chem. Res.*, **2011**, 45, 424-433.
126. Cheng, Y., He, C., Xiao, C., Ding, J., Zhuang, X., Huang, Y. and Chen, X. *Biomacromolecules*. **2012**, 13, 2053-2059.
127. Sajid, M. and McKerrow, J.H. *Mol. Biochem. Parasitol.*, **2002**, 120, 1-21.
128. Edwards, D.R. and Murphy, G. *Nature*. **1998**, 394, 527-528.
129. Basel, M.T., Shrestha, T.B., Troyer, D.L. and Bossmann, S.H. *ACS Nano*. **2011**, 5, 2162-2175.
130. Ulijn, R.V. *J. Mater. Chem.*, **2006**, 16, 2217-2225.
131. de la Rica, R., Aili, D. and Stevens, M.M. *Adv. Drug Deliv. Rev.*, **2012**, 64, 967-978.
132. Toledano, S., Williams, R.J., Jayawarna, V. and Ulijn, R.V. *Soc. Chem. Am. J.*, **2006**, 128, 1070-1071.
133. Aoi, K., Tsutsumiuchi, K. and Okada, M. *Macromolecules*. **1994**, 27, 875-877.
134. Krannig, K.-S., Sun, J. and Schlaad, H. *Biomacromolecules*. **2014**.
135. Moss, G.P. Nomenclature of glycoproteins, glycopeptides and peptidoglycans. *IUPAC-IUB Joint Commission on Biochemical Nomenclature (JCBN)*. [Online]. 1985, [Accessed 09.04.2017]. Available from: <http://www.chem.qmul.ac.uk/iupac/misc/glycp.html#4>.
136. Jacobs, J., Gathergood, N., Heuts, J.P.A. and Heise, A. *Polym. Chem.*, **2015**, 6, 4634-4640.
137. Krannig, K.-S. and Schlaad, H. *J. Am. Chem. Soc.*, **2012**, 134, 18542-18545.

138. Kramer, J.R. and Deming, T.J. *J. Am. Chem. Soc.*, **2010**, 132, 15068-15071.
139. Kramer, J.R. and Deming, T.J. *J. Am. Chem. Soc.*, **2012**, 134, 4112-4115.
140. Wang, J., Liu, C. and Chi, P. *J. Biomed. Mater. Res. B. Appl. Biomater.*, **2009**, 89B, 45-54.
141. Tian, Z., Wang, M., Zhang, A. and Feng, Z. *Front Mater Sci China*. **2007**, 1, 162-167.
142. Rüde, E., Westphal, O., Hurwitz, E., Fuchs, S. and Sela, M. *Immunochemistry*. **1966**, 3, 137-151.
143. Rüde, E. and Meyer-Delius, M. *Carbohydr. Res.*, **1968**, 8, 219-232.
144. Ben, R.N., Eniade, A.A. and Hauer, L. *Org. Lett.*, **1999**, 1, 1759-1762.
145. Tian, Z., Wang, M., Zhang, A.-y. and Feng, Z.-g. *Polymer*. **2008**, 49, 446-454.
146. Tang, H. and Zhang, D. *Biomacromolecules*. **2010**, 11, 1585-1592.
147. Cameron, C.B. and Bishop, C.D. *Proceedings of the Royal Society B: Biological Sciences*. **2012**, 279, 3041-3048.
148. Dmitrovic, V., Habraken, G.J., Hendrix, M.M., Habraken, W.J., Heise, A. and Sommerdijk, N.A. *Polymers*. **2012**, 4, 1195-1210.
149. Meldrum, F.C. *Int. Mater. Rev.*, **2003**, 48, 187-224.
150. Xu, A.-W., Ma, Y. and Cölfen, H. *J. Mater. Chem.*, **2007**, 17, 415-449.
151. Mochida, Y., Cabral, H., Miura, Y., Albertini, F., Fukushima, S., Osada, K., Nishiyama, N. and Kataoka, K. *ACS Nano*. **2014**, 8, 6724-6738.
152. Barrett, A.J., Woessner, J.F. and Rawlings, N.D. *Handbook of proteolytic enzymes*. Elsevier, **2012**.
153. Renukuntla, J., Vadlapudi, A.D., Patel, A., Boddu, S.H.S. and Mitra, A.K. *Int. J. Pharm.*, **2013**, 447, 75-93.
154. Harris, J.M. and Chess, R.B. *Nat. Rev. Drug Discov.*, **2003**, 2, 214-221.
155. Fischer, D., Li, Y., Ahlemeyer, B., Kriegelstein, J. and Kissel, T. *Biomaterials*. **2003**, 24, 1121-1131.
156. Larson, N. and Ghandehari, H. *Chem. Mater.*, **2012**, 24, 840-853.
157. Knop, K., Hoogenboom, R., Fischer, D. and Schubert, U.S. *Angew. Chem. Int. Ed.*, **2010**, 49, 6288-6308.
158. Birke, A., Huesmann, D., Kelsch, A., Weillbacher, M., Xie, J., Bros, M., Bopp, T., Becker, C., Landfester, K. and Barz, M. *Biomacromolecules*. **2014**, 15, 548-557.
159. Fetsch, C., Grossmann, A., Holz, L., Nawroth, J.F. and Luxenhofer, R. *Macromolecules*. **2011**, 44, 6746-6758.
160. Kwon, Y.-U. and Kodadek, T. *J. Am. Chem. Soc.*, **2007**, 129, 1508-1509.
161. Culf, A.S. and Ouellette, R.J. *Molecules*. **2010**, 15, p.5282.
162. Schneider, M., Fetsch, C., Amin, I., Jordan, R. and Luxenhofer, R. *Langmuir*. **2013**, 29, 6983-6988.
163. Amass, W., Amass, A. and Tighe, B. *Polym. Int.*, **1998**, 47, 89-144.
164. Ikada, Y. and Tsuji, H. *Macromol. Rapid Commun.*, **2000**, 21, 117-132.
165. Williams, C.K. *Chem. Soc. Revs.*, **2007**, 36, 1573-1580.
166. Langer, R. and Chasin, M. *Informa Health Care*. **1990**.
167. Huijser, S., HosseiniNejad, E., Sablong, R., de Jong, C., Koning, C.E. and Duchateau, R. *Macromolecules*. **2011**, 44, 1132-1139.
168. Klee, J.E., Schneider, C., Hölter, D., Burgath, A., Frey, H. and Mülhaupt, R. *Polymer. Adv. Tech.*, **2001**, 12, 346-354.
169. Wilbon, P.A., Chu, F. and Tang, C. *Macromol. Rapid Commun.*, **2013**, 34, 8-37.
170. Van Zee, N.J. and Coates, G.W. *Chem. Commun.*, **2014**, 50, 6322-6325.
171. Hillmyer, M.A. and Tolman, W.B. *Acc. Chem. Res.*, **2014**, 47, 2390-2396.
172. Labet, M. and Thielemans, W. *Chem. Soc. Revs.*, **2009**, 38, 3484-3504.
173. Platel, R.H., Hodgson, L.M. and Williams, C.K. *Polym. Rev.*, **2008**, 48, 11-63.
174. Uhrich, K.E., Cannizzaro, S.M., Langer, R.S. and Shakesheff, K.M. *Chem. Rev.*, **1999**, 99, 3181-3198.
175. Jeske, R.C., Rowley, J.M. and Coates, G.W. *Angew. Chem. Int. Ed.*, **2008**, 47, 6041-6044.
176. Bernard, A., Chatterjee, C. and Chisholm, M.H. *Polymer*. **2013**, 54, 2639-2646.

177. Nejad, E.H., Paoniasari, A., van Melis, C.G.W., Koning, C.E. and Duchateau, R. *Macromolecules*. **2013**, 46, 631-637.
178. Hosseini Nejad, E., van Melis, C.G.W., Vermeer, T.J., Koning, C.E. and Duchateau, R. *Macromolecules*. **2012**, 45, 1770-1776.
179. Chen, X., Lai, H., Xiao, C., Tian, H., Chen, X., Tao, Y. and Wang, X. *Polym. Chem.*, **2014**, 5, 6495-6502.
180. Thillaye du Boullay, O., Bonduelle, C., Martin-Vaca, B. and Bourissou, D. *Chem. Commun.*, **2008**, 1786-1788.
181. Lu, Y., Yin, L., Zhang, Y., Zhang, Z., Xu, Y., Tong, R. and Cheng, J. *ACS Macro Lett.*, **2012**, 1, 441-444.
182. Yin, Q., Yin, L., Wang, H. and Cheng, J. *Acc. Chem. Res.*, **2015**, 48, 1777-1787.
183. Lu, Y., Yin, L., Zhang, Y., Zhonghai, Z., Xu, Y., Tong, R. and Cheng, J. *ACS Macro Lett.*, **2012**, 1, 441-444.

Chapter 2. Instrumentations, General Methods and Materials

2.1. Nuclear Magnetic Resonance (NMR) Spectroscopy

^1H and ^{13}C NMR spectra were recorded on Bruker Avance 500 spectrometers. Chemical shifts (in ppm) were referenced to a trimethylsilane (TMS) standard whose chemical shift is 0 ppm. To avoid contamination and possible damage to the NMR probe, Norell® heavy-walled (1.4 mm thick) NMR tubes were used for ^1H NMR studies carried out in deuterated trifluoroacetic acid (TFA-d). Other NMR studies in common solvents, were carried out using standard 500 MHz Norell® NMR tubes. NMR spectra were analysed using MestreNova® Research Lab software. The following abbreviations are used in the ^1H NMR analyses: s = singlet, d = doublet, t = triplet, q = quartet, m = multiplet, dd = doublet of doublet, J = coupling constants (given in Hertz).

2.2. Fourier Transform Infrared (FTIR) Spectroscopy

Samples were dried *in vacuo* for 24 hours prior to infrared spectroscopic analysis. Spectra were then recorded on a Bruker ALPHA-P FTIR spectrometer, equipped with Bruker OPUS 7.0 software and a diamond attenuated total reflectance (ATR) accessory, accumulating 32 scans.

2.3. Melting Point Determination

Melting point determinations of previously purified compounds were assessed using a Griffin Edulab 12/04/082 melting point apparatus. Analyses were carried out in capillary tubes (1 mm diameter, 10 cm long). Thus, a small amount of the sample under consideration was placed in a thin-walled capillary tube (1 mm diameter) that had one of its ends heat-sealed.

2.4. Centrifugation, Sample-Drying and Lyophilisation

Samples were centrifuged using a Mistral 3000i MSE centrifuge unit, maintained at $-5\text{ }^\circ\text{C}$ (0 - 6000 rpm). Compounds were dried in a Fistreem vacuum oven that was equipped with a variable temperature control unit ($0\text{ }^\circ\text{C}$ - $200\text{ }^\circ\text{C}$) and a pressure gauge (0 mbar - 1020 mbar). A Thermoelectron Heto Powerdry LL1500 freeze-dryer, equipped with an Edwards two stage vacuum pump was used for lyophilisation of samples. Samples were lyophilised in distilled water in 50 mL poly(styrene) falcon tubes.

2.5. pH Measurements

Acidity values and basicity values were measured using a Thermo Scientific UY-58800-04 pH/mV/temperature meter. Sodium hydroxide standard solutions and hydrochloric acid standard solutions were used to adjust the pH of the buffered solutions to the required basic pH value or acidic pH value.

2.6. Mass Spectrometry (MS)

Positive electron impact (EI+) analyses of compounds were performed using a Thermo Scientific Ultimate 3000 electrospray ionisation mass spectrometer. Peptide-based samples were analysed in DMSO while low molecular weight compounds were analysed in suitable solvents that included DCM, methanol, THF and acetonitrile.

2.7. High Performance Liquid Chromatography (HPLC)

An Agilent Infinity 1260 HPLC instrument, equipped with an Ascentis C18 column and a UV detector, was used for all HPLC studies (Chapter 4.2.8).

2.8. Circular Dichroism (CD) Spectrometry

The Chirascan v.4.4.0 CD spectrometer was used to provide CD spectral information in the far UV region.

2.9. Differential Scanning Colorimetry (DSC) and Thermogravimetry (TGA)

Samples were weighed accurately using the Sartorius 4503 micro-balance. Differential scanning colorimetry analyses were then carried out using a DSC Q20 instrument, acquired from TA Instruments. The instrument was calibrated with indium. Aluminium pans were used to contain the samples that were heated at rates varying between 5 °C and 10 °C/ per minute, under an inert nitrogen atmosphere (40 mL/min). The sample purge was maintained at 10 mL per minute. Thermogravimetry studies were carried out using a TGA Auto Q20 instrument (TA Instruments). Samples were analysed in platinum pans using a controlled heating rate, either at 5 °C per minute or at 10 °C per minute.

2.10. Ultraviolet-Visible (UV-Vis) Spectrophotometry

Absorbance readings (190 - 750 nm) were performed on a dual beam Varian Cary 50 UV0902M112 UV-Vis spectrophotometer (Agilent Technologies), equipped with a xenon pulse lamp and Varian Cary WinUV 3.0 software. Samples were analysed in UV micro quartz cuvettes (10 mm, 700 μ L and 1700 μ L, black-walled). 'Simple-reads' at fixed wavelengths were carried out using a Jenway 6305 spectrophotometer (Cole-Parmer Ltd). All of the readings were taken in triplicate.

2.11. Fluorescence Microscopy

Fluorescence images were acquired using an Axio observer Z1 microscope (Zeiss Instruments), equipped with an AxioCam IC camera and an LD A-plan 5x0.15 Ph1 objective lens. Typically, samples were mounted onto and sandwiched between two microscope glass plates. Fluorescence imaging was then carried out at the relevant excitation wavelength and emission wavelength using an exposure time of 445 ms. The images obtained were edited using relevant software, such as Microsoft Office Picture Manager 2010.

2.12. Preparation of Phosphate Buffered Saline (PBS) Solutions

One Dulbecco 'A' PBS tablet was dissolved in ultrapure water (100 mL, 18.2 m Ω) under vigorous stirring. The solution obtained was sterilised by autoclaving at 115 °C for 10 minutes and then cooling down to ambient temperature. The buffer was sterilised further by passing through a 0.2 μ m Millipore PTFE filter.

2.13. Preparation of Sodium Acetate Buffers

Typically, 1 litre of a pH 5.0 sodium acetate buffer was prepared by homogenously mixing a 0.1M acetic acid glacial solution (357 mL) with a 0.1M sodium acetate tri-hydrate solution (643 mL). Typically, 400 mL of a pH 5.4 acetate buffer was prepared by homogenously mixing a 0.1M acetic acid glacial solution (58 mL) with a 0.1M sodium acetate tri-hydrate solution (342 mL). The buffers were pH-adjusted accordingly using either a standardised HCl solution or a standardised NaOH solution. The buffers were filter-sterilised by passing them through a 0.2 μ m Millipore PTFE filter.

2.14. Preparation of Nanoparticles (Nanoprecipitation)

The creation of particles by the self-aggregation of poly(amino acid)s in an aqueous medium was made possible by nanoprecipitation, using the dropping-in (co-solvent) method (Figure 2.1) [1-3]. A stock solution of the macromolecule was prepared in the relevant organic solvent (e.g. DMF, THF or acetone). A micropipette was then used to add a predetermined volume of macromolecule solution dropwise into an excess of the aqueous medium (PBS buffer), under vigorous stirring. The obtained suspension was then dialysed against PBS buffer for 48 hours. The nanoparticles were then either used in their aqueous suspension after dialysis or lyophilised for further use after reconstitution in the relevant aqueous buffer solutions.

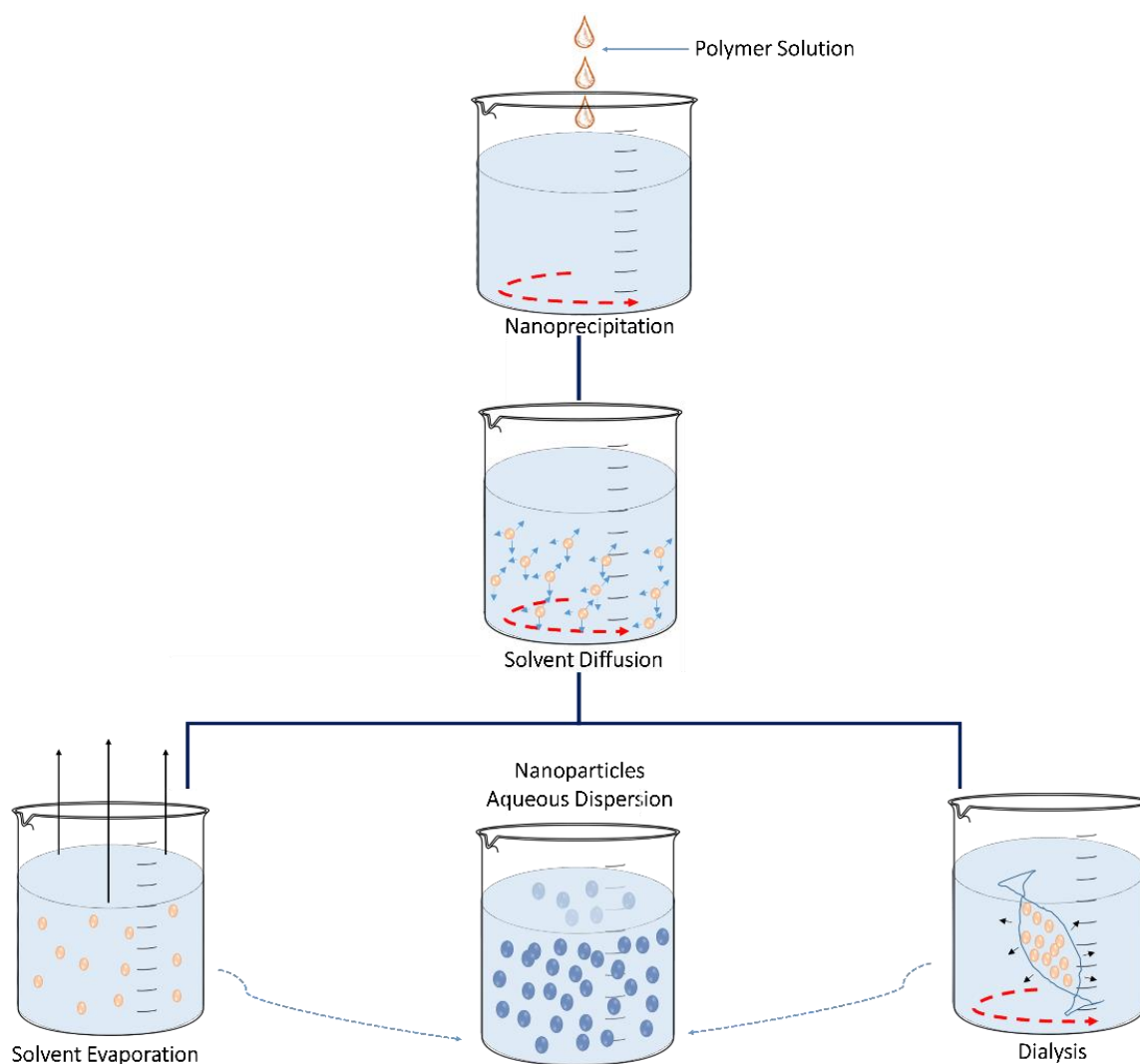


Figure 2.1. Illustration of the route to the generation of (nano)particles from poly(amino acid)-based macromolecules in solution, using the 'dropping-in' method. *Adapted from* [1, 2].

2.15. Dynamic Light Scattering (DLS) and Zeta Potential Studies

DLS analyses were performed on a Malvern Zetasizer Nano ZSP series instrument that was equipped with a 4 mW He-Ne laser, operating at a wavelength of 633 nm, and an avalanche photodiode (APD) detector. The non-invasive back-scatter-optic arrangement was used to collect the light scattered, at an angle of 173 °C. Samples were equilibrated for 2 minutes and then analysed at 37 °C in disposable 12 mm poly(styrene) cuvettes. Data were processed by the cumulative analysis of the experimental correlation function. Then the diameter of the particles was computed from the diffusion coefficients, using the Stokes-Einstein's equation. Measurements were carried out in triplicate. The instrument was furnished with DTS software (Windows 10). Zeta potential studies were carried out on a Malvern Zetasizer Nano ZSP instrument, at pH 7.4, 37 °C. No background electrolyte was added. A viscosity of 0.891 mPa.s, a dielectric constant equal to 78.6 and Henry function equal to 1.5 were used in the zeta potential computations.

2.16. Determination of Critical Aggregation Concentration (CAC)

The CACs of various macromolecules were determined by following an established DLS method [4-6]. The Malvern Zetasizer Nano ZSP series instrument was used for the light scattering measurements. The instrument was equipped with a 4 mW He-Ne laser, operated at a wavelength of 633 nm. The non-invasive back scatter optic arrangement was used to collect the light that was scattered by the particles, at an angle of 173°C. Stock solutions were prepared by dissolving the polymer in a relevant organic solvent, preferably a volatile solvent, e.g., acetone. Nanoprecipitation was carried out by independently dropping varying volumes of the stock solution into vigorously stirred nanopure water to yield a series of dispersions that contained the required polymer concentrations. The aqueous dispersions were subsequently analysed using DLS by monitoring the change in the intensity of the scattered light (in kilo counts per second (kcps)) in response to the loading of the polymer in the dispersion. The CAC of the polymer was then obtained, from the plot of kcps values versus the logarithms of polymer loadings (concentration), as the anti-logarithmic value of the inflexion point.

2.17. Sample Preparation, Sputter-Coating and Scanning Electron Microscopy (SEM)

With regard to solution-state samples (e.g., nanoparticles), a micropipette was used to extract approximately 20 μL of the sample from the parent suspension. The extracted sample was placed onto an SEM glass cover slip and air-dried in an extractor fume-hood, at ambient temperature. The cover slip was then mounted on an SEM stub using conductive tape. Solid samples, e.g., xerogels, were mounted directly onto SEM stubs using conductive prior to sputter-coating.

In order to enhance the surface conductivity, avoiding sample charging up, avoiding thermal damage and improving the electron signal, the samples that were intended for analyses using SEM were sputter-coated with a coherent film of gold for 3 minutes using a rotary-pumped Quorum Q150RS sputter-coater, powered by 20 mA current. The sample size and morphology were then determined using a JEOL JSM-6610LV microscope from Oxford Instruments, equipped with a field emission electron gun as an electron source. The accelerating voltage was varied between 5 - 15 kV and the working distance was varied between 10 mm and 17 mm.

2.18. Transmission Electron Microscopy (TEM)

All of the samples were contained in clean glass vials. Then, a glass pipette was used to deposit a drop of the nanoparticle sample onto a carbon-coated copper grid. The samples were left to stand in an extractor hood so that the solvent could be expelled prior to analyses. TEM measurements were performed on a Titan Themis G2300KV instrument from FEI Instruments, operated at an accelerating voltage of 80 kV. No staining was applied.

2.19. Mammalian Cell Culturing and Passaging

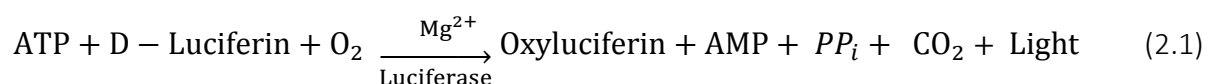
A generic procedure is given for all the mammalian cells that were cultured during the research program. Cells (e.g., C3H mouse dermal fibroblasts) were plated in 75 cm^2 Nunclon Δ^{TM} plastic cell culture flasks (T75) in 20 mL of Dulbecco's Modified Eagle Medium (DMEM), supplemented with 10 % (v/v) foetal bovine serum (FBS), L-glutamine (1 mM) and penicillin (100 U/mL)-streptomycin (100 $\mu\text{g}/\text{mL}$) solution. The flasks were then incubated in a humidified incubator

at 37 °C and 5 % (v/v) CO₂ in air. The culture medium was changed every 2 days. Upon reaching a 90 % confluence, the cells were passaged using a trypsin/EDTA solution (2 mL) for 5 minutes at 37 °C. An equal volume of culture medium was added to neutralise the trypsin, followed by washing under centrifugation, at 240 g for 10 minutes. Cells that were required for subsequent studies were counted on a Marienfeld-Superior Neubauer-improved haemocytometer using an Olympus CK40 light microscope. Excess cells were cryopreserved in a cryogenic-medium (DMEM supplemented with 20 % (v/v) FBS, L-glutamine (1mM) and penicillin (100 U/mL)-streptomycin (100 µg/mL) solution). The cells were then frozen in an isopropanol bath at a rate of 1 °C/minute in a freezer (-80 °C), and subsequently stored in liquid nitrogen.

Analogous procedures were used for the culturing and passing of pancreatic adenocarcinoma cells (Panc. 10.05), human retinal pigment epithelium cells (ARPE-19), T47D human breast cancer cells and MCF-7 human breast cancer cells.

2.20. ATPlite-M® Assay

ATP is present in all metabolically active cells. Thus, the production of ATP can be used as a marker of cell viability and proliferation, whereby an increase in cellular ATP content over time is indicative of cell proliferation. The ATPlite-M® assay is based on chemiluminescence and affords a facile route to quantitatively measuring the cellular ATP content. It utilises the reaction of ATP with the substrate D-luciferin in the presence of atmospheric oxygen to produce oxyluciferin, adenosine monophosphate, carbon dioxide, inorganic pyrophosphate and light. The intensity of the light produced from this reaction is directly proportional to the cellular ATP content and can be detected easily using a luminescence counter (Equation 2.1) [7].



The viability of previously seeded cells was assessed at predetermined time intervals. Generally, 100 µL of culture medium was pipetted from the respective wells and replaced with mammalian cell lysis solution (50 µL). The microplate was agitated at room temperature (700 rpm, 5 minutes) on an orbital microplate shaker. The lysed contents of the wells were then

transferred to a white 96-well ViewPlate microplate and a reconstituted substrate solution (50 μ L) was added. The microplate was sealed to prevent contamination, shielded from light by wrapping in an aluminium foil and agitated (700 rpm, 5 minutes) at room temperature. Bubbles formed during agitation were removed quickly by flaming and the microplate was re-sealed and dark-adapted inside the plate reader for 10 minutes. Luminescence counting was then carried out on a Hidex Chameleon plate reader, equipped with Mikrowin 2000 software from Mikrotek Laborsysteme GmbH.

2.21. Advanced Polymer Chromatography (APC)

Advanced Polymer Chromatography (APC) analyses (DMF eluent, 1 g/L LiBr) were carried out using an ACQUITY APC AQ (200 \AA , 2.5 μ m) column packed with bridged poly(ethylene) hybrid particles, on a Waters ACQUITY APC system, equipped with an ACQUITY refractive index (ACQ-RI) detector. The column temperature was maintained at 40 $^{\circ}$ C and the flow rate was 0.5 mL/minute. System calibration was carried out using poly(methyl methacrylate) standards and data were processed using Empower 3 software to provide polydispersity indices (PDI)s.

2.22. The Korsmeyer-Peppas (KP) model

The mechanism of the release of payload that is encapsulated in spherical delivery vehicles can be evaluated by fitting the experimental data to the Korsmeyer-Peppas (KP) model (Equation 2.2) [8, 9]. Using this model, the release exponent (n) can be determined by statistical analysis. For $n \leq 0.45$, the release of the encapsulated cargo follows Fickian diffusion, in which polymer relaxation dominates the rate of diffusion of the encapsulated cargo. Deviation from Fickian diffusion is indicated by values greater than 0.45, whereby the rates of diffusion of the encapsulated cargo and polymer relaxation are comparable. That is, for $0.45 < n < 0.89$ the release can be considered to be non-Fickian (anomalous), possibly because of a variety of factors, including the surface erosion or the bulk erosion of the delivery vehicle.

$$\frac{M_t}{M_{\infty}} = kt^n \quad (2.2)$$

Here, M_t and M_{∞} represent the cumulative amounts of payload that are released at time t and at infinite time, respectively. Hence, M_t/M_{∞} is the fractional payload release at time t , n is the

release exponent being indicative of the release mechanism and k is the rate constant that takes into account the geometric characteristics of the organogel and the encapsulated cargo. Using Equation 2.3, which is generated by the differentiation of Equation 2.2, a linear plot can be obtained, whose gradient is the release exponent (n), and may be used to determine whether or not the payload release follows a Fickian profile, or a non-Fickian diffusion profile.

$$\mathbf{Log (Release \%)} = \mathbf{Log \left[\frac{M_t}{M_\infty} \right]} = \mathbf{n Log t + Log k} \quad (2.3)$$

2.23. Drug Encapsulation Efficiency and Drug Loading Content

The drug encapsulation efficiency (EE) of nanoparticles and the drug loading content (LC) in the nanoparticles were determined using Equation 2.4 and Equation 2.5, respectively [10];

$$\mathbf{Encapsulation Efficiency (\%)} = \frac{\mathbf{W_o - W_n}}{\mathbf{W_o}} * \mathbf{100} \quad (2.4)$$

$$\mathbf{Drug Loading Content (\%)} = \frac{\mathbf{W_o - W_n}}{\mathbf{W_{np}}} * \mathbf{100} \quad (2.5)$$

Here, W_o is the total weight of the drug that was fed during nanoprecipitation, W_n is the net weight of drug that was not encapsulated by the nanoparticles, W_{np} is the weight of the drug-loaded nanoparticles.

2.24. Materials Inventory

All of the chemicals (Table 2.1 and Table 2.2) were used as received from the suppliers, except where it would be stated otherwise. In order to minimise exposure to either air or airborne contaminants, a Schlenk line was used to isolate air-sensitive reactions. The reactions were carried out under an inert nitrogen atmosphere. Nitrogen was dried over P_2O_5 and silica xerogels.

Table 2.1. Chemicals that were used during the research program.

Chemical	Supplier	Chemical	Supplier
L-Alanine ($\geq 99.8\%$)	Sigma Aldrich	Silica Gel	Sigma Aldrich
L-Phenylalanine ($\geq 99.8\%$)	Sigma Aldrich	Anhydrous THF ($\geq 99.9\%$)	Sigma Aldrich
N_ϵ -Cbz-L-Lysine ($\geq 99.8\%$)	Sigma Aldrich	2-Methyl-1-Propanol ($\geq 99.5\%$)	Sigma Aldrich
O-Benzyl-L-Serine ($\geq 99.8\%$)	Sigma Aldrich	4-Dimethylaminopyridine ($\geq 99\%$)	Sigma Aldrich
S-Tertbutylmercapto-L-Cysteine ($\geq 98\%$)	Sigma Aldrich	Diethyl Ether ($\geq 99\%$),	Sigma Aldrich
L-Aspartic Acid β -Benzyl Ester ($\geq 99\%$)	Sigma Aldrich	Pd/C (10 wt. %)	Sigma Aldrich
Sarcosine ($\geq 98\%$)	Alfa Aesar	Sodium Acetate trihydrate ($\geq 99\%$)	Sigma Aldrich
Triphosgene ($\geq 98\%$),	Alfa Aesar	Doxorubicin. HCl ($\geq 95\%$)	Fluorochem
Sodium Nitrite ($\geq 99.0\%$)	Sigma Aldrich	Thermolysin from <i>Bacillus thermoproteolyticus rokko</i> (~ 40 U/mg)	Sigma Aldrich
γ -Benzyl-L-Glutamic Acid ($\geq 99\%$)	Alfa Aesar	α -Chymotrypsin from bovine pancreas (≥ 40 U/mg protein)	Sigma Aldrich
Diphosgene ($\geq 98\%$)	Alfa Aesar	elastase from bovine pancreas (≥ 40 U/mg)	Sigma Aldrich
L-Valine ($\geq 99.8\%$)	Alfa Aesar	Anhydrous DMF (99.8%)	Sigma Aldrich

Table 2.2. Chemicals that were used during the research program (continued).

Chemical	Supplier	Chemical	Supplier
Lipase from <i>Candida antarctica</i> ≥ 1.0 U/mg	Sigma Aldrich	1,3,4,6-tetra- <i>o</i> -acetyl-2-amino-deoxy- β -D-glucopyranose ($\geq 98\%$)	Sigma Aldrich
Rhodamine B (98%)	Alfa Aesar	HBr/Acetic Acid (33 wt. %)	Sigma Aldrich
Concanavalin A from <i>Canavalia ensiformis</i>	Sigma Aldrich	Ricinus Communis (castor bean) Agglutinin RCA ₁₂₀	Sigma Aldrich
Dulbecco's Modified Eagle Medium	Sigma Aldrich	Dimethyl Sulfoxide (DMSO) for Cell Culturing ($\geq 99.7\%$)	Sigma Aldrich
L-glutamine (200 mM)	Sigma Aldrich	Trypsin-EDTA (0.25%)	Sigma Aldrich
Acetic Acid Glacial ($\geq 99.9\%$)	Sigma Aldrich	1,4 Dithiothreitol (DTT) ($\geq 97\%$)	Sigma Aldrich
Methanol (99.8%)	Sigma Aldrich	Albumin–Fluorescein Isothiocyanate Conjugate	Sigma Aldrich
Sulphuric Acid (99.99%)	Sigma Aldrich	L-glutathione ($\geq 99.8\%$)	Sigma Aldrich
Dulbecco 'A' PBS tablets	Thermo Fisher Scientific	HPLC-Grade Water (18.2 M Ω .cm).	VWR Int.
n-Hexane ($\geq 98\%$)	Sigma Aldrich	PEG Star Polymer (10,000 Da)	Sigma Aldrich
Anhydrous DCM (≥ 99.8)	Sigma Aldrich	Cobalt Phthalocyanine ($\geq 97\%$)	Sigma Aldrich
α -Pinene ($\geq 98\%$)	Thermo Fisher Scientific	Penicillin-Streptomycin	Sigma Aldrich
Anhydrous Ethyl Acetate ($\geq 99.8\%$)	Sigma Aldrich	Dopamine.HCl ($\geq 99\%$)	Alfa Aesar

2.25. References

1. Schubert, S., Delaney, J.J.T. and Schubert, U.S. *Soft Matter*. 2011, 7, 1581-1588.
2. Nicolas, J., Mura, S., Brambilla, D., Mackiewicz, N. and Couvreur, P. *Chem. Soc. Revs.*, 2013, 42, 1147-1235.
3. Mahapatro, A. and Singh, D.K. *J Nanobiotechnology*. 2011, 9, p.55.
4. Dorshow, R.B., Bunton, C.A. and Nicoli, D.F. *J. Phys. Chem. A.*, 1983, 87, 1409-1416.
5. Topel, Ö., Çakır, B.A., Budama, L. and Hoda, N. *J. Mol. Liq.*, 2013, 177, 40-43.
6. *Surfactant micelle characterization using dynamic light scattering.* <http://quimica.udea.edu.co/~coloides/Anexo1.pdf>. [Online database, Accessed: 09.04.2017].
7. Guardigli, M., Lundin, A. and Roda, A. Chapter 5 "Classical" Applications of Chemiluminescence and Bioluminescence. In: *Chemiluminescence and Bioluminescence: Past, Present and Future*. The Royal Society of Chemistry, 2011, 141-190.
8. Korsmeyer, R.W., Gurny, R., Doelker, E., Buri, P. and Peppas, N.A. *Int. J. Pharm.*, 1983, 15, 25-35.
9. Yang, Y.Q., Guo, X.D., Lin, W.J., Zhang, L.J., Zhang, C.Y. and Qian, Y. *Soft Matter*. 2012, 8, 454-464.
10. Kamba, S., Ismail, M., Hussein-Al-Ali, S., Ibrahim, T. and Zakaria, Z. *Molecules*. 2013, 18, p.10580.

Chapter 3. Cyclic Monomers Created from α -Amino Acids

The NCAs of α -amino acids and OCAs of α -amino acid derivatives (Figure 3.1) can be used as monomers in the creation of poly(amino acid)s by controlled ROPs. For this reason, the syntheses and characterisations of these materials have been important components of this research work. NCAs and OCAs are highly reactive monomers that present electrophilic reactivity at the 5-carbonyl group of the α -carbon.

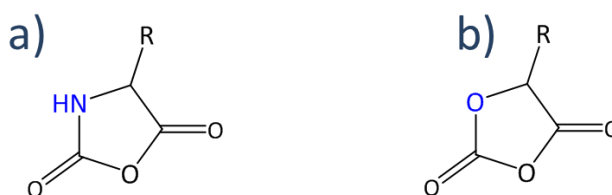


Figure 3.1. Generic illustration of a) NCA monomers and b) OCA monomers, which are applied in controlled ROPs to create poly(amino acid) and poly(ester) materials, respectively (R represents the various monomer side groups).

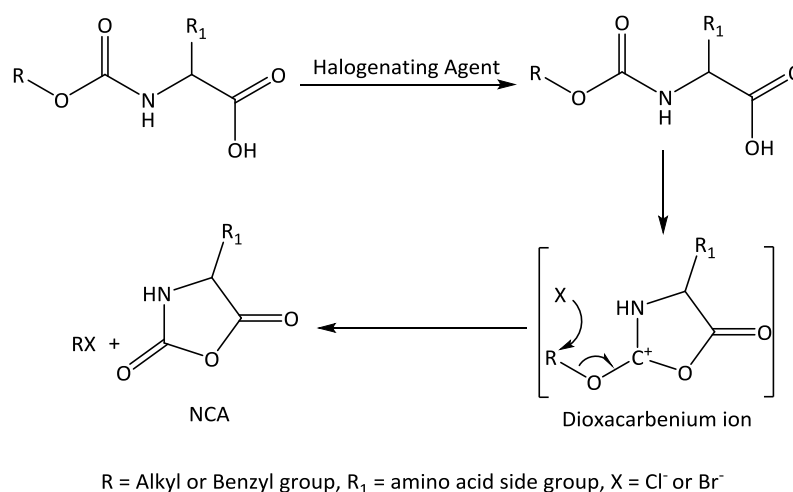
Optimised methods for the efficient generation of NCA monomers from α -amino acids have been developed [1, 2]. Methods have also been reported for the syntheses of OCA monomers which are derived from hydroxyacids of α -amino acids [3-5]. However, much research still needs to be conducted if one is to optimise and scale up the procedures for the syntheses of OCA monomers. This Chapter details the creation of NCA monomers from α -amino acids and OCA monomers from hydroxyacids which in turn are derived from α -amino acids.

3.1. Creation of α -Amino Acid NCA Monomers

α -Amino acid NCAs are important precursors for poly(amino acid)s. The feasibility of NCAs being polymerised to form smart poly(amino acid)s in a 'simple' manner by ROP has heightened the amount of research interest that has taken place in this field [6-8]. Leuchs' accidental discovery of the NCAs sparked research into synthesis of poly(amino acid)-based materials from α -amino acids. There are two documented methods for the synthesis of NCAs, based on Leuchs' initial findings from more than a century ago [9-11].

3.1.1. Leuchs' Anhydrides

Leuchs' attempts at distilling *N*-ethoxycarbonyl amino acid chlorides and *N*-methoxycarbonyl amino acid chlorides resulted in the accidental discovery of NCA monomers. When heated, instead of distillation, these compounds cyclised into NCAs that were in combination with alkyl chloride by-products. Subsequently, Leuchs' method (Scheme 3.1) involved reacting an *N*-alkyloxycarbonyl protected amino acid or an *N*-benzyloxycarbonyl protected α -amino acid with an acid halide. The ensuing cyclisation yielded the required NCA and an alkoxy halide or a benzyloxy halide, depending on the amino acid-protecting group [7, 12]. Commonly used acid halide-generating agents include thionyl chloride (which was originally used by Leuchs), phosphorus pentachloride, phosphorus trichloride and dichloromethyl methyl ether [7]. However, the reduced NCA yields arising from the much more demanding purification processes and the high cyclisation temperatures that are characteristic of Leuchs' method, limit its popularity [2].



Scheme 3.1. Leuchs' method for the synthesis of NCA synthesis.

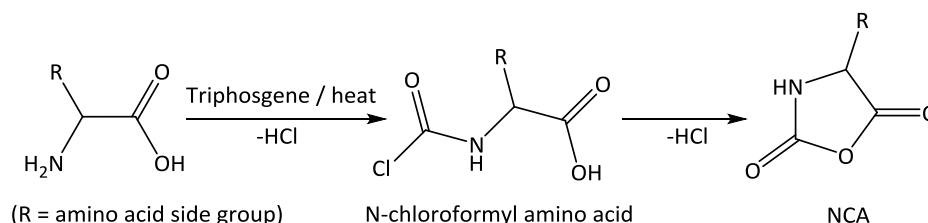
In subsequent reports it has been claimed that, on the contrary, NCAs can be obtained more readily below room temperature, from *n*-benzyloxycarbonyl amino acid halides, by using acid bromides for cyclisation [13]. Phosphorus tribromide is one of the more preferred generating agents. The basis of this argument is that the bromide ion is a better leaving group, and thus a better nucleophile that is needed for the cyclisation step. The ease of cyclisation into an NCA

is also complimented by the nature of the amino acid's substituent group. As such, the rate of cyclisation follows the sequence: methyl- < ethyl- < allyl- < benzyloxycarbonyl- [7, 13].

3.1.2. The Fuchs-Farthing Method

The Fuchs-Farthing method is a widely used pathway for the syntheses of NCA monomers because of the relatively favourable synthesis conditions that result in greater yields. Fuchs and Farthing's technique involved the direct phosgenation of free α -amino acids (i.e., α -*N*-unprotected amino acids) in anhydrous solvents. The solvents used should preferably possess a low boiling point to enable synthesis to take place under reflux. Some of the commonly used solvents include tetrahydrofuran, dioxane, ethyl acetate, toluene and chlorinated hydrocarbons that are inert to the phosgenating agent.

Upon phosgenation, *N*-chloroformyl amino acid intermediates are formed in a reaction step that involves the loss of an HCl molecule. The subsequent loss of a second HCl molecule completes the amino acid cyclisation into an NCA (Scheme 3.2).



Scheme 3.2. The Fuchs-Farthing method for NCA synthesis.

The gaseous nature of phosgene makes it a difficult reagent to handle, presenting a health risk. Moreover, it is hard to control accurately the quantity to be bubbled through the reagents. Thus, the crystalline trimer (triphosgene) is preferred because it is a solid at room temperature. NCA synthesis is usually performed under reflux to break down the trimers into individual, reactive phosgene molecules [13-15]. Diphosgene [16] and di-*tert*-butyltricarboxylate [17] have also been used as alternatives to phosgene.

Evidently, NCA syntheses by the Fuchs-Farthing method results in the generation of a considerable amount of the hydrochloric acid by-product. This presents challenges during NCA purification and in subsequent polymerisation processes. Therefore, several modifications,

aimed at improving the method, have been attempted. One of these includes using a mixture of solvents to counteract the high solubility of the hydrochloric acid. Reducing the solubility of the HCl also has the profound effect of suppressing the unwanted cleavage of the NCA ring due to attack by the HCl. This also reduces the quantity of amino acid hydrochloride impurities that are produced when the NCA ring is cleaved, thus improving purity and yields. Another attempt at improving the procedure is the incorporation of an HCl-scavenger in the reaction mixture, such as α -pinene [18].

The inherent generation of HCl in the direct phosgenation method has led to research in alternative ways of synthesising NCAs. Kricheldorf [7], Wilder and Mobashery [15], Johnstone *et al.* [19] have reported possible alternative NCA synthesis methods, some of which are minor variations of the Fuchs-Farthing method. Nevertheless, the Fuchs-Farthing's method remains the most preferred route to the generation of NCA monomers in greater yields.

3.1.3. Purification of NCA Monomers

The purity of NCAs is a limiting factor in NCA ROP because some of the electrophilic impurities are potential catalysts for side reactions during polypeptide synthesis. Some electrophilic impurities are potential chain transfer agents. Triphosgene [20], diphosgene [16] and di-*tert*-butyltricarboxylate [17] require an extra processing step to be removed. Furthermore, there is need to eliminate the by-products of NCA synthesis, such as HCl, the HCl-amino acid salts, 2-isocyanatoacyl chlorides and the *N*-chloroformyl amino acids [21-23]. NCAs produced by Leuchs' method may contain HBr, HCl, alkyl halides, and other undesirable by-products of the reaction involving halogenating agents [1, 12, 21].

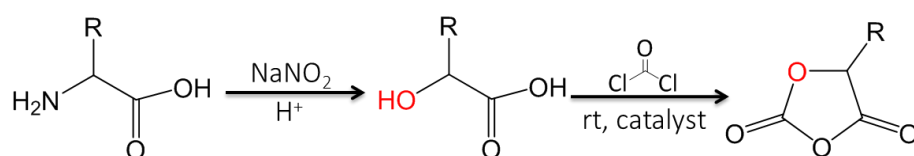
Repeated crystallisation under anhydrous conditions is the most applied purification method. The purity obtained with this method is satisfactory but recrystallisation itself is always a time consuming process. Furthermore, some highly functional and low melting NCAs are difficult to crystallise [1]. Purification by sublimation has also been reported, but it remains unpopular because there is a risk of the NCAs undergoing thermal polymerisation [24, 25]. Other measures aimed at obtaining pure NCAs include the incorporation of α -pinene or limonene during NCA synthesis, to scavenge for the HCl that is always hard to remove by recrystallisation. Re-phosgenation can also be carried out to eliminate residual HCl [22].

Kramer *et al.* [12] reported successfully purifying NCAs using silica gel flash chromatography, under anhydrous conditions. The level of purity achieved was highly satisfactory, the NCAs needing no further purification. Also, highly functional NCAs and low melting NCAs, which are usually difficult to crystallise, could be purified successfully using flash chromatography [1, 12].

3.2. Creation of α -Amino Acid OCA Monomers

The creation of poly(ester)s from the ROP of OCAs is a relatively new approach. As such, reactions for the synthesis of most OCA monomers are not yet fully optimised. However, as already discussed (Section 1), OCA monomers offer several advantages over conventional monomers, such as the ability to create poly(ester)s under mild conditions, that possess a wide array of side-chain functionalities because of the broad availability of functional α -amino acids [5]. The syntheses of Phe OCA [26], Glu(Bz) OCA [27], Ser(OBz) OCA [28] and Lys(Cbz) OCA [29], have previously been attempted.

The synthesis of OCAs (Scheme 3.3) incorporates a preliminary step that involves the conversion of α -amino acids to their corresponding α -hydroxyacids [30-32]. The α -amino acids are diazotised using sodium nitrite to generate the amino acid α -hydroxyacid. Formation of the required OCAs is then completed by carbonylating the α -hydroxyacids with cyclisation agents, such as phosgene, diphosgene or triphosgene [4, 33, 34].



Scheme 3.3. Generic illustration of the creation of α -amino acid OCAs by the diazotisation into α -hydroxyacids and subsequent cyclisation in the presence of a phosgenating agent (R represents amino acid side group).

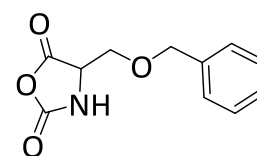
Synthesis of OCAs is usually carried out at ambient temperature. As such, the choice of phosgenating agent is an important factor in achieving relatively good yields within reasonable times. For example, the phosgenating agent has to be able to break down under the prevailing ambient conditions to furnish the phosgene molecules that drive the reaction to completion. For this reason the use of triphosgene, which is a solid at room temperature, is not popular because the reaction is time-consuming. The obvious replacement choice would be phosgene,

but its gaseous nature, coupled with its acute toxicity, present serious health and safety concerns. Therefore, the dimer diphosgene, which is in a liquid state at room temperature, is used to carbonylate the α -hydroxyacids. However, the downsides of OCA syntheses, which include the extended time of reactions (at least 18 hours), plus unsatisfactory yields, dictate that multiple repeat syntheses are required to build up adequate monomer quantities. Catalysis is usually employed to avert these shortcomings. Some of the catalysts that have been reported include the use of activated charcoal under basic conditions [29] and poly(styrene)-supported ammonium salts [27].

3.3. Experimental Details

3.3.1. Synthesis of *O*-benzyl-L-serine (Ser(OBz)) NCA

Ser(OBz) (5.0 g, 25.6 mmol) was weighed into a pre-dried three-neck round bottom flask that was evacuated and nitrogen purged three times prior to being used. Anhydrous ethyl acetate (60 mL) and α -Pinene were added (6.98 g, 51.2 mmol) and the resultant suspension was stirred under nitrogen whilst being heated to reflux. Triphosgene (9.0 g, 30.7 mmol) was dissolved in anhydrous ethyl acetate (20 mL) and the solution added dropwise *via* a dropping funnel into the refluxing reaction, for over 30 minutes. The reaction was allowed to reflux for 5 hours, after which time the initial suspension had turned into a solution. The volume was then reduced to a third of its initial volume using rotary evaporation. The concentrated solution was added dropwise to ice-cold hexane (200 mL) and subsequently stored at -16 °C for 12 hours to allow the NCA to precipitate fully out of solution. The crude NCA was isolated by filtration under vacuum and then purified by repeated recrystallisation from ethyl acetate: n-hexane (1:6 v/v), yielding the pure NCA as cream platelet crystals. The NCA was subsequently stored in the refrigerator (-16 °C) and shielded from moisture.



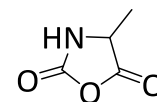
Yield: 4.98 g, 22.5 mmol, 88% (Off-white solids).

^1H NMR (500 MHz, DMSO, δ , ppm): 9.12 (s, 1H, NH), 7.39 - 7.29 (m, 5H, ArH, J = 50 Hz), 4.68 - 4.67 (t, 1H, αCH , J = 5 Hz), 4.58 - 4.52 (q, 2H, CH_2 , J = 30 Hz), 3.79 - 3.63 (m, 2H, CH_2 , J = 80 Hz). ^{13}C -NMR (125 MHz, CDCl_3 , δ , ppm): 58.1 (CH), 66.4 (CH_2CH), 72.7 (CH_2Ar), 126.9 (Ar), 128.1 (Ar), 128.5 (Ar), 135.9 (Ar), 152.6 (C(O)ONH), 169.9 (OC(O)CH). ESI MS (244 m/z , $\text{M} + \text{Na}^+$).

Melting Point: 99.5 °C. FTIR: $\nu_{\text{max}}/\text{cm}^{-1}$ (solid): 3273 cm^{-1} (NH), 2937 cm^{-1} (C-H, Ar), 1825 cm^{-1} (C=O), 1425 cm^{-1} (C=C, Ar), 1259 cm^{-1} (O-C=O). Elemental Analysis: *Theoretical*: Carbon 59.7%; Hydrogen 5.0%; Nitrogen 6.3%; *Found*: Carbon 59.8%; Hydrogen 5.1%; Nitrogen 6.6%

3.3.2. Synthesis of L-Alanine (Ala) NCA

The NCA of Ala was synthesised in anhydrous ethyl acetate by following a procedure that is similar to the one described for the synthesis of Ser(OBz) NCA.

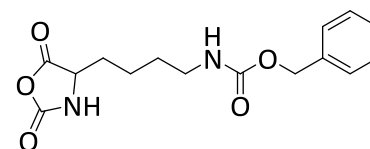


Yield: 2.28 g, 19.8 mmol, 31.9% (Off-white solids).

$^1\text{H-NMR}$ (500 MHz, DMSO- d_6 , δ , ppm): 8.97 (s, 1H, NH), 4.49 - 4.45 (q, 1H, αCH , $J = 20$ Hz), 1.33 - 1.32 (d, 3H, CH_3 , $J = 5$ Hz). $^{13}\text{C NMR}$ (125 MHz, DMSO- d_6 , δ , ppm): 175.4 ($\text{CHC}(\text{O})\text{O}$), 154.5 (CHNHCOO), 51.4 (αCH), 15.1 (CH_3). Melting Point: 90.5 °C. FTIR: $\nu_{\text{max}}/\text{cm}^{-1}$ (solid): 3280 cm^{-1} (NH), 1832 cm^{-1} (C=O, Anhydride), 2905 (CH, Alkyl). Elemental Analysis: *Theoretical*: Carbon 41.75%; Hydrogen 4.38%; Nitrogen 12.17%. *Found*: Carbon 41.72%; Hydrogen 4.39%; Nitrogen 12.20%.

3.3.3. Synthesis of N ϵ -Carbobenzyloxy-L-Lysine (Lys(Cbz)) NCA

The NCA of Lys(Cbz) was synthesised in anhydrous ethyl acetate, following a procedure that is similar to the one described for the synthesis of Ser(OBz) NCA.



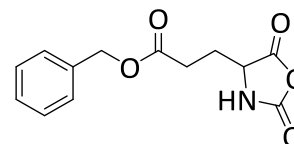
Yield: 4.83 g, 15.8 mmol, 88.1% (White crystals).

$^1\text{H-NMR}$ (500 MHz, DMSO, δ , ppm): 9.09 (s, 1H, NH), 7.39 - 7.26 (m, 5H, Ph, $J = 65$ Hz), 7.25 (s, 1H, COONH), 5.06 (s, 2H, Ar- CH_2), 4.45 - 4.43 (t, 1H, CH , $J = 10$ Hz), 3.02 - 2.98 (q, 2H, CH_2 , $J = 20$ Hz), 1.78 - 1.63 (m, 2H, CH_2 , $J = 75$ Hz), 1.46 - 1.26 (m, 4H, CH_2CH_2 , $J = 100$ Hz). $^{13}\text{C NMR}$ (125 MHz, DMSO- d_6 , δ , ppm): 172.4 ($\text{CHC}(\text{O})\text{O}$), 157.8 (CH_2NHCOO), 154.1 (CHNHCOO), 137.0, (Ar), 128.5 - 128.07 (Ar), 67.6 (CH_2Ar), 54.4 (αCH), 41.5 (NHCH_2), 29.8 (NHCH_2CH_2), 29.3 (CHCH_2), 24.2 (CHCH_2CH_2). Melting Point: 100 °C. ESI-MS: Calculated for $\text{C}_{15}\text{H}_{18}\text{N}_2\text{NaO}_5$ [M^+Na] $^+$ Calc: 329.111; Found: 329.111. FTIR: $\nu_{\text{max}}/\text{cm}^{-1}$ (solid): 3341 (NH), 2929 (CH), 1856, 1800 (CO anhydride), 1774 (benzyl ester), 1683 (aromatic C=C), 917 (aromatic C-H). Elemental Analysis:

Theoretical: Carbon 58.82%; Hydrogen 5.92%; Nitrogen 9.15%. *Found:* Carbon 58.79%; Hydrogen 5.91%; Nitrogen 9.17%.

3.3.4. Synthesis of γ -Benzyl-L-Glutamate (Glu(Bz)) NCA

The NCA of Glu(Bz) was synthesised in anhydrous ethyl acetate, following a procedure that is similar to the one described for the synthesis of Ser(OBz) NCA.

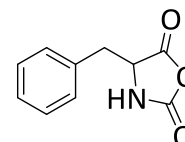


Yield: 4.89 g, 18.5 mmol, 88% (White crystals).

$^1\text{H-NMR}$ (500 MHz, CDCl_3 , δ , ppm): 7.33 - 7.27 (m, 5H, Ph, $J = 30$ Hz), 6.26 (s, 1H, NH), 5.10 - 5.05 (t, 2H, Ar- CH_2 , $J = 25$ Hz), 4.31 - 4.29 (t, 1H, αCH , $J = 10$ Hz), 2.54 - 2.48 (m, 2H, CH_2 , $J = 30$ Hz), 2.24 - 2.03 (m, 2H, CH_2 , $J = 105$ Hz). $^{13}\text{C NMR}$ (125 MHz, CDCl_3 , δ , ppm): 173.0 (CH_2COO), 172.4 (CHC(O)O), 154.6 (CHNHCOO), 137.1 (Ar), 128.3 (Ar), 128.1 (Ar), 66.3 (Ar- CH_2), 53.2, (αCH), 30.8 (CO(O)CH_2), 23.88 (CHCH_2). Melting Point: 93 °C. FTIR: $\nu_{\text{max}}/\text{cm}^{-1}$ (solid): 3247 (NH), 2932 (CH), 1860, 1778 (CO anhydride), 1702 (benzyl ester), 1400 (C=C aromatic), 740 - 930 (CH 'oop' bands). Elemental Analysis: *Theoretical:* Carbon 59.31%, Hydrogen 4.98%, Nitrogen 5.32%, *Found:* Carbon 59.28%, Hydrogen 4.97%, Nitrogen, 5.34%.

3.3.5. Synthesis of L-Phenylalanine (Phe) NCA

The NCA of Phe was synthesised in anhydrous THF, following a procedure that is similar to the one described for the synthesis of Ser(OBz) NCA.

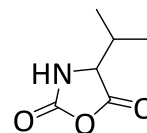


Yield: 4.33 g, 22.7 mmol, 74.9% (White crystals).

$^1\text{H NMR}$ (500 MHz, DMSO-d_6 , δ , ppm): 9.08 (s, 1H, NH), 7.33 - 7.17 (m, 5H, Ar, $J = 80$ Hz), 4.79 - 4.77 (t, 1H, αCH , $J = 10$ Hz), 3.03 - 3.02 (d, 2H, CH_2 , $J = 5$ Hz). $^{13}\text{C NMR}$ (125 MHz, DMSO-d_6 , δ , ppm): 172.9 (CHC(O)O), 154.7 (CHNHCOO), 137.6 (Ar), 129.4 (Ar), 129.1 (Ar), 127.2 (Ar), 56.66 (αCH), 38.32 (Ar- CH_2). FTIR: $\nu_{\text{max}}/\text{cm}^{-1}$ (solid): 3247 (NH, amide), 2922 (CH, alkyl), 1860, 1778 (CO, anhydride), 859 (C-H, Ar). Elemental Analysis: *Found:* Carbon 62.80%, Nitrogen 7.35%, Hydrogen 4.77%; *Theoretical:* Carbon 62.82, Nitrogen 7.33, Hydrogen, 4.75.

3.3.6. Synthesis of L-Valine (Val) NCA

The NCA of Val was synthesised in anhydrous THF, following a procedure that is similar to the one described for the synthesis of Ser(OBz) NCA.

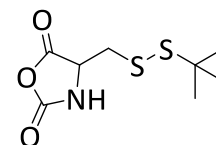


Yield: 4.96 g, 34.7 mmol, 73% (Cream crystals).

^1H NMR (500 MHz, DMSO, δ , ppm): 9.06 (s, 1H, NH), 4.34 - 4.33 (s, 1H, αCH), 2.08 - 2.02 (m, 1H, $\text{CH}(\text{CH}_3)_2$), 0.95 - 0.85 (q, 6H, $(\text{CH}_3)_2$). (^{13}C NMR (125 MHz, DMSO- d_6 , δ , ppm): 171.6 ($\text{CH}_2(\text{O})\text{O}$), 155.1 (CHNHCOO), 59.6 (αCH), 29.2 ($\text{CH}(\text{CH}_3)_2$), 19.4 (CH_3). Melting Point: 75 °C. FTIR: $\nu_{\text{max}}/\text{cm}^{-1}$ (solid): 3257 (NH, amide), 2942 (CH, alkyl), 1865, 1775 (CO, anhydride). Elemental Analysis: *Theoretical*: Carbon 50.35%; Hydrogen 6.34%; Nitrogen 9.79%. *Found*: Carbon 50.31%; Hydrogen 6.36%; Nitrogen 9.82%.

3.3.7. Synthesis of S-tertButylmercapto-L-Cysteine (STM-Cys) NCA

The NCA of STM-Cys was synthesised in anhydrous tetrahydrofuran, following a procedure that is similar to the one described for the synthesis of Ser(OBz) NCA.

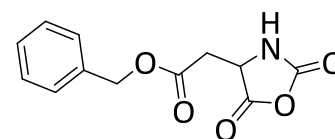


Yield: 3.57 g, 15.17 mmol, 64%. (White powder).

^1H NMR (500 MHz, CDCl_3 , δ , ppm): 6.37 (s, 1H, NH), 4.63 (dd, $J = 9.20, 2.9$ Hz, 1H, αCH), 2.99 (ddd, $J = 23.3, 14.0, 6.2$ Hz, 2H), 1.30 (s, 9H, *tert*-Butyl). FTIR: $\nu_{\text{max}}/\text{cm}^{-1}$ (solid): 3232 (NH secondary amine), 2959 (CH, alkyl), 1845 and 1805 (asymmetric anhydride C=O). (^{13}C NMR (125 MHz, CDCl_3 , δ , ppm): 168.18 ($\text{C}(\text{O})\text{OCH}$), 151.23 ($\text{NH}\text{C}(\text{O})\text{O}$), 57.24 (CH), 49.20 ($\text{C}(\text{CH}_3)_3$), 40.70 (CH_2S), 29.87 (CH_3). Melting Point: 106.3 °C. Elemental Analysis: *Theoretical*: Carbon 40.83%; Hydrogen 5.57%; Nitrogen 5.95%, Sulphur 27.25%. *Found*: Carbon 40.86%; Hydrogen 5.63%; Nitrogen 5.97%, Sulphur 27.32%.

3.3.8. Synthesis of L-Aspartic acid β -benzyl ester (Asp(Bz)) NCA

The NCA of Asp(Bz) was synthesised in anhydrous ethyl acetate, following a procedure that is similar to the one described for the synthesis of Ser(OBz) NCA.

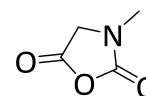


Yield: 4.98 g, 20 mmol, 89.3% (White crystals).

$^1\text{H-NMR}$ (500 MHz, DMSO- d_6 , δ , ppm): 8.99 (s, 1H, NH), 7.37 (m, 5H, ArH), 5.15 (s, 2H, CH_2O), 4.70 - 4.72 (t, 1H, αCH), 2.89 - 3.08 (m, 2H, CH_2). $^{13}\text{C NMR}$ (125 MHz, DMSO- d_6 , δ , ppm): 173.2 ($\text{CHC}(\text{O})\text{O}$), 171.1 ($\text{CH}_2\text{C}\text{OO}$), 154.6 ($\text{CHNH}\text{C}\text{OO}$), 137.1 (Ar), 128.3 (Ar), 128.1 (Ar), 66.1 (Ar- CH_2O), 52.8 (αCH), 33.8 (αCHCH_2). Melting Point: 119 °C. FTIR: $\nu_{\text{max}}/\text{cm}^{-1}$ (solid): 3250 (NH, secondary amine), 2963 (C-H, alkyl), 1885 and 1755 (C=O, anhydride and ester), 789 (C-H, aromatic). Elemental Analysis: *Theoretical*: Carbon 57.83%; Hydrogen 4.45%; Nitrogen 5.62%. *Found*: Carbon 57.83%; Hydrogen 4.46%; Nitrogen 5.68%.

3.3.9. Synthesis of Sarcosine (Sar) N-NCA

The cyclic monomer that is obtained from Sar is usually termed an N-NCA, rather than an NCA. This is because, unlike the conventional α -amino acids, Sar is N-substituted. The procedure for N-NCA synthesis differs marginally from that of NCAs. A detailed procedure, adapted from a previously reported protocol [35], is given.



Briefly, sarcosine (10 g, 112.2 mmol) was loaded into a three-neck round bottom flask and it was dried for 8 hours, under a stream of nitrogen flow that had been passed over silica and P_2O_5 . Then, α -pinene (29.9 g, 220 mmol) and anhydrous THF (150 mL) were added. The resultant suspension was heated to reflux. Triphosgene (16.6 g, 56 mmol) was dissolved in anhydrous THF (20 mL). The solution was added dropwise to the refluxing reaction medium. The reaction medium was refluxed for 5 hours, at which point the reaction medium had turned into a clear brown solution. The solution was concentrated under vacuum, yielding a brown solid residue which contained a clear brown oil. This mixture was heated to 75 °C and then dried under a high vacuum, until a solid residue was obtained. The crude solid was sublimed using a 'cold finger' apparatus. The sublimed compound was collected from the cooled surface and dissolved in anhydrous THF (30 mL) and filtered. The filtrate was added dropwise to cold n-hexane (150 mL). The resultant precipitate was allowed to stand in n-hexane (-18 °C), for 24 hours. The solvent was subsequently removed under vacuum. The residue was recrystallised twice, in anhydrous THF/n-hexane solution (1:5, v/v), yielding the pure N-NCA.

Yield: 8.83 g, 76.7 mmol, 68.4 % (Off-white crystals).

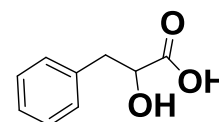
$^1\text{H NMR}$ (500 MHz, DMSO, δ , ppm): 4.23 (s, 2H, COCH_2), 2.87 (s, NCH_3). $^{13}\text{C NMR}$ (125 MHz, DMSO, δ , ppm): 167.3 ($\text{CH}_2\text{C}\text{O}_2$), 152.6 ($\text{N}\text{C}\text{O}_2$), 51.1 (CH_2), 29.8 (CH_3). FTIR: $\nu_{\text{max}}/\text{cm}^{-1}$ (solid):

3245 (N, Tertiary amine), 2898 (C-H alkyl), 1872, 1778 (CO anhydride). Elemental Analysis; *Theoretical*: Carbon 41.75%, Nitrogen 12.17%, Hydrogen 4.38%; *Found*: Carbon 41.70%, Nitrogen 12.21%, Hydrogen 4.41%.

3.3.10. Synthesis of Phe OCA

3.3.10.1. Synthesis of 2-Hydroxy-3-Phenyl Propanoic Acid

Phe (5 g, 30.3 mmol, 1 eqv) was dissolved in 1M sulphuric acid/acetone (100 mL; 1/1, v/v). The solution was cooled to 0 °C in an ice bath. Sodium nitrite (6.27 g, 90.9 mmol, 3 eqv) was dissolved in deionised water (10 mL) and the solution was added dropwise to the reaction medium, over a period of 30 minutes. The reaction was maintained at 0 °C for 2 hours, then it was stirred at room temperature, for 18 hours. Deionised water (500 mL) was added to the reaction medium. The reaction medium was then extracted three times, with ethyl acetate (300 mL). The combined organic layers were washed three times, using deionised water (500 mL). The layers were then washed twice using saturated brine (500 mL), and then were dried over magnesium sulphate. The drying agent was removed by filtration under vacuum. The product was subsequently isolated from ethyl acetate, by rotary evaporation.

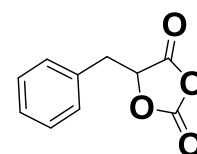


Yield: 4.60 g, 27.6 mmol, 91.2% (Yellow crystalline needles).

^1H NMR (500 MHz, $(\text{CD}_3)_2\text{CO}$, δ , ppm): 7.21 - 7.05 (m, 5H, Ph, $J = 7.13$ Hz), 4.27 - 4.25 (dd, 1H, αCH , $J = 4.26$ Hz), 3.01 - 2.97 (dd, 1H, Ph- CH , $J = 2.99$ Hz) 2.81 - 2.76 (dd, 1H, Ph- CH , $J = 2.78$ Hz). ESI-MS (189.1, $\text{M} + \text{Na}^+$).

3.3.10.2. Cyclisation into Phe OCA

Activated charcoal (0.34, 16.3 mmol, 1 eqv) was added to a solution of diphosgene (10.28 g, 32.6 mmol, 2 eqv) and 2-hydroxy-3-phenyl propanoic acid (4.6 g, 16.3 mmol, 1 eqv) in anhydrous THF (50 mL), in round bottom flask. The reaction medium was stirred at room temperature, under nitrogen flow, for 18 hours. Activated charcoal was removed by filtering the reaction medium through a pad of celite. The crude filtrate was then reduced to one-third of its initial volume using rotary evaporation. The solution was added dropwise to cold anhydrous THF/pentane



(1/9, v/v), to crystallise the OCA. The OCA product was collected, washed several times with cold pentane and then dried under vacuum.

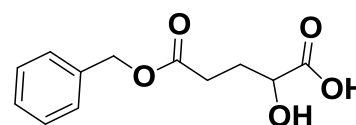
Yield: 3.51 g, 55% (Off-white crystals).

^1H NMR (500 MHz, Methanol- d_4 , δ , ppm): 7.20 - 7.08 (m, 5H, Ph), 4.27 - 4.25 (ddd, 1H, αCH , $J = 4.24$ Hz), 2.97 - 2.79 (m, 2H, Ph- CH_2). ^{13}C NMR (125 MHz, Methanol- d_4 , δ , ppm): 172.40 ($\text{C}=\text{O}$), 154.20 ($\text{C}=\text{O}$), 136.69 (Ar), 130.60 (Ar), 129.11 (Ar), 127.55 (Ar), 79.14 (αCH), 37.16 (Ar- CH_2). FTIR: $\nu_{\text{max}}/\text{cm}^{-1}$ (solid): 3040 cm^{-1} (C-H, Ar), 2899 cm^{-1} (C-H), 1850 cm^{-1} (C=O), 1460 cm^{-1} (O-C=O). ESI-MS (206.1, M + NH). Elemental Analysis; *Theoretical*: Carbon 62.50%, Hydrogen 4.20%; *Found*: Carbon 62.52%, Hydrogen 4.21%.

3.3.11. Synthesis of Glu(Bz) OCA

3.3.11.1. Synthesis of γ -Benzyl-2-Hydroxyglutaric Acid

Glu(Bz) (5 g, 21.1 mmol) was dissolved in a solution of 1M sulphuric acid and acetone (100 mL, 1:1 v/v). The solution was cooled to 0 °C in an ice bath. Sodium nitrite (4.40 g, 63.2



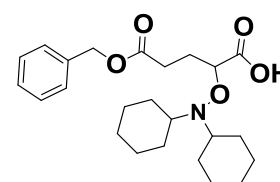
mmol) was dissolved in deionised water (10 mL). The solution was added dropwise to the cooled reaction medium, over a period of 30 minutes. The reaction medium was maintained at 0 °C for 2 hours, and then at room temperature for 18 hours. Further steps were carried out as described for the synthesis of 2-hydroxy-3-phenyl propanoic acid (Section 3.3.10.1). The crude hydroxyacid was purified by flash chromatography (Eluent: DCM (95)/MeOH (4.5)/AcOH (0.5) to give a light yellow oil. The hydroxy acid slowly crystallised upon standing.

Yield: 2.10 g, 8.83 mmol, 41.9%. ESI-MS (261.1 M + Na⁺).

^1H NMR (500 MHz, CDCl_3 , δ , ppm): 7.25 - 7.31 (m, 5H, Ph), 5.06 (s, 2H, CH_2Ph), 4.26 - 4.24 (dd, 1H, CH, $J = 4.25$ Hz), 2.59 - 2.46 (m, CH_2CO_2 , $J = 2.51$ Hz), 2.20 - 1.96 (m, 2H, CH_2CHCO_2).

3.3.11.2. Synthesis of γ -Benzyl-2-Hydroxyglutaric Acid Dicyclohexylamine Salt

γ -benzyl-2-hydroxyglutaric acid (3.34 g, 14.0 mmol) was dissolved in anhydrous diethyl ether (50 mL). The solution was injected into a round bottom flask and it was cooled in an ice bath. Dicyclohexylamine (2.54 g, 14.0 mmol) was added dropwise to the



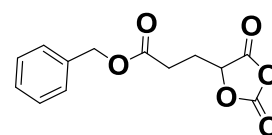
cooled solution. The reaction medium was removed from the ice bath and stirred at room temperature for 45 minutes. The precipitated salt was filtered and then it washed several times using cold diethyl ether. The salt was dried, *in vacuo*.

Yield: 3.34 g, 8.00 mmol, 57.1%.

^1H NMR (500 MHz, CDCl_3 , δ , ppm): 7.28 - 7.24 (m, 5H, Ph), 5.04 (s, 2H, CH_2Ph), 3.86 - 3.84 (dd, 1H, CH, $J = 3.85$ Hz), 2.98 - 2.93 (m, 2H, NCH), 2.56 - 2.36 (m, 2H, $\text{CH}_2\text{CH}_2\text{CO}_2$), 2.11 - 2.09 (m, 2H, CH_2CHCO_2), 2.00 - 1.48 (m, 22H, CH_2 , *cyclohexyl*). ^{13}C NMR (125 MHz, CDCl_3 , δ , ppm): 174.59 ($\text{C}=\text{O}$), 172.94 ($\text{CH}_2\text{C}=\text{O}$), 137.09 (Ar), 128.50 - 127.92 (Ar), 79.72 (αCH), 66.15 (BzCH_2O), 61.35 (N(CH)), 30.92 (s), 30.10 ($(\text{CH}_2)_2$, *cyclohexyl*), 26.32 (αCHCH_2), 25.99 (CH_2 , *cyclohexyl*), 24.77 ($(\text{CH}_2)_2$, *cyclohexyl*). ESI-MS (417.25), Elemental Analysis; *Theoretical*: Carbon 69.04%, Hydrogen 8.45%, Nitrogen 3.35%. *Found*: Carbon 69.07%, Hydrogen 8.42%, Nitrogen 3.38%.

3.3.11.3. Salt Cyclisation to form an OCA Monomer

Y-benzyl-2-hydroxyglutaric acid dicyclohexylamine salt (3.33, 8 mmol) was added to a suspension of poly(styrene)-supported diisopropylethylamine resin, in anhydrous diethyl ether (60mL).



Disphosgene (4.80 g, 24 mmol) was added. The reaction medium was degassed several times and then it was stirred under a nitrogen flow, at room temperature, for 18 hours. Further steps were carried out as described for the synthesis of Phe OCA.

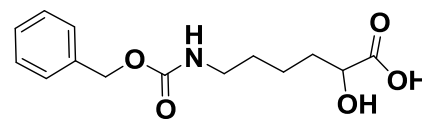
Yield: 1.06 g, 3.45 mmol, 50.2% (Light yellow oil that crystallises on standing).

^1H NMR (500 MHz, CDCl_3 , δ , ppm): 7.39 - 7.34 (m, 5H, Ph), (dd, 1H, CH, $J = 5.22$ Hz), 5.15 (s, 2H, CH_2Ph), 2.65 - 2.56 (m, 2H, CH_2CO_2 , $J = 2.61$ Hz), (m, CH_2CHCO_2). ^{13}C NMR (125 MHz, CDCl_3 , δ , ppm): 172 (αCHCO_2), 167 ($\text{CO}_2\text{CH}_2\text{Ph}$), 148 (αCHCO_3), 135 ($(\text{CH})_5\text{C}$ *aromatic*), 128 ($(\text{CH})_5$ *aromatic*), 78 (αCH) 67 (CH_2Ph), 28 (CO_2CH_2), 26 (CH_2CH). FTIR: $\nu_{\text{max}}/\text{cm}^{-1}$ (oil): 3033 (C-H, Ar stretch), 2896 (C-H, alkyl), 1853, 1776 (C=O, amide and ester overlap), 1457 (C-O), 732 (aromatic 'oop' bends). Elemental Analysis; *Theoretical*: Carbon 59.09%, Hydrogen 4.58%; *Found*: Carbon 59.12%, Hydrogen 4.59%.

3.3.12. Synthesis of Lys(Cbz) OCA

3.3.12.1. Synthesis of 6-(Benzyloxycarbonylamino)-2-Hydroxyhexanoic Acid

A similar procedure to that described for the synthesis of 2-hydroxy-3-phenyl propanoic acid was followed (Section 3.3.10.1). However, the reaction was worked up in ether.

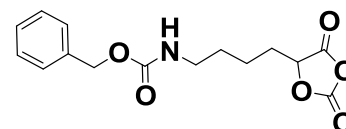


Yield: 4.74 g, 16.8 mmol, 93.7% (Yellow powder).

^1H NMR (500 MHz, CDCl_3 , δ , ppm): 7.40 - 7.19 (m, 5H, Ph), 5.43 (s, 2H, CH_2Ph), 4.16 - 4.14 (dd, 1H, CH, $J = 4.15$ Hz), 1.79 - 1.57 (m, 2H, CH_2CHCO_2), 1.47 - 1.26 (m, 4H, CH_2CH_2).

3.3.12.2. Cyclisation into Lys(Cbz) OCA

6-(benzyloxycarbonylamino)-2-hydroxyhexanoic acid (4.70 g, 16.7 mmol) was dissolved in anhydrous THF. The solution was added to a round bottom flask, which contained activated



charcoal (0.2 g, 16.7 mmol). Diphosgene (13.2 g, 66.8 mmol) and triethylamine (300 μL , 16.7 mmol) were injected dropwise into the reaction medium, under constant stirring. Further steps were carried out, as described for the synthesis of Phe OCA, with the exception that, the pure Lys(Cbz) OCA was obtained by recrystallisation of crude product in diethyl ether:diisopropyl ether solution (1:5 v/v), at -18 $^\circ\text{C}$, for 48 hours.

Yield: 4.52 g, 14.6 mmol, 87.6% (White waxy crystals).

^1H NMR (500 MHz, CDCl_3 , δ , ppm): 7.43 - 7.19 (m, 5H, Ph), 5.10 - 4.81 (m, 3H, Ph-CH_2 , αCH , $J = 5.06$ Hz), 3.75 - 3.57 (t, 1H, CONH , $J = 4.19$ Hz), 3.12 (d, 2H, NHCH_2 , $J = 3.15$ Hz), 2.03 - 1.73 (m, 2H, CHCH_2), 1.64 - 1.29 (m, 4H, CH_2CH_2). ^{13}C NMR (125 MHz, CDCl_3 , δ , ppm): 178 (αCHCO_2), 167.1 ($\text{CO}_2\text{CH}_2\text{Ph}$), 157 (αCHO_2), 148.2, (CCH_2OCONH), 128.6 (ArCH), 79.6 (αCH), 67.9 (PhCH_2OCO), 40.3 (OCONHCH_2), 30.3 (NHCH_2CH_2), 29.1 (αCHCH_2), 21.29 ($\text{NHCH}_2\text{CH}_2\text{CH}_2$). FTIR: $\nu_{\text{max}}/\text{cm}^{-1}$ (oil): 3601 (NH, amide stretch), 3029 (C-H, Ar stretch), 2787 (C-H, alkyl stretch), 1862, 1783 (C=O, amide and ester overlap), 758 (aromatic 'oop' bends). Elemental Analysis: *Theoretical*: Carbon 58.63%, Hydrogen 5.58%; Nitrogen 4.56%; *Found*: Carbon 58.65%, Hydrogen 5.59%, Nitrogen 4.52%.

3.4. References

1. Cheng, J. and Deming, T. Synthesis of Polypeptides by Ring-Opening Polymerization of α -Amino Acid N-Carboxyanhydrides. In: Deming, T. ed. *Peptide-Based Materials*. Springer Berlin Heidelberg, **2012**, 1-26.
2. Kricheldorf, H.R. *α -aminoacid-N-carboxy-anhydrides and related heterocycles: syntheses, properties, peptide synthesis, polymerization*. Springer Science & Business Media, **2012**.
3. Yin, Q., Yin, L., Wang, H. and Cheng, J. *Acc. Chem. Res.*, **2015**, 48, 1777-1787.
4. Lu, Y., Yin, L., Zhang, Y., Zhang, Z., Xu, Y., Tong, R. and Cheng, J. *ACS Macro Lett.*, **2012**, 1, 441-444.
5. Yu, Y., Zou, J. and Cheng, C. *Polym. Chem.*, **2014**, 5, 5854-5872.
6. Hadjichristidis, N., Iatrou, H., Pitsikalis, M. and Sakellariou, G. *Chem. revs.*, **2009**, 109, 5528-5578.
7. Kricheldorf, H.R. *Angew. Chem. Int. Ed.*, **2006**, 45, 5752-5784.
8. Deming, T.J. *J. Polym. Sci. A Polym. Chem.*, **2000**, 38, 3011-3018.
9. Deming, T. Polypeptide and Polypeptide Hybrid Copolymer Synthesis via NCA Polymerization. In: Klok, H.-A. and Schlaad, H. eds. *Peptide Hybrid Polymers*. Springer Berlin Heidelberg, **2006**, 1-18.
10. Habraken, G.J.M., Peeters, M., Dietz, C.H.J.T., Koning, C.E. and Heise, A. *Polym. Chem.*, **2010**, 1, 514-524.
11. Lu, H., Wang, J., Song, Z., Yin, L., Zhang, Y., Tang, H., Tu, C., Lin, Y. and Cheng, J. *Chem. Commun.* **2014**, 50, 139-155.
12. Kramer, J.R. and Deming, T.J. *Biomacromolecules*. **2010**, 11, 3668-3672.
13. Kralingen, L.v. *Controlled Polymerization of Amino acid Derivatives*. PhD thesis, Stellenbosch University, **2008**.
14. Farthing, A.C. *J. Chem. Soc.*, **1950**, 3213-3217.
15. Wilder, R. and Mobashery, S. *J. Org. Chem.*, **1992**, 57, 2755-2756.
16. Katakai, R. and Iizuka, Y. *J. Org. Chem.*, **1985**, 50, 715-716.
17. Nagai, A., Sato, D., Ishikawa, J., Ochiai, B., Kudo, H. and Endo, T. *Macromolecules*. **2004**, 37, 2332-2334.
18. Dmitrovic, V., Habraken, G.J.M., Hendrix, M.M.R.M., Habraken, W.J.E.M., Heise, A., de With, G. and Sommerdijk, N.A.J.M. *Polymers*. **2012**, 4, p.1195.
19. Johnson, R.P., John, J.V. and Kim, I. *Eur. Poly. J.*, **2013**, 49, 2925-2948.
20. Daly, W.H. and Poché, D. *Tetrahedron Lett.*, **1988**, 29, 5859-5862.
21. Katchalski, E. and Sela, M. Synthesis and Chemical Properties of Poly- α -Amino Acids. In: C.B. Anfinsen, M.L.A.K.B. and John, T.E. eds. *Advances in Protein Chemistry*. Academic Press, **1958**, 243-492.
22. Dorman, L.C., Shiang, W.R. and Meyers, P.A. *Synth. Commun.*, **1992**, 22, 3257-3262.
23. Iwakura, Y., Uno, K. and Kang, S. *J. Org. Chem.*, **1965**, 30, 1158-1161.
24. Waley, S.G. and Watson, J. *Proceedings of the Royal Society of London. Series A. Mathematical and Physical Sciences*. **1949**, 199, 499-517.
25. Ballard, D.G.H. and Bamford, C.H. *Proceedings of the Royal Society of London. Series A. Mathematical and Physical Sciences*. **1954**, 223, 495-520.

26. Yin, Q., Tong, R., Xu, Y., Dobrucki, L.W., Fan, T.M. and Cheng, J. *Biomacromolecules*. **2013**, 14, 920-929.
27. Thillaye du Boullay, O., Bonduelle, C., Martin-Vaca, B. and Bourissou, D. *Chem. Commun.*, **2008**, 1786-1788.
28. Lu, Y., Yin, L., Zhang, Y., Zhonghai, Z., Xu, Y., Tong, R. and Cheng, J. *ACS Macro Lett.* **2012**, 1, 441-444.
29. Chen, X., Lai, H., Xiao, C., Tian, H., Chen, X., Tao, Y. and Wang, X. *Polym. Chem.* **2014**, 5, 6495-6502.
30. Kimura, Y., Shirotani, K., Yamane, H. and Kitao, T. *Macromolecules*. **1988**, 21, 3338-3340.
31. Gerhardt, W.W., Noga, D.E., Hardcastle, K.I., García, A.J., Collard, D.M. and Weck, M. *Biomacromolecules*. **2006**, 7, 1735-1742.
32. Matthes, D., Richter, L., Muller, J., Denisiuk, A., Feifel, S.C., Xu, Y., Espinosa-Artiles, P., Sussmuth, R.D. and Molnar, I. *Chem. Commun.* **2012**, 48, 5674-5676.
33. Zhang, Z., Yin, L., Xu, Y., Tong, R., Lu, Y., Ren, J. and Cheng, J. *Biomacromolecules*. **2012**, 13, 3456-3462.
34. Pounder, R.J., Fox, D.J., Barker, I.A., Bennison, M.J. and Dove, A.P. *Polym. Chem.* **2011**, 2, 2204-2212.
35. Fetsch, C., Grossmann, A., Holz, L., Nawroth, J.F. and Luxenhofer, R. *Macromolecules*. **2011**, 44, 6746-6758.

Chapter 4. The Formation of Biodegradable Particles from a Therapeutic Initiator for Enzyme-Mediated Drug Delivery

Preamble

This Chapter is based on work published as:

Khuphe M.; Kazlauciusas A.; Huscroft M.; Thornton P. D. *Chem. Commun.*, **2015**, 51, 1520-1523.

Abstract

The direct grafting of amphiphilic macromolecules by the sequential NCA ROP from a model therapeutic molecule (dopamine hydrochloride) is detailed. Hydrophobic peptides of phenylalanine and alanine were grafted from the primary amino group of dopamine hydrochloride, followed by the grafting of hydrophilic sarcosine peptoids to yield an amphiphilic dopamine-terminated macromolecule, by a one-pot synthetic strategy. The monodisperse particles that were obtained from the self-aggregation of these macromolecules contained a peptide component that was capable of actuating dopamine release to an extent and rate, dependent on the protease enzyme with which it was reacted. To the author's knowledge, this is the first example of NCA ROP being carried out directly using a therapeutic molecule to afford peptide-peptoid-containing self-assembled structures that may be selectively degraded by protease enzymes to release a covalently-loaded, model therapeutic cargo.

4.1. Introduction

Highly controlled, stimuli-responsive release mechanisms permit the programmed release of payload molecules from a carrier vehicle on-demand [1-3]. Polymers are often employed as drug carriers to provide protection against premature drug metabolism and clearance *in vivo* [4]. Changes in environmental pH, temperature and ionic strength may be used to alter the properties of the polymer and to mediate the controlled delivery of guest molecules at a target site [5-10]. In addition, proteolytic enzymes may be exploited to trigger the swelling or degradation of (poly)peptide-containing carrier vehicles, resulting in payload release [11-15]. Such enzyme-responsive materials may be targeted towards proteases that are over-expressed at particular disease sites, thus providing this class of biomaterial significant medicinal relevance [16].

NCA ROP (Chapter 1.2) permits the generation of homopeptides that possess properties which are analogous to proteins, but are generated by a straightforward, controlled polymerisation that avoids the practical and economic demands that are associated with solid phase peptide synthesis [17-20]. Homopeptides are particularly useful as biomaterials as they possess the ability to form secondary structures, have general low toxicity, and may possess targeted biodegradability. Consequently, this class of polymer has been exploited for use in numerous applications including drug delivery, tissue regeneration and biomineralisation [21-23]. Along with providing a variety of polymeric architectures, NCA ROP also permits the creation of amphiphilic macromolecules. These are particularly useful because they can readily self-organise in aqueous media into one of the widely-researched versatile nanosystem, polymeric micelles (>100 nm) [24]. Polymeric micelles present cores that are relatively larger than the cores of micelles which are formed from the self-assembly of low molecular weight surfactant molecules. As such, polymeric micelles may encapsulate larger quantities of hydrophobic therapeutics and are usually characterised by longer circulation times, *in vivo* [25].

A frequently demonstrated method of controlled drug delivery involves the use of therapeutic molecules that are non-covalently loaded within polymeric nanocarriers, before their release upon interaction with a targeted stimulus [26-28]. This approach enables the achievement of relatively highly loaded quantities within the polymer nanocarriers. However, the process of drug loading can be challenging and may result in the loss of valuable drug molecules. A method that could restrict molecular loss, during payload loading into the polymer architecture, would be to initiate NCA ROPs directly using a suitable drug molecule, to create amphiphilic macromolecular structures that are capable of self-assembling into nanocarriers. The polymeric nanocarriers that are formed would then contain drug molecules that are covalently bound within a self-assembled biodegradable shell that, upon targeted degradation, could permit the on demand release of the therapeutic initiator. Dopamine hydrochloride, a hormone and neurotransmitter is prescribed to correct hemodynamic status in patients that suffer from shock syndrome. Thus, dopamine hydrochloride was selected as the therapeutic initiator in this proof-of-concept study. Patients suffering from Parkinson's disease lose dopaminergic cells in the substantia nigra region of the brain, resulting in depleted levels of dopamine. Dopamine is also prescribed to regulate the effects of Parkinson's disease [29].

4.2. Experimental Details

4.2.1. Dopamine-Mediated NCA ROP

A representative procedure is given using the dopamine-initiated sequential ROP of Ala NCA and Sar *N*-NCA. The other polymerisations were carried out by following the same procedure. Ala NCA (60 mg, 0.527 mmol) was dissolved in anhydrous DMF (20 mL). The solution was injected into a pre-dried, nitrogen-purged Schlenk tube that was sealed with a rubber septum and equipped with a magnetic stirrer bar. Dopamine hydrochloride (20 mg, 0.106 mmol) was dried under a continuous stream of nitrogen for 30 minutes, then dissolved in anhydrous DMF (10 mL). The solution was injected into the reaction medium under constant stirring and nitrogen flow. The reaction was allowed to proceed at room temperature for 96 hours. After 96 hours, the equivalent of 15 units of Sar *N*-NCA (180.3 mg, 1.582 mmol), dissolved in anhydrous DMF (10 mL), was injected into the reaction medium. The reaction was allowed to proceed for a further 96 hours, under a nitrogen flow. The product was precipitated in cold diethyl ether (300 mL), then isolated from the supernatant by centrifugation (3000 rpm, 10 min, -5 °C) and rinsed repeatedly using cold diethyl ether. The obtained macromolecule was subsequently dried in a vacuum oven (40 °C) for 24 hours, dialysed against distilled water and then lyophilised for 48 hours. Dop-(Ala)_m-(Sar)_n: 121 mg, 72.6 wt. % (Off-white powder). ¹H NMR (500 MHz, DMSO-d₆, δ, ppm): 8.25 (CH₂)₂NH), 8.15 - 7.80 (NH), 6.65 - 6.42 (Ar-H), 4.37 (α-CH), 4.30 - 4.23 (CH₂CO), 4.23 - 4.13 (CO(NH)CH₃), 1.23 - 1.10 (αCH(CH₃)). Elemental Analysis: C, 52.01; H, 7.21; N, 18.79. FTIR:ν_{max}/cm⁻¹ (solid): 2925 (alkyl C-H stretch), 1667 (C=O amide stretch), 1375 (C-H bending), 1253 (C-N stretch), 688 (aromatic C-H bending). Dop-(Phen)_m-(Sar)_n: 198 mg, 89.2 wt. % (White powder). ¹H-NMR (500 MHz, DMSO-d₆, δ, ppm): 7.97 (ArCH₂CH₂NH), 7.25 - 7.23 (Ar-H), 6.63 - 6.42 (Ar-H), 4.08 - 4.01 (αCH), 3.42 - 3.38 (Ar-CH₂), 3.03 - 2.97 (Ar-CH₂CH₂), 2.10 (Ar-CH₂CH), 1.12 - 1.09 (CH₂NCH₃). Elemental Analysis: C, 58.19; H, 6.87; N, 15.89. FTIR:ν_{max}/cm⁻¹ (solid): 2875 (alkyl C-H stretch), 1650 (C=O amide stretch), 702 (aromatic C-H bending).

4.2.2. Monitoring Progress of NCA ROP

The progress of the ROP of Ala NCA and the ROP of Phe NCA were monitored using ¹H NMR spectroscopy to determine the point at which the respective monomers were exhausted

before grafting the sarcosine peptoid. Aliquots (3 mL) were extracted from each reaction at selected time intervals and precipitated in cold diethyl ether, centrifuged and dried *in vacuo*. Using ^1H NMR spectroscopy, the monomer conversions were determined by comparing the integration value of aromatic protons of the dopamine with the integration value of the protons bonded to the α -carbon of Ala repeat units (i.e., for dop-(Ala)_m) and the integration value of the aromatic protons of Phe (i.e., for dop-Phe)_m).

4.2.3. Preparation of Nanoparticles

Dop-(Ala)₅-(Sar)₁₅ and Dop-(Phe)₄-(Sar)₁₈ particles were prepared in a PBS buffer (pH 7.4), by following the nanoprecipitation procedure that was described in Chapter 2.14.

4.2.4. Light Scattering Studies

A procedure similar to that described in Chapter 2.15 was followed. The respective particle dispersions were then stored at 37 °C without agitation for a period of up to 14 days, during which the dispersions were analysed at the predetermined time intervals using DLS.

4.2.5. Circular Dichroism (CD)

Dop-(Ala)₅-(Sar)₁₅ and Dop-(Phe)₄-(Sar)₁₈ particles were prepared in a PBS buffer (pH 7.4), as described in Chapter 2.14. The samples which had been equilibrated at 37 °C for 3 hours were then pipetted (200 μL) gently into CD quartz cuvettes (1 mm path length). CD spectra were then acquired in the far-UV region (190 nm - 260 nm) using a Chirascan v.4.4.0 CD spectrometer, equipped with a 150 W, air-cooled Xe arc lamp.

4.2.6. Enzyme-Mediated Degradation of Particles

Triplicate sets of dop-(Ala)₅-(Sar)₁₅ and dop-(Phe)₄-(Sar)₁₈ particles (0.1 mg/mL) were incubated within independent PBS solutions (pH 7.4, 37 °C) that contained 20 units of thermolysin (from *Bacillus thermoproteolyticus rokko*), 20 units of α -chymotrypsin and 20 units of elastase (from bovine pancreas), within dialysis tubing (MWCO = 1200 Da). The three sets-up were dialysed against a blank PBS buffer solution (pH 7.4, 37 °C). Samples of another triplicate set of the respective particles (0.1 mg/mL) were incubated within independent PBS buffer solutions (pH 7.4, 37 °C) only, maintained within dialysis tubing (MWCO = 1000 Da) and then dialysed against blank PBS buffer solution (pH 7.4, 37 °C). The experimental sets-up were maintained under

constant agitation. Dopamine released into the dialysate was quantified, at predetermined intervals, using HPLC.

4.2.7. Calibration of High Performance Liquid Chromatography (HPLC)

Table 4.1. HPLC instrumentation settings and experimental conditions applied in the study of enzyme-mediated dopamine-release.

Column	Ascentis Express C18.5 cm x 2.1 mm, 2.7 μ m Particle Size		
Mobile Phase	A: Water + 0.1% TFA B: Acetonitrile + 0.1% TFA		
Flow Rate	0.5 mL/min		
Sample Injection Volume	10 μ L		
Gradient	Time (Min)	A (%)	B (%)
	0	100	0
	5	100	0
	10	97	3
	11.5	0	100
	13.0	0	100
	13.5	100	0
15.0	100	0	
Column Compartment/ Autosampler Temperature	5 $^{\circ}$ C		
Detector	Photodiode Array UV Detector		

Calibration standards were prepared by the serial dilution of a stock solution of dopamine (1mg/mL) in HPLC-grade water (18.2 M Ω). The concentration of dopamine in dilute standard solutions ranged from 0 μ g/mL to 100 μ g/mL. The solutions were analysed by HPLC to provide data that were the basis of a linear calibration graph, for the accurate quantification of the dopamine content. The optimised settings and experimental conditions that were used for the HPLC calibration and, subsequently, for the study of dopamine-release from particles are given in Table 4.1.

4.2.8. Verification of Dopamine Release

Dialysate samples of Dop-(Ala)₅-(Sar)₁₅ and of Dop-(Phe)₅-(Sar)₁₅ that were previously incubated within enzymatic solutions were fractionated by HPLC. The fraction consistent with

dopamine's elution peak was collected. Repetitive fractionation was carried out, to accumulate enough of the dopamine fractions, to be able to carry out analyses using electrospray ionisation mass spectrometry (ESI MS). The fractions were lyophilised. The resulting powders were reconstituted in methanol and then analysed by ESI-MS, to substantiate the composition.

4.2.9. Biological Studies

C3H mouse dermal fibroblasts were cultured and passaged, as described in Chapter 2.19. Solutions of Dop-(Ala)₅-(Sar)₁₅ and of Dop-(Phe)₄-(Sar)₁₈ (1 mg/mL) were prepared in sterile-filtered DMSO that was suitable for cell culture. The stock solutions were serial-diluted in DMEM culture medium that was supplemented with 10% (v/v) FBS, 1 mM L-glutamine and 100 U/mL penicillin-100 µg/mL streptomycin mixture, to obtain 0.5 µg/mL, 1 µg/mL, 5 µg/mL, 100 µg/mL and 1000 µg/mL Dop-(Ala)₅-(Sar)₁₅ and Dop-(Phe)₄-(Sar)₁₈ solutions, respectively. Five sets of triplicate Nunclon Δ™ surface wells were seeded with 5 × 10⁴ C3H mouse dermal fibroblasts and then topped to the 200 µL mark with polymer solutions of the respective concentration (Figure 4.1).

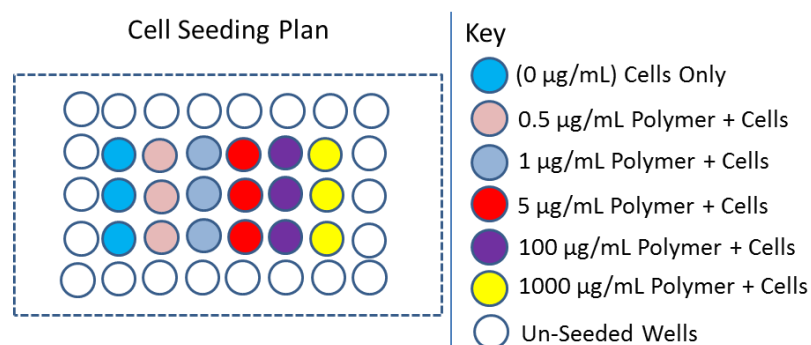


Figure 4.1. Cell-seeding plan for the determination of the cytotoxicity of Dop-(Ala)₅-(Sar)₁₅ and of Dop-(Phe)₄-(Sar)₁₈, against C3H mouse dermal fibroblasts.

In another set of triplicate Nunclon Δ™ surface wells, 5 × 10⁴ C3H mouse dermal fibroblasts were seeded and the wells were topped with a DMEM culture medium, supplemented with 10% (v/v) FBS, 1 mM L-glutamine and penicillin (100 U/mL)-streptomycin (100 µg/L) mixture, containing none of the macromolecules. The unseeded peripheral wells were filled with sterilised PBS buffer solution to maintain the 96-well microplate's humid environment and to reduce any evaporation from the seeded wells. The seeded microplates were incubated in a humidified incubator, at 37 °C and 5% (v/v) CO₂ in air, for 72 hours. ATPlite-M® assay was subsequently carried out, as described in Chapter 2.20.

4.3. Results and Discussion

The required cyclic monomers were synthesised using the Fuchs-Farthing method of direct phosgenation [30]. L-ala NCA and L-phe NCA were then independently reacted with dopamine hydrochloride to induce their ring opening and the formation of short hydrophobic peptides that were conjugated to the dopamine initiator (Figure 4.2a). The presence of a primary amine group that was capable of initiating NCA ROP, and the dopamine hydrochloride's complete solubility in DMF make this therapeutic molecule a suitable candidate for the grafting of peptides from it. In addition, Dimitrov and Schlaad [31] have disclosed that primary amine hydrochlorides promote highly-controlled NCA ROP by negating the formation of NCA anions that would otherwise cause significant premature chain termination.

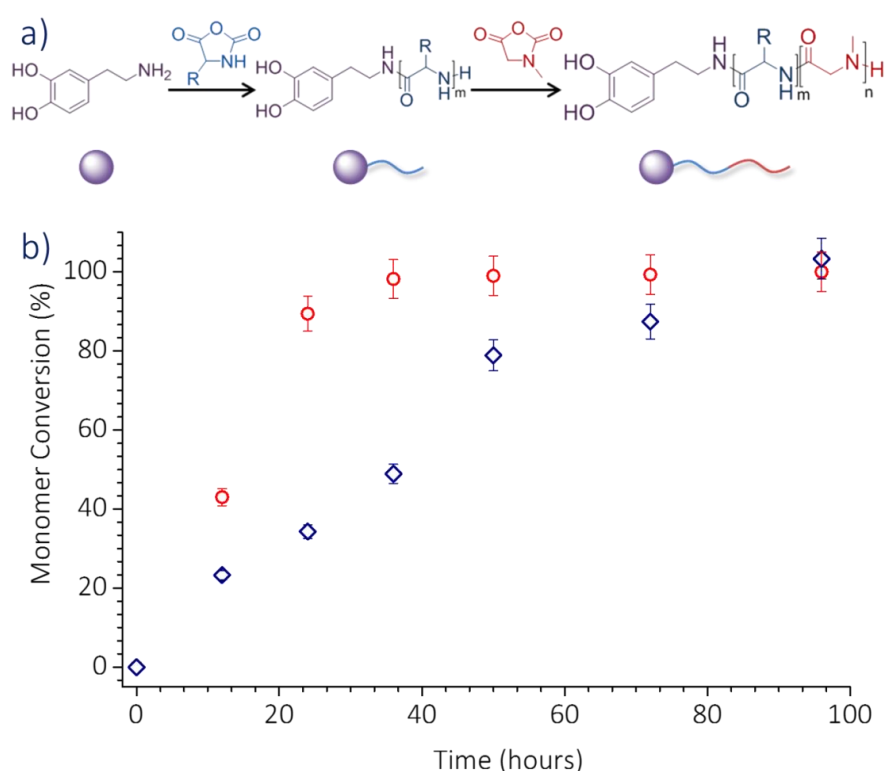


Figure 4.2. (a) Scheme for dopamine acting as a model therapeutic molecule that initiates the sequential ROP of a hydrophobic amino acid NCA, followed by sarcosine NCA. (b) The kinetic aspects of the dopamine-initiated ROP of Ala NCA (○) and Phe NCA (◇).

Various monomer-to-initiator (M/I) feed ratios were trialed initially, to establish the viability of the ROP grafting of Ala and Phe peptides from dopamine. The length of the hydrophobic peptide segment was limited by the solubility of the growing dopamine-peptide conjugate, in

DMF. The optimum number of Ala and Phe amino acidic repeat units that could be grafted from dopamine was subsequently determined by ^1H NMR. The ROP was limited to an average of five repeat amino acid units and four repeat amino acid units, for Ala and Phe per dopamine-initiated chain, respectively. As such, subsequent NCA ROPs were carried out using the optimised M/I ratios in order to avoid the premature precipitation of the hydrophobic dop-peptide segments. ^1H NMR supported kinetic studies, to determine the rate of ROP of the amino acid NCAs, revealed that the grafting of the peptide segment was completed within 96 hours in both cases (Figure 4.2 b). The kinetic profiles reveal a greater conversion rate of NCAs from initiation to approximately 60 hours, followed by a gradual conversion until completion.

The NCA of sarcosine, created from a hydrophilic but charge-neutral amino acid, was then reacted with the respective dopamine-peptide conjugates in order to yield a dopamine-terminated amphiphilic block macromolecule that could be capable of self-organisation into particles. Sarcosine was selected as the hydrophilic component within the macromolecular structures due to its reported non-toxicity, contrasting with other peptides such as poly(L-lysine) [32]. It has been demonstrated that poly(sarcosine) possesses excellent resistance to non-specific protein adsorption and to cell attachment [33], and possesses biocompatibility [34]. ^1H NMR spectroscopy analyses (Figure 4.3 a, Figure 4.4 a) confirmed the creation after 192 hours, of the desired amphiphilic architectures. Because of their relatively low molecular weights, these macromolecules were also conveniently analysed by ESI MS (Figure 4.3 b and 4.4 b). The compositions of the diblock copolymers that were produced were shown to be Dop-(Ala)₅-(Sar)₁₅ and Dop-(Phe)₄-(Sar)₁₈, according to ^1H NMR analyses, and Dop-(Ala)₅-(Sar)₁₇ and Dop-(Phe)₄-(Sar)₂₀, according to ESI-MS analyses. The former composition has been used to describe aspects of the further studies on these materials.

Table 4.2. The theoretical composition and molecular weights of the dopamine-conjugated macromolecules that were produced, as determined using ESI-MS and ^1H NMR.

Theoretical composition	M_w by ^1H NMR (g/mol)	M_w by ESI MS (g/mol)
Dop-(Ala) ₅ -(Sar) ₁₅	1573	1715
Dop-(Phe) ₅ -(Sar) ₁₅	2019	2160

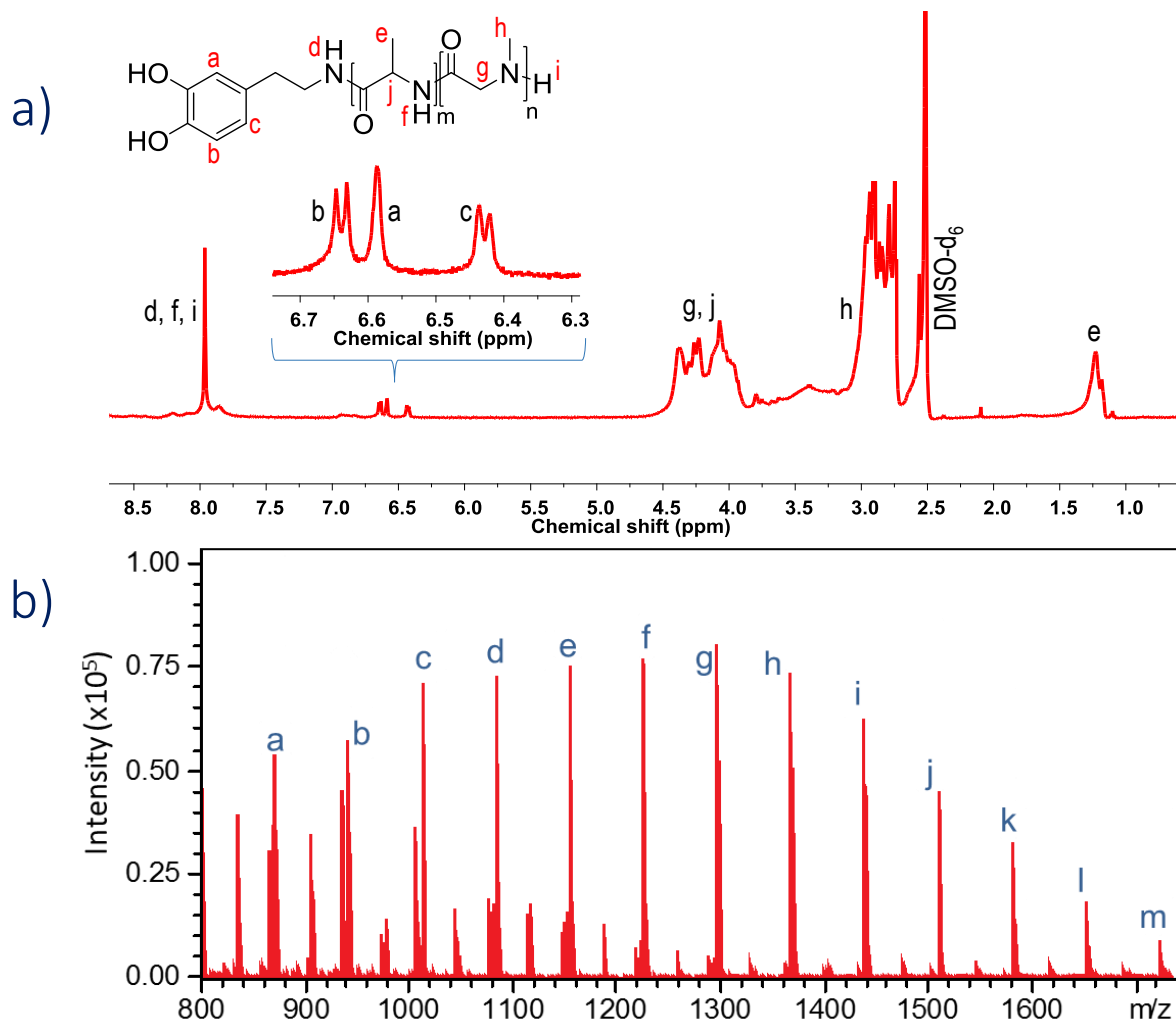


Figure 4.3. (a) ^1H NMR spectrum of Dop-(Ala)₅-(Sar)₁₅ in DMSO- d_6 ; (b) The ESI-MS spectrum of Dop-(Ala)₅-(Sar)₁₅. The peaks can be assigned to the various possible fragments of the macromolecule, i.e., a: dop-(ala)₅-b-(sar)₅, b: dop-(ala)₅-b-(sar)₆, c: dop-(ala)₅-b-(sar)₇, d: dop-(ala)₅-b-(sar)₈, e: dop-(ala)₅-b-(sar)₉, f: dop-(ala)₅-b-(sar)₁₀, g: dop-(ala)₅-b-(sar)₁₁, h: dop-(ala)₅-b-(sar)₁₂, i: dop-(ala)₅-b-(sar)₁₃, j: dop-(ala)₅-b-(sar)₁₄, k: dop-(ala)₅-b-(sar)₁₅, l: dop-(ala)₅-b-(sar)₁₆, m: dop-(ala)₅-b-(sar)₁₇.

The ability of the dopamine-containing amphiphilic macromolecules that were produced, to self-assemble into potentially useful payload delivery vehicles by nanoprecipitation in PBS buffer solutions (Figure 4.5, *top*), was assessed by using DLS and by using SEM. SEM studies revealed that both macromolecules were capable of self-assembly to yield uniform spherical particles (Figure 4.5a, b). Experimental findings from SEM analyses were consistent with those from DLS, revealing that the particles formed from Dop-(Ala)₅-(Sar)₁₅ possessed a mean diameter of 204.7 ± 12.7 nm and particles formed from Dop-(Phe)₄-(Sar)₁₈ possessed a mean diameter of 250 ± 31.4 nm (Figure 4.5 c, d).

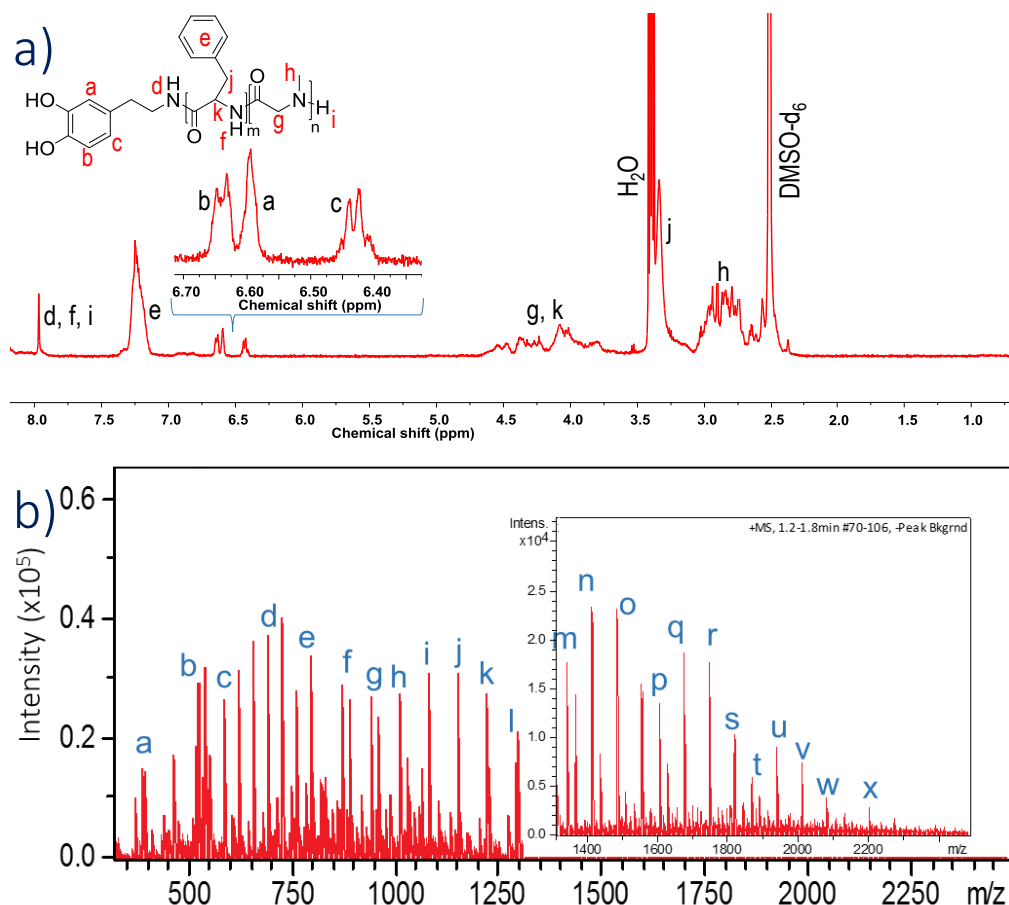


Figure 4.4. (a) ^1H NMR spectrum of Dop-(Phe) $_4$ -(Sar) $_{15}$ in DMSO- d_6 ; (b) The ESI-MS spectrum of Dop-(Phe) $_4$ -(Sar) $_{15}$. The peaks can be assigned to the various possible fragments of the macromolecule, i.e., a: Dop-(phe) $_2$, b: dop-(phe) $_2$ -(sar), c: dop-(phe) $_3$, d: dop-(phe) $_4$, e: dop-(phe) $_4$ -(sar), f: dop-(phe) $_4$ -(sar) $_2$, g: dop-(phe) $_4$ -(sar) $_3$, h: dop-(phe) $_4$ -(sar) $_4$, i: dop-(phe) $_4$ -(sar) $_5$, j: dop-(phe) $_4$ -(sar) $_6$, k: dop-(phe) $_4$ -(sar) $_7$, l: dop-(phe) $_4$ -(sar) $_8$, m: dop-(phe) $_4$ -(sar) $_9$, n: dop-(phe) $_4$ -(sar) $_{10}$, o: dop-(phe) $_4$ -(sar) $_{11}$, p: dop-(phe) $_4$ -(sar) $_{12}$, q: dop-(phe) $_4$ -(sar) $_{13}$, r: dop-(phe) $_4$ -(sar) $_{14}$, s: dop-(phe) $_4$ -(sar) $_{15}$, t: dop-(phe) $_4$ -(sar) $_{16}$, u: dop-(phe) $_4$ -(sar) $_{17}$, v: dop-(phe) $_4$ -(sar) $_{18}$, w: dop-(phe) $_4$ -(sar) $_{19}$, x: dop-(phe) $_4$ -(sar) $_{20}$.

One of the desired attributes of payload delivery vehicles that are intended for application *in vivo* is that they should be able to maintain their stability, and not sediment rapidly or disassemble in the absence of a stimulus [35]. As such, the stability of the particles formed was assessed over time. It was found that after remaining in a PBS solution, at 37 °C, in the absence of a dispersing agent, the particle size remained unchanged over the initial 90 minutes. Overall, the average diameter of the Dop-(Ala) $_5$ -(Sar) $_{15}$ particles increased by 2.4% over 14 days. The average diameter of Dop-(Phe) $_4$ -(Sar) $_{18}$ particles increased by 5.0% over 14 days. These

observed increments are relatively small, demonstrating the considerable stability of these particles.

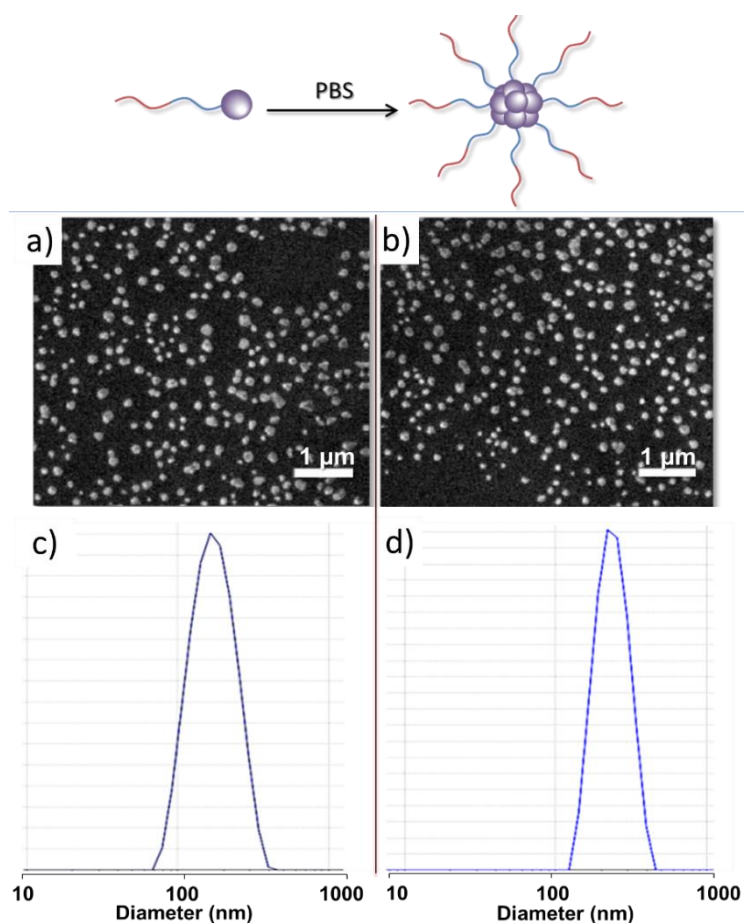


Figure 4.5. (top) Graphical illustration of the self-aggregation of the amphiphilic architectures. SEM images obtained from (a) Dop-(Ala)₅-(Sar)₁₅ particles and (b) Dop-(Phe)₄-(Sar)₁₈ particles. Scale bars represent 1 μm. DLS charts revealing the size distribution of (c) Dop-(Ala)₅-(Sar)₁₅ particles and (d) Dop-(Phe)₄-(Sar)₁₈ particles in PBS buffer solution. The PDIs were measured as 0.24 and 0.22, respectively.

The critical aggregation concentration (CAC) of amphiphilic architectures can be determined by DLS [36-38]. Thus, DLS was subsequently used to determine the CAC of both macromolecule types, to ascertain their suitability for use as self-assembled materials, *in vivo*. The CAC of Dop-(Ala)₅-(Sar)₁₅ (Figure 4.6b) was revealed to be 4.01×10^{-6} mol/L (i.e. 5.99 μg/mL) and the CAC of Dop-(Phe)₄-(Sar)₁₈ was revealed to be 3.58×10^{-7} mol/L (i.e., 0.724 μg/mL) (Figure 4.6 c). DLS studies also revealed that Dop-(Ala)₅-(Sar)₁₅ particles and Dop-(Phe)₄-(Sar)₁₈ particles possess polydispersity indices of 0.24 and 0.22 respectively, another indication of the stability of the two colloidal dispersions.

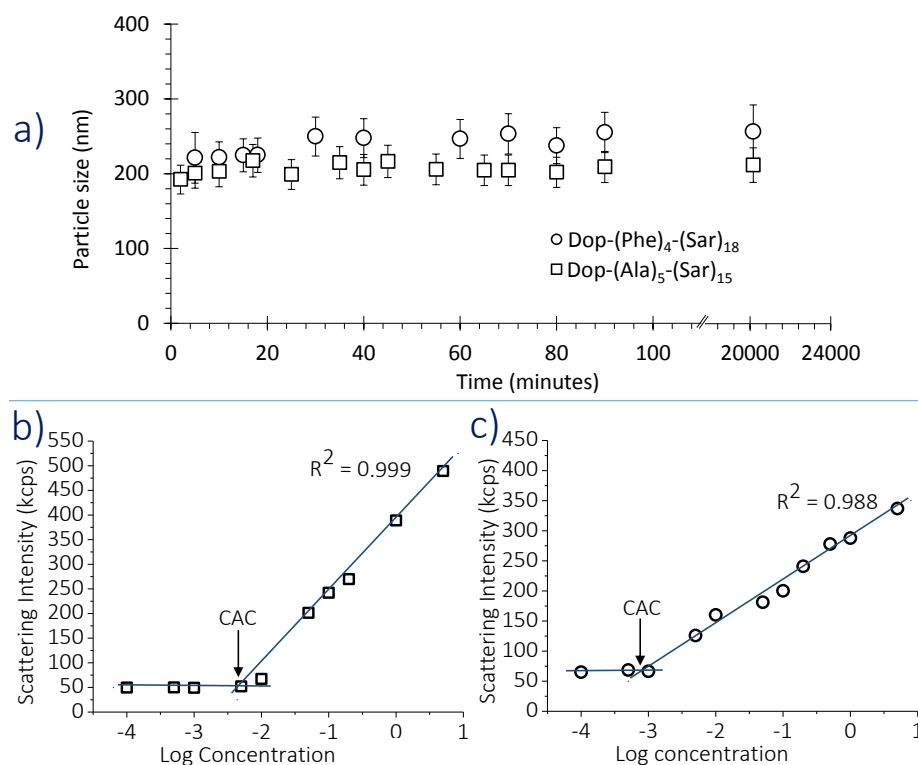


Figure 4.6. (a) Chart detailing the stability of Dop-(Ala)₅-(Sar)₁₅ particles and Dop-(Phe)₄-(Sar)₁₈ particles incubated in PBS buffer, at 37 °C for over 14 days. The variation of the intensity of the scattered light at various concentrations of Dop-(Ala)₅-(Sar)₁₅ (b) and Dop-(Phe)₄-(Sar)₁₈ (c), leading to the determination of the critical aggregation concentration of the respective macromolecules.

Circular dichroism (CD) spectroscopy is a versatile technique that can be used to determine the secondary structure that might be adopted by poly(amino acid)s in solution [39, 40]. The CD spectra of Dop-(Ala)₅-(Sar)₁₅ and Dop-(Phe)₄-(Sar)₁₈ in PBS buffer were obtained at pH 7.4, at 37 °C. The profile of the spectrum obtained from Dop-(Ala)₅-(Sar)₁₅ (Figure 4.7b) resembles an α -helix conformation, showing a negative profile between 210 nm and 200 nm, that becomes positive at *ca.*196 nm, is displayed. The spectrum obtained from Dop-(Phe)₄-(Sar)₁₈ (Figure 4.7a) shows distinct minima that are located close to 210 nm and close to 230 nm. These are reminiscent of a β -sheet conformation, probably emanating from the π - π stacking of the aromatic groups of Phe [34].

Following the creation of monodisperse particles, studies were undertaken to demonstrate the controlled release of covalently encapsulated dopamine, during targeted peptide degradation by targeted protease enzymes (Figure 4.8, *top*). As a proof-of-concept study, the release activities of three serine protease enzymes were analysed against time for the dopamine-

containing nanoparticles. It has been previously demonstrated that serine proteases may be used as highly effective triggers in activating enzyme-responsive materials, particularly in mediating the release of payload molecules in controlled drug delivery processes [41].

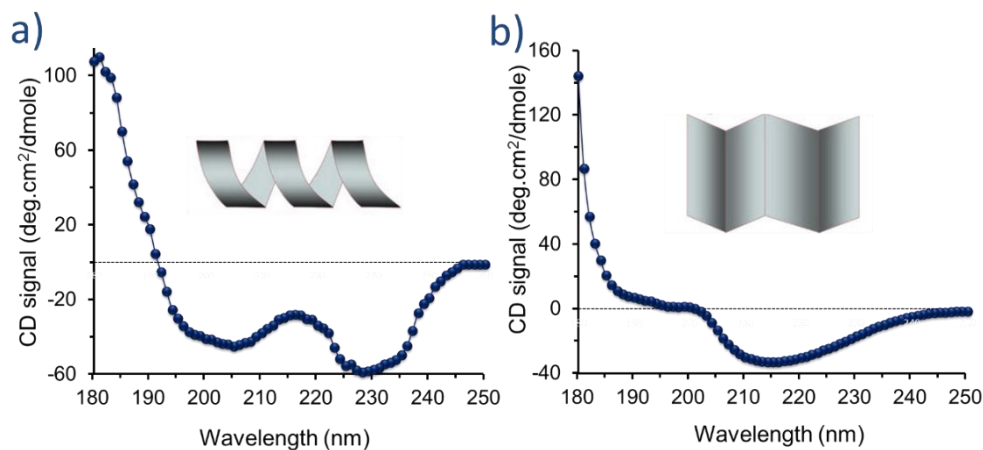


Figure 4.7. CD spectra obtained from the analysis of a) Dop-(Ala)₅-(Sar)₁₅ particles and of b) Dop-(Phe)₄-(Sar)₁₅ particles in aqueous an BS buffer solution (pH 7.4, 37 °C).

Chymotrypsin from bovine pancreas possesses the selective ability to cleave peptide bonds that are flanked by aromatic amino acids located at the P1 position, but is rather non-specific for the P'1 amino acid [42]. Thermolysin from *Thermoproteolyticus rokko* possesses low cleavage selectivity [43]. However, elastase from bovine pancreas overwhelmingly selectively cleaves peptide bonds that are flanked by small amino acids, for example, Ala, [44]. As such, it may be hypothesised that elastase should demonstrate extensive activity against Dop-(Ala)₅-(Sar)₁₅ compared to the activity against Dop-(Phe)₄-(Sar)₁₈, while chymotrypsin should cleave more extensively Dop-(Phe)₄-(Sar)₁₈ than it does to to Dop-(Ala)₅-(Sar)₁₅, because of the presence of the aromatic Phe. Also, thermolysin should demonstrate activity against both sets of particles because of its relatively non-specific ability. Conversely, extremely limited amounts of dopamine would be anticipated to be detected in response to incubation in PBS buffer solution since this would lack a protease enzyme.

Dopamine release was detected to some extent when both sets of particles were incubated in the enzymatic solutions. In contrast, detected dopamine release from the sets of particles that were incubated in the PBS buffer solution that lacked a protease enzyme was significantly less in either set of particles. The differences in selectivity that the enzymes possess for the

peptides created demonstrated that the composition might be able to be tuned to target a particular protease enzyme. For example, dopamine release from Dop-(Ala)₅-(Sar)₁₅ was greatest when the particles were incubated with elastase (Figure 4.8 a), demonstrating the relatively high activity that elastase has in cleaving peptide bonds that are flanked by small amino acid residues, such as from Ala.

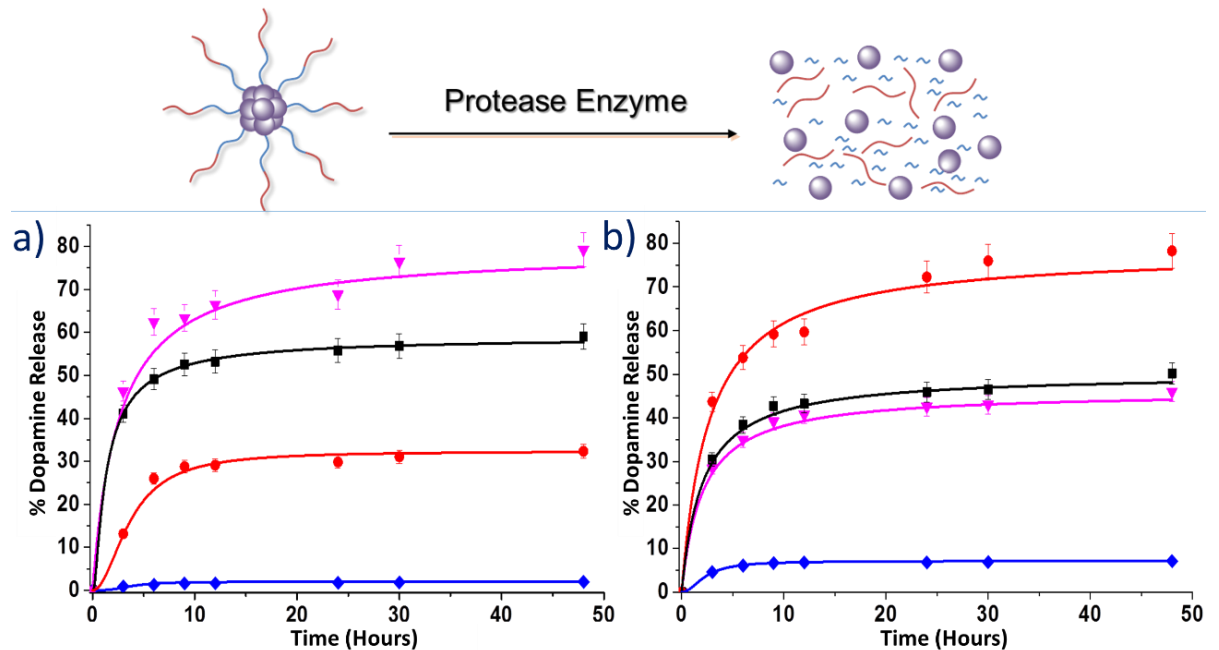


Figure 4.8. (top), Graphical illustration of Dop-(Peptide)-(Peptoid) particles being degraded in the presence of a relevant protease enzyme. The release of dopamine from (a) Dop-(Ala)₅-(Sar)₁₅ particles and from (b) Dop-(Phe)₄-(Sar)₁₈ particles in response to elastase (▼), to thermolysin (■), to chymotrypsin (●) and to the PBS buffer solution only (◆).

In excess of 79% of the total dopamine content was released to the exterior of the dialysis tubing for detection, after 48 hours. In excess of 59% of the total dopamine content was released from the dialysis tubing after incubation with thermolysin. Also, approximately 32% of the total dopamine content was released from the particles when incubated with chymotrypsin. The amount of dopamine released from Dop-(Phe)₄-(Sar)₁₈ particles was greatest (in excess of 78%) when the particles were incubated with chymotrypsin (Figure 4.8 b), demonstrating this enzyme's preference towards the cleavage of peptide bonds that link one or more aromatic amino acid residues. Both elastase and thermolysin showed some activity towards Dop-(Phe)₄-(Sar)₁₈ particles, but less than that observed with chymotrypsin (46% release and 50% release, respectively). In all cases, each of the time points shown in

Figure 4.8 represents an independent experiment that was repeated to confirm method reproducibility.

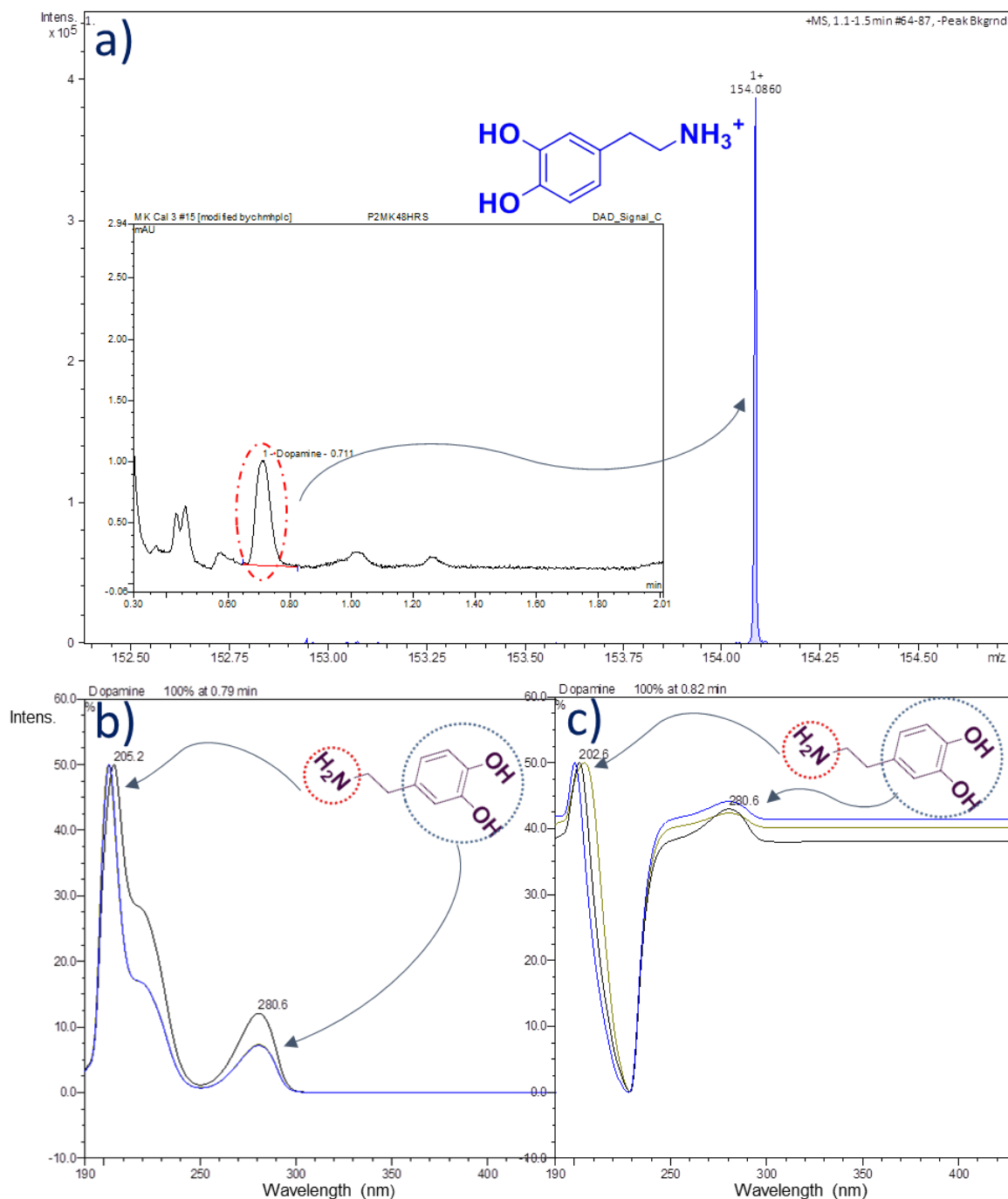


Figure 4.9. (a) Representative ESI-MS spectrum of the samples obtained from HPLC analyses (inset), showing that the m/z of the released sample matched the m/z of a dopamine ion. (b) Representative UV spectra of pure dopamine and (c) representative UV spectra of dopamine samples that were released from particles. (The characteristic peaks (amine group UV absorption band at 205 nm and phenol group UV absorption band at 280 nm) are present in free dopamine and released samples).

The free, un-oxidised dopamine exhibits spectral properties, and a molecular weight, that are different from the oxidation products of dopamine [45]. ESI-MS analyses of the fractions collected by HPLC, whose retention time corresponded to the retention time of free dopamine, confirmed the release of dopamine, ($m/z = 153$) (Figure 4.9 a). This was confirmed from the UV spectra of the dopamine that was released from particles. The absorption band of the amino group (*ca.* 205 nm - 230 nm) and the absorption band of the phenolic group (*ca.* 280 nm), can be seen in the UV absorption spectrum of the free dopamine (Figure 4.9 b) and also in the UV absorption spectrum of the dopamine that was released from particles (Figure 4.9 c).

The results of the release experiments demonstrate that the release profile may be adapted to target particular protease enzymes. For instance, grafting an (Ala)₅-(Sar)₁₅ from a therapeutic initiator, may be used to target diseases that are linked with the presence of enhanced elastase concentrations at the disease site. These include non-healing chronic wounds, atherosclerosis, pulmonary emphysema and cystic fibrosis [46, 47]. Alternatively, an appropriate enzyme, that is capable of hydrolysing the peptide bonds present within the polymer structure, may be encapsulated within the particles, to release the therapeutic initiator in a controlled manner.

Biocompatibility is another important requirement of Dop-(Ala)₅-(Sar)₁₅ macromolecules and Dop-(Phe)₅-(Sar)₁₅ macromolecules if they are to be potential candidates for use as self-assembled materials, *in vivo*. Thus, *in vitro* biocompatibility studies were conducted by assessing both sets of particles, in excess, against mammalian cells (C3H mouse dermal fibroblasts). It was observed that the concentration of the macromolecules can be increased in the cell culture medium to values that are above 1000 times their respective critical aggregation concentrations whilst still retaining cell viabilities that are above 50%, over a period of 72 hours (Figure 4.10). The viability of the cells that were cultured with the particles was also evidenced by the yellow colouring of culture medium, similar to the control experiments (i.e., cells that were cultured in ideal conditions, with no particles present) (Figure 4.10, *Insets*). The colour change is consistent even at greater particle loadings. This change of colour of the DMEM medium, from the initial pink colour to a yellow colour, is expected of viable cells, showing the occurrence of a metabolic process.

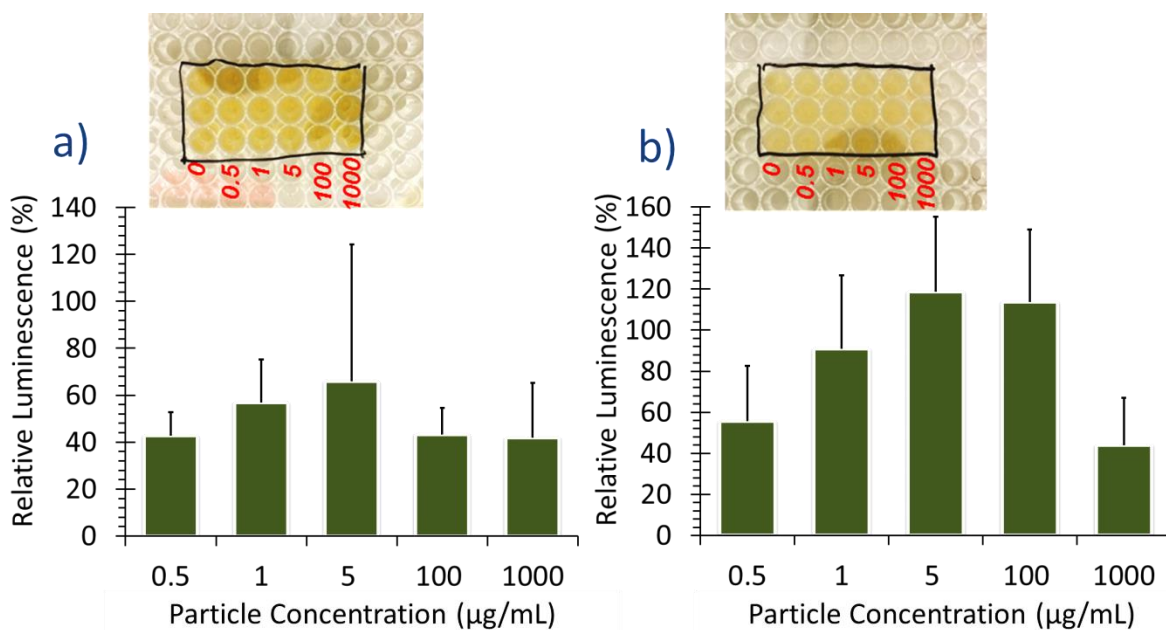


Figure 4.10. The determination of the cytotoxicity of, (a) Dop-(Ala)₅-(Sar)₁₅ particles and (b) Dop-(Phe)₅-(Sar)₁₅ particles against C3H mouse dermal fibroblasts (5×10^4 cells) over a period of 72 hours. Data ($n=3$) were collected as counts per second (cps) and are presented as % mean cps \pm 95% CL [(2-way ANOVA ($p < 0.05$) and the Tukey method for computing mean square deviation (MSD) [48].

4.4. Conclusions

NCA ROPs that were initiated from a model therapeutic molecule have been used as a highly effective strategy for the creation of monodisperse particles that were able to selectively release the covalently-loaded dopamine, in a controlled manner. The direct, one-pot, grafting of amphiphilic block copolymers from dopamine enables the achievement of facile payload loading within the self-assembled structures. The biodegradable and biocompatible shells of the structures are susceptible to selective degradation by enzyme-mediated hydrolysis, resulting in dopamine release upon protease interaction and activity. The process is tuneable, allowing control over the release to be realised profile in response to particular target proteases by altering the peptide component of the structures formed. It is anticipated that this NCA ROP-based delivery strategy could be applied to the encapsulation and subsequent controlled delivery of a wide-range of therapeutic initiators that are associated with the treatment of numerous diseases.

4.5. References

1. Ge, Z. and Liu, S. *Chem Soc Rev.* **2013**, 42, 7289-325.
2. Yu, S., He, C., Ding, J., Cheng, Y., Song, W., Zhuang, X. and Chen, X. *Soft Matter.* **2013**, 9, 2637-2645.
3. Thornton, P.D. and Heise, A. *J. Am. Chem. Soc.*, **2010**, 132, 2024-2028.
4. Schroeder, A., Heller, D.A., Winslow, M.M., Dahlman, J.E., Pratt, G.W., Langer, R., Jacks, T. and Anderson, D.G. *Nat Rev Cancer.* **2012**, 12, 39-50.
5. Mura, S., Nicolas, J. and Couvreur, P. *Nat Mater.* **2013**, 12, 991-1003.
6. Xiao, D., Jia, H.-Z., Zhang, J., Liu, C.-W., Zhuo, R.-X. and Zhang, X.-Z. *Small.* **2014**, 10, 591-598.
7. Yu, Z., Li, N., Zheng, P., Pan, W. and Tang, B. *Chem. Commun.*, **2014**, 50, 3494-3497.
8. Byrne, M., Thornton, P.D., Cryan, S.-A. and Heise, A. *Polym. Chem.*, **2012**, 3, 2825-2831.
9. Li, J., Han, Y., Chen, Q., Shi, H., ur Rehman, S., Siddiq, M., Ge, Z. and Liu, S. *J. Mater. Chem. B.*, **2014**, 2, 1813-1824.
10. Yang, P., Li, D., Jin, S., Ding, J., Guo, J., Shi, W. and Wang, C. *Biomaterials.* **2014**, 35, 2079-2088.
11. Coll, C., Mondragón, L., Martínez-Mañez, R., Sancenón, F., Marcos, M.D., Soto, J., Amorós, P. and Pérez-Payá, E. *Angew. Chem. Int. Ed.*, **2011**, 50, 2138-2140.
12. Thornton, P.D., Billah, S.M.R. and Cameron, N.R. *Macromol. Rapid Commun.*, **2013**, 34, 257-262.
13. Thornton, P.D. and Heise, A. *Chem. Commun.*, **2011**, 47, 3108-3110.
14. Su, T., Tang, Z., He, H., Li, W., Wang, X., Liao, C., Sun, Y. and Wang, Q. *Chem. Sci.*, **2014**, 5, 4204-4209.
15. Zhang, C., Pan, D., Luo, K., She, W., Guo, C., Yang, Y. and Gu, Z. *Adv Healthc Mater.*, **2014**, 3, 1299-1308.
16. Zelzer, M., Todd, S.J., Hirst, A.R., McDonald, T.O. and Ulijn, R.V. *Biomater. Sci.*, **2013**, 1, 11-39.
17. Hadjichristidis, N., Iatrou, H., Pitsikalis, M. and Sakellariou, G. *Chem. revs.*, **2009**, 109, 5528-5578.
18. Huang, J. and Heise, A. *Chem. Soc. Revs.*, **2013**, 42, 7373-7390.
19. Habraken, G.J.M., Heise, A. and Thornton, P.D. *Macromol. Rapid Commun.*, **2012**, 33, 272-286.
20. Krannig, K.-S. and Schlaad, H. *Soft Matter.* **2014**, 10, 4228-4235.
21. Wibowo, S.H., Sulistio, A., Wong, E.H.H., Blencowe, A. and Qiao, G.G. *Chem. Commun.*, **2014**, 50, 4971-4988.
22. Deng, Z., Habraken, G.J.M., Peeters, M., Heise, A., de With, G. and Sommerdijk, N.A.J.M. *Soft Matter.* **2011**, 7, 9685-9694.
23. Yan, S., Zhang, K., Liu, Z., Zhang, X., Gan, L., Cao, B., Chen, X., Cui, L. and Yin, J. *J. Mater. Chem. B.* **2013**, 1, 1541-1551.
24. Safari, J. and Zarnegar, Z. *J. Saudi Chem. Soc.*, **2014**, 18, 85-99.
25. He, X., Wu, X., Gao, C., Wang, K., Lin, S., Huang, W., Xie, M. and Yan, D. *React. Funct. Polym.*, **2011**, 71, 544-552.
26. Han, F.Y., Thurecht, K.J., Whittaker, A.K. and Smith, M.T. *Front Pharmacol.*, **2016**, 7, p.185.
27. Chen, H., Khemtong, C., Yang, X., Chang, X. and Gao, J. *Drug Discov Today.* **2011**, 16, 354-360.
28. Honglwan, A., Ni, H., Weissman, D. and Yang, S. *Polym. Chem.*, **2013**, 4, 3667-3675.
29. Cheng, H.-C., Ulane, C.M. and Burke, R.E. *Neurol. Ann.*, **2010**, 67, 715-725.
30. Habraken, G.J.M., Peeters, M., Dietz, C.H.J.T., Koning, C.E. and Heise, A. *Polym. Chem.*, **2010**, 1, 514-524.

31. Dimitrov, I. and Schlaad, H. *Chem. Commun.* **2003**, 2944-2945.
32. Fischer, D., Li, Y., Ahlemeyer, B., Krieglstein, J. and Kissel, T. *Biomaterials.* **2003**, 24, 1121-1131.
33. Lau, K.H.A., Ren, C., Sileika, T.S., Park, S.H., Szleifer, I. and Messersmith, P.B. *Langmuir.* **2012**, 28, 16099-16107.
34. Fetsch, C., Grossmann, A., Holz, L., Nawroth, J.F. and Luxenhofer, R. *Macromolecules.* **2011**, 44, 6746-6758.
35. Schubert, S., Delaney, J.J.T. and Schubert, U.S. *Soft Matter.* **2011**, 7, 1581-1588.
36. Dorshow, R.B., Bunton, C.A. and Nicoli, D.F. *J. Phys. Chem. A.* **1983**, 87, 1409-1416.
37. Topel, Ö., Çakır, B.A., Budama, L. and Hoda, N. *J. Mol. Liq.*, **2013**, 177, 40-43.
38. *Surfactant micelle characterization using dynamic light scattering.* <http://quimica.udea.edu.co/~coloides/Anexo1.pdf>. [Online database], [Accessed 08.04.2017].
39. Greenfield, N.J. *Anal Biochem.*, **1996**, 235, 1-10.
40. Krannig, K.-S., Sun, J. and Schlaad, H. *Biomacromolecules.* **2014**.
41. Wang, J., Yue, Y., Chen, G. and Xia, J. *Soft Matter.* **2011**, 7, 7217-7222.
42. KA, W. *Proceedings of the National Academy of Sciences of the United States of America.* **1964**, 52, 884-889.
43. Ambler, R.P. and Meadway, R.J. *Biochem. J.*, **1968**, 108, 893-&.
44. Altas, D. and Berger, A. *Biochemistry.* **1973**, 12, 2573-2577.
45. Pham, C.L.L., Leong, S.L., Ali, F.E., Kenche, V.B., Hill, A.F., Gras, S.L., Barnham, K.J. and Cappai, R. *J. Mol. Biol.*, **2009**, 387, 771-785.
46. Owen, C.A. and Campbell, E.J. *J. Leukoc. Biol.*, **1999**, 65, 137-150.
47. Grinnell, F. and Zhu, M. *J. Invest. Dermatol.* **1996**, 106, 335-341.
48. Kao, L.S. and Green, C.E. *J. Surg. Res.*, **2008**, 144, 158-170.

Chapter 5. A Vegetable Oil-Based Organogel for Use In pH-Mediated Drug Delivery

Preamble

This Chapter is based on work published as:

Khuphe M.; Mukonoweshuro B.; Kazlauciusas A.; Thornton P. D. *Soft Matter*, **2015**, 11, 9160-9167.

Abstract

Organogels that are prepared with vegetable oils as the liquid organic phase, present an excellent platform for the controlled delivery of hydrophobic guest molecules. A graft copolymer is disclosed, that is comprised of an oligo(L-serine) backbone which is linked to alkyl side-chains by hydrolytically susceptible ester bonds. The copolymer is capable of gelating edible safflower oil. The thermoresponsive organogel formed, which is non-cytotoxic, is capable of withholding guest molecules, before undergoing targeted disassembly upon incubation in solutions of acidic pH, permitting the directed release of payload molecules. The presented material offers a promising candidate for the controlled delivery of hydrophobic agents within acidic environments, such as cancer tumour sites.

5.1. Introduction

Organogels are semi-solid materials in which an organic liquid forms a continuous phase that is immobilised within an extensive three-dimensional (3D) entwinement of gelator molecules (usually ≤ 5 wt. %) [1-3]. Various factors are considered when classifying organogels (Figure 5.1 5.1). Organogelation is usually achieved by warming or heating the gelator molecules in an organic liquid. The subsequent aggregation of the gelator molecules, upon cooling of the solution to below the gelation temperature (T_{gel}), yields a supersaturated, semi-solid, self-supporting 3D network [4-7]. The entanglements in the 3D network are complemented by a balance between various intermolecular interactions, to create a stable solid-like structure. Gelator interactions within physical organogels are non-covalent, and include dispersion forces, hydrogen bonds, π - π stacking and dipole-dipole interactions [8, 9]. Some of the

common chemical groups which are found in gelator molecules include amides and ureas (for complementary hydrogen bonding), long chain alkanes (for van der Waals forces and solvophobic forces), nucleobases (for π - π stacking and hydrogen bonds) and hydroxyl groups (for hydrogen bonding) [6].

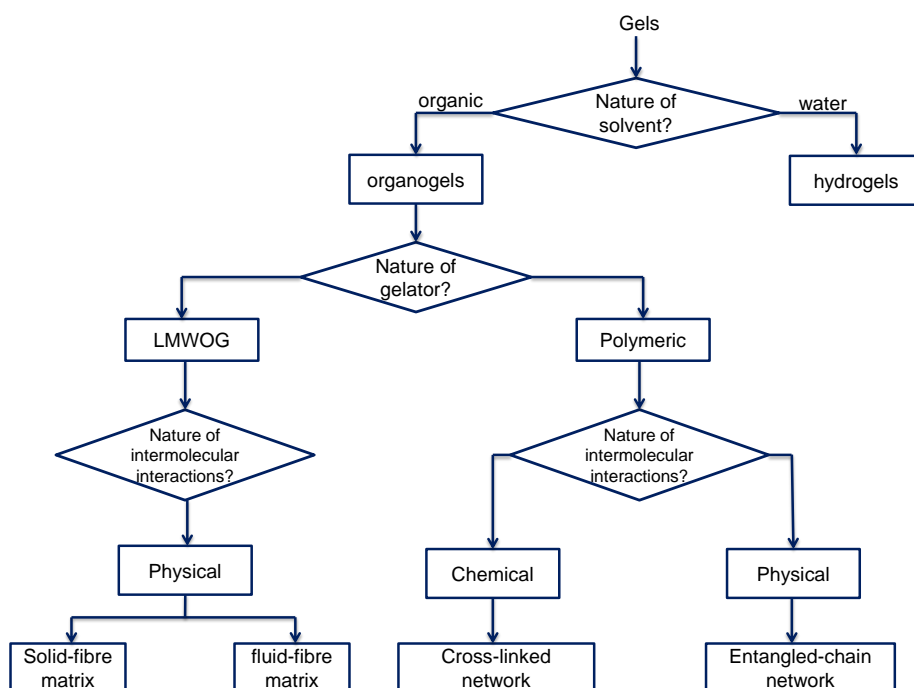


Figure 5.1. Classification of gels, in particular, organogels. *Adapted from* [5, 10].

The vast network that organogels present ensures their significant potential in employment as contemporary biomaterials, including their use as vehicles for the delivery of unbound drug molecules. Physical organogels entrap solvent molecules within a mesh that is fashioned by non-covalent interactions between polymer chains, dictating that the formation of such gels is often thermally reversible [11]. This feature may readily be utilised within an injectable drug delivery system that flows during injection, before undergoing thermally-mediated gelation within the body [12]. Additionally, organogels possess non-susceptibility to microbial attack because, unlike the aqueous phase within hydrogels, the organic phase can inhibit microbial contamination [13].

Despite these advantageous features, the application of organogels within a biomedical context has been hindered largely because of the cytotoxicity that is associated with numerous organic solvents. For example, the majority of organogels that have been reported have been

formed using solvents such as acetone [14], THF [15], toluene [16], propanol [8], chloroform [16], hexane [17], benzene [18], methanol [19], dichloromethane [16], acetonitrile [14, 16] and DMF [20]. Most of these solvents are either irritants, carcinogens, mutagens, teratogens or acute toxicants. Consequently, organogels have more commonly been employed within non-biological settings, such as in oil spill clean-up [2, 17, 18, 21], dye spill clean-up [22, 23], electronic sensors [24-29] and in fuel cells for energy harvesting [30, 31].

Bhattacharya *et al.* [32] reported the phase-selective gelation of alanine-based amphiphilic gelators for the recovery of oil spills from water. Basak *et al.* [18] formulated organogels using a phenylglycine amphiphile that was derivatised with a long fatty acyl chain. This gelator was phase-selective as it preferentially gelled the organic phase and, thus could be recovered from an oil-in-water emulsion. Some of the oils that were gelled include paraffin, kerosene, diesel, petroleum-benzene. Recently, Soner *et al.* [17] created a range of poly(alkoxysilane) gelators by reacting 1,3-benzenedimethanol with alkoxysilane monomers of different chain lengths. The polymers obtained preferentially absorbed various organic solvents and oils from water. These include, petrol, diesel oil and cyclohexane. Mukherjee *et al.* [2] synthesised two β -glycoside organogelators that were derived from an eco-friendly per-*O*-acetylated glucosamine. These organogelators were phase selective too, and could gel organic liquids at ambient conditions. Other organogel systems that have been shown to possess potential application in oil spill-recovery have been reported by Trivedi and Dastidar [33], Zhang *et al.* [30, 31], Jadhav *et al.* [34] and Pathrap and Sureshan [35].

Recently, Mukherjee and Mukhopadhyay [22] synthesised a galactose-based phase-selective organogelator that not only showed potential for use in oil spill-recoveries, but also was able to adsorb preferentially dye molecules from water. Debnath *et al.* [23] synthesised dipeptide-based gelators that were derivatised with alkyl groups of various chain lengths. These self-assembled into organogels that were able to adsorb dye molecules from water. The use of organogels is widespread in energy harvesting cells, where they can be used as scaffolds in organic-based electronic devices and in photonic devices, e.g. fuel cells and solar cells [30, 31]. The principle involves the use of conjugated (chromophoric) gelators e.g., oligo(*p*-phenylenevinylene), that can self-assemble in suitable organic liquids to form 3D networks, through which energy (electrons) can flow from one end (donor) and be harnessed by

connecting the scaffold to a suitable acceptor [36-40]. The use of organogels in fuel cells has been reported by several authors. These include Sangeetha and Maitra [41], Desvergne *et al.* [42], Ishi-i and Shinkai [43], Sagawa *et al.* [44], Yang *et al.* [45], Nakashima and Kimizuka [46], Sakamoto and Dunn [47] and Sivakkumar *et al.* [48].

Due to their reversible nature and their ability to respond to various stimuli (thermo, pH, photo, humidity or moisture, etc.), supramolecular organogels show great potential for use in sensors [24, 25, 30]. For example, the sensitivity of the gel system can be tuned by incorporating stimuli-responsive functional groups into the design. Typical examples are azobenzyl units and anthraceny units that can be used to achieve photo-responsivity through photo-isomerisation, while pH-responsiveness may be achieved by incorporating acidic or basic sites in the organogel structure [49]. For example, Shinkai *et al.* [25] designed a stimuli-response organogelator by coupling chromophoric perylene bismide groups to cholesterol. The resultant organogel matrix could be used in fluorescence-based sensors. Other examples of organogels in sensing applications have been disclosed [26-29, 50].

Vegetable oils offer an alternative to conventional organic solvents for use as the continuous phase and may permit the creation of non-cytotoxic organogels that were suitable for application *in vivo*. Examples of vegetable oil-based organogels include organic gelators that are dispersed within sunflower oil [51], safflower oil [52] and linseed oil [53]. Barbut and co-workers demonstrated that an ethylcellulose-canola oil organogel was a potential replacement for the animal fat in frankfurters [54]. Also, Marangoni and co-workers demonstrated the use of canola oil as the solvent in 12-hydroxystearic acid-containing organogels that displayed tuneable crystallinity and oil binding capacity, depending on their storage temperature [55]. The use of organogels as biomaterials is more limited. Leroux and co-workers reported the formation of a number of alanine methyl ester-terminated fatty acid organogelators [56]. They revealed that *N*-lauroyl-L-alanine and the *N*-lauroyl-L-alanine methyl ester could independently gelate soybean oil to yield organogels that may be used in the controlled release of dextran molecules [57]. Additionally, biocompatible *N*-stearoyl-L-alanine methyl ester organogels that were formed in the presence of safflower oil showed promise for the controlled delivery of rivastigmine [58]. Lukyanova *et al.* [59] reported the formation of an organogel consisting of 12-hydroxystearic acid as the gelator within non-toxic soybean oil. The

organogel formed, which was susceptible to degradation by lipase enzymes, was able to support the attachment and proliferation of Chinese hamster ovary fibroblast cells, highlighting the potential that the material possesses for application as a scaffold for tissue engineering. Work by Kakemi and co-workers demonstrated the use of 12-hydroxystearic acid-soybean oil organogels in the delivery of lipophilic drug molecules [60] and hydrophilic drug molecules [61]. Lipase-mediated organogel degradation resulted in payload release, which was also demonstrated *in vivo*.

Biomaterials which are intended for drug delivery applications *in vivo* are required to be biocompatible and to be able to undergo programmed biodegradation [62, 63]. Poly(amino acid)s form a class of macromolecule that offer both traits, and may be synthesised in a highly-controlled manner by *N*-carboxyanhydride ring-opening polymerisation (NCA ROP) reactions [64-66]. In addition, amino acids offer an extensive array of functional groups, including carboxylic acid, amino, thiol and hydroxyl groups, that translate to the corresponding polymer [67]. These enable the facile post-polymerisation functionalisation of poly(amino acid)s with groups that facilitate their hierarchical self-assembly into precisely defined, nano and microstructures that may be exploited for use as drug delivery vehicles [68, 69].

Organogels that have been formed from poly(amino acid) gelators, dispersed in vegetable oils, have the potential to comprise an extremely effective class of drug delivery vehicle. If designed and synthesised appropriately, such materials offer biocompatibility and biodegradability, in addition to being created from renewable sources. This Chapter details the synthesis and characterisation of a novel organogel that was formed from a poly(amino acid)-containing polymer, dispersed within edible safflower oil. A graft copolymer consisting of an oligo(L-serine) (Oligo(Ser)) backbone, conjugated with pendant octadecanoic acid branches, acts as a biodegradable gelator, that is susceptible to hydrolysis under acidic conditions. The organogel formed is thermoresponsive and possesses the ability to encapsulate a molecular cargo, before undergoing acid-induced degradation and consequent payload release. The material generated is a candidate for use as an injectable drug carrier vehicle for the controlled delivery of non-polar therapeutic agents, within acidic environments, such as cancerous tissue zones [70] and the vagina [71] and may possess further scope in use as a scaffold for tissue engineering.

5.2. Experimental

5.2.1. Synthesis of *O*-Benzyl-L-Serine (Ser(OBz) NCA

The synthesis of Ser(OBz) NCA is described in Chapter 3.3.1.

5.2.2. Synthesis of Oligo(Ser(OBz))

The NCA of Ser(OBz) (830 mg, 3.74 mmol) was dissolved in anhydrous DMF (20 mL) in a nitrogen-purged Schlenk tube that was equipped with a magnetic stirrer bar. To this, a solution of benzylamine (20 mg, 0.19 mmol) in anhydrous DMF (10 mL) was added. The reaction stirred under an inert nitrogen atmosphere, at room temperature for 96 hours. The product was subsequently precipitated in cold diethyl ether and isolated by centrifugation. The recovered solid product was washed three times using cold diethyl ether, dialysed against distilled water and subsequently lyophilised to obtain the polymer. Yield: 422.6 mg, 62 wt. %. ¹H NMR (500 MHz, TFA-d, ppm): 8.53 (NH), 7.45 - 7.30 (ArH), 5.04 - 4.81 (αCH), 4.81 - 4.49 (Ar-CH₂O), 4.35 - 3.79 (CHCH₂O). FTIR $\nu_{\max}/\text{cm}^{-1}$ (solid): 3278 cm^{-1} (NH), 2929 (C-H, Ar), 1822 (C=O), 1423 (C=C, Ar), 1255 (O-C=O).

5.2.3. Deprotection of Oligo(Ser(OBz))

Oligo(Ser(OBz)) (350 mg) was weighed into a 50 mL round bottom flask that was equipped with a magnetic stirrer bar. Trifluoroacetic acid (7 mL) was added to dissolve the polymer. 3 mL of an HBr solution in acetic acid (33 wt. %) was added and the solution was left to stir at room temperature for 16 hours. The polymer was then precipitated in cold diethyl ether (100 mL) and isolated by centrifugation. The recovered polymer was washed three times using cold diethyl ether and subsequently dried *in vacuo* (30 °C) for 48 hours. Yield: 87 wt. %. GPC (DMF + LiBr, PMMA standards): $M_n = 1862$, $M_w = 1959$, PDI = 1.05. ¹H NMR (500 MHz, TFA-d, ppm): 8.52 (NH), 7.45 - 7.30 (ArH), 5.04 - 3.79 (αCH, CH₂OH, Ar-CH₂). ESI-MS in DMSO (1847 Da, M⁺ H⁺). FTIR $\nu_{\max}/\text{cm}^{-1}$ (solid): 3278 cm^{-1} (NH), 1822 (C=O, amide). Elemental Analysis: Carbon (36.5%), Nitrogen (12.1%), Hydrogen (5.40%).

5.2.4. Synthesis of Poly[(Ser)-*g*-Octadecanoic Acid] (PSOA)

Octadecanoic acid (1.54 g, 5.41 mmol) was dissolved in anhydrous DMF (10 mL). The solution was injected into a 100 mL round bottom flask sealed with a rubber septum and nitrogen-

purged. Oligo(Ser) (250 mg, 0.134 mmol) was dissolved in anhydrous DMF and the solution was added to the reaction mass. 4-Dimethylaminopyridine (DMAP) (33.1 mg, 0.271 mmol) was dissolved in anhydrous DMF (10 mL) and also added to the reaction mass. The reaction was cooled to 0 °C. Dicyclohexylcarbodiimide (DCC) (0.670 g, 3.25 mmol) was dissolved in anhydrous DMF (10 mL) and the solution was added dropwise to the cooled reaction over a period of 15 minutes. The reaction was stirred at 0 °C for a further 30 minutes and then allowed to proceed at room temperature for 48 hours. The precipitated dicyclohexylurea (DCU) was then isolated by filtration. The filtrate was added drop-wise to cold diethyl ether (500 mL) and the precipitate obtained was isolated by centrifugation (6000 rpm, 20 min, -10 °C) and dialysed ($MWCO = 2000$ Da) against distilled water for 72 hours. The product was subsequently recovered by lyophilisation. Yield: 77.3 wt. %. $^1\text{H NMR}$ (500 MHz, TFA-d, ppm): 8.53 (NH), 7.45 - 7.30 (ArH), 5.04 - 3.79 (αCH , CH_2OH , Ar- CH_2), 2.22 - 2.64 (CH_2) $_2$ COO), 1.53 - 1.41 (CH_2) $_{14}$, 0.99 - 0.97 (CH_3). Elemental Analysis: Carbon (69.4%), Nitrogen (5.10%), Hydrogen (10.7%). FTIR $\nu_{\text{max}}/\text{cm}^{-1}$ (solid): 3278 cm^{-1} (NH), 2917 (C-H, alkyl stretch), 1822 (C=O, amide).

5.2.5. Rheological Studies

Limited rheological measurements were carried out at 37 °C using a stress-controlled AR 1500ex rheometer (TA instruments). The instrument was equipped with steel-parallel plate geometry (40 mm in diameter). The geometry gap distance was maintained at 0.05 mm. Gelation was carried out on the plate of the rheometer. Then the linear viscoelastic region (LVER) of the gel sample was determined by conducting a stress sweep test at a constant frequency (6.28 rad/s). The storage modulus (G') and the loss modulus (G'') were determined by performing a frequency sweep test (0.1 rad/s to 628 rad/s) at a constant stress (5 Pa).

5.2.6. Preparation of Xerogels

A previously reported procedure was adopted in the preparation of xerogels that would be suitable for analysis by SEM [35]. Briefly, organogel samples were immersed in n-hexane/acetone solutions (8:2 v/v) for a period of 24 hours to induce the extraction of the vegetable oil from the gel matrix. The obtained xerogels were subsequently mounted carefully onto SEM stubs using conducting tap, then allowed to air-dry, prior to sputter-coating with a thin layer of gold as described in Chapter 2.17.

5.2.7. Preparation of Organogel-Coated Cell Culture Wells

A 2 wt. % composition of organogel was prepared by dispersing PSOA (36.5 mg) in safflower oil at 50 °C (1.79 g). A 50 µg/mL solution of type 1 rat tail collagen was prepared in PBS solution and then pH-adjusted to pH 7. Two sets of triplicate wells per a 96-well microplate were either coated at their internal base with the organogel (30 µL per well), rat tail collagen (30 µL per well) or left uncoated (i.e. Nunclon Δ™ surface). One more set of triplicate wells was coated with a cyanoacrylate ('super glue') (30 µL per well). All the coated microplates were incubated for 3 hours at room temperature, in a class II biohazard cabinet, prior to use.

5.2.8. Cell-Seeding

Mammalian cells were cultured as detailed in Chapter 2.19. Then, triplicate wells, coated with PSOA–safflower oil organogel, type 1 rat tail collagen, Nunclon Δ™ surface and a cyanoacrylate were seeded with 5×10^4 C3H mouse dermal fibroblasts, respectively (Figure 5.2). Dulbecco's Modified Eagle Medium (DMEM) supplemented with a 10% (v/v) foetal bovine serum, L-glutamine (1 mM) and penicillin (100 U/mL)-streptomycin (100 µg/mL) solution was then added to bring the total volume in each well to 200 µL. In another set of triplicate wells that were coated with the PSOA-safflower oil organogel, type 1 rat tail collagen and Nunclon Δ™ surface, no cells were seeded but the wells were filled with DMEM (200 µL). Empty peripheral wells were filled with sterilised PBS solution to keep the environment humid and to reduce evaporation from the seeded wells. The seeded microplates (×3) were incubated in a humidified incubator at 37 °C and 5% (v/v) CO₂ in air for 24 hours, for 72 hours and for 120 hours, respectively.

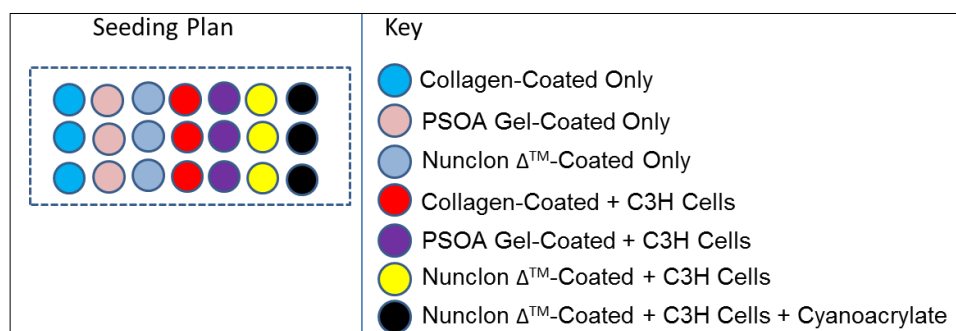
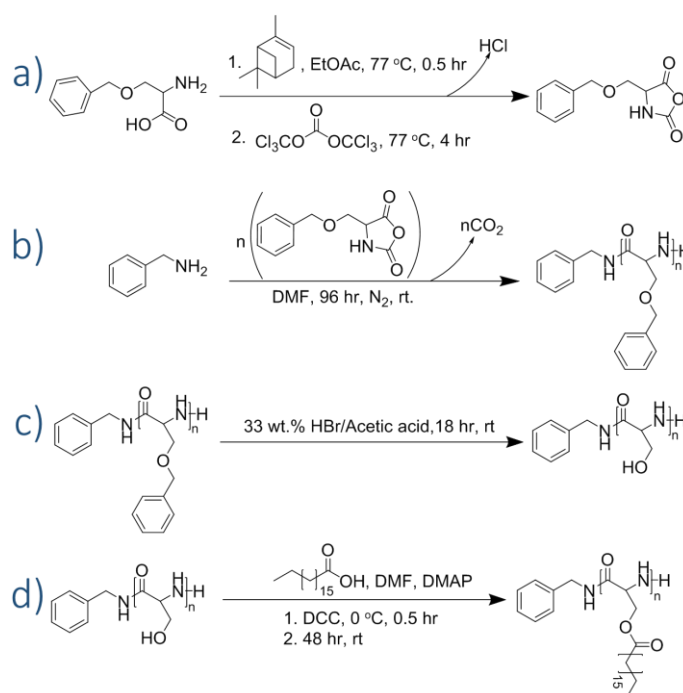


Figure 5.2. General illustration of the plate-coating and cell-seeding layout plan in the biological analyses (Only the experimental wells from a 96-well microplate are shown).

5.3. Results and Discussion

A polymer gelator was synthesised, that was designed to possess the ability to form hydrogen bonds between adjacent poly(amino acid) backbone chains [72], and to form hydrophobic interactions between adjacent, grafted, alkyl chains [6], thus facilitating organogel formation. Initially, Ser(OBz) NCA was synthesised in high purity by following the Fuchs-Farthing method (Scheme 1 a) (Chapter 3.3.1).



Scheme 5.1. The synthesis route to the PSOA gelator. (a) Synthesis of the NCA of Ser(OBz), (b) synthesis of oligo(Ser(OBz)) by NCA ROP, (c) deprotection of oligo(Ser(OBz)) in hydrobromic acid solution and (d) post-polymerisation modification of oligo(Ser) by Steglich esterification, yielding the PSOA gelator.

Oligo(Ser(OBz))₂₀ was then synthesised by the ROP of Ser(OBz) NCA, using benzylamine as the initiator (Scheme 5.1 b). Following the polymerisation, the benzyl ether protecting group was cleaved from the polymer using hydrobromic acid solution (Scheme 5.1 c), as confirmed by ¹H NMR spectroscopy (Figure 5.3) and by FTIR spectroscopy (Figure 5.4 a, b). The former displayed a substantial reduction in the integration value that corresponds to aromatic protons; the peaks remaining can be attributed to the aromatic protons of the benzylamine initiator. FTIR spectroscopy revealed a reduction in the strength of the signal for the peaks that correspond to aromatic C-H bending (862 cm⁻¹ - 685 cm⁻¹).

The molecular weight of oligo(Ser) was calculated from ^1H NMR by comparing the integration value of the aromatic protons of benzylamine (7.45 ppm - 7.30 ppm) with the integration value of the protons that are bonded to the α -carbons of the amino acid repeat units (5.04 ppm - 4.81 ppm), and was 1773.1 g/mol. A comparable value was obtained using GPC (1862 g/mol) (Figure 5.5) and ESI MS (1847 g/mol), suggesting further the complete polymerisation and complete removal of the benzyl ether protecting groups. ESI MS revealed a fragmentation pattern that is characterised by an increment of 87 m/z, representative of the Ser repeat unit (Figure 5.6).

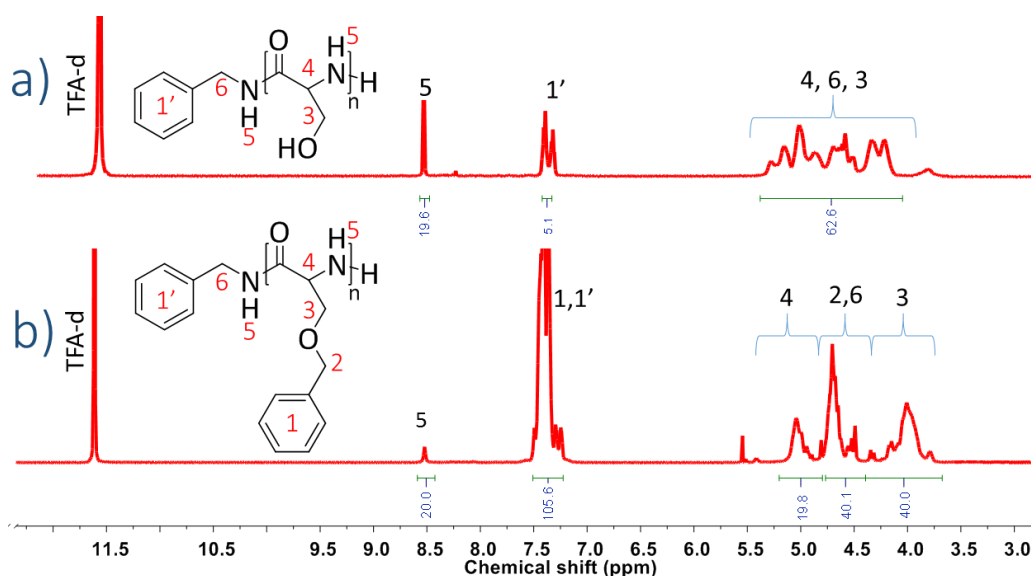


Figure 5.3. ^1H NMR spectra of oligo(Ser) after deprotection of the Ser side groups to expose the hydroxyl groups (a), and of oligo(Ser(OBz)) before carrying out the deprotection (b).

The PSOA gelator was then obtained by grafting octadecanoic acid molecules to the hydroxyl groups of oligo(Ser) (Scheme 5.1 d) by DCC-mediated esterification. The use of FTIR spectroscopy confirmed the successful grafting of octadecanoic acid by revealing the presence of a strong signal at *ca.* 2917 cm^{-1} , which is characteristic of the CH_2 alkyl chain (Figure 5.4 c). ^1H NMR analysis revealed further that alkyl grafting had occurred by displaying peaks that are characteristic of the alkyl chain of octadecanoic acid (i.e., from 0.97 ppm - 2.22 ppm, Figure 5.7). The DSC thermogram of octadecanoic acid (Figure 5.4 d) reveals a thermal transition corresponding to the melting point endotherm (71.5 $^\circ\text{C}$). This thermal transition is present in the thermogram of the derivatised polymer (Figure 5.4 f), but is absent from the thermogram of PS (Figure 5.4 e), further confirming successful esterification. The successful grafting of alkyl

chains was also demonstrated by an increase in the overall carbon content from 36.5 % to 69.4 % when the oligo(Ser) was converted to PSOA, as determined by elemental analysis (Table 5.1).

Table 5.1. Atomic composition of oligo(Ser) and the PSOA gelator

	% Carbon	% Nitrogen	% Hydrogen
Oligo(Ser)	36.5	12.1	5.35
PSOA	69.4	5.1	10.7

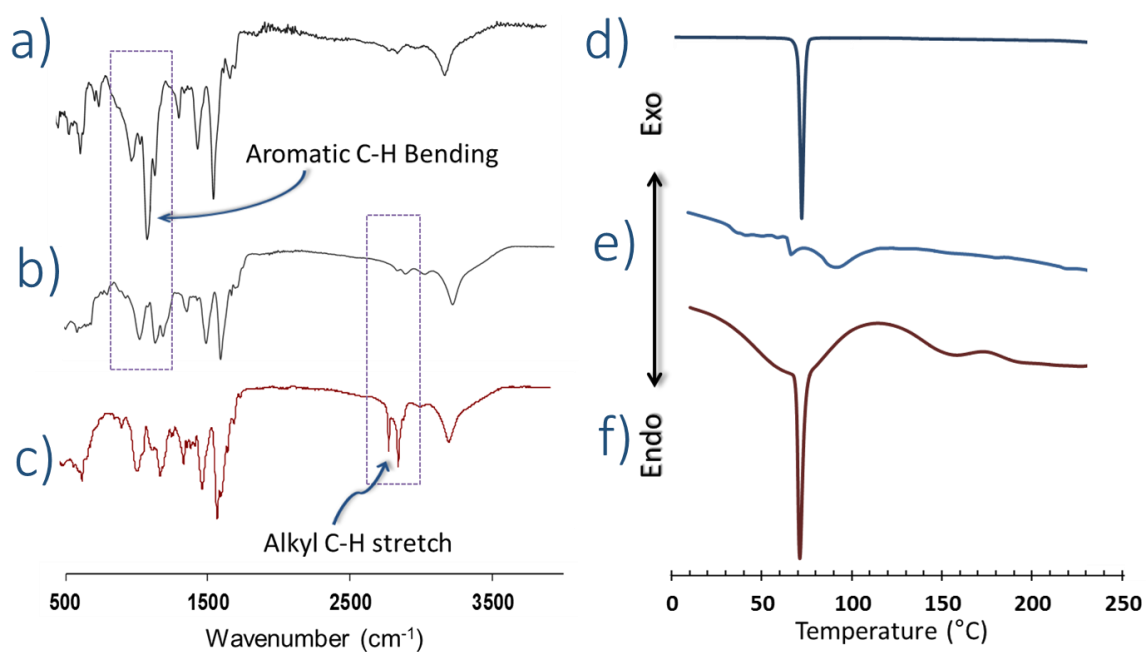


Figure 5.4. FTIR spectra of oligo(Ser(OBz)) (a), and of the deprotected oligo(Ser) (b) showing the diminishing of the aromatic C-H bends arising from the removal of the benzyl groups. Successful grafting of octadecanoic acid is evidenced by the emergence of a C-H alkyl stretch emanating from the octadecanoic acid component (c). The DSC thermograms obtained from the analysis of octadecanoic acid (d), oligo(Ser) (e) and the PSOA gelator (f). (Endo = endotherm, Exo = exotherm).

The grafting of alkyl groups to the oligo(Ser) side groups was accompanied by an increase in the overall hydrogen content and a decrease in the nitrogen content. By comparing the overall carbon content of PSOA to the theoretical carbon content that equates to complete oligo(Ser) modification, the grafting efficiency was calculated to be 97.3 %.

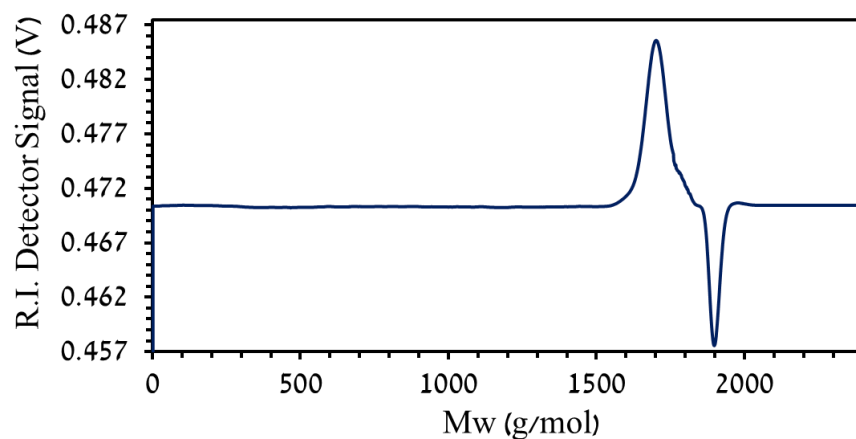


Figure 5.5. GPC trace of oligo(Ser).

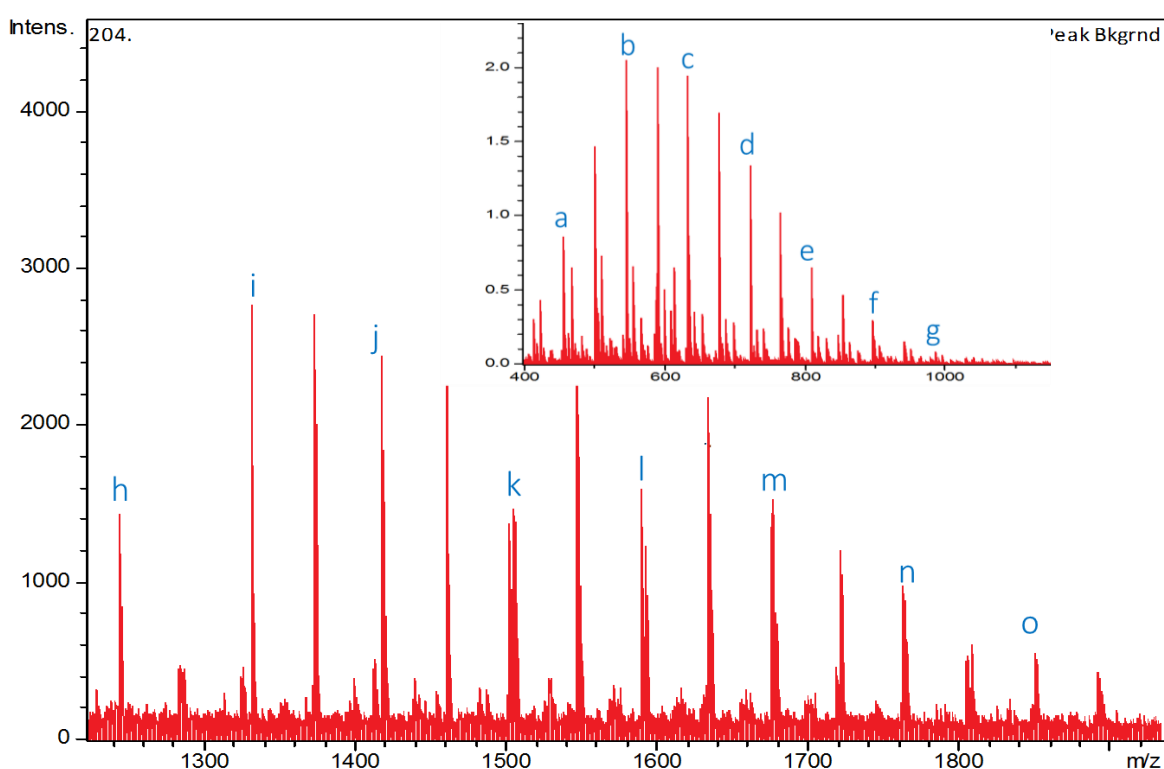


Figure 5.6. ESI-MS fragmentation pattern obtained from oligo(Ser). The lettered peaks may be assigned to the various fragments of the macromolecule; a: Benzylamine (Benz)-(Ser)₄, b: Benz-(Ser)₅, c: Benz-(Ser)₆, d: Benzylamine-(Ser)₇, e: Benz-(Ser)₈, f: Benz-(Ser)₉, g: Benz-(Ser)₁₀, h: Benz-(Ser)₁₃, i: Benz-(Ser)₁₄, j: Benz-(Ser)₁₅, k: Benz-(Ser)₁₆, l: Benz-(Ser)₁₇, m: Benz-(Ser)₁₈, n: Benz-(Ser)₁₉, o: Benz-(Ser)₂₀.

Thermogravimetric analysis revealed that the grafting of alkyl chains onto oligo(Ser) conferred thermal stability to PSOA by acting as a heat-sink (Appendix 5). PSOA formation was characterised by having a low rate of weight loss when heated between 150 °C and 325 °C,

compared to unmodified oligo(Ser). As such, PSOA maintains structural integrity when subjected to elevated temperatures, within the range studied.

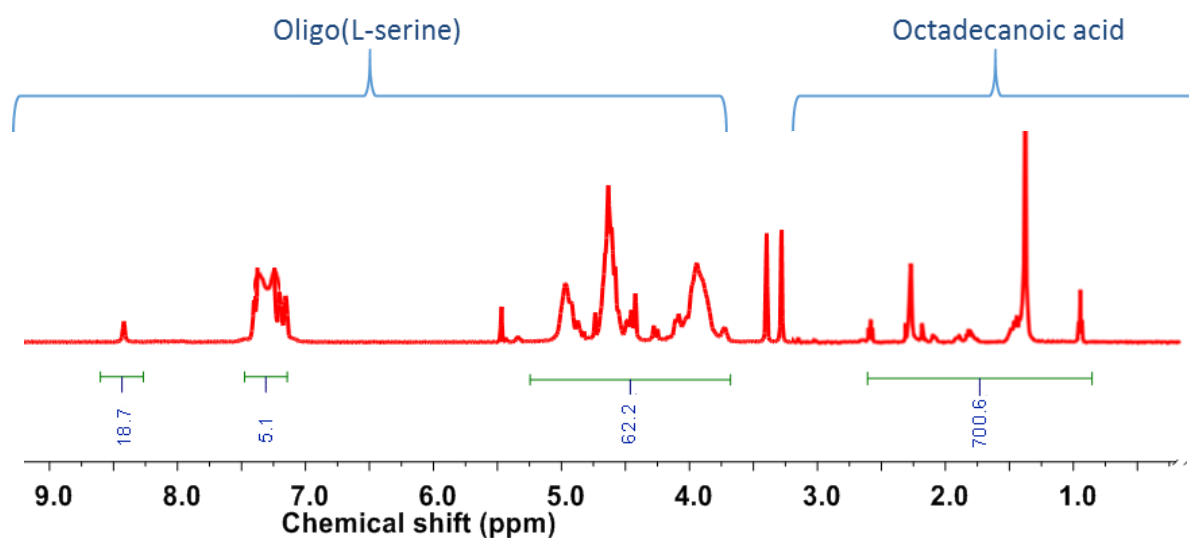


Figure 5.7. ¹H NMR of PSOA gelator showing new peaks to have emerged in the region 0.97 ppm - 2.64 ppm, emanating from the grafted octadecanoic acid.

The ability of PSOA to induce the gelation of safflower oil was assessed by heating the gelator in safflower oil to achieve PSOA dissolution. Gelation was observed upon cooling, arising from the self-aggregation of the PSOA macromolecules (Figure 5.8, top). This gelation, arising as a result of the development of supramolecular hydrophobic interactions between the alkyl chains and hydrogen bonding between amino acid repeat units is illustrated in Figure 5.8. PSOA induced the gelation of safflower oil at polymer loadings of 2 wt. % or greater. DSC was employed to analyse the thermal properties of the 2 wt. % organogel using a heating cycle of between -20 °C and 80 °C as it is within the confines of the envisaged application temperatures.

The thermogram produced displayed an endotherm having a minimum point at 45.9 °C, which can be attributed to a gel/sol transition (Figure 5.9). This endothermic trough was present in six heat-cool cycles (Figure 5.10), demonstrating the thermal reversibility that the material possesses. The broad nature of the peak indicates that the aggregates are polydisperse [73]. The sol/gel transition represented as a maximum point at 37.2 °C in the cooling cycle (Figure 5.10 a). The temperature corresponding to the gel/sol (Figure 5.10 b) transition is greater than the one corresponding to sol/gel transition. This is a consequence of hysteresis behaviour, a common feature of thermoreversible organogel behaviour [74].

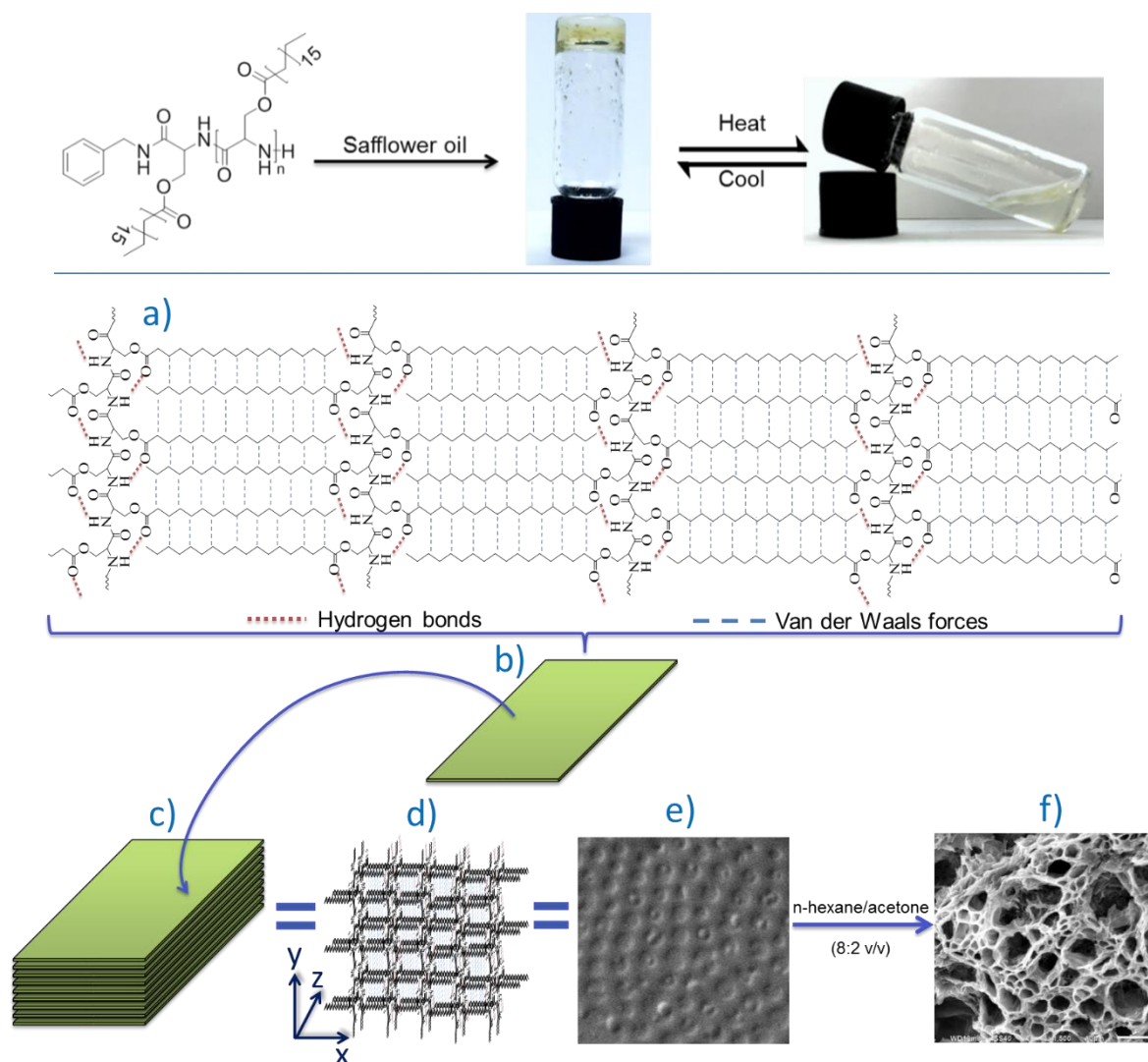


Figure 5.8. (top) PSOA forms an organogel when dispersed in safflower oil, which is thermoreversible. (a) The envisaged supramolecular interactions that take place in the PSOA-safflower oil organogel, (b) possibly resulting in planar aggregations of PSOA macromolecules, (c, d) that can stack into a 3D organogel network. (e) SEM microphotograph of the organogel in its 'wet' state (before de-oiling), showing a pattern that resembles the envisaged stacking of PSOA macromolecules and (f) a 3D SEM microphotograph of xerogels obtained after de-oiling.

A gel/sol temperature that is in excess of 37 °C is very significant for self-assembled gels that are intended for use as injectable drug delivery media, as the solution must form a gel that is capable of withholding guest molecules, *in vivo*, following injection. Additionally, it is paramount that an organogel that is intended to be applied as a scaffold for tissue engineering possesses a gel/sol temperature greater than 37 °C, to maintain its structural integrity ability to support cell growth and proliferation, *in vivo* [6].

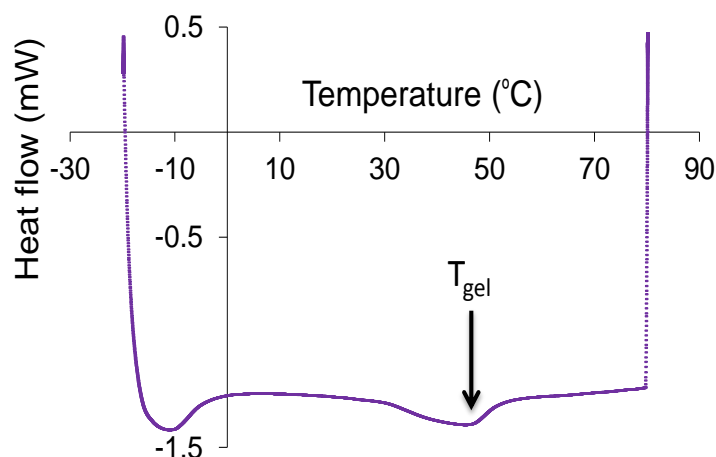


Figure 5.9. A representative DSC thermogram obtained from PSOA-safflower oil organogels reveals the sol-gel transition (T_{gel}) at 45.9 °C.

The structural integrity of the organogel was determined by measuring its weight loss upon heating, by TGA. The organogel was found to be thermally stable when heated within the confines of the envisaged application temperatures, losing only 0.29 % of its original mass when heated to 80 °C for 9 minutes (Appendix 5).

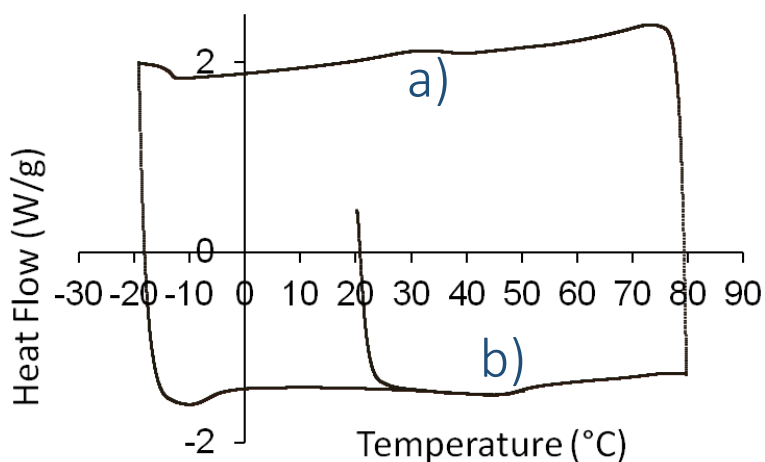


Figure 5.10. Representative DSC thermogram obtained from six heating-cooling cycles of the synthesised organogels, showing the sol/gel transition (a) and the gel/sol transition (b).

In the intended application, the porosity of the organogel would strongly influence the success of cell proliferation and of the encapsulation and the release of molecular cargoes, thus, heavily impacting upon material performance. Thus, the morphology of the 2 wt. % polymer loading organogel was assessed by imaging the xerogels of the polymers formed by SEM. The microstructure formed possessed an interconnected porous 3D network (Figure 5.11 a) with

large pores, as observed at higher magnification (Figure 5.11 b). The porous nature of the organogels confirmed their suitability for employment as a drug delivery carrier in which hydrophobic therapeutic agents may occupy the voids that would be present within the structure.

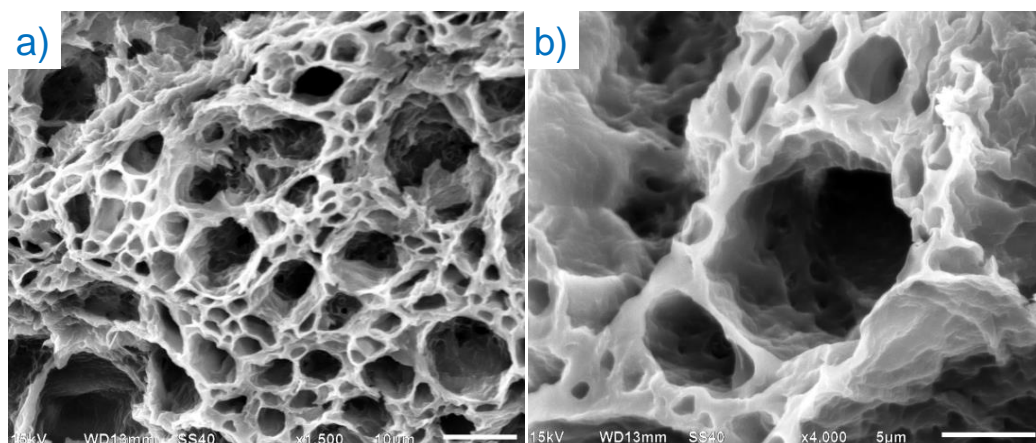


Figure 5.11. SEM micrographs showing the morphology of the 2 wt. % organogel. Scale bars represent a) 10 μm , b) 5 μm .

Rheometry was used in the determination of the properties of the organogels formed. Ideal gels behave as viscous flowing liquids over long time scales and so the storage modulus (G') must dominate the loss modulus (G'') for a composition to qualify as a gel [75]. The 2 wt. % polymer-loading organogel was used as the model sample for all of the rheometric evaluations. Initially, the linear viscoelastic region (LVER) of the gel was determined by performing an amplitude sweep at a constant angular frequency (6.28 rad/s) (Figure 5.12 a). The gel was subjected to an increasing amount of sinusoidal stress to disturb the network structure so that the material began to flow. At low stress values, the elastic modulus dominates the loss modulus by almost one order of magnitude, indicating the presence of a wholly elastic, intact organogel. Partial break-up of the organogel was evidenced by the decrease in the value of G' when the stress was gradually increased. Structural failure was more pronounced at the yield stress (35 Pa), when the gel began to flow. The limit of the LVER was noted as the point at which the storage modulus reduced to 90% of the initial value (*ca* 20 Pa). Subsequently, a frequency sweep test (Figure 5.12 b) was conducted within the limits of the LVER of the organogel by subjecting the gel to a constant stress (5 Pa). The storage modulus of the

organogel was greater than the loss modulus over the entire frequency range (0.1 - 628 rad/s) and no cross-over point was observed.

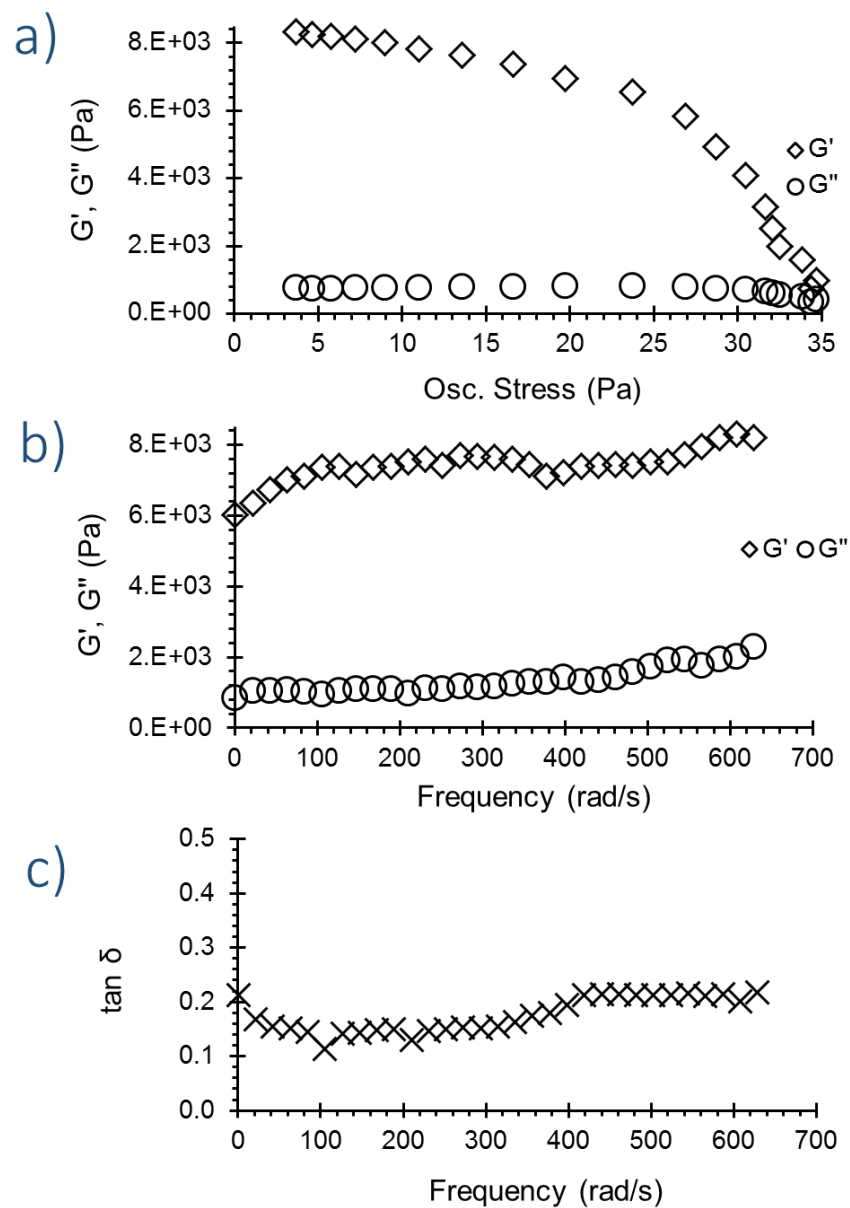


Figure 5.12. Rheological study of the PSOA-safflower oil organogel a) amplitude sweep test, b) frequency sweep test and c) variation of the tangent of the phase angle (δ) with change in frequency.

The observed elastic dominance confirms that the material possessed an internal network. Furthermore, the moduli of the organogel (both G' and G'') do not exhibit a dependency on the applied frequency, which suggests that the organogel has a good tolerance for the external forces being exerted on it. For viscoelastic materials, this is a desirable attribute as it ensures structural integrity during the application cycle. The G' value of the organogel was 8.3×10^3 Pa,

which is comparable with the G' values of other organogels, as reported in the literature [76, 77].

The loss factor ($\tan \delta$), may also be used as an indicator for the structural integrity of a deformed viscoelastic material [78]. In the current study, it was observed that, initially, $\tan \delta$ decreased slightly with an increase in frequency (Figure 5.12 c), indicating that the gel had become more elastic and dissipated less energy. The loss factor then remained nearly constant throughout the frequency sweep, with values far less than one, thereby confirming that the elastic characteristics (G') dominated the viscous characteristics (G'').

To investigate the biocompatibility of the material created, and hence the suitability of using the PSOA-safflower oil organogel as an injectable biomaterial, C3H mouse dermal fibroblasts were cultured in triplicate wells (that were coated with the 2 wt. % PSOA-safflower oil organogel) for 24 hours, for 72 hours and for 120 hours. Cells cultured on a cured super-glue (80 - 100 % (v/v) cyanoacrylate) surface and cells cultured on Nunclon Δ^{TM} -coated surfaces (tissue culture plastic) were used as controls for non-viable and for viable cells respectively. Cells were also cultured in type I collagen-coated wells as a control. Unseeded wells (filled with culture medium only) that were coated with the organogel, type I collagen and Nunclon Δ^{TM} surface, respectively, were also set up to determine whether or not any of these substrates could interfere with the ATPlite-M[®] assay.

The results obtained from the unseeded wells showed that none of the tested substrates interfered with the ATPlite-M[®] assay. After 24 hours, the results showed that the cellular ATP levels of the cells that were cultured on the organogel were not significantly different to those of cells cultured on the collagen surface and on the Nunclon Δ^{TM} surface, but were significantly different to those cultured on the cured cyanoacrylate ($p < 0.05$, 2-way ANOVA) (Figure 5.13). After 72 hours, the ATP content of all the cells, on the three test substrates, increased markedly, although no significant difference in ATP levels was found between cells that were present on the collagen and on the organogels. The ATP levels of the cells that were seeded on the Nunclon Δ^{TM} surface were significantly greater than these two substrates however (3x greater than collagen and 4x greater than the organogel). Importantly, the ATP levels of the cells seeded on the organogel quadrupled between 24 hours and 72 hours.

After 120 hours, there was no further increase in the ATP content of the cells that were cultured on the organogel (compared to 72 hours). For cells cultured on the Nunclon Δ^{TM} surface, there was a decline between 72 and 120 hours, although this was not significant. Conversely, there was a significant increase in the ATP content measured for the cells that were cultured on collagen, between 72 hours and 120 hours.

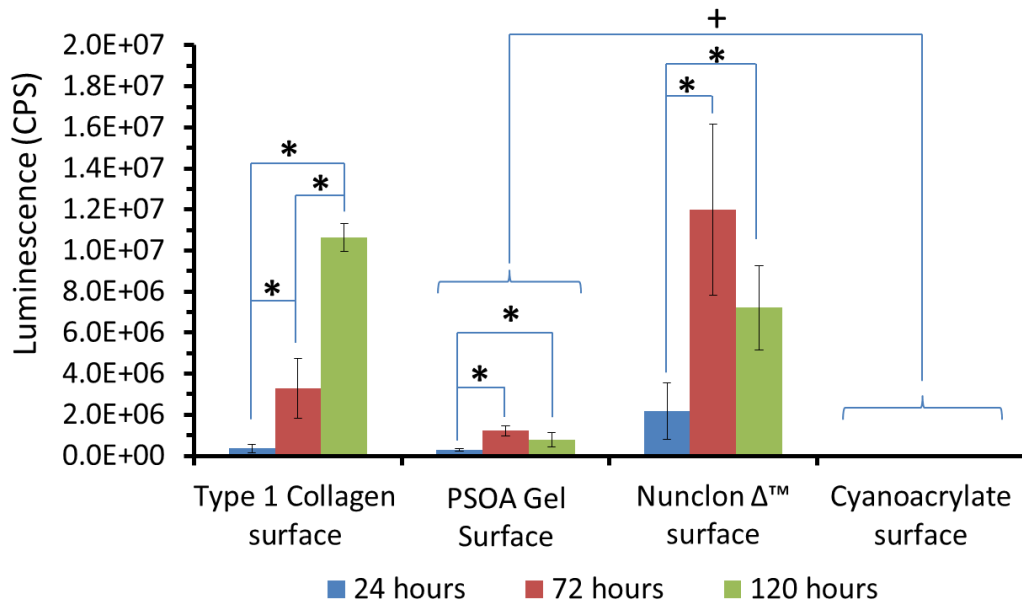


Figure 5.13. Experimental results from the determination of the suitability of the PSOA gel in supporting cell growth and proliferation. Data (n = 3) are presented as mean counts per second (cps) \pm 95 % CL following analysis by 2-way ANOVA ($p < 0.05$) and the Tukey method for computing MSD to determine individual differences between time points and surface coating. * represents significant differences between time points and + represents significant differences between PSOA-safflower oil gel and the cured cyanoacrylate surfaces.

These findings demonstrate that the organogel presented is able to support cell adhesion, cell growth and cell proliferation. It is not a cytotoxic material. Although the ATP amounts of the cells cultured on the organogel were less than those from the cells that were cultured on the Nunclon Δ^{TM} surface, the trend was similar across these surfaces. The cells grown on the organogel increased their ATP amount four-fold between 24 hours to 72 hours, which is indicative of cell proliferation.

Notably, the ATP levels did not decline between 72 hours and 120 hours, suggesting that the cells were viable and that the gel was not cytotoxic; as was observed with cells cultured on the

cured cyanoacrylate (a well-known cytotoxic substrate). The culture medium in the seeded coated wells (with the exception of cured cyanoacrylate-coated wells) turned from pink (unseeded control) to yellow (seeded) after 120 hours. This is indicative of cellular metabolism due to lactic acid accumulation, which lowers the pH of the culture medium (Figure 5.14).

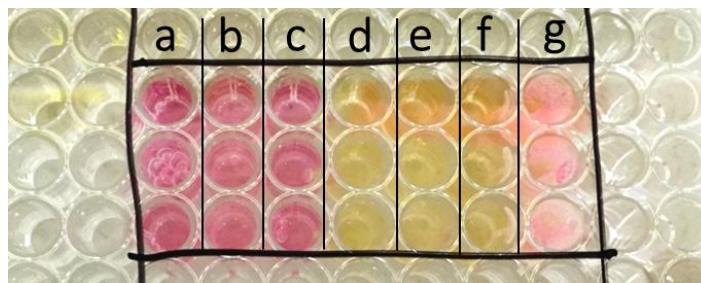


Figure 5.14. Illustration of the plate seeding plan showing the appearance of the culture medium after 120 hours; a) collagen coated (unseeded); b) PSOA-safflower gel coated (unseeded); c) Nunclon Δ^{TM} surface (unseeded); d) collagen coated + cells; e) PSOA-safflower gel coated + cells; f) Nunclon Δ^{TM} surface + cells; g: cyanoacrylate coated + cells.

Thermoreversibility and responsiveness to external stimuli are attributes that organogels should possess to demonstrate their appropriateness for us as stimuli-responsive, injectable drug delivery compositions. Acid-catalysed organogel degradation may be exploited as a trigger to release a therapeutic payload within the acidic cancerous tissue. The pH values within the primary lysosomes and the secondary lysosomes of the cancer cells that form solid tumours has been reported to be as low as pH 4 [79, 80]. This acidic environment has been exploited for the intracellular release of drug molecules and of fluorescent dyes from pH-sensitive polymeric carriers [81-85]. In addition, the acidic pH of vaginal fluid (pH 4.2) ensures that the reported organogels may be of significance in the delivery of antiviral therapies by vaginal administration [71]. Research conducted by Wu *et al.* [86] and by Bunzen and Kolehmainenhas [87] demonstrated the targeted, acid-catalysed hydrolysis of imine links to induce organogel disassembly. Consequently, studies were conducted to assess the ability of organogels, formed at 2 wt.% polymer loading and 4 wt.% polymer loading in safflower oil, to release rhodamine B in response to the cleavage of the ester bonds that link the graft copolymer by acid-catalysed hydrolysis, thereby, resulting in polymer degradation and organogel disruption. Rhodamine B was used as a model payload due to its fluorescence insensitivity upon changes in solution pH. The release of rhodamine B from the organogels was greatest when the organogel was

incubated in an acidic (pH 4.2) acetate buffer solution; in excess of 75% of total rhodamine B was released from the 2 wt. % gel after 78 hours (Figure 5.15). In contrast, the release of rhodamine B from the gel that was incubated in pH 7.4 PBS buffer solution was negligible, with less than 5% of total rhodamine B being expelled over the 78 hour period. When the PSOA content within the organogel was increased from 2 wt. % to 4 wt. %, the release of rhodamine B being monitored at pH 4.2, the amount of rhodamine B that was released was 32%. This effect can be attributed to the greater crosslink density that is achieved with PSOA loadings greater than 2 wt. %. Such traits can be exploited in drug delivery as a way of varying the release profile of the encapsulated payload, according to medicinal requirements [88-90].

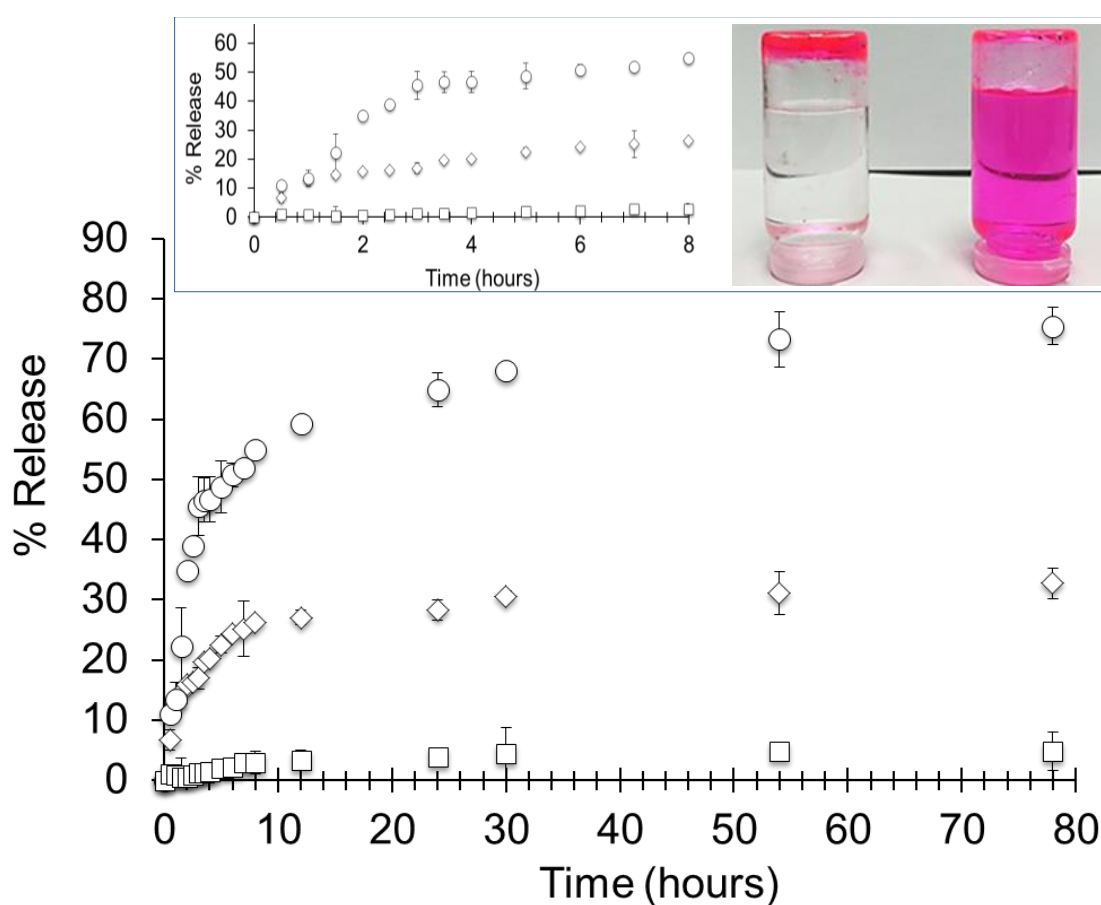


Figure 5.15. The release of rhodamine B from a 2 wt. % PSOA-safflower oil organogel in response to incubation in PBS buffer solution, maintained at pH 7.4 (\square) and pH 4.2 (\circ), and release from the 4 wt. % PSOA-safflower oil organogel, at pH 4.2 (\diamond). The inset (*top*) shows the release of rhodamine B from the gels within the first 8 hours (*far left*), rhodamine B-loaded 2 wt. % PSOA-safflower oil organogel maintained within solution of pH 7.4 for 78 hours (*middle*), and the remains of rhodamine B-loaded 2 wt. % PSOA-safflower oil organogel, maintained within solution of pH 4.2 for 78 hours (*far right*).

Macroscopic images of the release compositions after 78 hours show that the encapsulated molecules are retained within the gel structure to a greater extent at pH 7.4 (Figure 5.15, *inset middle*) compared to an acidic pH 4.2 (Figure 5.15, *inset right*), as indicated by the concentration of rhodamine B within the released media (extent of staining). Fluorescence microscopy was used to image the residual gel samples obtained after 78 hours of incubation, at pH 7.4 and at pH 4.2, respectively (Figure 5.16). The organogel stored at pH 4.2 can barely be seen because of a very low concentration of fluorescent molecules remaining in the gel, whilst the organogel stored at pH 7.4 is extremely prominent due to the high concentration of fluorescent rhodamine B molecules remaining in the gel network. Upon increasing the brightness of the images by 30%, and then by a further 30%, it can be observed that the gel stored at pH 4.2 becomes noticeable but still lacks significant fluorescence. On the contrary, the image of the organogel that was stored at pH 7.4 is saturated, further highlighting the successful release of rhodamine B from the organogels maintained within acidic solution in contrast to the relative non-release from the organogel maintained in pH 7.4 solution.

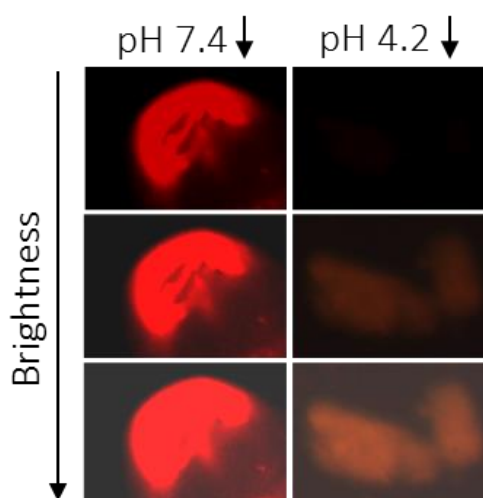


Figure 5.16. Fluorescence microscopy images, obtained from a 2 wt. % PSOA-safflower oil organogel after 78 hours of incubation in pH 7.4 medium and in pH 4.2 medium.

The mechanisms of the release of the encapsulated rhodamine B molecules was studied by fitting the experimental data to the Korsmeyer-Peppas (KP) model (Equation 5.1) [91]. Fitting the experimental data to the KP model afford the linear plots of the logarithm of rhodamine B release (%) against the logarithm of time (Figure 5.17). The gradient of the linear plot is equal to the release exponent (n) at that time interval and pH (Table 5.2).

$$\log (\text{release } \%) = \log \left[\frac{M_t}{M_\infty} \right] = n \log t + \log k \quad (5.1).$$

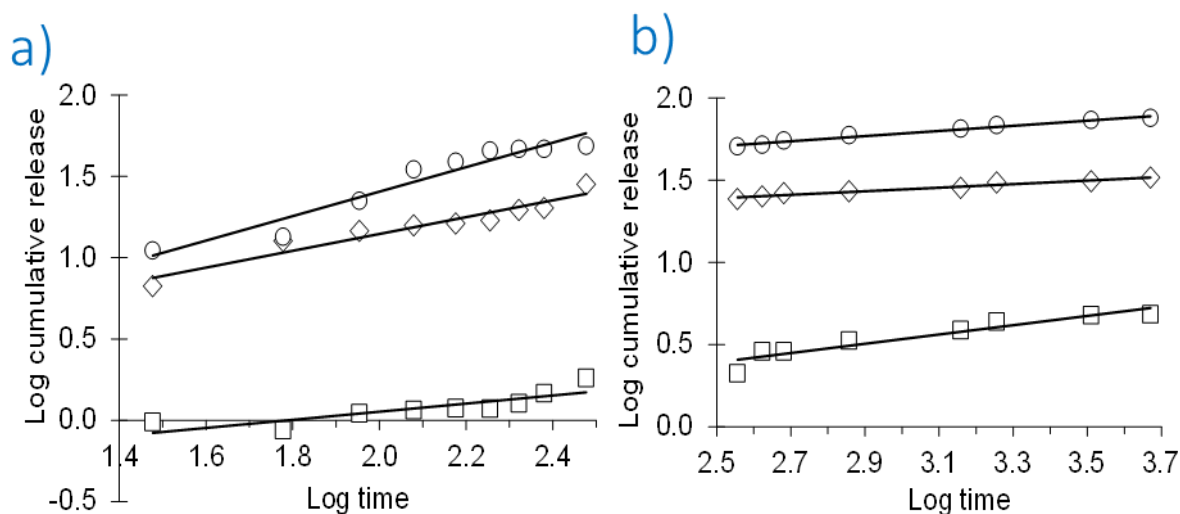


Figure 5.17. KP model Plots for; 2 wt.% PSOA-safflower oil organogel, incubated in PBS buffer solution, maintained at pH 7.4 (\square) and at pH 4.2 (\circ), and a 4 wt. % PSOA-safflower oil organogel, incubated in PBS buffer maintained at pH 4.2 (\diamond); from 0-5 hours (a) and from 6-78 hours (b).

Table 5.2. Release exponents (n) and correlation coefficients (r^2), computed from the KP model.

pH	PSOA loading in Safflower oil	0 - 5 hours		6 - 78 hours	
		n	r^2	n	r^2
4.2	2 wt. %	0.75	0.94	0.16	0.98
4.2	4 wt. %	0.52	0.93	0.11	0.96
7.4	2 wt. %	0.25	0.72	0.28	0.91

Analysis of the experimental data revealed that $0.45 < n < 0.89$ in the period ranging from 0 to 5 hours for the PSOA-safflower oil organogels that were incubated in the buffer maintained at pH 4.2. Specifically, the value of n was 0.75 for the 2 wt. % organogel, and was 0.52 for the 4 wt. % organogel. According to the KP model, these values suggest that release of the encapsulated rhodamine B was anomalous (non-Fickian), within the period studied. Surface erosion, driven by the acid hydrolysis of the organogel matrix, is possibly the dominant mechanism by which the payload was released. Increasing the loading of the gelator, from 2

wt. % to 4 wt. %, caused the delayed and sustained release of rhodamine B due to the accompanying increase in the crosslink density of the gel matrix. However, over the same period of time, the release of rhodamine B from the 2 wt. % organogel, incubated in PBS buffer maintained at pH 7.4, followed Fickian diffusion ($n = 0.25$). This is to be expected as a pH 7.4 solution cannot induce the degradation of the organogel matrix. This explanation also supports the negligible release of rhodamine B at pH 7.4, in contrast to enhanced release from the organogels in the pH 4.2 solution. In contrast, the release of rhodamine B from the organogels, between 6 and 78 hours of incubation, followed Fickian diffusion profile ($n < 0.45$), regardless of the solution pH. This effect could be due to the greater time required for the rhodamine B molecules to migrate from deep within the gel matrix to the surrounding medium.

5.4. Conclusions

The hydroxyl groups of oligo(Ser) were used to graft octadecanoic acid, yielding a macromolecule that was capable of gelating edible safflower oil. Organogels were formed at polymer loadings as low as 2 wt. %, the effect being thermoreversible, offering the material great potential for use as an injectable biomaterial. Additionally, the organogel that was produced possessed considerable mechanical strength, with an elastic modulus of almost 10^4 Pa. The organogel was pH-responsive and able to be eroded to release encapsulated rhodamine B, when incubated at 37 °C in an acidic environment. Statistical analysis, performed by applying the KP model, revealed that initially, the release of the encapsulated molecular cargo follows non-Fickian diffusion at acidic pH values and a Fickian diffusion at pH 7.4. Then, a wholly Fickian diffusion process occurred at greater time intervals (after 5 hours) regardless of solution pH. The organogel composition possessed biocompatibility that was comparable to that of collagen, and so offers a conducive environment for the growth and proliferation of mammalian cells. As such, this organogel offers significant promise for use as an injectable carrier vehicle in the controlled delivery of therapeutic molecules to disease-infected cells, such as cancerous cells, that present an acidic environment, *in vivo*.

5.5. References

1. Lupi, F.R., Gabriele, D., Baldino, N., Mijovic, P., Parisi, O.I. and Puoci, F. *Food Funct.*, **2013**, 4, 1512-1520.
2. Mukherjee, S., Shang, C., Chen, X., Chang, X., Liu, K., Yu, C. and Fang, Y. *Chem. Commun.* **2014**, 50, 13940-13943.
3. Abdallah, D.J. and Weiss, R.G. *J. Braz. Chem. Soc.*, **2000**, 11, 209-218.
4. van Esch, J.H. and Feringa, B.L. *Angew. Chem. Int. Ed.*, **2000**, 39, 2263-2266.
5. Vintiloiu, A. and Leroux, J.-C. *J. Control. Release.* **2008**, 125, 179-192.
6. Skilling, K.J., Citossi, F., Bradshaw, T.D., Ashford, M., Kellam, B. and Marlow, M. *Soft Matter.* **2014**, 10, 237-256.
7. Bastiat, G., Plourde, F., Motulsky, A., Furtos, A., Dumont, Y., Quirion, R., Fuhrmann, G. and Leroux, J.-C. *Biomaterials.* **2010**, 31, 6031-6038.
8. Terech, P. and Weiss, R.G. *Chem. revs.*, **1997**, 97, 3133-3160.
9. Hanabusa, K., Yamada, M., Kimura, M. and Shirai, H. *Angew. Chem. Int. Ed.*, **1996**, 35, 1949-1951.
10. Flory, P.J. *Faraday Discuss Chem Soc.*, **1974**, 57, 7-18.
11. Murdan, S. *Drug Deliv.*, **2005**, 2, 489-505.
12. Yu, G., Yan, X., Han, C. and Huang, F. *Chem. Soc. Revs.*, **2013**, 42, 6697-6722.
13. Anand, B., Pisal, S., Paradkar, A. and Mahadik, K. *J Sci Ind Res (India)*. **2001**, 60, 311-318.
14. Suzuki, M., Nakajima, Y., Yumoto, M., Kimura, M., Shirai, H. and Hanabusa, K. *Org. Biomol. Chem.*, **2004**, 2, 1155-1159.
15. Zhang, T. and Guo, Q. *Chem. Commun.*, **2013**, 49, 11803-11805.
16. Yang, H.-K., Su, M.-M., Ren, L.-J., Zheng, P. and Wang, W. *RSC Adv.*, **2014**, 4, 1138-1145.
17. Kizil, S., Karadag, K., Ozan Aydin, G. and Bulbul Sonmez, H. *J. Environ. Manage.*, **2015**, 149, 57-64.
18. Basak, S., Nanda, J. and Banerjee, A. *J. Mater. Chem. A.*, **2012**, 22, 11658-11664.
19. Kim, K.T., Park, C., Vandermeulen, G.W.M., Rider, D.A., Kim, C., Winnik, M.A. and Manners, I. *Angew. Chem. Int. Ed.*, **2005**, 44, 7964-7968.
20. Zou, J., Zhang, F., Chen, Y., Raymond, J.E., Zhang, S., Fan, J., Zhu, J., Li, A., Seetho, K., He, X., Pochan, D.J. and Wooley, K.L. *Soft Matter.* **2013**, 9, 5951-5958.
21. Zhang, T., Wu, Y., Gao, L., Song, Z., Zhao, L., Zhang, Y. and Tao, J. *Soft Matter.* **2013**, 9, 638-642.
22. Mukherjee, S. and Mukhopadhyay, B. *RSC Adv.*, **2012**, 2, 2270-2273.
23. Debnath, S., Shome, A., Dutta, S. and Das, P.K. *Chem. Eur. J.*, **2008**, 14, 6870-6881.
24. Sanchez, C., Julian, B., Belleville, P. and Popall, M. *J. Mater. Chem. A.*, **2005**, 15, 3559-3592.
25. Sugiyasu, K., Fujita, N. and Shinkai, S. *Angew. Chem. Int. Ed.*, **2004**, 43, 1229-1233.
26. Xue, P., Xu, Q., Gong, P., Qian, C., Ren, A., Zhang, Y. and Lu, R. *Chem. Commun.*, **2013**, 49, 5838-5840.
27. Lin, Q., Zhu, X., Fu, Y.-P., Zhang, Y.-M., Fang, R., Yang, L.-Z. and Wei, T.-B. *Soft Matter.* **2014**, 10, 5715-5723.
28. Xue, P., Sun, J., Yao, B., Gong, P., Zhang, Z., Qian, C., Zhang, Y. and Lu, R. *Chem. Eur. J.*, **2015**, 21, 4712-4720.
29. Rajamalli, P. and Prasad, E. *Org. Lett.*, **2011**, 13, 3714-3717.
30. Banerjee, S., Das, R.K. and Maitra, U. *J. Mater. Chem. A.*, **2009**, 19, 6649-6687.

31. Oelkrug, D., Tompert, A., Gierschner, J., Egelhaaf, H.-J., Hanack, M., Hohloch, M. and Steinhuber, E. *J. Phys. Chem. B.*, **1998**, 102, 1902-1907.
32. Bhattacharya, S. and Krishnan-Ghosh, Y. *Chem. Commun.*, **2001**, 185-186.
33. Trivedi, D.R. and Dastidar, P. *Chem. Mater.*, **2006**, 18, 1470-1478.
34. Jadhav, S.R., Vemula, P.K., Kumar, R., Raghavan, S.R. and John, G. *Angew. Chem. Int. Ed.*, **2010**, 49, 7695-7698.
35. Prathap, A. and Sureshan, K.M. *Chem. Commun.* **2012**, 48, 5250-5252.
36. Ajayaghosh, A., Praveen, V.K. and Vijayakumar, C. *Chem. Soc. Revs.* **2008**, 37, 109-122.
37. Hoeben, F.J.M., Shklyarevskiy, I.O., Pouderoijen, M.J., Engelkamp, H., Schenning, A.P.H.J., Christianen, P.C.M., Maan, J.C. and Meijer, E.W. *Angew. Chem. Int. Ed.*, **2006**, 45, 1232-1236.
38. Zhang, J., Hoeben, F.J.M., Pouderoijen, M.J., Schenning, A.P.H.J., Meijer, E.W., De Schryver, F.C. and De Feyter, S. *Chem. Eur. J.*, **2006**, 12, 9046-9055.
39. Hoeben, F.J.M., Wolffs, M., Zhang, J., De Feyter, S., Leclère, P., Schenning, A.P.H.J. and Meijer, E.W. *J. Am. Chem. Soc.*, **2007**, 129, 9819-9828.
40. Li, X., Sinks, L.E., Rybtchinski, B. and Wasielewski, M.R. *J. Am. Chem. Soc.*, **2004**, 126, 10810-10811.
41. Sangeetha, N.M. and Maitra, U. *Chem. Soc. Revs.*, **2005**, 34, 821-836.
42. Desvergne, J.-P., Olive, A.G., Sangeetha, N.M., Reichwagen, J., Hopf, H. and Del Guerzo, A. *Pure Appl. Chem.*, **2006**, 78, 2333-2339.
43. Ishi-i, T. and Shinkai, S. Dye-Based Organogels: Stimuli-Responsive Soft Materials Based on One-Dimensional Self-Assembling Aromatic Dyes. In: Würthner, F. ed. *Supramolecular Dye Chemistry*. Springer Berlin Heidelberg, 2005, 119-160.
44. Sagawa, T., Fukugawa, S., Yamada, T. and Ihara, H. *Langmuir*. **2002**, 18, 7223-7228.
45. Yang, X., Lu, R., Xue, P., Li, B., Xu, D., Xu, T. and Zhao, Y. *Langmuir*. **2008**, 24, 13730-13735.
46. Nakashima, T. and Kimizuka, N. *Adv. Mater.*, **2002**, 14, 1113-1116.
47. Sakamoto, J.S. and Dunn, B. *J. Electrochem. Soc.*, **2002**, 149, A26-A30.
48. Sivakkumar, S., MacFarlane, D.R., Forsyth, M. and Kim, D.-W. *J. Electrochem. Soc.*, **2007**, 154, A834-A838.
49. Murata, K., Aoki, M., Nishi, T., Ikeda, A. and Shinkai, S. *J. Chem. Soc., Chem. Commun.*, **1991**, 1715-1718.
50. Choi, M.M.F. and Shuang, S. *Analyst*. **2000**, 125, 301-305.
51. Gandolfo, F., Bot, A. and Flöter, E. *Soc. Oil Chem. Am. J.*, **2004**, 81, 1-6.
52. Toro-Vazquez, J.F., Morales-Rueda, J.A., Dibildox-Alvarado, E., Charó-Alonso, M., Alonzo-Macias, M. and González-Chávez, M.M. *J. Am. Oil Chem. Soc.*, **2007**, 84, 989-1000.
53. Laredo, T., Barbut, S. and Marangoni, A.G. *Soft Matter*. **2011**, 7, 2734-2743.
54. Zetzl, A.K., Marangoni, A.G. and Barbut, S. *Food Funct.* **2012**, 3, 327-37.
55. Rogers, M.A., Wright, A.J. and Marangoni, A.G. *Soft Matter*. **2008**, 4, 1483-1490.
56. Motulsky, A., Lafleur, M., Couffin-Hoarau, A.-C., Hoarau, D., Boury, F., Benoit, J.-P. and Leroux, J.-C. *Biomaterials*. **2005**, 26, 6242-6253.
57. Couffin-Hoarau, A.-C., Motulsky, A., Delmas, P. and Leroux, J.-C. *Pharm Res.*, **2004**, 21, 454-457.
58. Vintiloiu, A., Lafleur, M., Bastiat, G. and Leroux, J.-C. *Pharm Res.*, **2008**, 25, 845-852.
59. Lukyanova, L., Franceschi-Messant, S., Vicendo, P., Perez, E., Rico-Lattes, I. and Weinkamer, R. *Colloids Surf B Biointerfaces*. **2010**, 79, 105-112.
60. Iwanaga, K., Sumizawa, T., Miyazaki, M. and Kakemi, M. *Int. J. Pharm.*, **2010**, 388, 123-128.

61. Iwanaga, K., Kawai, M., Miyazaki, M. and Kakemi, M. *J. Pharm.*, **2012**, 436, 869-872.
62. Thornton, P.D., Billah, S.M.R. and Cameron, N.R. *Macromol. Rapid Commun.*, **2013**, 34, 257-262.
63. Thornton, P.D. and Heise, A. *Chem. Commun.* **2011**, 47, 3108-3110.
64. Khuphe, M., Kazlauciunas, A., Huscroft, M. and Thornton, P.D. *Chem. Commun.*, **2015**, 51, 1520-1523.
65. Hehir, S. and Cameron, N.R. *Polym Int.*, **2014**, 63, 943-954.
66. Habraken, G.J.M., Heise, A. and Thornton, P.D. *Macromol. Rapid Commun.*, **2012**, 33, 272-286.
67. Thornton, P., Brannigan, R., Podporska, J., Quilty, B. and Heise, A. *J. Mater. Sci. Mater. Med.*, **2012**, 23, 37-45.
68. Gibson, M.I. and Cameron, N.R. *Angew. Chem. Int. Ed.*, **2008**, 47, 5160-5162.
69. Bonduelle, C. and Lecommandoux, S. *Biomacromolecules*. **2013**, 14, 2973-2983.
70. Manchun, S., Dass, C.R. and Sriamornsak, P. *Life Sci.*, **2012**, 90, 381-387.
71. Ramyadevi, D. and Rajan, K.S. *RSC Adv.*, **2015**, 5, 12956-12973.
72. Pal, A., Ghosh, Y.K. and Bhattacharya, S. *Tetrahedron*. **2007**, 63, 7334-7348.
73. Bairi, P., Roy, B., Routh, P., Sen, K. and Nandi, A.K. *Soft Matter*. **2012**, 8, 7436-7445.
74. Daniel, C., Dammer, C. and Guenet, J.-M. *Polymer*. **1994**, 35, 4243-4246.
75. Lejardi, A., Hernández, R., Criado, M., Santos, J.I., Etxeberria, A., Sarasua, J.R. and Mijangos, C. *Carbohydr Polym.*, **2014**, 103, 267-273.
76. Haldar, U., Bauri, K., Li, R., Faust, R. and De, P. *ACS Appl. Mater. Interfaces*. **2015**, 7, 8779-8788.
77. Fan, J., Zou, J., He, X., Zhang, F., Zhang, S., Raymond, J.E. and Wooley, K.L. *Sci. Chem.*, **2014**, 5, 141-150.
78. Moura, M.J., Figueiredo, M.M. and Gil, M.H. *Biomacromolecules*. **2007**, 8, 3823-3829.
79. De Duve, C., De Barsy, T., Poole, B., Trouet, A., Tulkens, P. and Van Hoof, F.o. *Biochem Pharmacol.*, **1974**, 23, 2495-2531.
80. Fehrenbacher, N. and Jäätelä, M. *Cancer Res.*, **2005**, 65, 2993-2995.
81. Haag, R. and Kratz, F. *Angew. Chem. Int. Ed.*, **2006**, 45, 1198-1215.
82. Krüger, H.R., Nagel, G., Wedepohl, S. and Calderón, M. *Nanoscale*. **2015**, 7, 3838-3844.
83. Cortese, B., D'Amone, S., Gigli, G. and Palamà, I.E. *MedChemComm*. **2015**, 6, 212-221.
84. Palama, I.E., Cortese, B., D'Amone, S., Arcadio, V. and Gigli, G. *Biomater. Sci.*, **2015**, 3, 361-372.
85. Hakeem, A., Duan, R., Zahid, F., Dong, C., Wang, B., Hong, F., Ou, X., Jia, Y., Lou, X. and Xia, F. *Chem. Commun.*, **2014**, 50, 13268-13271.
86. Wu, H., Ni, B.-B., Wang, C., Zhai, F. and Ma, Y. *Soft Matter*. **2012**, 8, 5486-5492.
87. Bunzen, H. and Kolehmainen, E. *Molecules*. **2013**, 18, 3745-3759.
88. Ge, Z. and Liu, S. *Chem. Soc. Revs.* **2013**, 42, 7289-7325.
89. Lin, L.-J., Larsson, M. and Liu, D.-M. *Soft Matter*. **2011**, 7, 5816-5825.
90. Ganguly, S. and Das, N.C. *RSC Advs.*, **2015**, 5, 18312-18327.
91. Korsmeyer, R.W., Gurny, R., Doelker, E., Buri, P. and Peppas, N.A. *Int. J. Pharm.*, **1983**, 15, 25-35.

Chapter 6. Polymer Hydrogels for Glutathione-Mediated Protein Release

Preamble

This Chapter is based on work published as:

B.S. McAvan*, M. Khuphe* and P.D. Thornton, *Eur. Polym. J.*, **2017**, 87, 468-477 (*The authors contributed equally to this research).

Abstract

The use of amine-terminated poly(ethylene glycol) star polymers as macroinitiators for the ring-opening polymerisation of S-tert-butylmercapto-L-cysteine N-carboxyanhydride is described. This results in the creation of amphiphilic copolymers that are capable of forming discrete particles in aqueous solution. Poly(amino acid) deprotection liberates the pendant thiol groups that can then form covalent disulfide crosslinks with adjacent thiol groups, yielding a crosslinked polymer that is capable of hydrogel formation. The model protein albumin–fluorescein isothiocyanate conjugate was encapsulated within the hydrogels produced, prior to its release upon hydrogel interaction with the glutathione reducing agent. Consequently, the resulting stimuli-responsive polymers have great promise as biomaterials that are capable of releasing a protein molecular cargo upon interaction with glutathione.

6.1. Introduction

Stimuli-responsive polymers form an important class of material that can readily be applied to the production of advanced biomaterials [1-3]. The controlled release of payload molecules, from a polymeric carrier upon external stimulation, enables the delivery of therapeutic agents on-demand, as part of a highly-effective drug delivery system [4, 5]. In addition, stimuli-responsive polymers may be used as scaffolds for tissue regeneration [6-8]. Consequently, polymers that are susceptible to a controlled response and/or degradation upon interaction with stimuli, including alterations in environmental temperature [9], pH [10-12], and the presence of particular enzymes, are highly sought [13].

Polymers that undergo physical/chemical alterations upon interaction with reducing agents are also of significance in their use within a biomedical context [14-16]. Glutathione (GSH) is a natural tripeptide that is abundant in the majority of animal cells. The thiol group of the cysteine unit of glutathione dictates that glutathione is a reducing agent. For instance, the disulfide bonds that are formed within cytoplasmic proteins are reduced to cysteine units, the glutathione being an electron donor [17]. Micromolar concentrations of GSH occur within the blood plasma, compared to intracellular GSH concentrations of between 0.5 mM and 10 mM. Thus, glutathione is a particularly valid target in therapeutic treatments as extracellular drug release is minimised [18].

Using a polymeric hydrogel as a carrier vehicle permits the controlled delivery of biomolecules, such as the proteinaceous drugs Trastuzumab, Bevacizumab and Rituximab, *in vivo* [19]. Polymer hydrogels are well-suited to the controlled delivery of proteins as they present an aqueous environment that prevents protein denaturation. The hydrogel enables the efficient encapsulation of the protein cargo, restricting its metabolisation whilst maintaining its bioactivity. It also enables protein release at a pre-programmed rate, upon stimulation. Such materials have been used for the delivery of growth factors as part of tissue regeneration, and for the controlled delivery of proteins that act as therapeutic agents [20, 21]. The relative ease of polymer hydrogel synthesis, coupled with the feasibility of creating materials that often possess biocompatibility, adds to their suitability as drug delivery vehicles and scaffolds for promotion of tissue regeneration.

This chapter concerns the generation of PEG star polymers that are terminated with cysteine oligomers for use as protein delivery vehicles. Cysteine is a particularly useful component of functional materials due to its pendant thiol group that may be used either in thiol-ene 'click' reactions [22], or in the formation of disulfide bridges [23]. The terminal cysteine units were grafted by NCA ROP and possessed tertiary butyl protecting units, thus producing an amphiphilic structure that possessed the ability to form discrete particles in an aqueous medium. Cysteine deprotection liberated the thiol groups, enabling the polymers to undergo chemical crosslinking, *via* the formation of disulfide bridges, to yield a polymeric network. This polymeric network was able to uptake appreciable amounts of water, due to its considerable PEG content, and to form hydrogels that are susceptible to reduction upon incubation with

glutathione. The polymer hydrogels formed are able to encapsulate and to selectively release the fluorescently labelled model protein bovine serum albumin, deeming them highly-applicable for the controlled release of protein payloads, within reductive environments. It is envisaged that the hydrogels formed may act as scaffolds for tissue engineering that permit the release of protein growth factors, and/or as protein delivery vehicles, that perform payload release upon interaction with a reducing agent that is either present, or injected at the intended site of action, in both instances.

6.2. Experimental Details

6.2.1. Synthesis of S-tertbutylmercapto (STBM)-L-cysteine NCA

The synthesis of the cyclic monomer is detailed in Chapter 3.3.7.

6.2.2. Synthesis of Poly[(STBM-L-Cysteine)_n]₄-b-(StarPEG_{10k}) Macromolecules

A representative procedure for the syntheses of poly[(STBM-L-cysteine)_n]₄-b-(StarPEG_{10k}) macromolecules is given for a monomer-to-macroinitiator feed ratio of 40:1, which had the intention of furnishing each of the four arms of StarPEG with 10 oligomer repeat units, on average. STBM-L-cysteine NCA (0.19 g, 0.81 mmol) was dissolved in anhydrous DMF (20 mL) under a nitrogen flow. The solution was injected into a suba-sealed Schlenk tube that was previously dried, evacuated, nitrogen-purged and equipped with a magnetic stirrer bar. An amino group-terminated PEG star polymer (0.20 g, 0.02 mmol) was dissolved in anhydrous DMF (10 mL). The solution was introduced under nitrogen flow into the NCA solution in the Schlenk tube. The reaction was stirred under a nitrogen flow for 96 hours, at ambient temperature. The product was subsequently precipitated by adding the reaction mass dropwise into cold diethyl ether (1:10 v/v). The precipitate was left to stand in a freezer (-18 °C) for 24 hours. The polymer was eventually isolated by centrifugation (2000 rpm, 10 min, -5 °C) and dried *in vacuo* (35 °C) for 24 hours. The same procedure was followed for the synthesis of the other macromolecules created using M/I molar feed ratios of 20:1 and 80:1.

Yields: 78.3% (M/I 10:1), 86.5% (M/I 5:1), 62.1% (M/I 20:1). ¹H NMR (500 MHz, TFA, δ, ppm): 7.48 (s, NH), 5.53 - 4.75 (m, αCH), 4.25 - 3.76 (m, PEG), 2.45 - 2.34 (d, -S-S-CH₂), 1.73 - 1.38 (m,

tert-Butyl). FTIR: $\nu_{\max}/\text{cm}^{-1}$ (solid): 3325 (NH, amine stretch), 2879 (CH, alkyl stretch), 1676 (C=O amide stretch).

6.2.3. Deprotection of Poly[(STBM-L-Cysteine)_n]-*b*-(StarPEG_{10k}) Macromolecules

A representative procedure for the deprotection of the macromolecules is given using an outline for the deprotection of poly[(STBM-L-cysteine₁₀)₄-*b*-(StarPEG_{10k})]. Poly[(STBM-L-cysteine₁₀)₄-*b*-(StarPEG_{10k})] (0.21 g, 0.02 mmol) was dissolved in anhydrous DMF (20 mL) and injected into a Schlenk tube that was equipped with a magnetic stirrer bar. DTT (0.20 g, 1.3 mmol) was dissolved in anhydrous DMF (5 mL) and added to the polymer solution. The reaction solution was stirred at 60 °C for 120 hours and then then dialysed against deionised water for 96 hours. The deprotected polymer was subsequently obtained *via* lyophilisation.

Yield: 57.2 wt. % (M/I 10:1), 54.4 wt. % (M/I 5:1), 67.8 wt. % (M/I 20:1). ¹H NMR (500 MHz, DMSO, δ , ppm): 7.97 (s, NH), 5.23 - 5.22 (d, α CH), 3.52 - 3.33 (m, PEG), 2.77 - 2.51 (m, -S-S-CH₂). FTIR: $\nu_{\max}/\text{cm}^{-1}$ (solid): 3305 (NH, amine stretch), 2875 (CH, alkyl stretch), 1682 (C=O, amide stretch).

6.2.4. Polymer Crosslinking

A representative procedure is given. Poly[(L-cysteine₁₀)₄-*b*-(StarPEG_{10k})] (0.20 g, 0.02 mmol) was dissolved in anhydrous DMF. The solution was injected into a Schlenk tube. Cobalt phthalocyanine (10 mg, 0.02 mmol) was dissolved in anhydrous DMF (5 mL) and this solution was added to the polymer solution. The reaction solution was stirred at room temperature for 24 hours. The reaction mass was then poured into an excess of cold diethyl ether (1:10 v/v) and allowed to stand at -18 °C for 24 hours. The product was isolated by centrifugation (2000 rpm, 20 min) and dried *in vacuo* (30 °C) for 48 hours. FTIR: $\nu_{\max}/\text{cm}^{-1}$ (solid): 3270 (NH, amine stretch), 2864 (C-H, alkyl stretch), 1667 (C=O, amide stretch).

6.2.5. Nanoprecipitations, DLS Studies and SEM Studies

Nanoprecipitations were carried out as described in Chapter 2.14, by dropwise addition (40 μ L) of poly[(STBM-L-cysteine)_n]-*b*-(StarPEG_{10k}) solutions (5 mg/mL) to ultra-pure water (18.2

Megohms, 10 mL). The particle sizes, size distributions and morphologies were subsequently assessed using DLS and SEM.

6.2.6. Water Uptake

Hydrogels were dried *in vacuo* (48 hours, 37 °C). The obtained xerogels (10 mg) were then soaked in an excess of deionised water. The uptake of water by the scaffolds was determined by monitoring the weight increase of the scaffolds to the point of saturation.

6.2.7. Protein Loading Within the Hydrogels

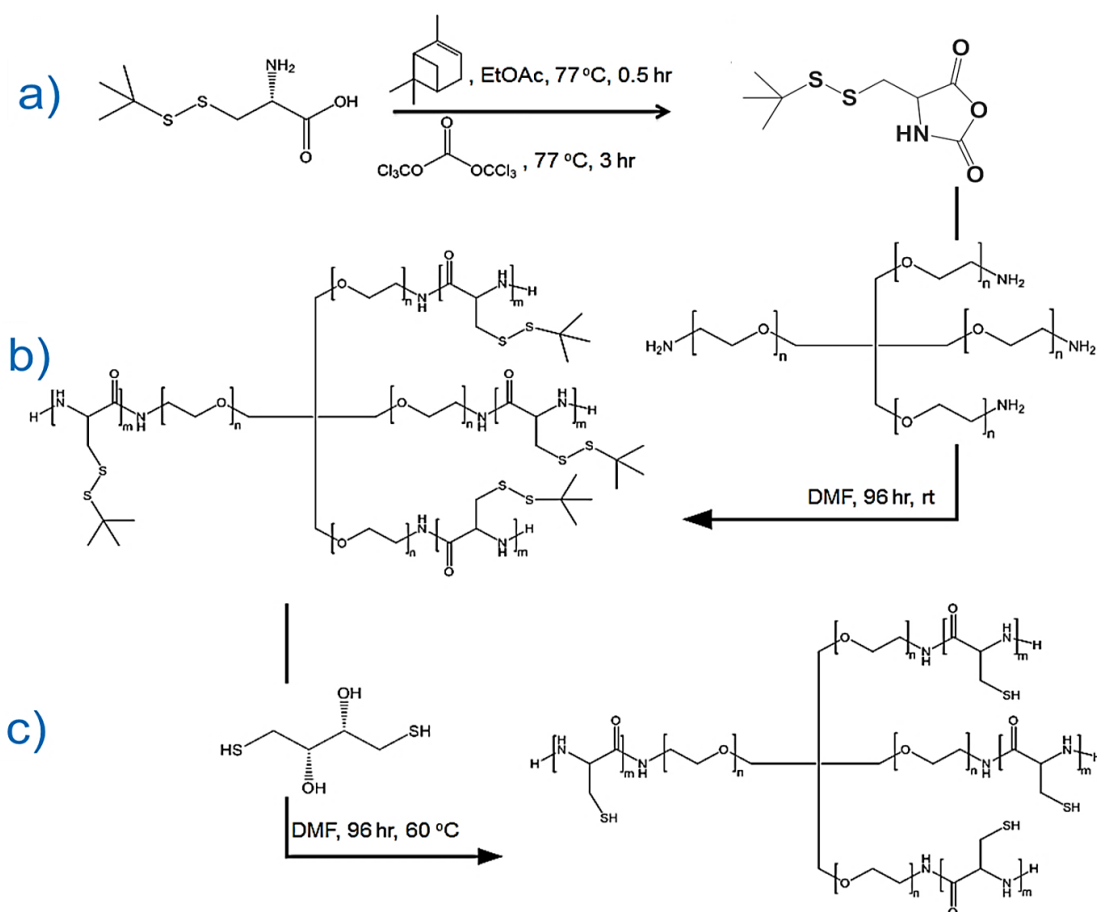
A solution of albumin fluorescein isothiocyanate conjugate (FITC-albumin) (1 mg/mL) was obtained by dissolving the protein in PBS buffer solution (pH 7.4) and its absorbance was determined. Pre-weighed poly[(L-cysteine₅)₄-(StarPEG_{10k})] and poly[(L-cysteine₁₀)₄-(StarPEG_{10k})] were soaked independently in FITC-albumin solutions, in the dark, for 48 hours. The resulting saturated hydrogels were rinsed free of un-encapsulated FITC-albumin, using PBS buffer solution and retained for GSH-mediated protein release and fluorescence microscopy imaging. The supernatants that were recovered after hydrogel soaking were retained and analysed for their absorbance to ascertain the amount of protein that was encapsulated.

6.2.8. The Glutathione-Mediated, *In Vitro* Degradation of Hydrogels

Hydrogel degradation was monitored by tracking the release of the previously-encapsulated protein payload. Triplicate sets of FITC-Albumin-loaded hydrogels were stored in glass vials that contained the PBS buffer solution only (10 mL, pH 7.4) and L-glutathione in PBS buffer solution (5 mM, 10 mL, pH 7.4). The vials, which were masked with aluminium foil, were incubated in an oven maintained at 37 °C. At selected intervals, aliquots (70 µL) were obtained from each vial. These aliquots were analysed in semi-micro, self-masking quartz cuvettes, by UV-Vis spectrophotometry. Samples were returned immediately to their parent vials after each analysis. The amount of protein that was released at each time interval was quantified from a previously obtained linear calibration graph.

6.3. Results and Discussion

The NCA of *S-tert*-Butylmercapto-L-cysteine (STBM-L-cysteine NCA) was obtained in good purity using an established protocol (Scheme 6.1 a) [25]. Then, a four-arm, amine-terminated poly(ethylene glycol) (starPEG, Mw: 10,000 Da) was used to initiate the ring-opening polymerisation of STBM-L-cysteine NCA in monomer feed ratios of 5, 10 and 20 monomer units per starPEG arm (Scheme 6.1 b) [26].



Scheme 6.1. The route to the generation of thiol-ene cross-linkable macromolecules: the synthesis of STBM-L-cysteine NCA (a), starPEG amine-mediated NCA ROP to generate poly[(STBM-L-cysteine)_n]₄-*b*-(StarPEG_{10k}) macromolecules (b) and the DTT-mediated reductive removal of STBM groups to generate macromolecules that possess pendant thiol groups (c).

NCA ROP was performed in anhydrous DMF enabling the dissolution of the macroinitiator, the NCA monomer and the resulting polymer products. The feasibility of the starPEG-mediated ROP of STBM-L-cysteine NCA was confirmed by ^1H NMR spectroscopy (Figure 6.1 b) and by

FTIR spectroscopy (Figure 6.2 a-c). Comparison of the ^1H NMR integration values corresponding to the STBM protons (1.46 - 1.81 ppm) and the ^1H NMR integration values corresponding to the PEG star polymer initiator protons (3.25 - 4.50 ppm) allows the composition of the polymers to be determined (Table 6.1).

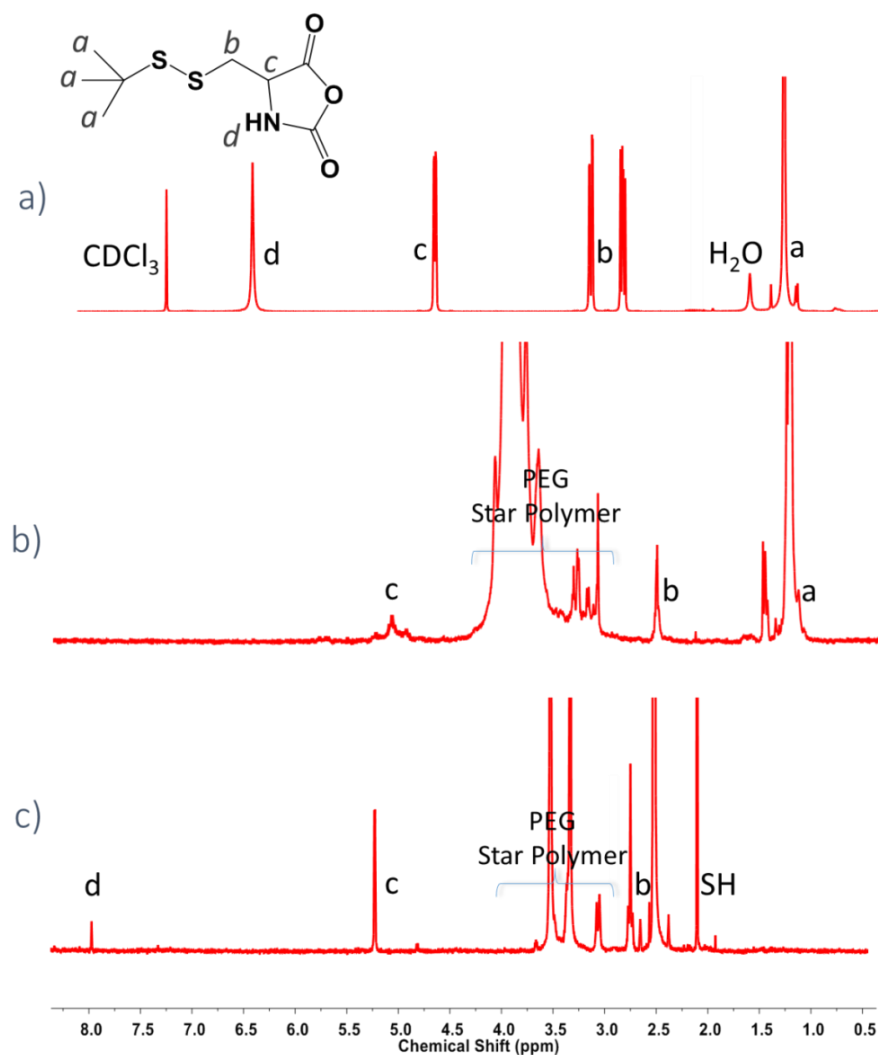


Figure 6.1. ^1H NMR spectrum of STBM-L-Cysteine NCA (a), representative ^1H NMR spectra in TFA-d for poly[(STBM-L-cysteine) $_n$] $_4$ -b-(StarPEG $_{10k}$)] macromolecules before removal of STBM protecting groups (b) and after deprotection to remove STBM protecting groups (c).

The polymerisations to produce the polymers stated in Table 6.1 (entries 1 and 2) went to completion within the allocated reaction period. According to analysis carried out using ^1H NMR spectroscopy, the polymerisation detailed in entry 3 did not go to completion due to the increased monomer concentration. This polymerisation was terminated after 96 hours,

immediately prior to the reaction mixture becoming turbid; an occurrence that was observed in another, separate reaction.

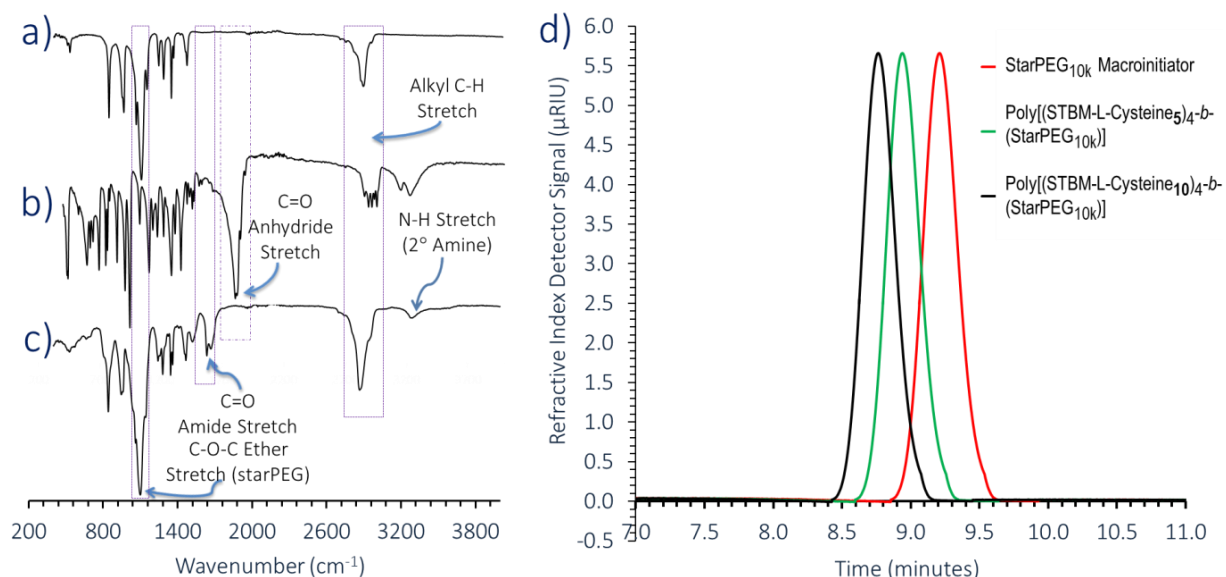


Figure 6.2. FTIR spectra of the PEG star polymer macroinitiator (a), STBM-L-Cysteine NCA (b), representative spectrum for the resultant hybrid macromolecules, obtained from the starPEG-initiated ROP of STBM-L-Cysteine NCA (c), APC chromatograms of the macromolecules (d).

FTIR spectra (Figure 6.2) revealed the disappearance of the anhydride stretch (1806 cm^{-1}) of the NCA monomer and the subsequent emergence of the amide stretch, after NCA ROP for 96 hours. The emergence of the ether signal (*ca.* 1200 cm^{-1} - 1012 cm^{-1}) on the infrared spectrum of the hybrid macromolecules, due to the presence of PEG, also confirmed the successful grafting of peptide oligomers from the PEG star polymer initiator. The formation of copolymers was supported further by thermal analyses (Figure 6.3). The DSC thermograms of the STBM-protected macromolecules (Figure 6.3 b) reveals the emergence of an endothermic trough (i) at $262\text{ }^{\circ}\text{C}$ - $310\text{ }^{\circ}\text{C}$ that is absent on the DSC thermogram of the PEG star polymer macroinitiator (Figure 6.3 a). This endotherm is attributed to the energy required to degrade the carbon content which is mostly provided by the STBM protecting groups. This interpretation of the endothermic behaviour was confirmed further by TGA, where it is observed as a weight-loss shoulder, which is attributable to fragmentation, degradation and mass loss (Figure 6.3 e (iii)). This shoulder is absent from the TGA thermogram of the PEG star polymer macroinitiator (Figure 6.3, v). The successful grafting of poly(amino acid)s was also indicated by the emergence of an endothermic trough indicating the melting of the PEG star polymer

macroinitiator, at 50 °C, in the thermograms of the poly(amino acid)-grafted macromolecules. The hybrid macromolecules that were produced possessed a monomodal molecular weight distribution, as determined by APC (Figure 6.2 d).

Table 6.1. Composition of the copolymers obtained from StarPEG_{10k}-initiated NCA ROPs.

Entry	Theoretical Macromolecule	Composition Estimated from ¹ H NMR
1	Poly[(STBM-L-cysteine ₅) ₄ - <i>b</i> -(StarPEG _{10k})]	Poly[(STBM-L-cysteine ₅) ₄ - <i>b</i> -(StarPEG _{10k})]
2	Poly[(STBM-L-cysteine ₁₀) ₄ - <i>b</i> -(StarPEG _{10k})]	Poly[(STBM-L-cysteine ₁₀) ₄ - <i>b</i> -(StarPEG _{10k})]
3	Poly[(STBM-L-cysteine ₂₀) ₄ - <i>b</i> -(StarPEG _{10k})]	Poly[(STBM-L-cysteine ₁₆) ₄ - <i>b</i> -(StarPEG _{10k})]

A standard deprotection procedure was then adopted for the elimination of STBM groups, by DTT-mediated reduction of the disulfide linkages, to generate free thiol groups (Scheme 6.1 c) [10]. ¹H NMR spectroscopic spectra of the deprotected macromolecules (Figure 6.1 c) revealed the complete disappearance of the peaks that belonged to the STBM groups (1.26 - 1.71 ppm) and the emergence of a singlet peak that is characteristic of alkyl thiol protons (≈ 2.15 ppm).

DSC and TGA analyses of the deprotected macromolecules supported the removal of STBM groups through the disappearance of the endotherm trough (Figure 6.3 c) and a diminished weight-loss shoulder (Figure 6.3, iv), which was observed prior to carrying out the deprotection of the macromolecules (Figure 6.3 b and Figure 6.3, iii), respectively.

It was anticipated that poly((STBM-L-cysteine)-*b*-(StarPEG_{10k})) might self-assemble in aqueous media to form discrete particles due to the inherent amphiphilicity of the block copolymer. Nanoprecipitation in PBS resulted in the generation of monodisperse particles, the size of which were observed to vary inversely with the length of the poly(amino acid) block (Figure 6.4). For example, poly((STBM-L-cysteine₁₆)₄-*b*-(StarPEG_{10k})) aggregated into particles with an average size of 138.8 nm, poly((STBM-L-cysteine₁₀)₄-*b*-(StarPEG_{10k})) aggregated into particles

with an average size of 274.7 nm and poly((STBM-L-cysteine₅)₄-b-(StarPEG_{10k})) aggregated into particles with an average size of 368.8 nm.

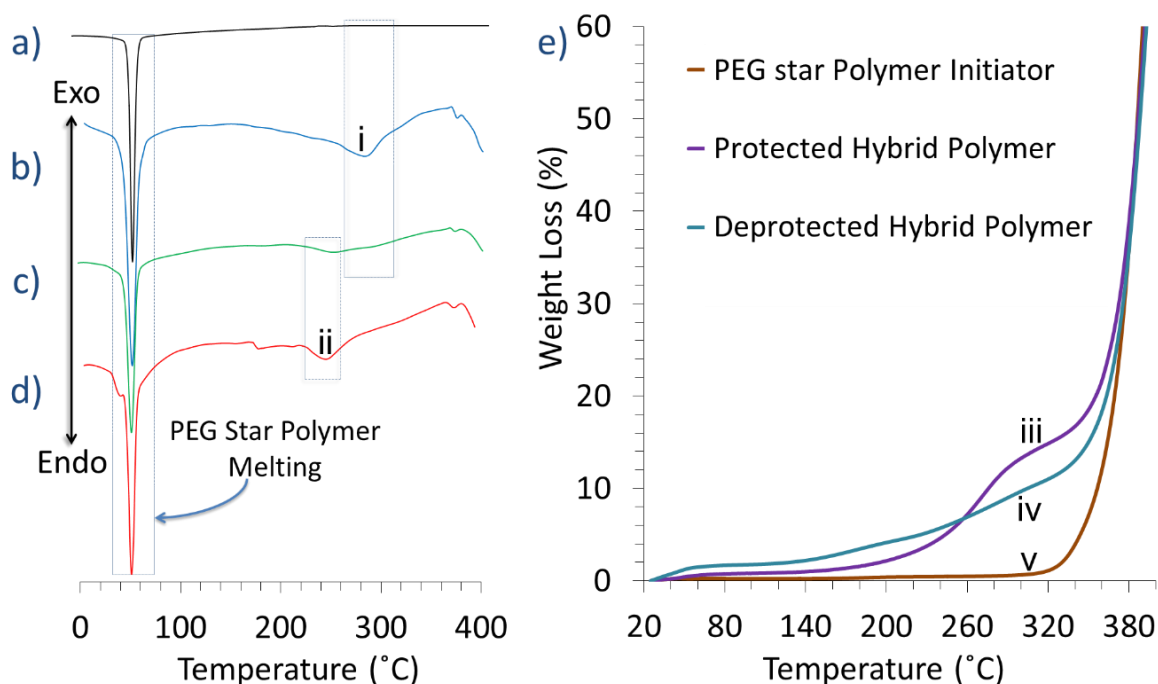


Figure 6.3. Left; Differential scanning calorimetry thermograms corresponding to the PEG star polymer initiator (a), poly[(STBM-L-cysteine₁₀)₄-b-(StarPEG_{10k})] (b) poly[(L-cysteine₁₀)₄-b-(StarPEG_{10k})] (c) and the crosslinked xerogel of poly[(L-cysteine₁₀)₄-b-(StarPEG_{10k})] (d). Right (e); the TGA thermograms corresponding to the PEG star polymer initiator, poly[(STBM-L-cysteine₁₀)₄-b-(StarPEG_{10k})] and poly[(L-cysteine₁₀)₄-b-(StarPEG_{10k})].

A literature-reported procedure was then adopted to crosslink the deprotected macromolecules, forming disulfide linkages between adjacent polymer chains (Figure 6.5) [27]. Due to the insolubility of the crosslinked networks formed, solution-based forms of analyses were impossible. DSC analyses of the crosslinked networks revealed the emergence of an endotherm trough (ii) at 220 °C - 255 °C (Figure 6.3 d), which was absent prior to crosslinking (Figure 6.3 c). The observed endotherm is attributed to the thermal energy that is required to cleave the disulfide crosslinks that were present [28].

The morphology of polymer hydrogels is paramount in their successful application as biomaterials. For example, in tissue engineering, the success of cell-proliferation on polymeric scaffolds is reliant upon the perfusion of nutrients to those cells that are able to migrate throughout the polymer network [29, 30]. In addition, a porous structure within drug delivery

vehicles is advantageous since it enables the loading of sufficiently high concentrations of therapeutic agents within the carrier. SEM analysis of the polymer xerogels reveals that they possess a microstructure that is characterised by an interconnected, porous 3D network, (Figure 6.6 a, b). The pores that existed within the hydrogels' microstructure are evident in the 3D microphotograph (Figure 6.6 b).

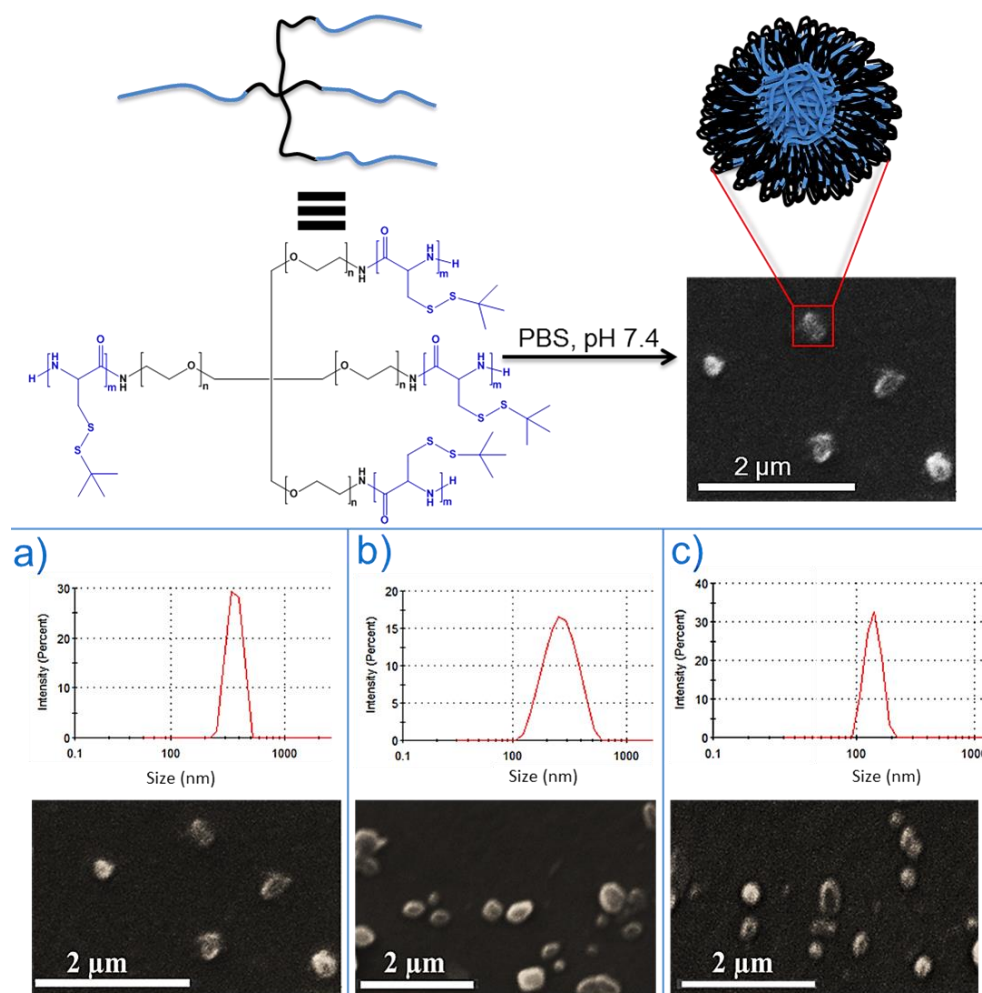


Figure 6.4. STBM-protected macromolecules self-organise in aqueous medium into spherical particles (top). DLS traces and SEM micrographs obtained from the self-assembly of (a) poly[(STBM-L-cysteine₅)₄-*b*-(StarPEG_{10k})], (b) poly[(STBM-L-cysteine₁₀)₄-*b*-(StarPEG_{10k})] and (c) poly[(STBM-L-cysteine₁₆)₄-*b*-(StarPEG_{10k})] macromolecules in aqueous medium.

The ability to take up and to hold aqueous media is paramount for the successful encapsulation of aqueously-dispersed therapeutic agents and subsequent application of hydrogels, *in vivo*. The effect of the crosslink density on the polymers' ability to take up and hold aqueous media

was investigated by monitoring PBS solution uptake. The uptake varied inversely with the lengths of the peptide oligomers (or with the number of cysteine monomer units) that were grafted onto each arm of starPEG (Figure 6.7). PBS solution uptake was greatest (66.1 wt. %) with the hydrogel possessing the shortest peptide oligomers (an average of five cysteine monomer units grafted on each arm of starPEG), but was the least (37.5 wt. %) with the hydrogel possessing the longest peptide block (an average of 16 cysteine monomer units grafted on each arm of starPEG). This effect could arise because of the greater crosslink density within those polymers containing a greater number of cysteine repeat units, resulting in a decrease in the porosity and in the swelling ability of the hydrogels [31, 32].

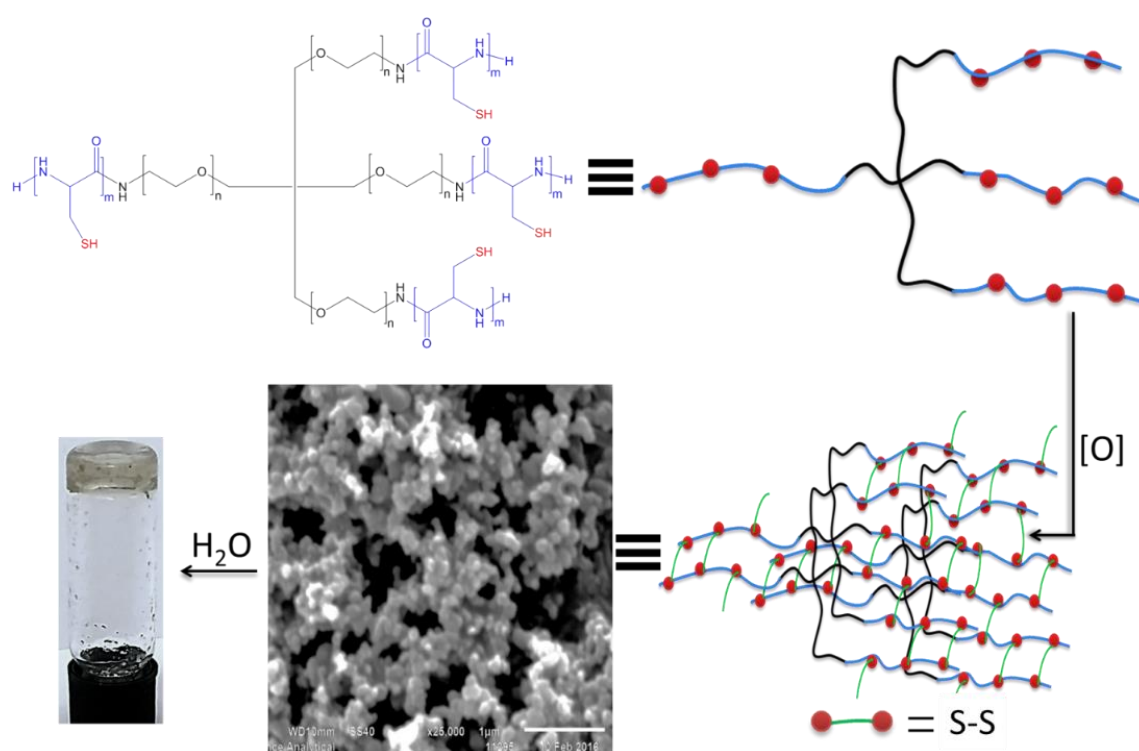


Figure 6.5. Graphical illustration of the generation of disulfide crosslinked chemical hydrogels.

The poly[(L-cysteine₅)₄-*b*-(StarPEG_{10k})] and poly[(L-cysteine₁₀)₄-*b*-(StarPEG_{10k})] hydrogels were then investigated for their ability to hold the model protein FITC-albumin. The protein-loaded hydrogels were analysed by fluorescence microscopy to ascertain the extent of FITC-albumin loading and retention, following hydrogel washing (Figure 6.8 c, d). The uniform distribution of green fluorescence within the hydrogels confirms the retention of FITC-labelled protein within the hydrogel networks. UV-Vis spectroscopic analysis of the respective supernatants, obtained

after the washing cycles, revealed that 46 wt. % of FITC-albumin was successfully loaded into the poly[(L-cysteine₅)₄-*b*-(StarPEG_{10k})] hydrogel and 49 wt. % was successfully loaded into the poly[(L-cysteine₁₀)₄-*b*-(StarPEG_{10k})] hydrogel (0.46 mg and 0.49 mg of FITC-albumin per mg of hydrogel respectively).

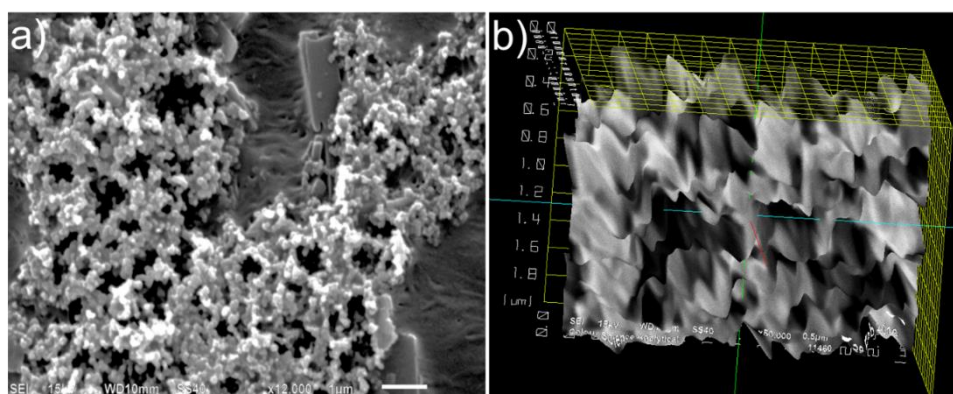


Figure 6.6. a) SEM micrographs of a poly((L-cysteine₁₀)₄-*b*-(starPEG_{10k})) chemical hydrogel and b) A 3-dimensional micrograph of the hydrogel reveal the presence of the pores within the microstructure.

An assessment of the use of GSH to activate FITC-albumin release from the hydrogels, by the reduction of the disulfide bridges that maintain the network structure, was then carried out. The release of FITC-albumin from the hydrogels, in response to an excessive amount of GSH, was monitored for up to 6 hours.

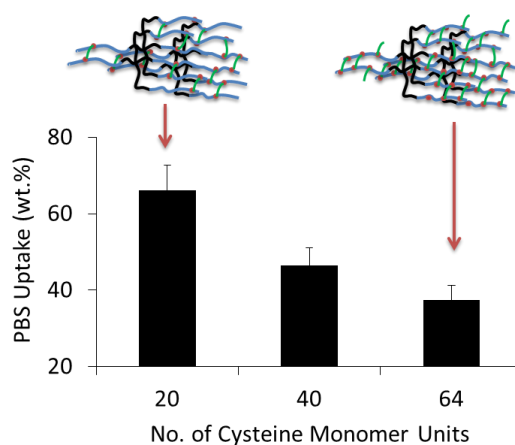


Figure 6.7. Variation of PBS solution uptake by hydrogel scaffolds in relation to the number of cysteine repeat units that were grafted to the PEG star polymer macroinitiator.

33.3% of the protein was released from the poly[(L-cysteine₁₀)₄-*b*-(StarPEG_{10k})] hydrogel after 6 hours. 37.1% of the protein was released from the poly[(L-cysteine₅)₄-*b*-(StarPEG_{10k})]

hydrogel after 6 hours of incubation at 37 °C, respectively (Figure 6.8 a, b). Beyond this time point, hydrogel degradation prevented the extent of release to be determined with accuracy as isolation of the supernatant from the impaired hydrogel became impossible. On the contrary, less than 2% of the encapsulated FITC-albumin was released when the hydrogels were incubated in PBS solution only. Complete disruption of the crosslinked networks, to release the encapsulated cargo, was observed when the hydrogels were left for a prolonged period (48 hours) in GSH solutions, as revealed by fluorescence microscopy (Figure 6.8 e).

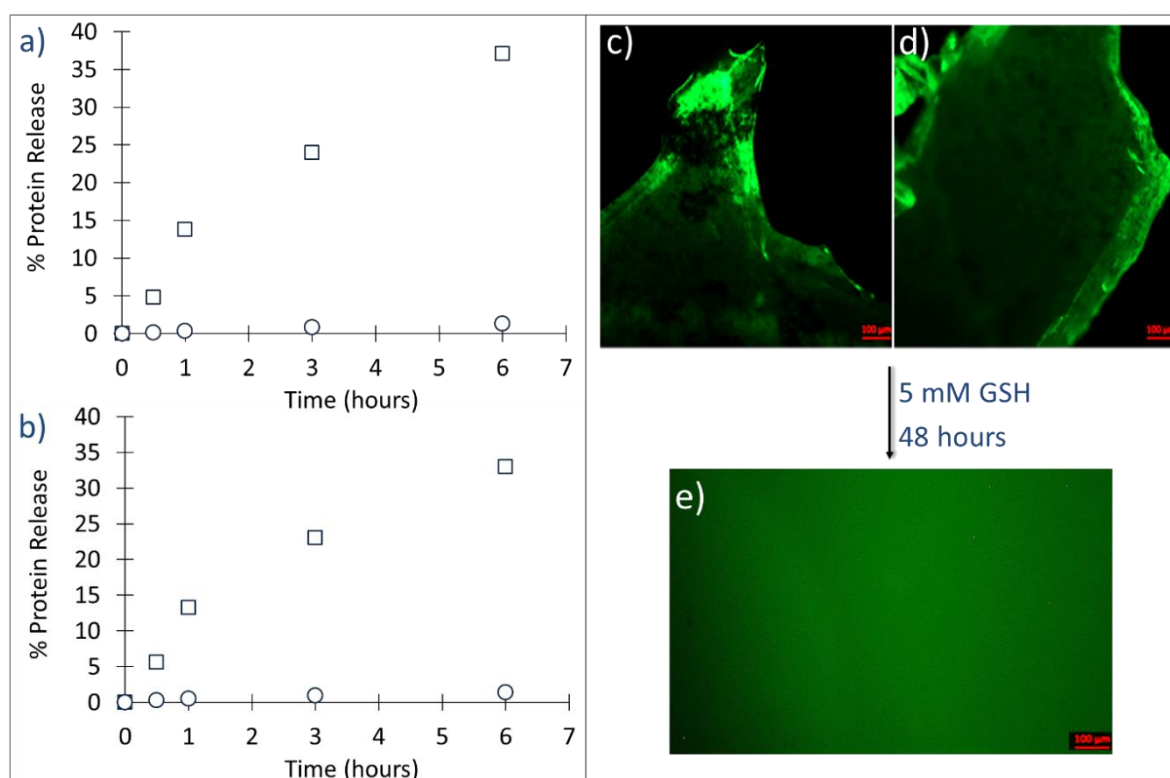


Figure 6.8. The release of FITC-albumin from a poly[(L-cysteine₅)₄-b-(StarPEG_{10k})] hydrogel (a) and from a poly[(L-cysteine₁₀)₄-b-(StarPEG_{10k})] hydrogel (b) in response to incubation in glutathione (□) and in response to incubation in PBS solution only (○). Fluorescence microscopy photographs, obtained from the protein-loaded poly[(L-cysteine₅)₄-b-(StarPEG_{10k})] hydrogel (c) and poly[(L-cysteine₁₀)₄-b-(StarPEG_{10k})] hydrogel (d) and a representative microphotograph depicting the complete breakdown of the hydrogel structures to release the encapsulated molecular cargo in response to incubation in glutathione solutions (e). Scale bars represent 100 μm.

These results greatly support the suitability of employing the reported materials in the controlled release of protein molecules, with potential applications as therapeutic delivery vehicles and/or as scaffolds to promote tissue regeneration.

6.4. Conclusions

NCA ROP has been used to furnish StarPEG with terminal cysteine units. Initially, the grafted cysteine units presented tertiary butyl protecting groups, dictating that the modified PEG would possess amphiphilicity and the ability to self-assemble in aqueous solution to form discrete particles. Upon cysteine deprotection, a polymer capable of undergoing chemical crosslinking, through the formation of disulfide bridges, was isolated. Covalently crosslinked polymer hydrogels were consequently formed. These were capable of entrapping FITC-albumin, prior to its release upon disulfide reduction and hydrogel disassembly, mediated by GSH. The hydrogels reported have particular potential in the delivery of (bio)macromolecules at reductive sites. They may further be used as scaffolds for tissue regeneration that could aid cell growth and proliferation, through the release of protein growth factors.

6.5. References

1. Y. Shen, X. Fu, W. Fu, Zhibo Li, *Chem. Soc. Rev.* **2015**, 44, 612-622.
2. S. Zhang, Z. Li, *J. of Poly. Sci. B: Poly. Phys.* **2013**, 51, 546-555.
3. R. Cheng, F. Meng, C. Deng, H.-A. Klok, Z. Zhong, *Biomaterials.* **2013**, 34, 3647-3657.
4. J. Nicolas, S. Mura, D. Brambilla, N. Mackiewicz, P. Couvreur, *Chem. Soc. Rev.* **2013**, 42, 1147-1235.
5. H. Wei, R.-X. Zhuo, X.-Z. Zhang, *Progress in Poly. Sci.* **2013**, 38, 503-535.
6. R. Langer, J. Vacanti, *J. of Pediatric Surgery.* **2016**, 51, 8-12.
7. F. Khan, M. Tanaka, S.R. Ahmad, *J. of Materials Chem. B.* **2015**, 3, 8224-8249.
8. H. Cui, Y. Liu, Y. Cheng, Z. Zhang, P. Zhang, X. Chen, Y. Wei, *Biomacromol.* **2014**, 15, 1115-1123.
9. Y. Pei, O. R. Sugita, J. Y. Quek, P. J. Roth, A. B. Lowe, *Eur. Poly. J.* **2015**, 62, 204-213.
10. S. V. Lale, A. Kumar, F. Naz, A. C. Bharti, V. Koul, *Polym. Chem.* **2015**, 6, 2115-2132
11. L. Liu, L. Fu, T. Jing, Z. Ruan, L. Yan, *ACS App. Mater. & Interfaces.* **2016**, 8, 8980-8990.
12. M. Khuphe, B. Mukonoweshuro, A. Kazlauciusas, P.D. Thornton, *Soft Matter.* **2015**, 11, 9160-9167.
13. M. Khuphe, A. Kazlauciusas, M. Huscroft, P. D. Thornton, *Chem. Commun.* **2015**, 51, 1520-1523.
14. F. Meng, W.E. Hennink, Z. Zhong, *Biomaterials.* **2009**, 30, 2180-2198.
15. H. Zhang, X. Kong, Y. Tang, W. Lin, *ACS App. Mater. & Interfaces.* **2016**, 8, 16227-39.
16. Q. Zhou, L. Xu, F. Liu, W. Zhang, *Polymer.* **2016**, 97, 323-334.
17. B. Arunachalam, U. T. Phan, H. J. Geuze, P. Cresswell, *Proc. Natl. Acad. Sci. USA.* **2000**, 97, 745-750.
18. C. Wu, C. Belenda, J.-C. Leroux, M. A. Gauthier, *Chem.-Eur. J.* **2011**, 17, 10064-10070.
19. T. Vermonden, R. Censi, W. E. Hennink, *Chem. Rev.* **2012**, 112, 2853-2888.
20. D. Seliktar. *Science.* **2012**, 336, 1124-1128.
21. P. D. Thornton, A. Heise, *Chem. Commun.* **2011**, 47, 3108-3110.
22. T. Hayashi, P. D. Thornton, *Dyes Pigments.* **2015**, 121, 235-237; T Hayashi, A. Kazlauciusas, P. D. Thornton, *Dyes Pigments.* **2015**, 123, 304-316.
23. S-Y. Lee, S. Kim, J. Y. Tyler, K. Park, J-X. Cheng, *Biomaterials.* **2013**, 34, 552-561.
24. P. D. Thornton, R. Brannigan, J. Podporska, B. Quilty, A. Heise, *J. Mater. Sci: Mater. Med.* **2012**, 23, 37-45.
25. B.J. Sparks, J.G. Ray, D.A. Savin, C.M. Stafford, D.L. Patton. *Chem. Commun.* **2011**, 47, 6245-6247.
26. P.D. Thornton, S.M.R. Billah, N.R. Cameron, *Macromol. Rapid Commun.* **2013**, 34, 257-262.
27. G.J.M. Habraken, C.E. Koning, J.P.A. Heuts, A. Heise, *Chem. Commun.* **2009**, 24, 3612-3614.
28. Y. Dou, B. Zhang, M. He, G. Yin, Y. Cui, I.N. Savina, **2015**, 7, 580-591.
29. G. Ahuja, K. Pathak, *Indian J. of Pharma. Sci.* **2009**, 71, 599-607;
30. S.-E. Lamhamedi-Cherradi, M. Santoro, V. Ramammoorthy, B.A. Menegaz, G. Bartholomeusz, L.R. Iles, H.M. Amin, A.J. Livingston, A.G. Mikos, J.A. Ludwig, *Adv. Drug Deliv. Revs.* **2014**, 79-80, 155-171.
31. J. Maitra, V.K. Shukla, *American J. of Poly. Sci.* **2014**, 4, 25-31; K.Y. Lee, J.A. Rowley, P. Eiselt, E.M. Moy, K.H. Bouhadir, D.J. Mooney, *Macromol.* **(2000)**, 33, 4291-4294.
32. H.V. Chavda, C.N. Patel, *Int. J. of Pharma. Investigation*, **2011**, 1, 17-21.

Chapter 7. Glucose-Bearing Biodegradable Poly(Amino Acid) and Poly(Amino Acid)-Poly(Ester) Conjugates for Controlled Payload Release

Preamble

This Chapter is based on work published as:

Khuphe M.; Mahon C. S.; Thornton P. D., *Biomater. Sci.*, **2016**, 4, 1792-1801.

Abstract

The glucoseamine-initiated ring-opening polymerisation of amino acid N-carboxyanhydrides and O-carboxyanhydrides to yield amphiphilic block copolymers that are capable of self-assembly in aqueous solution to form well-defined, glucose-presenting, particles is reported. The particles formed are susceptible to enzyme-mediated (lipase and protease) degradation, and to pH-induced degradation. These can selectively bind the lectin, concanavalin A. Such glycoparticles are of significance to the controlled release of payload molecules in response to an acidic environment, for instance cancerous tissue, and upon interaction with target enzymes.

7.1. Introduction

Stimuli-responsive materials enable the delivery of therapeutic agents, upon interaction with a targeted stimulus, in a highly-controlled manner [1]. Such materials are highly suited to drug delivery as they permit payload protection and transportation *in vivo*, prior to drug release and subsequent deployment at the target site [2]. In particular, materials that are capable of releasing payload molecules, in response to a reduced environmental pH, are particularly well-suited to the transportation and delivery of poorly water soluble anticancer agents [3], due to the acidic nature of tumour tissue [4]. Degradation of the pH-responsive polymers by acid-mediated hydrolysis is a particularly effective method for the delivery of therapeutic agents to cancerous sites [5].

Amphiphilic block copolymers may be designed and created to adopt discrete nanoparticulate structures in aqueous media. Commonly, poly(ethylene glycol) (PEG) is used as the hydrophilic block that forms the shell of the nanoparticle, and thus aids nanoparticle dispersion, *in vivo* [6].

PEG has numerous advantageous properties that render it highly-appropriate for this role. These include its wide-ranging solubility in organic media and in aqueous media, non-fouling capabilities and commercial availability. However, PEG has restricted susceptibility to enzymatic degradation and is associated with hypersensitivity after intravenous administrations and oral administrations. There is also an accelerated blood clearance phenomenon arising as a result of the generation of anti-PEG antibodies [7]. Consequently, there is a clear demand for the generation of non-toxic, biodegradable and hydrophilic polymers that may serve as an alternative to PEG in the production of nanoparticles (NPs) for controlled drug delivery.

The secondary structures that poly(amino acid)s can possess are features that are rarely presented by synthetic non-poly(amino acid) macromolecules [8, 9]. NCA ROP readily proceeds from a primary amine-bearing initiator, so polymer grafting from a wide-range of functional initiators is possible [10]. In addition, the extensive and varied functionalities that such polymers present enables straightforward post-polymerisation (bio)molecular grafting. *O*-carboxyanhydride (OCA) monomers offer a relatively straightforward route to the synthesis of functional poly(ester)s [11]. Consequently, OCA ROP offers a route to biodegradable polymers that are capable of undergoing self-assembly in aqueous solution, and can be readily functionalised with chosen (bio)molecules.

Carbohydrates and carbohydrate-containing (macro)molecules are essential components within biology. Glycoproteins are a particular example of carbohydrate-bearing macromolecules that play a key role in numerous biological processes, including cell-cell interactions [12]. Carbohydrate ligands may be conjugated to protein molecules to target protein receptors at sites of localisation (glycotargeting), as part of a targeted drug delivery mechanism [13]. Alternatively, synthetic poly(amino acid)s may be used as a substitute for proteins in the creation of well-defined glycopolymers, designed for targeted drug delivery [14]. Such polymers have good biological activity and the ability to withhold payload molecules. The conjugation of glucose to biodegradable poly(amino acid)s is of particular significance to the creation of a highly-effective drug delivery system; glucose transporters are membrane-embedded proteins that facilitate the transport of glucose across the cell membrane [15]. Glucose uptake and metabolism by cancerous cells is greater than glucose uptake and

metabolism by non-cancerous cells, asserting the logic of using glucose moieties to enable molecular uptake by cancer cells [16].

Carbohydrate (macro)molecules may be used as initiators of polymerisations. They may also undergo chain-growth polymerisation upon the introduction of vinyl groups to the sugar unit. For instance, Nakamura *et al.* [17] disclosed the use of the polysaccharide, chitosan as a macroinitiator for the generation of chitosan-*graft*-polysarcosine copolymers using NCA ROP. Wong *et al.* [18] demonstrated the acrylate modification of glucoseamine (GluAm) to yield a sugar-bearing monomer that could undergo controlled, reversible addition-fragmentation chain-transfer (RAFT) polymerisation. Yamada *et al.* [19] have described the production of amphiphilic block copolymers of vinyl ethers (VEs) that were furnished with pendant *N*-acetyl-D-glucosamine (GlcNAc) units. The copolymers were produced using the living cationic polymerisation of isobutyl vinyl ether and a vinyl ether carrying 3,4,6-tri-O-acetyl-2-deoxy-2-phthalimido- β -D-glucose. Aoi *et al.* [20] demonstrated the ROP of 2-oxazolines, initiated by GlcNAc to yield glucosamine-terminated, 2-oxazoline polymers upon the removal of the acetyl-protecting groups. Continuation of the use of carbohydrate molecules to initiate polymerisations may be extended further to include GluAm for the initiation of NCA ROP, thus affording glucose-terminated poly(amino acid)s and poly(amino acid)-poly(ester) conjugates.

This chapter details the creation of poly(amino acid) block copolymers and poly(sarcosine)-*b*-poly(ester) block copolymers, formed by an initial NCA ROP that is initiated from GluAm. The glycosylated polymer that is produced can then independently initiate a second amino acid NCA, or an amino acid OCA, to yield a second poly(amino acid) block or poly(ester) block, respectively. To the best of the author's knowledge, this is the first example of the combination of NCA ROP and OCA ROP to produce a block copolymer consisting of discrete poly(ester) blocks and poly(peptoid) blocks. Using glucosamine in this manner removes the requirement of post-polymerisation functionalisation to be conducted for the production of glycopeptides; a glucose-presenting amphiphilic block copolymer is created in a one-pot reaction. The polymers formed may self-assemble in aqueous media to yield discrete NPs and have been shown to possess the ability to encapsulate and withhold rhodamine B molecules, prior triggered glycoparticle degradation and payload release upon interaction with an acidic environmental medium and/or an appropriate lipase or protease enzyme. The glycoparticles

formed demonstrated excellent selectivity to the binding of concavalin A, signifying that glucose is present on their exterior. The glycoparticles detailed offer promise as biodegradable drug delivery vehicles, for the targeted and controlled delivery of therapeutic agents.

7.2. Experimental Details

7.2.1. Syntheses of Cyclic Monomers

Sarcosine (Sar) *N*-NCA, L-phenylalanine (Phe) NCA and Phe OCA were synthesised following the procedures described in Chapter 3.3.

7.2.2. Polymer Syntheses

The ROP procedure used for polymer syntheses is described using the example of the synthesis of Glu-poly[(Sar)_m-*b*-(PheLA)_n]. Sar *N*-NCA (420 mg, 3.65 mmol) was dissolved in anhydrous DMF (10 mL). The solution was injected into a nitrogen-purged Schlenk tube that was equipped with a magnetic stirrer bar. To this, a solution of 1,3,4,6-tetra-*O*-acetyl-2-amino-deoxy-β-D-glucopyranose (Glu) (64 mg, 0.183 mmol), dissolved in anhydrous DMF (5 mL), was added. The reaction was stirred at room temperature, under nitrogen for 96 hours. Aliquots (1 mL) were isolated from the reaction at 24 hour, 72 hour and 96 hour intervals. These were added to cold diethyl ether and the precipitated solids, obtained after centrifugation, were analysed using ESI MS, to affirm the ROP of Sar *N*-NCA from the glucose molecule. Then, Phe OCA (350.6 mg, 1.83 mmol) was dissolved in anhydrous DMF (5 mL). The solution was injected gently into the reaction medium, together with a solution of 4-dimethylaminopyridine (DMAP) (22.3 mg, 0.183 mmol) in anhydrous DMF (2 mL). The reaction stirred at room temperature for a further 96 hours. The product was subsequently precipitated in cold diethyl ether (200 mL), isolated using centrifugation (4000 rpm, 10 min) and dried *in vacuo* (37 °C) for 24 hours. An analogous procedure was followed for the synthesis of Glu-poly[(Sar)_m-*b*-(Phe)_n], with Phe NCA to generate the poly(amino acid) block.

Glu-poly[(Sar)_m-*b*-(PheLA)_n]: 53.4%. ¹H NMR (500 MHz, TFA, δ) 8.53 (s, NH), 7.67 - 7.16 (m, ArH), 7.02 (t, OCHC(O)CH₃), 6.32 - 5.28 (m, OC(O)CH₃(CH₃)₃NH), 4.73 - 4.62 (m, C(O)αCHCH₂ArH), 4.62 - 4.51 (m, COCH₂N(CH₃)₃), 4.12 - 4.07 (m, CHNHCO, CH₂CHO), 3.52 - 3.00 (m, Ar-CH₂, NCH₃), 2.41 - 2.33 (q, COCH₃, 12H).

Glu-poly[(Sar)_m-b-(Phe)_n]: 75.9%. ¹H NMR (500 MHz, TFA, δ): 8.55 (s, NH), 7.50 - 7.15 (m, ArH), 5.40 - 5.36 (m, CH(OCOCH₃)), 5.01 m - 4.92 (m, CH₂(OCOCH₃)), 4.72 - 4.49 (m, CH₂N(CH₃), αCHNH), 3.78 - 3.74 (t, CH(O)OCOCH₃), 3.68 - 3.63 (t, CHCONHCH₂), 3.39 - 3.09 (m, CH₂Ar, N(CH₃)), (d, OCOCH₃).

7.2.3. Acetyl Deprotection

An example of acetyl deprotection is provided for the deprotection of Glu-poly[(Sar)_m-b-(PheLA)_n]. Briefly, Glu-poly[(Sar)_m-b-(PheLA)_n] (400 mg) was dissolved in 0.2 M LiOH(aq)/THF (40 mL, 1:3 v/v). The solution was introduced into a 2-neck round bottom flask equipped with a magnetic stirrer bar. The reaction was stirred at room temperature for 12 hours, under a nitrogen flow. Tetrahydrofuran (THF) was then removed under vacuum. The resulting deacetylated polymer was dialysed against HPLC-grade water for 96 hours, with the dialysate being replenished at 8 hour intervals. Yields after dialysis and lyophilisation: Glu-poly[(Sar)_m-b-(PheLA)_n]: 63 wt. %; Glu-poly[(Sar)_m-b-(Phe)_n]: 72 wt. %.

7.2.4. Turbidimetry Studies

Concanavalin A (Con A) solution (2 mg/mL) and *Ricinus Communis* Agglutinin (RCA₁₂₀) solution (2 mg/mL) were prepared in a PBS buffer solution (pH 7.4). Polymeric NPs (5 mg/mL) were also prepared in a PBS buffer solution (pH 7.4). Lectin-binding assessments, using UV-Vis spectrophotometry, were then carried out by monitoring the change in turbidity (absorbance) at 450 nm, when the lectin solution was mixed with the glycopolymer solution. Typically, 400 μL of Con A was pipetted into a UV-Vis quartz cuvette and the background absorbance was measured. NPs (200 μL) were added to the lectin solution and the solution was mixed thoroughly by pipetting up and down. The absorbance was then monitored continuously for 10 minutes. From then on, the concentration of NPs was increased gradually in the mixture, by adding 100 μL NPs at 10 minute intervals and monitoring the absorbance. The final loading of NPs in the medium was ca 3.18 mg/mL. An analogous procedure was repeated using RCA₁₂₀.

7.2.5. Preparation of Rhodamine B-Loaded Glyconanoparticles

Glycopolymer solutions were obtained by dissolving the respective polymers (20 mg) in DMSO (1 mL). Then, rhodamine B solution (34 μM) was prepared in a PBS buffer solution (pH 7.4), its

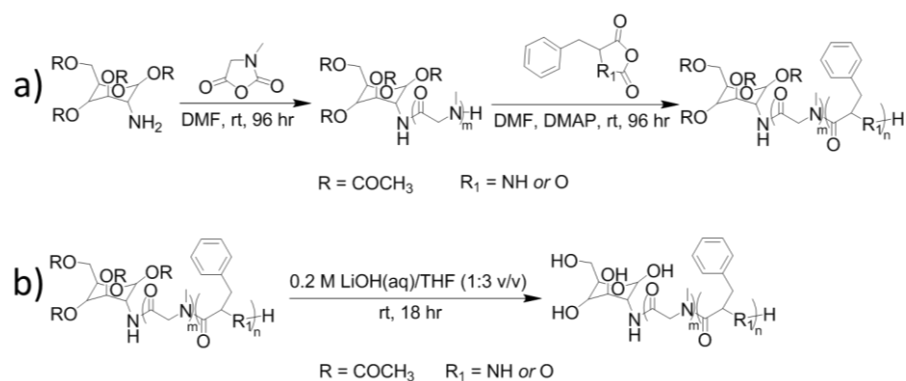
absorbance being confirmed using UV-Vis spectrophotometry. The glycopolymer solution (1 mL) was added gradually to the aqueous rhodamine-B solution (20 mL), under vigorous stirring. After complete addition, the suspensions generated were incubated at room temperature and left to stir for 18 hours in the dark, to afford enough time for encapsulation of the rhodamine B. The respective suspensions were then centrifuged. Rhodamine B-loaded NPs were subsequently isolated from free, un-encapsulated, rhodamine B and DMSO by decanting off the supernatant. The particles were rinsed using neat PBS buffer solution. The NPs were collected and dialysed against a PBS buffer solution (2000 Da MWCO) for 48 hours and subsequently lyophilised. The absorbance of the supernatant that was obtained after centrifugation was recorded at 554 nm.

7.2.6. Enzyme and pH-Mediated Polymer Degradation

Rhodamine B-loaded Glu-poly[(Sar)_m-*b*-(PheLA)_n] NPs and Glu-poly[(Sar)_m-*b*-(Phe)_n] NPs were reconstituted in a PBS buffer (pH 7.4, 5 mL) only, in a PBS buffer (pH 7.4, 5 mL) containing 40 units of lipase, in a PBS buffer (pH 7.4, 5 mL) containing 40 units of α -chymotrypsin and in an acetate buffer (pH 5.4, 5 mL) only, respectively. The respective mixtures were then contained in glass vials that were masked with aluminium foil. Evaporation was prevented by capping the vials. The final loading of NPs in each vial set-up was 5 mg/mL. The vials were subsequently incubated in the dark at 37 °C. At predetermined time intervals, 1 mL aliquots were isolated from each experimental set-up, transferred into Eppendorf microcentrifuge safe-lock tubes and centrifuged. The respective supernatants (0.7 mL) were transferred into micro-cell quartz cuvettes and their absorbance determined using UV/Vis spectrophotometry, at the λ_{max} (554 nm). Analysed samples were returned immediately to their respective parent sample vials to achieve accumulative rhodamine B release. Rhodamine B release at each time interval was then computed from a prepared calibration graph.

7.3. Results and Discussion

The NCA cyclic monomers and OCA cyclic monomers were obtained in good purity, using previously reported protocols (Chapter 3.3). Then, amphiphilic block copolymers, that contained poly(Sar) as the hydrophilic segment, were synthesised from acetyl-protected GluAm, for use as drug delivery vehicles (Scheme 7.1a).



Scheme 7.1. The syntheses of biodegradable poly[(sar)-b-(ester)] and poly[(sar)-b-(amino acid)] macromolecules from a carbohydrate-initiated ROP (a). The removal of acetyl protecting groups (b).

Initially, Phe NCA was grafted from acetyl-protected Glu-poly(Sar) to yield a poly(peptoid)-*b*-poly(amino acid) block copolymer (Scheme 7.1 a). Secondly, phenylalanine lactic acid (PheLA) OCA was grafted from acetyl-protected Glu-poly(Sar) to yield a poly(peptoid)-*b*-poly(ester) block copolymer (Scheme 7.1 a). Poly(amino acid)-containing Glu-poly[(Sar)_m-*b*-(Phe)_n] and poly(ester)-containing Glu-poly[(Sar)_m-*b*-(PheLA)_n] were produced in reasonable yields, 75.9% and 53.4% respectively.

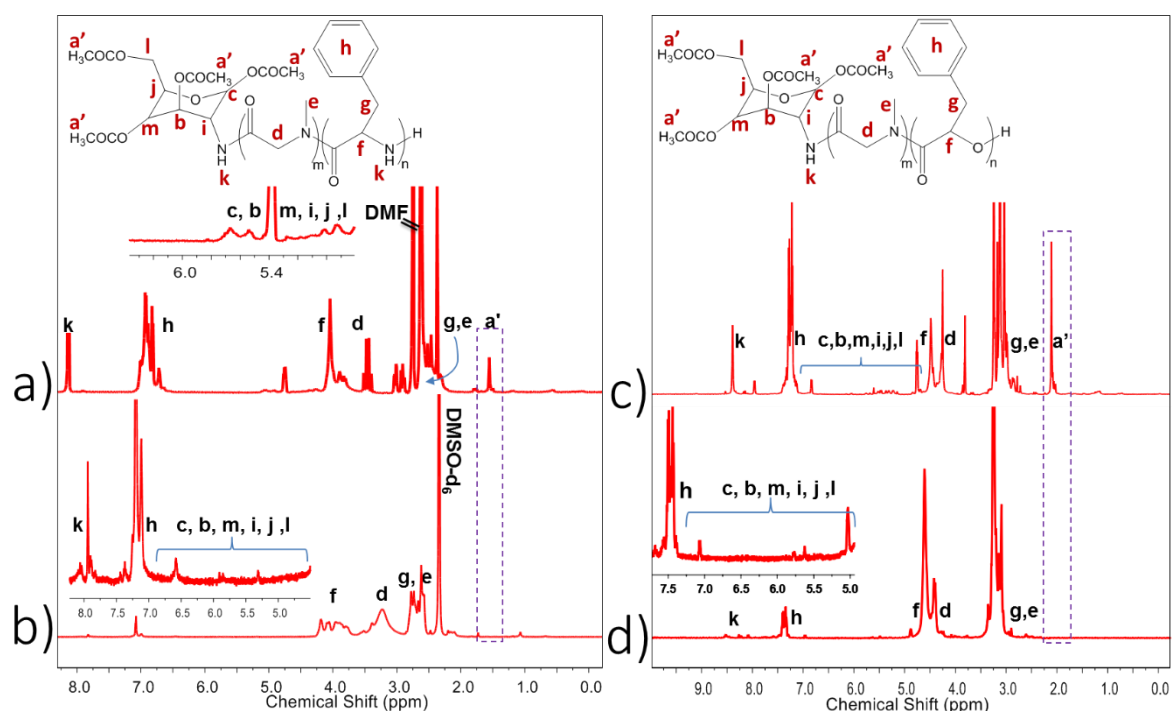


Figure 7.1. ¹H NMR spectra of Glu-poly[(Sar)_m-*b*-(Phe)_n] before (a) and (b) after the removal of acetyl protecting groups from the GluAm moieties. ¹H NMR spectra of Glu-poly[(Sar)_m-*b*-(PheLA)_n] before (c) and (d) after the removal of acetyl protecting groups from the GluAm moieties.

^1H NMR (Figure 7.1 a, c) and FTIR (Figure 7.2 a, c) confirmed the production of the desired polymers. The compositions of the polymers were approximated from ^1H NMR spectroscopy. This revealed that 24.4 units of Sar and 10.8 units of Phe were successfully grafted from GluAm to yield Glu-poly[(Sar) $_m$ -*b*-(Phe) $_n$], and that 20 units of Sar and 11 units of PheLA were successfully grafted from GluAm to yield Glu-poly[(Sar) $_m$ -*b*-(PheLA) $_n$]. Removal of the acetyl groups, that had previously protected the hydroxyl groups of glucosamine, was conducted using a LiOH and THF aqueous solution (Scheme 7.1 b).

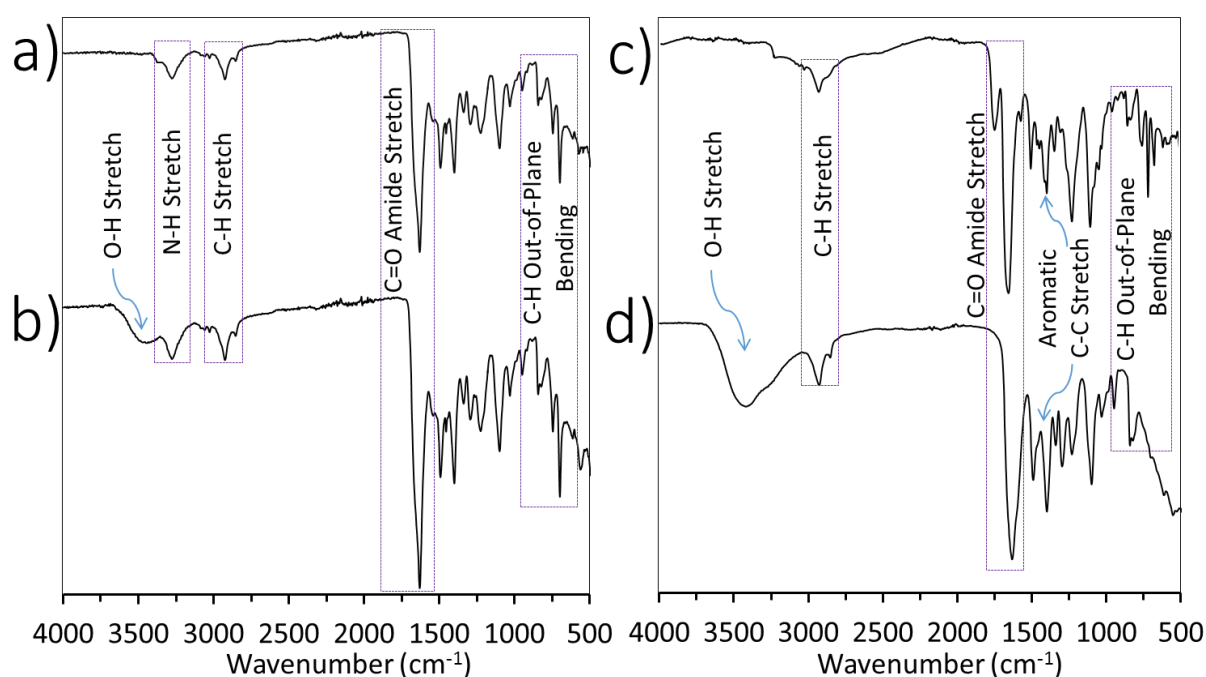


Figure 7.2. FTIR spectra of Glu-poly[(Sar) $_m$ -*b*-(Phe) $_n$] before (a) and after (b) the removal of the acetyl protecting groups from the GluAm moieties. FTIR spectra of Glu-poly[(Sar) $_m$ -*b*-(PheLA) $_n$] before (c) and after (d) the removal of the acetyl protecting groups from the GluAm moieties.

The M_n , M_w and PDI values of the polymers produced were assessed using Advanced Polymer Chromatography (APC) (Figure 7.3), as are summarised in Table 7.1. The results confirm that, in both instances, acetyl deprotection did not result in polymer hydrolysis. Both of the polymers that were produced possessed PDI values close to 1.00, an imperative requirement of effective polymeric drug delivery vehicles. Further confirmation that acetyl deprotection had occurred was gained from the data that were obtained using ^1H NMR spectroscopy (Figure 7.1 b, d) and FTIR spectroscopy (Figure 7.2 b, d). ^1H NMR spectroscopic analyses confirmed the disappearance of the peak belonging to the protons from acetyl groups (α'). FTIR spectroscopic

analyses revealed the emergence of a peak (hydroxyl stretch ($\nu(\text{OH}) = 3500 \text{ cm}^{-1}$), emanating from the deprotected glucose moieties.

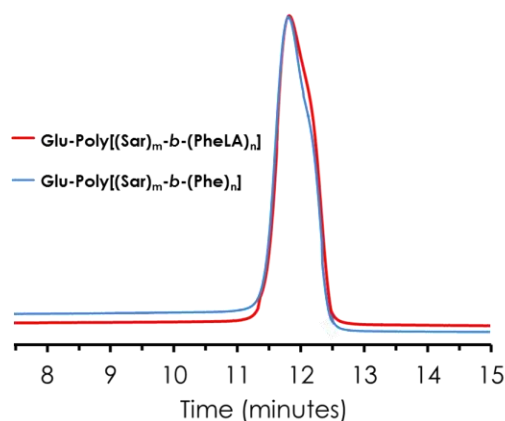


Figure 7.3. APC traces of Glu-poly[(Sar)_m-b-(PheLA)_n] and of Glu-poly[(Sar)_m-b-(Phe)_n].

Table 7.1. The molecular weight of the polymers produced.

Polymer	M_n (g/mol)	M_w (g/mol)	PDI *
Glu-poly[(Sar) _m -b-(Phe) _n]	4221	4449	1.05
Glu-poly[(Sar) _m -b-(PheLA) _n]	4234	4466	1.05

* Determined by advanced polymer chromatography (APC).

The ability of the polymers that were produced to form particles in aqueous media is essential if they are to be used as drug delivery vehicles. NPs were formed by dissolving the respective polymers in DMF and then dialysing the solutions against a PBS buffer solution (pH 7.4). The morphologies of the NPs produced was assessed using TEM (Figure 7.4 a, b) and by SEM (Appendix 7), both of which revealed the formation of discrete spherical NPs.

DLS can be used to determine the critical aggregation concentration (CAC) of the polymers produced [21]. DLS Analysis revealed that the particles consisting of Glu-poly[(Sar)_m-b-(Phe)_n] had a hydrodynamic radius of $66.8 \pm 10.0 \text{ nm}$ (Figure 7.4 d) and a CAC of 0.079 mg/mL. The particles formed from Glu-poly[(Sar)_m-b-(PheLA)_n] possessed a hydrodynamic radius of $59.6 \pm 12.0 \text{ nm}$ (Figure 7.4 c) and a CAC of 0.061 mg/mL. In both instances, the particles that were

formed were of suitable dimensions to be used as drug delivery vehicles *in vivo*, and the polymers were able to form stable particles from suitably low concentrations to be applied *in vivo* [22].

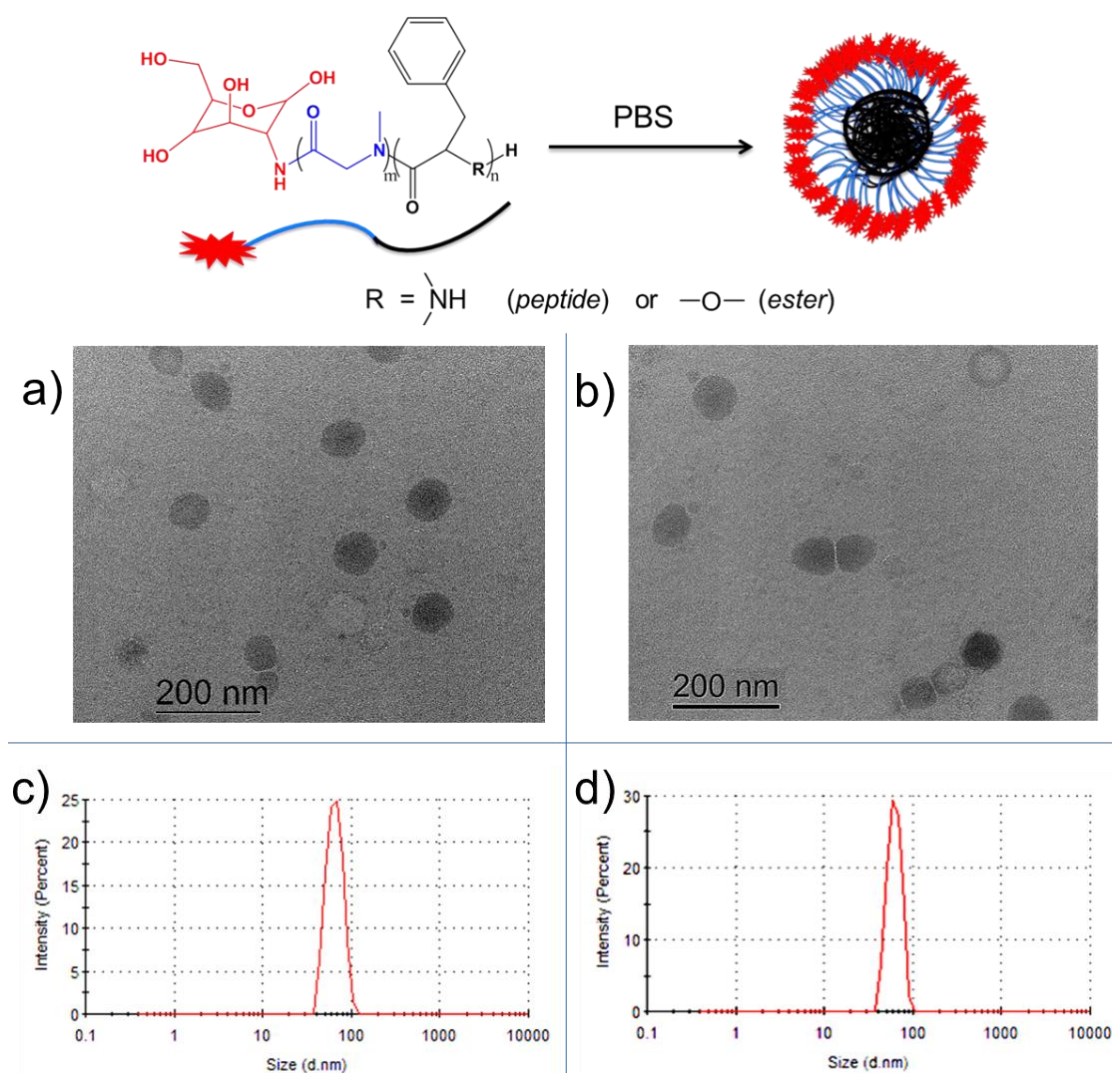


Figure 7.4. (Top) A schematic representation of the formation of NPs, in aqueous medium. TEM microphotographs of NPs formed from the synthesis of biodegradable block copolymers from Glu-poly[(Sar)_m-b-(PheLA)_n] (a) and from Glu-poly[(Sar)_m-b-(Phe)_n] (b). DLS size distribution traces of Glu-poly[(Sar)_m-b-(PheLA)_n] NPs (c) and Glu-poly[(Sar)_m-b-(Phe)_n] NPs (d).

The stability of particles that were formed from Glu-poly[(Sar)_m-b-(Phe)_n] was assessed initially over a period of 300 mins, before the particles were stored and re-analysed after 5 days and after 25 days (Figure 7.5 a, c). The particle size remained relatively stable at 67.9 nm and at 68.2 nm, after 5 days and after 25 days, respectively. Analogous analysis of the particles that

were formed from Glu-poly[(Sar)_m-b-(PheLA)_n] was performed and revealed that the size of these particles remained relatively stable at 62.3 nm and at 62.4 nm, after 5 days and after 25 days, respectively (Figure 7.5 b, d).

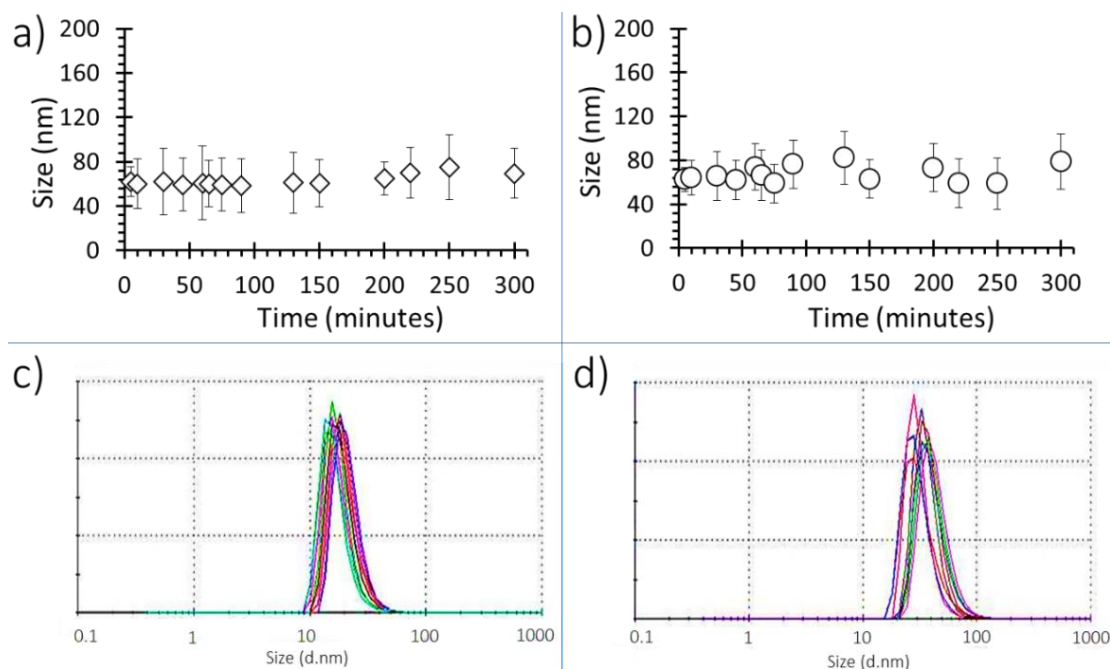


Figure 7.5. Graphs detailing the stability of Glu-poly[(Sar)_m-b-(Phe)_n] NPs (a) and of Glu-poly[(Sar)_m-b-(PheLA)_n] NPs (b), monitored continuously for 300 minutes. Error bars represent the SD values for DLS measurements, done in triplicate. An overlay of the DLS traces which were obtained at 1 hour intervals for the duration of 10 hours, for Glu-poly[(Sar)_m-b-(Phe)_n] NPs (c) and for Glu-poly[(Sar)_m-b-(PheLA)_n] NPs (d). The close fit of the traces reveals the stability of the dispersions.

Central to the design of the polymers produced is their ability to present glucose units on their exterior, upon self-assembly into particles. The recognition abilities of the glycopolymers formed was determined using Con A, a tetrameric lectin. This possesses four binding sites that can specifically bind to glucosyl residues. Successful interaction between the NPs and lectin macromolecules results in particle aggregation, and in an increase in the turbidity of the medium in which they are found. Figure 7.6 reveals the tendency of the NPs formed from Glu-poly[(Sar)_m-b-(Phe)_n] and from Glu-poly[(Sar)_m-b-(PheLA)_n] to aggregate in the presence of Con A, but not in the presence of the non-glucose-binding RCA₁₂₀. Each step increase in absorbance that is evidenced in Figure 7.6 c and in Figure 7.6 d is a result of further NP addition (0.5 mg) to the medium, before a total polymer loading of 3.18 mg/mL was reached, after 50 minutes.

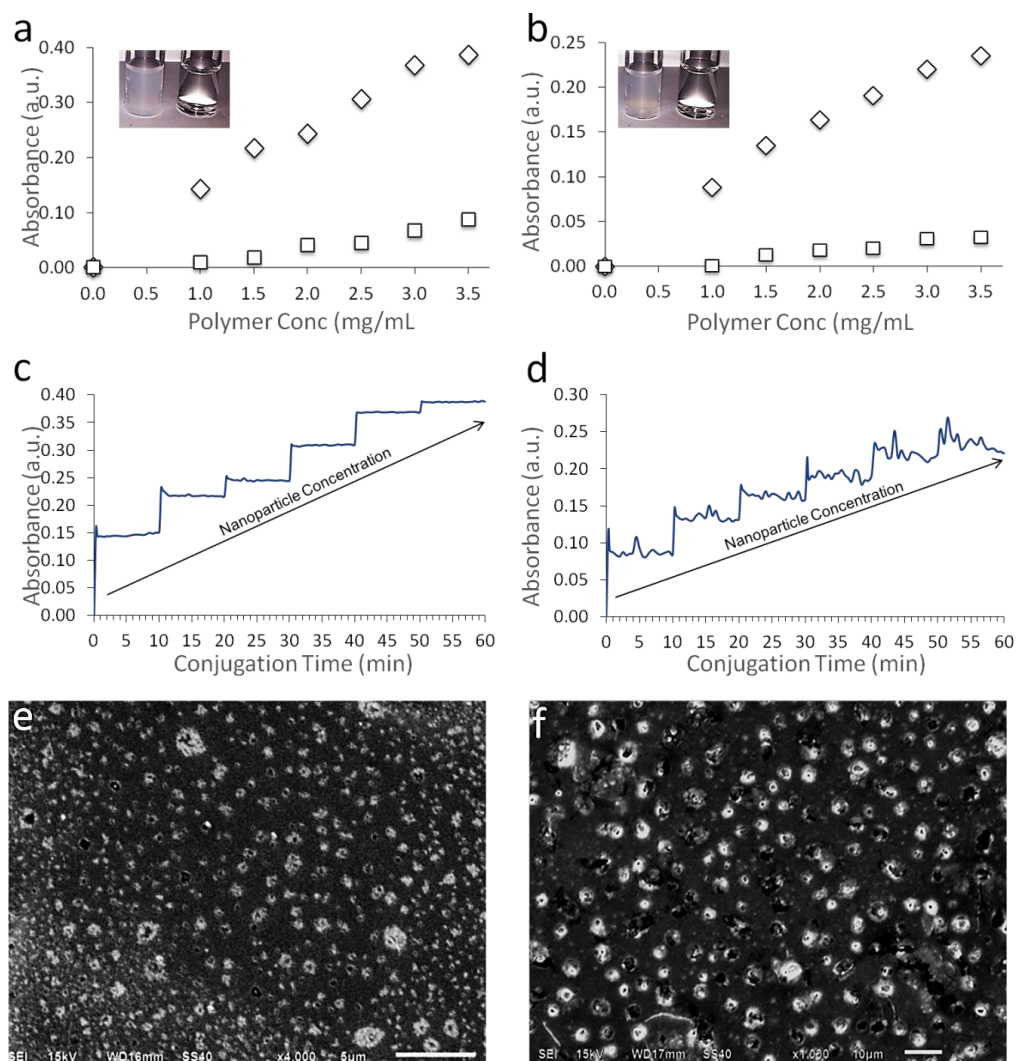


Figure 7.6. (a and b) UV-Vis spectrophotometry data revealing the aggregation of NPs created from Glu-poly[(Sar)_m-b-(Phe)_n] and Glu-poly[(Sar)_m-b-(PheLA)_n] when incubated with Con A (◇) and RCA₁₂₀ (□) at increasing concentrations. The inset reveals the turbid suspensions that formed when the polymers were incubated with Con A and the clear solutions that were found when the polymers were incubated with RCA₁₂₀. The binding of NPs created from Glu-poly[(Sar)_m-b-(Phe)_n] (c) and Glu-poly[(Sar)_m-b-(PheLA)_n] (d) to Con A resulted in an increase in absorbance as the NP concentration was progressively increased over time. SEM analysis confirmed the formation of aggregates when Con A was incubated with NPs created from Glu-poly[(Sar)_m-b-(Phe)_n] (e, scale bar represents 5 μm) and Glu-poly[(Sar)_m-b-(PheLA)_n] (f, scale bar represents 10 μm).

Nanoparticle aggregation was also confirmed by carrying out SEM analyses of the media that contained NPs produced from Glu-poly[(Sar)_m-b-(Phe)_n] and from Glu-poly[(Sar)_m-b-(PheLA)_n], independently incubated with Con A (Figure 7.6 e and Figure 7.6 f, respectively). Size analyses of the aggregates that were formed were conducted using DLS and revealed that Glu-

poly[(Sar)_m-b-(Phe)_n] particles, that were incubated with Con A, had aggregated resulting in a mean aggregate size of 2.40 ± 0.30 μm (Appendix 7). Glu-poly[(Sar)_m-b-(PheLA)_n] particles, that were incubated with Con A, had aggregated resulting in a mean aggregate size of 2.93 ± 0.40 μm (Appendix 7). In both instances, the polydispersity indices of the dispersions was in excess of 0.67, indicating that the particles in the media were unstable and highly aggregated.

Reducing the environmental pH gives a suitable stimulus to triggering the release of a molecular cargo within an acidic environment, such as that provided by the acidic tumour tissue. The creation of polymeric structures that contain ester linkages, which are susceptible to acid-mediated hydrolysis, offers a highly-effective mechanism for the delivery of anticancer agents to targeted cancerous cells. The abilities of the glycoparticles formed, to encapsulate and then to selectively release low molecular weight molecules, was investigated using rhodamine B as a model payload compound. NPs that were produced from Glu-poly[(Sar)_m-b-(PheLA)_n] were independently incubated in aqueous solutions at pH values of pH 5.4 and of pH 7.4. A pH value of 5.4 was selected to simulate a (late) endosomal pH, whilst a pH of 7.4 is equal to the value of the physiological pH [23]. When incubated in a pH 5.4 acetate buffer, the release of rhodamine B (in excess of 97%) occurred because of the disruption of the NPs, upon acid hydrolysis of the ester bonds (Figure 7.7 a).

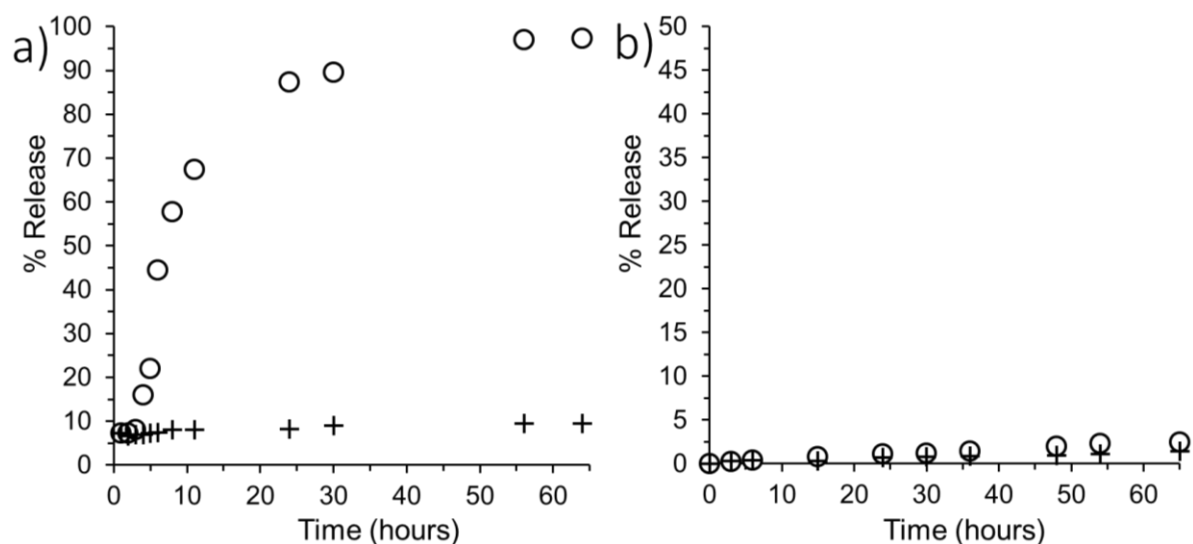


Figure 7.7. The release of rhodamine B from Glu-poly[(Sar)_m-b-(PheLA)_n] NPs (a) and from Glu-poly[(Sar)_m-b-(Phe)_n] NPs (b) in response to incubation in PBS buffer solution, maintained at pH 7.4 (+) and acetate buffer maintained at pH 5.4 (o).

However, the particles maintained in a pH 7.4 PBS buffer solution released less than 11% of the loaded rhodamine B, over a 65 hour period. Payload release from exclusively poly(amino acid)-containing Glu-poly[(Sar)_m-b-(Phe)_n] particles (control experiment), in response to incubation in the pH 5.4 acetate buffer solution was extremely limited owing to the peptide bonds that formed the polymer backbone being non-susceptible to acid hydrolysis (Figure 7.7 b). In addition, the composition of the block copolymers that were formed, was selected for them to be susceptible to hydrolysis when independently incubated with α -chymotrypsin (Phe-containing polymers) and lipase (PheLA-containing polymers). The proteolytic enzyme α -chymotrypsin possesses selectivity in cleaving peptide bonds that are flanked by amino acids that possess aromatic side groups, for instance Phe. The lipase possesses the broad selectivity to cleave ester bonds [24]. The ability of the particles produced to release their molecular cargo, in response to an enzymatic trigger, is presented in Figure 7.8.

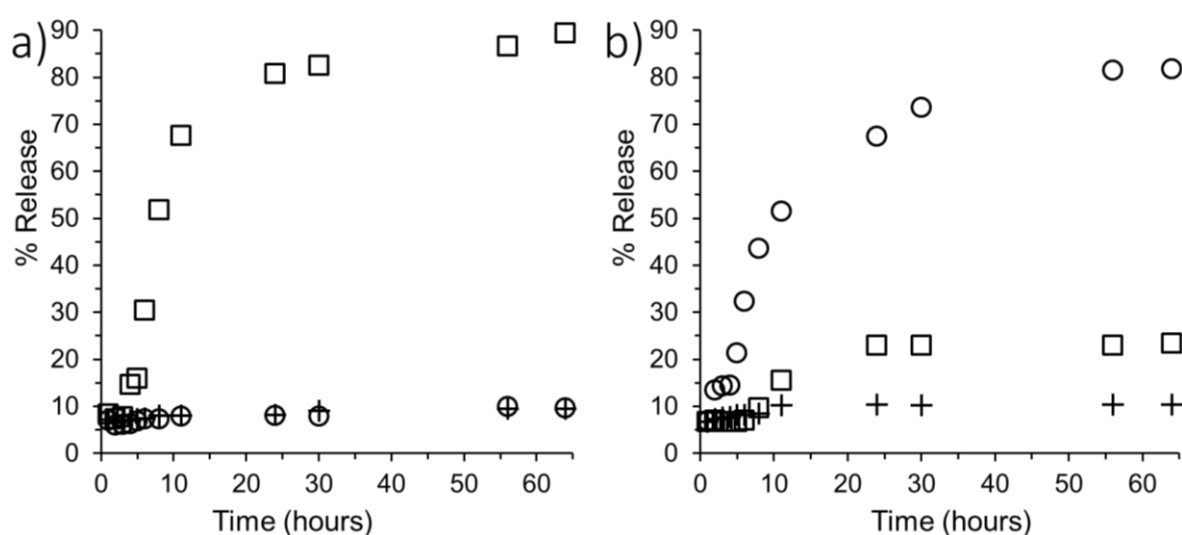


Figure 7.8. The release of rhodamine B, at 37 °C, from Glu-poly[(Sar)_m-b-(Phe)_n] NPs (a) and from Glu-poly[(Sar)_m-b-(PheLA)_n] NPs (b) in response to incubation in a PBS solution (pH 7.4) only (+), PBS solution (pH 7.4), containing 40 Chymotrypsin units (□) and PBS solution (pH 7.4) containing 40 Lipase units (o).

As anticipated, α -chymotrypsin demonstrated extensive activity against the Phe-containing polymer, with 89.4% of rhodamine B release occurring after 65 hours of incubation. The activity of α -chymotrypsin against the PheLa-containing polymer was markedly less (23.3% release following 65 hours incubation), but is still noteworthy. This suggests the potential of this polymer for gradual payload release upon interaction with α -chymotrypsin. The activity of

lipase was profound against the PheLA-containing polymers (81.8% release after 65 hours), but negligible against the Phe-containing polymers. As such, these polymers possessed the ability to release their molecular cargo in response to acidic pH environment (PheLA-containing polymers), and the presence of lipase enzymes and of protease enzymes.

The Korsmeyer-Peppas (KP) model [25] (Chapter 2.22), was then used in an estimation of the release profile of rhodamine B from the NPs. Analysis of the experimental data from enzyme-mediated degradation studies (Figure 7.9 a, b) revealed release exponential (n) values of $n \leq 0.43$ for Glu-poly[(Sar)_m-*b*-(Phe)_n] NPs and for Glu-poly[(Sar)_m-*b*-(PheLA)_n] NPs (Table 7.2). It is suggested that payload release followed a Fickian diffusion profile, indicating that comparable erosion control factors and the diffusion factors were responsible for the payload release.

Table 7.2. The release exponents (n) that were determined using the KP model.

	n (0 - 8 hours)	n (9 - 65 hours)
Glu-poly[(Sar) _m - <i>b</i> -(Phe) _n] in PBS only (pH 7.4)	0.10	0.09
Glu-poly[(Sar) _m - <i>b</i> -(Phe) _n] + Chymotrypsin (pH 7.4)	0.40	0.23
Glu-poly[(Sar) _m - <i>b</i> -(Phe) _n] + Lipase (pH 7.4)	0.18	0.13
Glu-poly[(Sar) _m - <i>b</i> -(PheLA) _n] in PBS only (pH 7.4)	0.11	0.07
Glu-poly[(Sar) _m - <i>b</i> -(PheLA) _n] + Chymotrypsin (pH 7.4)	0.11	0.37
Glu-poly[(Sar) _m - <i>b</i> -(PheLA) _n] + Lipase (pH 7.4)	0.43	0.30
Glu-poly[(Sar) _m - <i>b</i> -(PheLA) _n] in acetate buffer (pH 5.4)	1.94	0.20
Glu-poly[(Sar) _m - <i>b</i> -(Phe) _n] in acetate buffer (pH 5.4)	0.77 (0 - 65 hrs)	

However, analysis of data obtained from the pH-mediated degradation of Glu-poly[(Sar)_m-*b*-(Phe)_n] NPs (Figure 7.9 c, Table 7.2) revealed a value of $n > 0.85$, at acidic pH (case II transport-dominated release mechanism). This indicates a rapid diffusion of rhodamine B from the NPs

relative to the relaxation process of the polymer chains. This is most likely due to polymer erosion and the subsequent dis-assembly of NPs [26]. The nominal payload release that was recorded from the control experiment (Glu-poly[(Sar)_m-b-(Phe)_n] NPs that were incubated in acidic pH) could be because of the swelling of the polymeric NPs over time (Figure 7.9 d, Table 7.2).

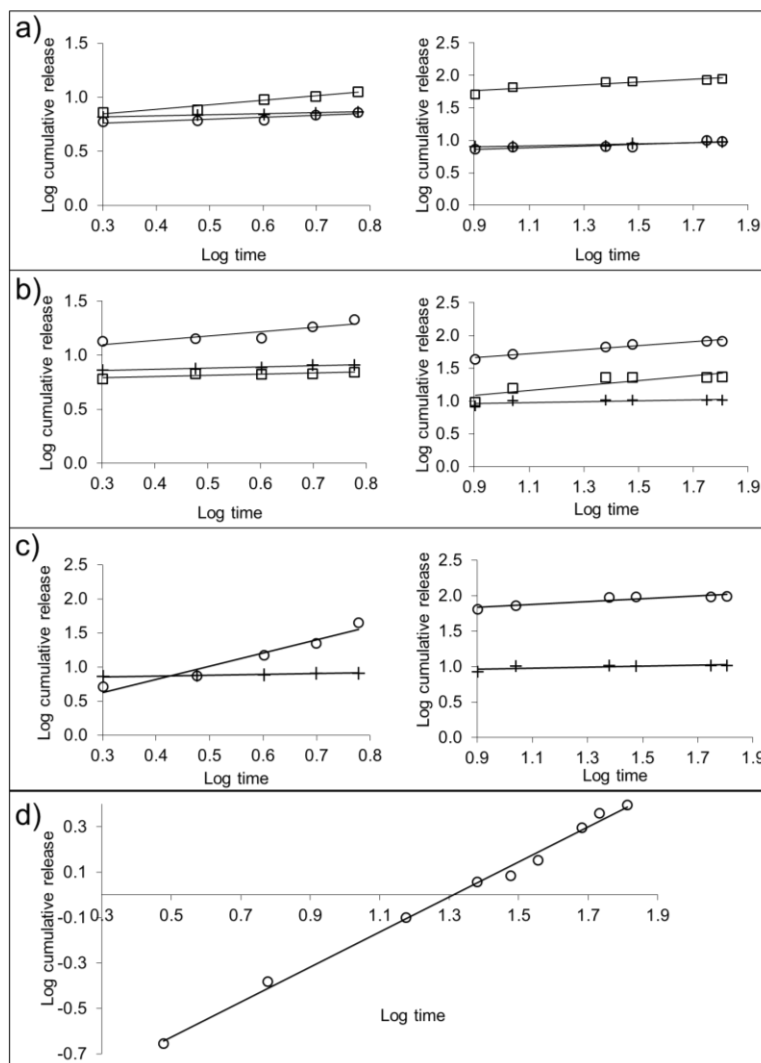


Figure 7.9. Korsmeyer-Peppas (K-P) model plots for the release of the molecular cargo from (a) Glu-poly[(Sar)_m-b-(Phe)_n] NPs and from (b) Glu-poly[(Sar)_m-b-(PheLA)_n] NPs incubated in PBS buffer (pH 7.4) only (+), in PBS buffer (pH 7.4) plus Chymotrypsin (□), in PBS buffer (pH 7.4) plus Lipase (○). Also, K-P model plots for the release of molecular cargo from (c) Glu-poly[(Sar)_m-b-(PheLA)_n] NPs and from (d) Glu-poly[(Sar)_m-b-(Phe)_n] NPs incubated in PBS buffer (pH 7.4, 37 °C) (+) and in an acetate buffer (pH 5.4, 37 °C) (○).

7.4. Conclusion

Amphiphilic block polymers, consisting of discrete poly(ester) and/or poly(amino acid) segments, which were independently conjugated to a poly(peptoid) segment, were produced using glucoseamine as the functional initiator. Using the glucose initiator enabled NPs to be generated that present glucose on their exterior, a feature that may be exploited for enhanced cellular uptake by cancerous cells. The selective binding of the particles was demonstrated by the ability of glucose-bearing particles to bind with the target, lectin Con A, but not with the control, lectin RCA₁₂₀. The controlled release of entrapped payload molecules was achieved when the PheLA-containing particles were incubated in an acidic medium. Additionally, the enzyme-mediated hydrolysis of both poly(amino acid)-containing polymers and poly(ester)-containing polymers was achieved using protease and lipase enzymes, respectively. As such, the resulting biodegradable particles are of significance as carrier vehicles for subsequent payload release on interaction with a targeted stimulus.

7.5. References

1. (a) S. Mura, J. Nicolas, and P. Couvreur, *Nat. Mater.*, **2013**, 12, 991-1003; (b) S. Ganta, H. Devalapally, A. Shahiwala, and M. Amiji, *J. Control. Release*, **2008**, 126, 187-204; (c) Q. Zhang, N. Re Ko, and J. Kwon Oh, *Chem. Commun.*, **2012**, 48, 7542-7552; (d) A.K. Bajpai, S.K. Shukla, S. Bhanu, and S. Kankane, *Prog. Polym. Sci.*, **2008**, 33, 1088-1118; (e) P. D. Thornton and A. Heise, *Chem. Commun.* **2011**, 47, 3108-3110.
2. (a) R. Chenga, F. Menga, C. Denga, H-A. Klok, and Z. Zhong, *Biomaterials*, **2013**, 34, 3647-3657; (b) S. Wang, P. Huang, and X. Chen, *ACS Nano*, **2016**, 10, 2991-2994; (c) C.J. Kearney, and D.J. Mooney, *Nat. Mater.* **2013**, 12, 1004-1017.
3. (a) T. Vasconcelos, B. Sarmiento, and P. Costa, *Drug Discov. Today*, **2007**, 12, 1068-1075; (b) J.-Z. Du, X.-J. Du, C.-Q. Mao, and J. Wang, *J. Am. Chem. Soc.*, **2011**, 133, 17560-17563.
4. (a) J. Hua,; S. Miurab, K. Nac, and Y. H. Bae, *J. Control. Release*, **2013**, 172, 69-76; (b) C. Zhao, L. Shao, J. Lu, X. Deng, and Y. Wu, *ACS Appl. Mater. Interfaces*, **2016**, 8, 6400-6410; (c) T. Wang, D. Wang, H. Yu, M. Wang, J. Liu, B. Feng, F. Zhou, Q. Yin, Z. Zhang, Y. Huang, and Y. Li, *ACS Nano*, **2016**, 10, 3496-3508; (d) C. Li, G.-F. Luo, H.-Y. Wang, J. Zhang, Y.-H. Gong, S.-X. Cheng, R.-X. Zhuo, and X.-Z. Zhang, *The J. of Phy. Chem., C* **2011**, 115, 17651-17659.
5. (a) X. Zhang, Y. Huang, M. Ghazwani, P. Zhang, J. Li, S. H. Thorne, and S. Li, *ACS Macro Lett.*, **2015**, 4, 620-623 (b) H. Chen, D. Zheng, J. Liu, Y. Kuang, Q. Li, M. Zhang, H. Ye, H. Qin, Y. Xu, C. Li, and B. Jiang, *Int. J. Biol. Macromol.*, **2016**, 85, 596-603; (c) S.-S. Han, Z.-Y. Li, J.-Y. Zhu, K. Han, Z.-Y. Zeng, W. Hong, W.-X. Li, H.-Z. Jia, Y. Liu, R.-X. Zhuo, and X.-Z. Zhang, *Small*. **2015**, 11, 2543-2554.
6. (a) N. Larson, and H. Ghandehari, *Chem. Mater.*, **2012**, 24, 840-853 (b) R. Ji, J. Cheng, T. Yang, C.C. Song, L. Li, F.-S. Du, and Z.-C. Li, *Biomacromolecules*, **2014**, 15, 3531-3539; (c) J. Zhai, T.M. Hinton, L.J. Waddington, C. Fong, N. Tran, X. Mulet, C.J. Drummond, and B.W. Muir, *Langmuir*, **2015**, 31, 10871-10880.
7. (a) M. Barz, R. Luxenhofer, R. Zentel, and M. J. Vicent, *Polym. Chem.*, **2011**, 2, 1900-1918; (b) A. Chanan-Khan, J. Szebeni, S. Savay, L. Liebes, N.M. Rafique, C.R. Alving, and F.M. Muggia, *Annals of Oncology*, **2003**, 14, 1430-1437 (c) J. Szebeni, *Toxicology*, **2005**, 216, 106-121; (d) J.K. Armstrong, G. Hempel, S. Koling, L.S. Chan, T. Fisher, H.J. Meiselman, and G. Garratty, *Cancer*, **2007**, 110, 103-111; (e) N.J. Ganson, S.J. Kelly, E. Scarlett, J.S. Sundry, and M.S. Hershfield, *Arth. Res. & Therapy*, **2005**, 8, 1-10.
8. (a) M. Khuphe, B. Mukonoweshuro, A. Kazlauciusas, and P. D. Thornton, *Soft Matter*, **2015**, 11, 9160-9167; (b) Y. Sun, Y. Hou, X. Zhou, J. Yuan, J. Wang, and H. Lu, *ACS Macro Lett.*, **2015**, 4, 1000-1003 (c) G.J.M. Habraken, A. Heise, and P.D. Thornton, *Macromol. Rapid Commun.*, **2012**, 33, 272-286; (d) H. Peng, J. Ling, and Z. Shen, *J. of Poly. Sci. Part A: Poly. Chem.*, **2012**, 50, 1076-1085.
9. (a) R. Jones, *Nat. Nanotechnol.*, **2008**, 3, 699-700; (b) H. Lu, J. Wang, Y. Bai, J.W. Lang, S. Liu, Y. Lin, and J. Cheng, *Nat. Commun.*, **2011**, 2, 206.
10. (a) M. Khuphe, A. Kazlauciusas, M. Huscroft, and P. D. Thornton, *Chem Commun.*, **2015**, 51, 1520-1523; (b) I. Dimitrov, and H. Schlaad, *Chem. Commun.*, **2003**, 23, 2944-2945; (c) P. D. Thornton, R. Brannigan, J. Podporska, B. Quilty and A. Heise, *J. Mater. Sci.: Mater. Med.*, **2012**, 23, 37-45.
11. (a) R. J. Pounder, D. J. Fox, I. A. Barker, M. J. Bennison, and A. P. Dove, *Polym. Chem.*, **2011**, 2, 2204-2212; (b) Y. Lu, L. Yin, Y. Zhang, Z. Zhang, Y. Xu, R. Tong, and J. Cheng, *ACS Macro Lett.*, **2012**, 1, 441-444.

12. (a) G. Yu, Y. Ma, C. Han, Y. Yao, G. Tang, Z. Mao, C. Gao, and F. Huang, *J. Am. Chem. Soc.*, **2013**, 135, 10310–10313; (b) T. Nakamura, K.-W. Peng, S. Vongpunsawad, M. Harvey, H. Mizuguchi, T. Hayakawa, R. Cattaneo, and S.J. Russell, *Nat Biotech.*, **2004**, 22, 331-336.
13. (a) V. Ladmiral, M. Semsarilar, I. Canton, and S. P. Armes, *J. Am. Chem. Soc.*, **2013**, 135, 13574-13581; (b) N. Yamazaki, S. Kojima, N.V. Bovin, S. André, S. Gabius, and H.J. Gabius, *Adv. Drug Deliv. Rev.*, **2000**, 43, 225-244.
14. (a) J. Huang, G. Habraken, F. Audouin, and A. Heise, *Macromolecules*, **2010**, 43, 6050-6057; (b) J.R. Kramer, and T.J. Deming, *J. Am. Chem. Soc.*, **2010**, 132, 15068-15071; (c) D. Pati, S. Das, N.G. Patil, N. Parekh, D.H. Anjum, V. Dhaware, A.V. Ambade, and S. Sen Gupta, *Biomacromolecules*, **2016**, 17, 466-475; (d) J. Liu, Z. Sun, Y. Yuan, X. Tian, X. Liu, G. Duan, Y. Yang, L. Yuan, H.-C. Lin, and X. Li, *ACS Appl. Mater. Interfaces*, 2016, 8, 6917-6924; (e) K.-S. Krannig, and H. Schlaad, *J. Am. Chem. Soc.*, **2012**, 134, 18542-18545.
15. (a) Y-S. Lin, R. Tungpradit, S. Sinchaikul, F-M. An,; D-Z. Liu, S. Phutrakul, and S-T. Chen, *J. Med. Chem.*, **2008**, 51, 7428–7441; (b) E.C. Calvaresi, C. Granchi, T. Tuccinardi, V. Di Bussolo, R.W. Huigens, H.Y. Lee, R. Palchadhuri, M. Macchia, A. Martinelli, F. Minutolo, and P.J. Hergenrother, *Chembiochem : Europ. J. of Chem. Bio.*, **2013**, 14, 2263-2267.
16. O. Warburg, *Science*, **1956**, 123, 309-314.
17. R. Nakamura, K. Aoi, and M. Okada, *Macromol. Rapid Commun.*, **2006**, 27, 1725-1732.
18. E. H. H. Wong, M. M. Khin, V. Ravikumar, Z. Si, S. A. Rice and M. B. Chan-Park, *Biomacromolecules*, **2016**, 17, 1170–1178.
19. K. Yamada, M. Minoda and T. Miyamoto, *Macromolecules*, **1999**, 32, 3553–3558.
20. K. Aoi, H. Suzuki and M. Okada, *Macromolecules*, **1992**, 25, 7073-7075
21. (a) S. C. Owen, D. P.Y. Chan and M. S. Shoichet, *Nano Today*, **2012**, 7, 53-65; (b) Dorshow, R.B., Bunton, C.A. and Nicoli, D.F. *The J. of Phys. Chem.* **1983**, 87, 1409-1416; (c) Topel, Ö., Çakır, B.A., Budama, L. and Hoda, N. *J. of Molecular Liquids*. 2013, 177, 40-43.
22. S. Parveen, R. Misra, and S. K. Sahoo, *Nanomedicine*, **2012**, 8, 147-166.
23. (a) S. Modi, M. G. Swetha D. Goswami, G. D. Gupta, S. Mayor, and Y. Krishnan, *Nat. Nanotechnol.*, **2009**, 4, 325-330; (b) H. Wu, L. Zhu, and V.P. Torchilin, *Biomaterials*, **2013**, 34, 1213-1222; (c) H. Yin, E.S. Lee, D. Kim, K.H. Lee, K.T. Oh, and Y.H. Bae, *J. Control. Release*, **2008**, 126, 130-138.
24. (a) P. D. Thornton, G. McConnell, and R. V. Ulijn, *Chem. Commun.*, **2005**, 47, 5913-5915; (b) K. Herzog, R.J. Müller, and W.D. Deckwer, *Poly. Degrad. and Stability*, **2006**, 91, 2486-2498; (c) N. Honda, I. Taniguchi, M. Miyamoto, and Y. Kimura, *Macromol. Biosci.*, **2003**, 3, 189-197.
25. (a) Y.Q. Yang, X.D. Guo, W.J. Lin, L.J. Zhang, C.Y. Zhang, and Y. Qian, *Soft Matter*, **2012**, 8, 454-464; (b) P. Costa, and J.M. Sousa Lobo, *Europ. J. of Pharm. Sci.*, **2001**, 13, 123-133; (c) R. Huang, W. Qi, L. Feng, R. Su, and Z. He, *Soft Matter*, **2011**, 7, 6222-6230.
26. W. Lin, S. Nie, Q. Zhong, Y. Yang, C. Cai, J. Wang, and L. Zhang, *J. of Mater. Chem. B*, **2014**, 2, 4008-4020.

Chapter 8. Poly[(Amino Acid)-(Ester)] Graft Copolymer Nanoparticles for the Acid-Mediated Release of Doxorubicin

Abstract

NCA ROP and OCA ROP were combined in a sequential ROP designed to synthesise a novel poly[(amino acid)-graft-(ester)] copolymer. The macromolecule created was capable of self-aggregating into discrete nanoparticles that encapsulated, and subsequently released doxorubicin (dox) via an acid-mediated hydrolysis. The dox-loaded nanoparticles exhibited significant anticancer activity against the T47D human breast cancer cells, as revealed by the complete loss of cell viability, after 72 hours. As such, the nanoparticles detailed are a promising candidate for the controlled delivery of hydrophobic chemotherapeutics to the acidic cancerous tissues.

8.1. Introduction

The pharmaceutical industry is in a constant state of flux, with the past 30 years seeing the rise of multiple, paradigm-shifting scientific advances such as high-throughput screening, combinatorial chemistry, genomics, proteomics and computational chemistry [1, 2]. These have resulted in an increase in the number of viable targets and chemical substrates available, often in the form of vast compound libraries and databases [3]. In the past decade alone, the number of therapeutic compounds that are in development has increased by 62% [2]. However, somewhat counter-intuitively, the number of new drugs and drug delivery strategies approved by the USA Food Drug Administration (FDA) has been in decline since the 1990s, with only 25% being approved between 2000 - 2010, relative to the number that was approved between 1990 - 2000 [4].

Utilising polymeric carriers for targeted drug delivery enables the distribution of hydrophobic drug molecules, *in vivo*, prior to drug release and deployment at a target site [5, 6]. In addition, the polymer restricts undesired and non-selective drug-receptor interactions, an imperative requirement for the delivery of toxic anti-cancer drugs where there is need to minimise the extremely unpleasant side effects that are

associated with prolonged chemotherapy [7]. Biodegradable polymers, including polyesters [8], poly(anhydride)s [9], poly(amino acid)s [10], poly(alkyl cyanoacrylate)s [11] and poly(orthoester)s [12] have been highlighted as promising drug delivery vehicles. Such polymers are designed to undergo programmed hydrolysis at a target site to liberate the therapeutic agent, following polymer degradation.

Poly(amino acid)s, created by NCA ROP are attractive candidates for drug delivery vehicles because they can readily self-assemble in aqueous solution to form discrete nanostructures. Additionally, poly(amino acid)s provide functional versatility [13-15]. However, poly(amino acid)s are not susceptible to acid hydrolysis. As such, they have limited applicability in pH-mediated drug delivery. pH-responsive polymer segments may be incorporated in the design of poly(amino acid) composites in order to afford polymer degradation and payload release upon interaction with the targeted pH stimulus. Poly(ester)s are susceptible to hydrolysis at pH values that are comparable to the cancerous tumour microenvironment [16]. The extracellular pH of many solid tumours ranges from pH 6.5 to pH 7.2. Also, the pH within cancerous cells may be between pH 5.0 and pH 6.0 in endosomes, and between pH 4.0 and pH 5.0 in lysosomes [17]. The synthesis of pendant-functionalised poly(ester)s may be achieved using OCA ROP. Combining NCA ROP and OCA ROP can enable the production of polymers that are capable of self-assembly to form nanoparticles (NPs) in aqueous media and can entrap therapeutic cargoes, and crucially, polymers that are susceptible to acid hydrolysis to permit payload release.

8.2. Experimental Procedures

8.2.1. Syntheses of Oligo(Ser(OBz)) Macromolecules

A generic procedure is given for the syntheses of a series of poly(*O*-benzyl-L-serine) macromolecules. Briefly, Ser(OBz) NCA was dissolved in anhydrous DMF (10 mL) and added to a Schlenk tube, which was previously evacuated and purged with nitrogen. Benzylamine (1 equivalent) was dissolved in anhydrous DMF (2 mL). The solution was injected into the reaction vessel. The reaction medium was degassed and then stirred under nitrogen for 96 hours, at room temperature. The polymer was precipitated in cold diethyl ether (250 mL) and left

overnight in the freezer to facilitate greater yields. The obtained polymer was isolated *via* centrifugation and dried, *in vacuo*. Yields: 71% - 91%. FTIR: $\nu_{\max}/\text{cm}^{-1}$ (solid): 3200 cm^{-1} (C-H, Aromatic stretch), 2850 cm^{-1} (C-H, alkyl stretch), 1800 cm^{-1} (C=O, Amide stretch). ^1H NMR (500 MHz, TFA-d, δ , ppm): 8.51 (s, NH), 7.50 ppm (m, Ar), 4.51 - 5.49 (m, CH).

8.2.2. Deprotection of Oligo(Ser(OBz)) Macromolecules

This generic procedure relates to the deprotection of the polymers. oligo(Ser(OBz)) was dissolved in trifluoroacetic acid (10 mL) and the solution was added to a round bottom flask. HBr in acetic Acid (33 wt. %, 3 mL) was added dropwise to the polymer solution and the reaction was stirred at room temperature, for 18 hours. The product was precipitated out of solution in cold diethyl ether (200 mL), isolated by centrifugation, dialysed and lyophilised. Yields: 84 wt. % - 95 wt. %. FTIR: $\nu_{\max}/\text{cm}^{-1}$ (solid): 3185 cm^{-1} (C-H, Aromatic bending), 2870 cm^{-1} (C-H, alkyl stretch), 1830 cm^{-1} (C=O, amide stretch). ^1H NMR (500 MHz, TFA-d, δ , ppm): 8.51 ppm (s, NH), δ 7.50 (m, Ar (benzylamine initiator)), 4.50 - 5.52 (m, CH).

8.2.3. Oligo(Ser)-Mediated OCA ROP

Phe OCA was dissolved in anhydrous DMF (5 mL). The solution was injected into a Schlenk tube that was equipped with a magnetic stirrer bar. Then, DMAP (10 wt. % of oligo(Ser)) was dissolved in anhydrous DMF and injected into the Schlenk tube. Oligo(Ser) was dissolved in anhydrous DMF (20 mL). The solution was injected into the reaction medium. The reaction medium was degassed and stirred under nitrogen for 168 hours. The product was precipitated in cold diethyl ether, collected *via* centrifugation, dialysed (2000 Da MWCO) and lyophilised. Yields: 61 wt. % - 78 wt. %. FTIR: $\nu_{\max}/\text{cm}^{-1}$ (solid): 3150 cm^{-1} (C-H, Aromatic bends), 2850 cm^{-1} (C-H, alkyl stretch), 1850 cm^{-1} (C=O, amide stretch), 1765 cm^{-1} (C=O, Ester). ^1H NMR (500 MHz, TFA-d, δ , ppm): 8.52 (s, NH), 7.00 - 7.51 (m, Ar), 4.50 - 5.51 (m, CH), 3.09 - 3.52 (m, CH).

8.2.4. Preparation of the Doxorubicin (Dox) Free-Base

Dox hydrochloride (3.00 mg, 5.50 μmol) was added to a solution of triethylamine (20 μL , 55 μmol) in anhydrous chloroform (3 mL). The solution was stirred, at room temperature, for 4 hours.

8.2.5. Preparation of Dox-Loaded NPs

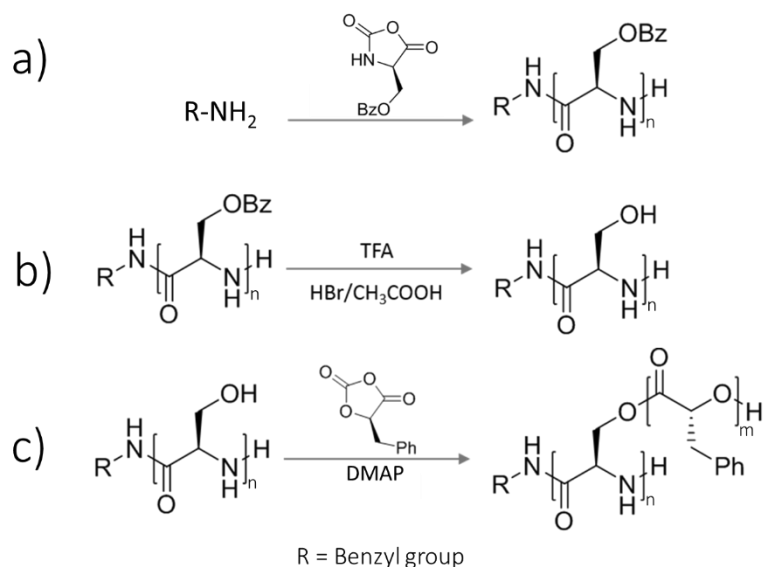
Poly(Ser)-*graft*-(Phe AHA)] (6 mg) was dissolved in DMF (1 mL). Dox was then encapsulated by adopting an established protocol [18, 19]. Briefly, the poly(Ser)-*graft*-(Phe AHA)] solution and dox-free base solution (3 mg/mL, 5.5 μ mol) were added simultaneously to vigorously-stirred PBS buffer (pH 7.4, 10 mL). The NPs were dialysed against PBS buffer and obtained *via* lyophilisation.

8.2.6. pH-Mediated Release of Dox

Dox-loaded NPs were reconstituted in an acetate buffer solution (pH 5.0) only, and in a PBS buffer solution (pH 7.4) only. NPs that were reconstituted in an acetate buffer solution were collected into a dialysis tubing membrane (2000 Da MWCO) and dialysed against an acetate buffer (pH 5.0). Similarly, NPs that were reconstituted in PBS buffer were collected into a dialysis tubing membrane (2000 Da MWCO) and dialysed against a PBS buffer solution (pH 7.4). The set-ups were incubated in the dark, under constant agitation, at 37 °C. Then, 1 mL samples were extracted from the dialysate at predetermined time intervals and analysed by UV-Vis spectrophotometry. The amount of dox released at each time point was then quantified using a pre-prepared standard calibration curve. In addition, a sample was isolated from medium that contained the dox-loaded NPs that had been stored at pH 7.4 and from the medium that contained the dox-loaded NPs that had been stored at pH 5.0. The samples were analysed using DLS and SEM.

8.3. Results and Discussion

The NCAs of Ser(OBz) and Phe were synthesised in high purity by following the procedures which are detailed in Chapter 3.3 (Figure 8.3 a, c). Then, oligo(Ser(OBz)) macromolecules were produced using a benzylamine-initiated NCA ROP, in various monomer-to initiator (M/I) feed ratios (Scheme 8.1 a). The formation of macromolecules was confirmed by FTIR spectroscopy (Figure 8.1 a) and ¹H NMR spectroscopy (Figure 8.2 b). It was then considered to be paramount to cleave the benzyl-protecting groups to generate a macroinitiator that possessed hydroxyl groups, which could be used to initiate the OCA ROP. Benzyl protecting groups were removed by following an established facile method, that uses trifluoroacetic acid and hydrogen bromide solution (33 wt. %) in acetic acid (Scheme 8.1 b) [20].



Scheme 8.1. (a) The benzylamine-initiated ROP of Ser(Obz) NCA to produce oligo(Ser(Obz)) macromolecules; (b) deprotection of oligo(Ser(Obz)) to yield oligo(Ser). Oligo(Ser)-initiated ROP of Phe OCA (c).

Analyses of the resultant oligo(Ser) macromolecules using FTIR spectroscopy (Figure 8.1 b) revealed the emergence of the O-H stretch signal ($\nu(\text{OH}) = 3500 - 3200 \text{ cm}^{-1}$) and the disappearance of the aromatic C-H bends ($\nu(\text{CH}) = 860 - 680 \text{ cm}^{-1}$), arising from the removal of benzyl-protecting groups. Analysis that was carried out using ^1H NMR spectroscopy (Figure 8.2d) revealed a decrease in the integration values of the aromatic protons, leaving only the integration value which equated to the aromatic protons of the benzylamine (benz) initiator. The composition of the resultant oligo(Ser) macromolecules was computed from the ^1H NMR spectra, which revealed that the three macromolecules that were created consisted of 9.6, 18.7 and 19.6 amino acid monomer repeat units (Table 8.1).

The oligo(Ser) macromolecules were then used as the macroinitiators for the ROP of phenylalanine OCA (Scheme 8.1 c). The OCA ROP reaction was catalysed by DMAP because the base activation of the monomer using the multiple hydrogen bonds from DMAP is reported to be more energetically favourable than the standard nucleophilic activation that would be achieved by the monomer alone [21]. In addition, it was hypothesised that DMAP might act *via* a ‘two-pronged’ activation approach, through its basic nitrogen atom centre and acidic O-hydrogen atoms, making it a bifunctional catalyst. OCA ROP resulted in the grafting of varying degrees of oligomers of Phe α -hydroxyacid (AHA) from the pendant hydroxyl groups, yielding

copolymers that possessed varying ratios of the peptide and the ester segments within their composition (Table 8.2). FTIR spectroscopy (Figure 8.1 c) confirmed the grafting of the ester oligomers by revealing an increase in the magnitude of the peaks that represent aromatic C-H bending (*ca.* 860 - 680 cm^{-1}), and a decrease in the OH-stretch signals (3500 - 3200 cm^{-1}) that had previously overlapped with the alkyl C-H stretch peaks and with the secondary amine N-H stretch peaks, prior to the grafting of the Phe AHA groups. Analysis carried out using ^1H NMR spectroscopy (Figure 8.2 e) confirmed the emergence of signals that are associated with the CH_2 methylene groups (*ca.* 3.25 - 3.73 ppm) of the Phe AHA repeat units.

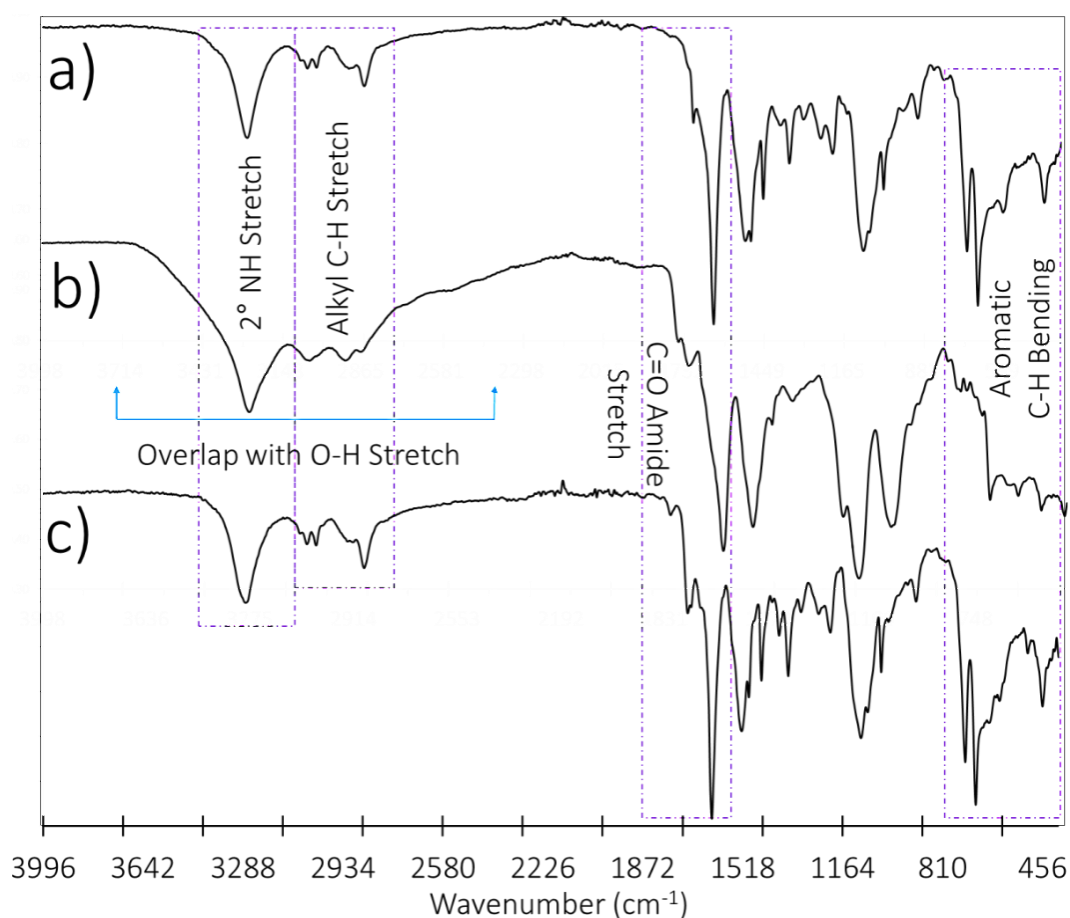


Figure 8.1. Representative FTIR spectra for, (a) oligo(Ser(OBz)) macromolecules, (b) oligo(Ser) macromolecules and (c) poly[(Ser)-graft-(Phe AHA)] macromolecules.

The ability of the macromolecules that were produced to self-assemble and form NPs in aqueous media was then assessed using the ‘dropping-in’ method of self-assembly [22], in which the polymer was expelled from the organic phase into the aqueous PBS buffer solution (pH 7.4). This method enabled the creation of discrete spherical NPs (Figure 8.3) as confirmed

by the results obtained from SEM studies (Figure 8.3 b). The size of the NPs that were obtained from the macromolecules ranged between 90 nm and 104 nm. DLS studies revealed that the NP dispersions possessed narrow size distributions and sustained stability ($PDI \leq 0.7$), as demonstrated by PDI values that ranged from 0.07 to 0.28 (Table 8.3). This is a desirable attribute of nanomaterials that are intended for use in drug delivery, *in vivo* [23-25].

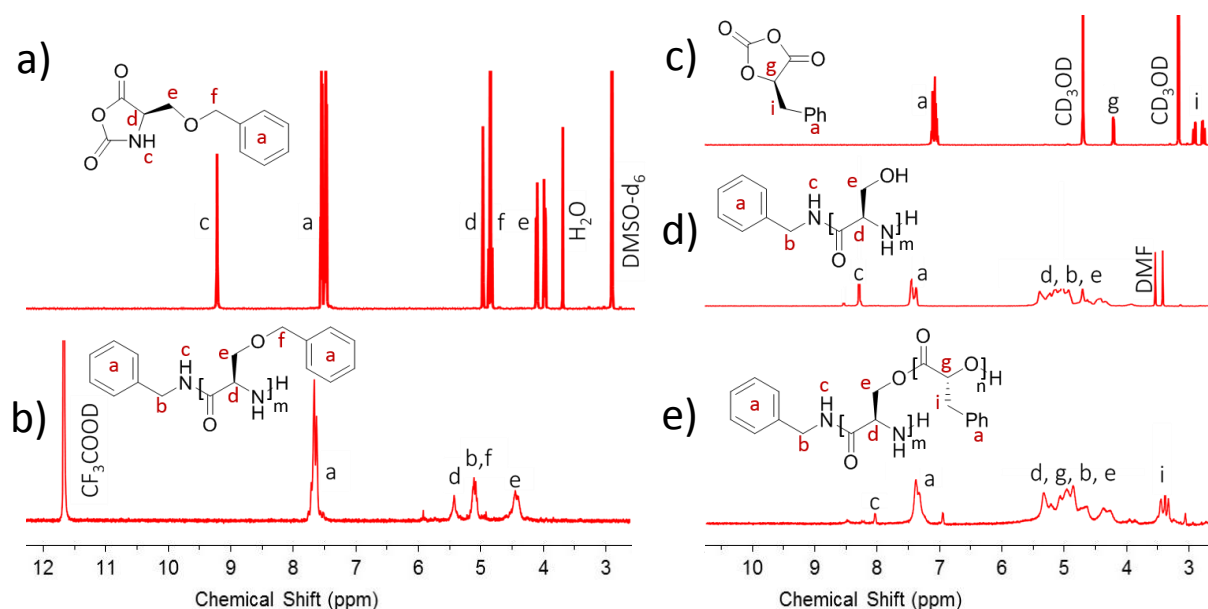


Figure 8.2. Representative ¹H NMR spectra for Ser(Obz) NCA (a), oligo(Ser(Obz)) (b), Phe OCA (c), oligo(Ser) (d) and the resulting poly[(Ser-g-(Phe AHA))] macromolecules after grafting ester repeat units from the pendant OH-groups, using OCA ROP (e).

Table 8.1. Composition of variants of oligo(Ser) produced by NCA ROP, computed by ¹H NMR and APC

Theoretical No. of Repeat Units	Actual No. of Repeat Units	Theoretical Mass (Da)	Actual Mass (Da)	PDI*
20	19.6	1847	1792.6	1.07
15	18.7	1412	1715.2	1.12
10	9.6	977	932.6	1.08

* Determined by APC

Table 8.2. Hybrid polymers produced by OCA ROP initiated from the OH-groups of oligo(Ser)

Theoretical Oligo(Ser):Oligo(Phe AHA) Ratio	Actual Oligo(Ser):Oligo(Phe AHA) Ratio	PDI *
20 : 5.0	19.6 : 6.0	1.13
20 : 2.5	19.6 : 3.1	1.17
15 : 5.0	18.7 : 3.0	1.13
15 : 2.5	18.7 : 3.0	1.13
10 : 5.0	9.6 : 5.2	1.14
10 : 2.5	9.6 : 1.8	1.14

* Determined by APC

The experimental findings that are detailed in Table 8.2 and Table 8.3 suggest that there is no clear relationship between the copolymer molecular weight and the resultant size of NPs.

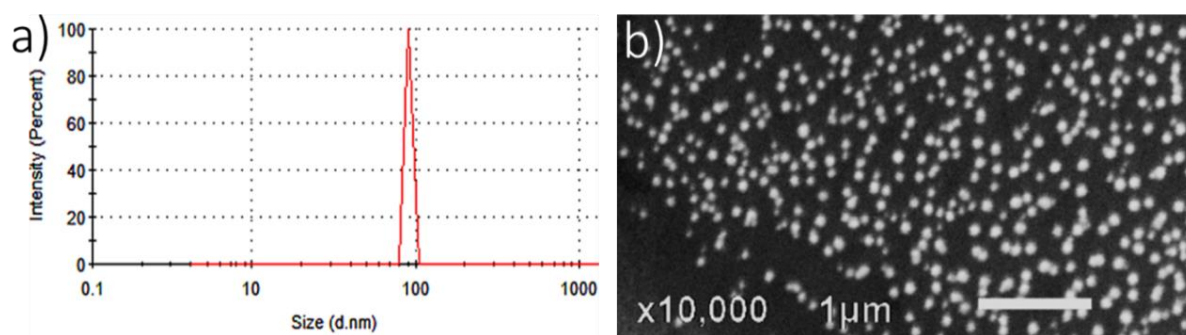


Figure 8.3. Representative DLS trace (a) and SEM microphotograph (b) obtained from poly[(Ser)_{19.6}-g-(Phe AHA)_{6.0}] NPs.

Due to their relatively narrow PDI, poly[(Ser)_{19.6}-g-(Phe AHA)₆] NPs (Table 8.3, Entry 1) were deemed to be the most attractive candidate for use as a drug delivery vehicle [25]. As such, these NPs were progressed into proof-of-concept studies, which aimed to demonstrate the successful encapsulation and the subsequent release of the chemotherapeutic dox from the copolymer NPs.

Table 8.3. Mean particle size and PDI values obtained from DLS analyses

Entry	Copolymer	Particle Size (d.nm)	PDI
1	Poly[(Ser) _{19.6} - <i>g</i> -(Phe AHA) ₆]	90	0.07
2	Poly[(Ser) _{19.6} - <i>g</i> -(Phe AHA) _{2.5}]	100	0.11
3	Poly[(Ser) _{18.7} - <i>g</i> -(Phe AHA) ₅]	96	0.28
4	Poly[(Ser) _{18.7} - <i>g</i> -(Phe AHA) _{2.5}]	95	0.10
5	Poly[(Ser) _{9.6} - <i>g</i> -(Phe AHA) ₅]	97	0.14
6	Poly[(Ser) _{9.6} - <i>g</i> -(Phe AHA) _{2.5}]	104	0.23

Dox is commonly supplied as its hydrochloride salt form, which is very soluble in aqueous media. To maximise drug-loading into the hydrophobic NP core, and thus reduce the amount of drug which remains dissolved in solution, dox was converted to its free-base (hydrophobic form) prior to carrying out the nanoprecipitation [18, 19]. Dox-loaded NPs were then prepared by nanoprecipitation from the aqueous PBS buffer solution (Figure 8.4 a).

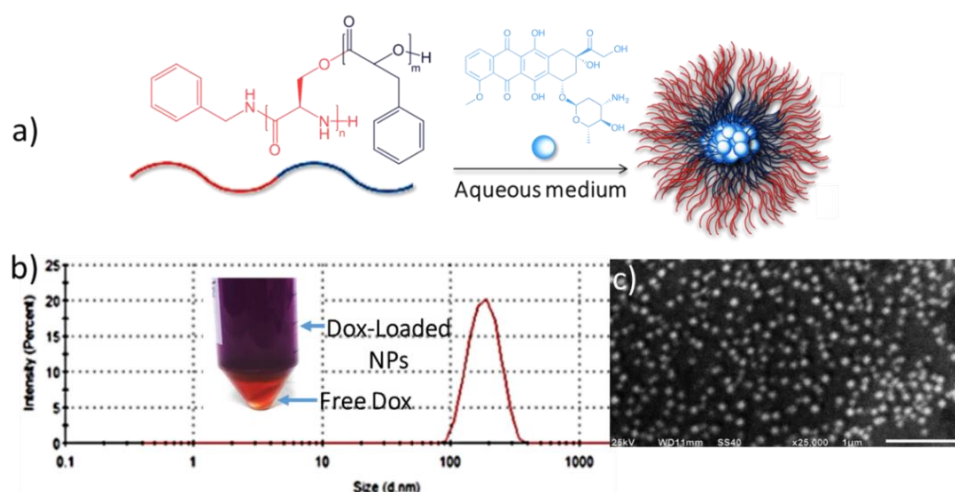


Figure 8.4. (a) Schematic illustration of the formation of Dox-loaded poly[(Ser)_{19.6}-*g*-(Phe AHA)₆] NPs upon nanoprecipitation, (b and c) Dox-loading within NPs, resulting in the formation of a purple suspension (inset) and an increase in NP diameter (scale bar represents 1 μm).

The encapsulation of the free-base into the hydrophobic cores of the NPs could be linked to the observed change in colour from the clear pink dox solution to a brownish/purple NP suspension (Figure 8.4 b, *inset*) [26]. The use of dialysis enabled the expulsion of un-encapsulated dox from the NPs. DLS analyses and SEM analyses, that were conducted after the encapsulation of dox, revealed an increase in the particle size from 90 nm to 118 nm, the spherical nature of the NPs being retained (Figure 8.4 b, c). This observation confirms further the successful loading of the drug molecules into the NPs, this being consistent with scientific findings that drug-encapsulation may alter the diameter of NPs [25]. The drug-encapsulation efficiency of poly[(Ser)_{19.6}-*g*-(Phe AHA)₆] NPs was 52.3% ± 6.2% and the NPs possessed a substantial drug loading of 2.90% ± 1.3% (w/w).

The potential for the acid-mediated release of dox from the NPs was then assessed. For this purpose, the dialysis method [27] was adopted, whereby the dox-loaded NPs were suspended in an aqueous medium, within a dialysis tubing membrane. Upon polymer hydrolysis, the released dox could pass freely through the dialysis bag, into the external medium and be quantified; whilst un-hydrolysed dox-loaded NPs would be retained within the dialysis bag. The release of dox from the NPs was greatest when the NPs were incubated at pH 5 (Figure 8.5 a).

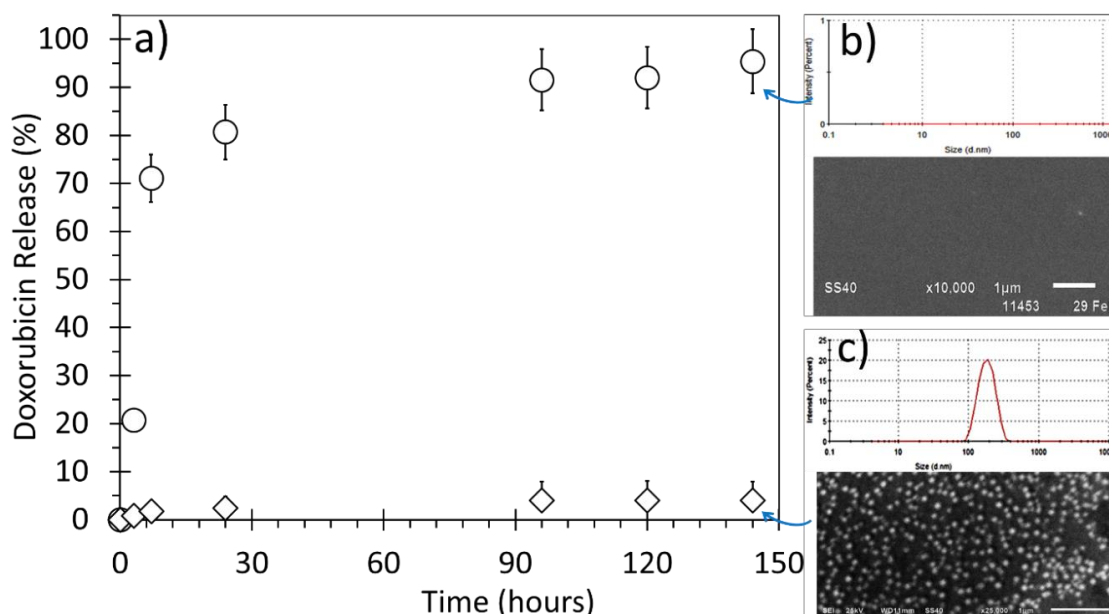


Figure 8.5. (a) The release of dox from NPs that consisted of poly[(Ser)_{19.6}-*g*-(Phe AHA)_{6.0}], being incubated in a pH 5.0 acetate buffer solution (○) and in a pH 7.4 PBS buffer solution (◇). DLS and SEM analyses of NPs, maintained for over 6 days at pH 7.4 (Inset c) and at pH 5.0 (Inset b). Scale bars represent 1 μm.

In excess of 95.4% dox was released from the NPs that were maintained at pH 5.0, after six days. In contrast, only 4.0% of the encapsulated dox was released from the NPs that were maintained at pH 7.4, after six days. DLS analyses and SEM analyses revealed the maintained presence of the NPs when they were incubated at pH 7.4 (Figure 8.5, Inset c). However, the presence of NPs in the media that was incubated at pH 5.0 was not detected by SEM analyses and by DLS analyses, thus confirming the occurrence of acid-mediated hydrolysis (Figure 8.5, Inset b).

An MTT assay was then carried out to determine the *in vitro* cytotoxicity of poly[(Ser)_{19.6}-*g*-(Phe AHA)₆] NPs and dox-loaded poly[(Ser)_{19.6}-*g*-(Phe AHA)₆] NPs against T47D human breast cancer cells (Figure 8.6). The blank polymer NPs exhibited nominal cytotoxicity against the cells, during a prolonged period of 72 hours. This was revealed by the cell viability values which were sustainably significant (remained close to 100%) (Figure 8.6 a).

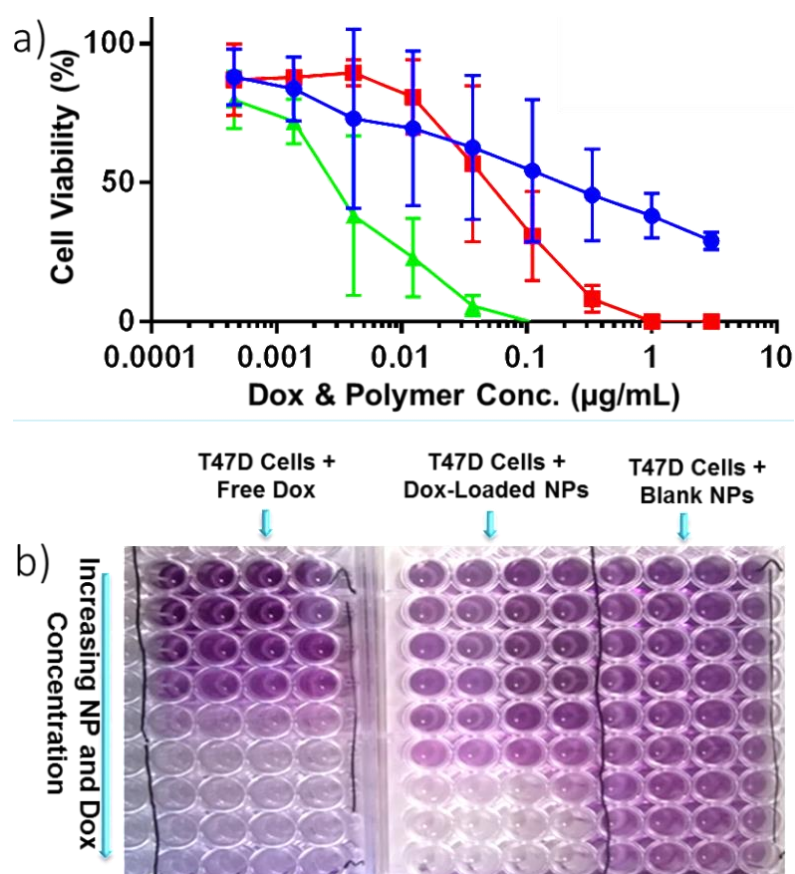


Figure 8.6. (a) The effect of blank polymer NPs (●), dox-loaded polymer NPs (■) and free dox (▼) on the viability of T47D cells. Data is presented as mean ± SD (n = 4). (b) Representative macro images obtained from the colorimetric MTT assays in which the purple colouring indicates viable cells.

The macro images that were obtained from the colorimetric MTT assay revealed the maintained presence of the purple colouring in the seeded wells, thus confirming the maintained presence of viable cells, whose viability was affected marginally by culturing them in the presence of blank NPs for 72 hours (Figure 8.6 b). In contrast, the dox-loaded NPs exhibited significant cytotoxicity against the cancerous cells (the IC_{50} value of dox-loaded NPs on T47D cells was 0.065 $\mu\text{g}/\text{mL}$). The viability of the cancerous cells reduced to zero after 72 hours of incubation with dox-loaded NPs (dox loadings $\geq 1 \mu\text{g}/\text{mL}$). The images obtained from colorimetric MTT assay confirm the absence of viable cells in the presence of dox-loaded NPs (absence of purple colouring) (Figure 8.6 b). These results suggest that the polymer NPs are internalised by the T47D breast cancer cells. These would then be hydrolysed by the prevailing acidic pH environment, releasing the dox that causes tumour-recession (cell death) [17].

8.4. Conclusions

NCA ROP and OCA ROP were combined to create poly[(amino acid)-(ester)] graft copolymers that were capable of self-assembly in aqueous media to form discrete NPs. The poly[(Ser)_{19.6}-*graft*-(Phe AHA)₆] NPs were proven to be able of encapsulating chemotherapeutic dox. The drug was retained within the NPs that were maintained at pH 7.4, because of the absence of polymer degradation at this pH value. However, the poly(ester) functionality granted an innate susceptibility to acid-mediated polymer hydrolysis. Consequently, NP degradation, resulting in dox-release, occurred when the NPs were maintained within pH 5.0 acetate buffer solution. MTT assay revealed that poly[(Ser)_{19.6}-*g*-(Phe AHA)₆] has limited cytotoxicity against T47D cells. In contrast, the dox-loaded poly[(Ser)_{19.6}-*g*-(Phe AHA)₆] NPs exhibited significant anticancer activity against the T47D cells. As such, poly[(Ser)_{19.6}-*g*-(Phe AHA)₆] NPs are a promising candidate for controlled drug delivery to acidic, cancerous tumour sites.

8.5. References

1. Lipinski, C. *Am Pharm Rev.* **2002**, 5, 82-85.
2. Hay, M., Thomas, D.W., Craighead, J.L., Economides, C. and Rosenthal, J. *Nat Biotech.* **2014**, 32, 40-51.
3. Zheng, W., Jain, A., Papoutsakis, D., Dannenfelser, R.-M., Panicucci, R. and Garad, S. *Drug Dev Ind Pharm.* **2012**, 38, 235-247.
4. Cohen, F.J. *Nat Rev Drug Discov.* **2005**, 4, 78-84.
5. Chen, W.-H., Luo, G.-F., Lei, Q., Jia, H.-Z., Hong, S., Wang, Q.-R., Zhuo, R.-X. and Zhang, X.-Z. *Chem. Commun.* **2015**, 51, 465-468.
6. Xu, Z., Liu, S., Liu, H., Yang, C., Kang, Y. and Wang, M. *Chem. Commun.* **2015**, 51, 15768-15771.
7. Bae, Y.H. and Park, K. *J. Control. Release.* **2011**, 153, 198-205.
8. Khuphe, M., Mahon, C.S. and Thornton, P.D. *Biomater. Sci.*, **2016**, 4, 1792-1801.
9. Wang, J., Yang, G., Guo, X., Tang, Z., Zhong, Z. and Zhou, S. *Biomaterials.* **2014**, 35, 3080-3090.
10. Khuphe, M., Mukonoweshuro, B., Kazlauciusas, A. and Thornton, P.D. *Soft Matter.* **2015**, 11, 9160-9167.
11. Vauthier, C., Dubernet, C., Chauvierre, C., Brigger, I. and Couvreur, P. *J. Control. Release.* **2003**, 93, 151-160.
12. Li, L., Knickelbein, K., Zhang, L., Wang, J., Obrinske, M., Ma, G.Z., Zhang, L.-M., Bitterman, L. and Du, W. *Chem. Commun.* **2015**, 51, 13078-13081.
13. Lavilla, C., Byrne, M. and Heise, A. *Macromolecules.* **2016**, 49, 2942-2947.
14. McAvan, B.S., Khuphe, M. and Thornton, P.D. *Eur. Polym. J.*, **2017**, 87, 468-477.
15. Murphy, R., Borase, T., Payne, C., O'Dwyer, J., Cryan, S.A. and Heise, A. *RSC Adv.*, **2016**, 6, 23370-23376.
16. Manchun, S., Dass, C.R. and Sriamornsak, P. *Life Sci.*, **2012**, 90, 381-387.
17. Liu, Y., Wang, W., Yang, J., Zhou, C. and Sun, J. *Asian J. Pharmacol.*, **2013**, 8, 159-167.
18. Kim, D., Gao, Z.G., Lee, E.S. and Bae, Y.H. *Mol. Pharm.*, **2009**, 6, 1353-1362.
19. Li, S., Wu, W., Xiu, K., Xu, F., Li, Z. and Li, J. *J. Biomed. Nanotechnol.*, **2014**, 10, 1480-1489.
20. Sulistio, A., Blencowe, A., Widjaya, A., Zhang, X. and Qiao, G. *Polym. Chem.*, **2012**, 3, 224-234.
21. Bonduelle, C., Martín-Vaca, B., Cossío, F.P. and Bourissou, D. *Chem. Eur. J.*, **2008**, 14, 5304-5312.
22. Zhu, Y., Sun, J., Yi, C., Wei, W. and Liu, X. *Soft Matter.* **2016**, 12, 7577-7584.
23. Desai, M.P., Labhassetwar, V., Walter, E., Levy, R.J. and Amidon, G.L. *Pharm Res.*, **1997**, 14, 1568-1573.
24. Albanese, A. and Chan, W.C.W. *ACS Nano.* **2011**, 5, 5478-5489.
25. Mato, E., Puras, G., Bell, O., Agirre, M., Hernández, R., Igartua, M., Moreno, R., Gonzalez, G., de Leiva, A. and Pedraz, J. *J Nanomed Nanotechnol.*, **2015**, 6, p.1.
26. Wang, Y., Chen, L. and Liu, P. *Chem. Eur. J.*, **2012**, 18, 5935-5943.
27. Hua, S. *Int J Nanomedicine.*, **2014**, 9, 735-744.

Chapter 9. Biodegradable Poly(Ester) Nanoparticles Created by Sequential ROP of α -Amino Acid OCAs for the Controlled Release of Chemotherapeutics

Abstract

Diblock poly(ester) copolymers were created by the sequential ROP of L-phenylalanine OCA and L-lysine(Cbz), and by the sequential ROP of L-phenylalanine OCA and γ -benzyl L-glutamic acid OCA. The protected diblock poly(ester)s, and the amphiphilic poly(ester)s obtained after removing the benzyl ester and carbobenzyloxy protecting groups, self-organised in aqueous media to yield spherical nanoparticles. The nanoparticles were proven to be capable of encapsulating at least 45% of a doxorubicin feed and subsequently releasing it in a controllable manner, in response to an acidic pH stimulus, in vitro.

9.1. Introduction

The desirable properties of poly(ester)s that have been created by OCA ROP, that include their functional versatility and their susceptibility to hydrolysis by an acidic pH stimuli, have been detailed in Chapter 1.6 and Chapter 8.1. Anticancer drugs are toxic in inappropriate use and can cause damage to heart muscle, which leads to heart failure [1, 2]. For example, doxorubicin (dox) and other anthracyclines [3, 4], fluorouracil [5] and paclitaxel [6] are among the cancer drugs that have been reported to cause abnormalities in heart rate or rhythm, leading to cardiac toxicity. One particular note is the established dox cardiomyopathy, which has a mortality rate of at least 50%, and has no effective treatment [3]. Established dox cardiomyopathy can be prevented by reducing the drug dosage during the direct administering of dox. Furthermore, the drug molecules can be encapsulated in biodegradable nanocarriers, to achieve controlled and targeted administration of the drug, directly at the site of action, thus reducing the potential toxic effects that would otherwise be due to dose dumping and burst release [7, 8].

Although several nanocarriers have been developed for the delivery of anticancer therapeutics [9-13], there remains a need to devise more effective delivery systems that are able to reduce established dox cardiomyopathy and myelosuppression. Biodegradable and biocompatible polymers are excellent candidates for use as dox delivery vehicles due to their potentially high

loading efficiencies. Designed poly(ester)s, in particular, can be created in a straightforward manner by the ROP of α -amino acid OCAs, and then employed in the controlled delivery of chemotherapeutic drugs to cancerous tumour sites that usually present a slightly acidic pH environment [14]. In this chapter, a report is given of the sequential ROP of α -amino acid OCAs, conducted to create diblock poly(ester) copolymers, being reported for the first time. The macromolecules created self-organised in PBS buffer to yield monodisperse, spherical nanoparticles, that encapsulated and subsequently release dox in a controllable manner, in response to environmental acidic pH.

9.2. Experimental Details

9.2.1. Syntheses of Poly(Ester)s

A representative procedure is given, using the synthesis of poly[(PheLA)_{10.4}-*b*-(Lys(Cbz)LA)_{31.4}]. Phe OCA (0.31 g, 1.6 mmol) was dissolved in anhydrous THF (5 mL) and the solution was transferred to a previously flame-dried and nitrogen-purged Schlenk tube. 4-DMAP (0.02 g, 0.16 mmol) was dissolved in anhydrous THF (2 mL) and the solution was added to the OCA solution in the Schlenk tube. 2-methyl-1-propanol (11.86 mg, 0.16 mmol) was dissolved in THF (5 mL) and the solution was injected into the reaction medium. The reaction medium was stirred at room temperature, under a nitrogen flow. A small sample was extracted from the reaction medium at predetermined time intervals and analysed by ¹H NMR, to ascertain the degree of polymerisation. When all of the Phe OCA had been polymerised, the poly(pheLA) macromolecule was precipitated in cold diethyl ether and then redissolved in anhydrous THF in the Schlenk tube. The reaction medium was degassed and nitrogen-purged. Lys(Cbz) OCA (1.48 g, 4.8 mmol) was dissolved in anhydrous THF (10 mL). The solution was injected into the reaction medium together with a solution of DMAP in anhydrous THF (0.02 g, 0.16 mmol). The reaction medium was degassed and then stirred under nitrogen at room temperature until all the Lys(Cbz) OCA had been polymerised fully, as determined by ¹H NMR spectroscopy. The macromolecules were precipitated in cold diethyl ether (1:5 v/v), isolated by centrifugation, dialysed (2000 MWCO) against distilled water for 72 hours and lyophilised. Yield: 58.7%. ¹H NMR (500 MHz, CDCl₃, δ , ppm): 7.62 - 7.22 (m, Ph), 5.61 - 5.42 (d, α CH), 5.28 - 4.71 (m, Ph-CH₂OCO), 3.90 - 3.81 (d, α CH), 3.25 - 2.51 (m, CONHCH₂, Ph-CH₂, CONH), 1.73 - 1.29 (CH(CH₃)₃), 0.79 - 0.65 (6H, d, (CH₃)₂). FTIR: $\nu_{\max}/\text{cm}^{-1}$ (solid): 3632 (OH Stretch), 3109 (NH Stretch), 2910

(C-H Stretch), 1749 (Ester C=O Stretch), 1405 (Aromatic C=C Stretch). An analogous procedure was used for the synthesis of poly[(PheLA)_{10.4}-*b*-(Glu(Bz)LA)_{30.2}]. Yield: 59.8%. 7.25 - 7.05 (m, Ph), 5.13 - 4.88 (α CH), 4.88 - 4.63 (m, Ph-CH₂OCO), 3.31 - 3.12 (CH₂O, α CH), 2.60 - 1.91 (m, Ph-CH₂, (CH₂)₂COO), 0.69 - 0.49 (6H, d, (CH₃)₂). FTIR: $\nu_{\text{max}}/\text{cm}^{-1}$ (solid): 3654 (OH Stretch), 2926 (C-H Stretch), 1737 (Ester C=O Stretch), 1439 (Aromatic C=C Stretch).

9.2.2. Deprotection of Poly(Ester)s

A 10 wt. % palladium-on-carbon catalyst (40 mg, 20 wt. % of polymer) was added to a pre-dried round bottom flask. The flask was equipped with a magnetic stirrer bar and then sealed. The catalyst was then purged with nitrogen. Poly[(PheLA)_{10.4}-*b*-(Glu(Bz)LA)_{30.2}] (200 mg) was dissolved in anhydrous THF (20 mL) and the polymer solution was injected into the flask containing the catalyst. The reaction medium was degassed several times and then stirred at room temperature under hydrogen flow for 48 hours. Then, it was filtered through a pad of celite. The polymer solution was dialysed against distilled water for 72 hours and the purified polymer isolated by lyophilisation. Yield: 80 wt. %. An analogous procedure was followed for the deprotection of poly[(PheLA)_{10.4}-*b*-(Lys(Cbz)LA)_{31.4}]. Yield: 75.4 wt. %.

9.2.3. Preparation of Dox-Loaded Nanoparticles

Dox-loaded nanoparticles (NPs) were prepared from the deprotected poly[(PheLA)_{10.4}-*b*-(GluLA)_{30.2}] and from the protected poly[(PheLA)_{10.4}-*b*-(Lys(Cbz)LA)_{31.4}] copolymers. The NPs were prepared by the simultaneous addition of the poly(ester) solution (10 mg/mL, 2 mL) and the dox-free base solution (2.5 mg/mL, 2 mL), into vigorously stirred PBS buffer solution (20 mL, pH 7.4). The samples were then dialysed against a PBS buffer solution for 72 hours in the dark. NPs were obtained after lyophilisation.

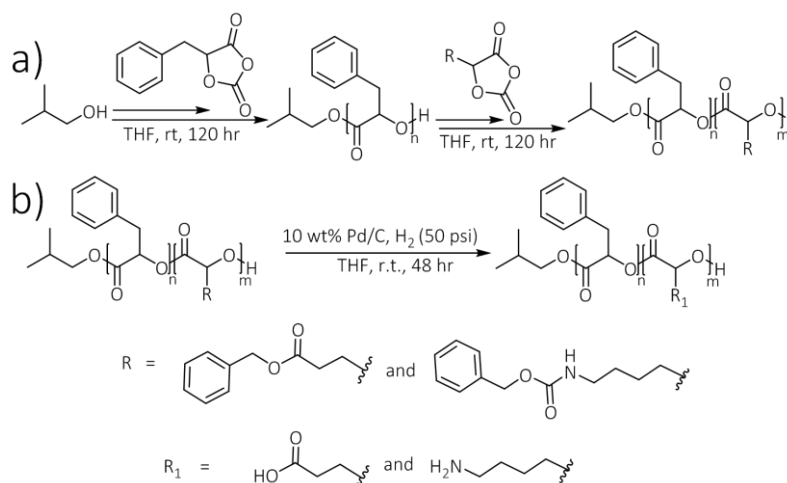
9.2.4. Doxorubicin Release

Dox-loaded NPs were reconstituted in an acetate buffer solution (pH 5.0) only, and in a PBS buffer solution (pH 7.4) only. NPs, reconstituted in an acetate buffer solution, were collected into a dialysis tubing membrane (2000 Da MWCO) and dialysed against an acetate buffer solution (pH 5.0). Similarly, NPs that were reconstituted in the PBS buffer were collected into a dialysis tubing membrane (2000 Da MWCO) and dialysed against a PBS buffer solution (pH 7.4). The experimental set-ups were incubated at 37 °C in the dark, under constant agitation.

Then, 750 μL samples were extracted from the dialysate at predetermined time intervals and analysed by UV-Vis spectrophotometry. The amount of dox released at each time point was then quantified using a pre-prepared standard calibration graph.

9.3. Results and Discussion

The OCA monomers of carbobenzyloxy L-lysine (Lys(Cbz)), L-phenylalanine (Phe) and γ -benzyl-L-glutamic acid (Glu(Bz)) were synthesised by following the experimental procedures that are reported in Chapter 3.3. Phe was selected to provide the hydrophobic poly(ester) block, while (Lys(Cbz) and (Glu(Bz)) were selected to provide the hydrophilic ester repeat units, after poly(ester) deprotection. The ROP of OCA monomers can be initiated from the hydroxyl functional groups of a small molecule or macromolecule [15]. Here, isobutanol was selected to initiate the ROP of the phenylalanine OCA to generate a hydrophobic poly(pheLA) macromolecule (Scheme 9.1 a).



Scheme 9.1. (a) The syntheses of diblock poly(ester)s by isobutanol-mediated sequential OCA ROP, and (b) deprotection of poly(ester) macromolecules by catalytic Pd/C hydrogenolysis.

The conversion of the OCA monomer into a macromolecule was monitored by ¹H NMR spectroscopy (Figure 9.1), by comparing the integration value of the CH₃ protons of the isobutanol initiator with the integration value of the aromatic protons of phenylalanine. ¹H NMR spectroscopy revealed that the conversion of phe OCA monomer was complete after approximately 120 hours of polymerisation (Figure 9.1 c, Figure 9.2 a). The poly(pheLA)

oligomers were then precipitated out of solution and then re-dissolved in neat anhydrous THF, in order to ensure that none of the phe OCA monomer was present in the reaction medium.

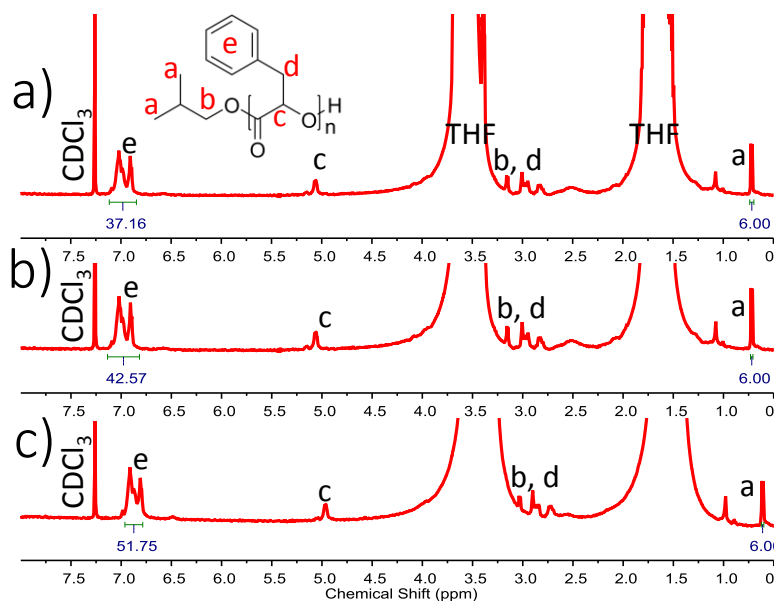


Figure 9.1. ^1H NMR spectra revealing the progress of the 2-methyl-1-propanol-mediated ROP of phenylalanine OCA, (a) at 24 hours, (b) after 48 hours, and (c) after 96 hours showing complete conversion of the OCA monomer.

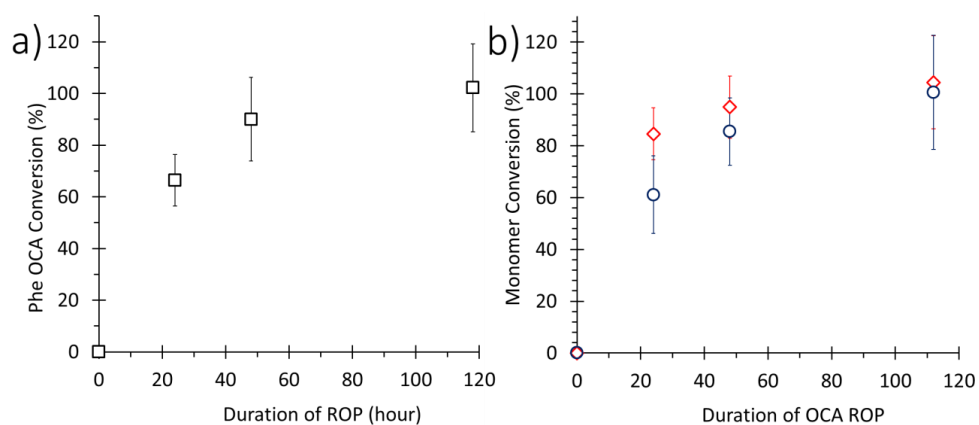


Figure 9.2. Charts detailing the conversion of OCA monomers into poly(ester)s. (a) The ROP of phe OCA (\square) from isobutanol to produce hydrophobic poly(pheLA) macromolecules. (b) The kinetics of the ROP of Lys(Cbz) OCA (\circ) and of the ROP of Glu(Bz) OCA (\diamond) from a poly(pheLA) macroinitiator.

Subsequently, the poly(pheLA) macromolecules were then used to initiate the ROP of Lys(Cbz) OCA and to initiate the ROP of Glu(Bz) OCA, respectively (Scheme 9.1a). The conversion of the respective monomers into the desired poly(ester) macromolecules was monitored by ^1H NMR spectroscopy. The polymerisation of Lys(Cbz) OCA was monitored by comparing the ^1H NMR

integration value corresponding to the CH₃ protons of the initiator (*ca* 0.75 ppm) with the integration values of the protons that are bonded to the alpha carbon of the amino acid repeat unit (*ca* 3.95 ppm) (Figure 9.3). ¹H NMR spectroscopy revealed that *ca* 31.4 Lys(Cbz) repeat units were grafted from the poly(PheLA) block to give the required diblock macromolecule (Figure 9.3 c).

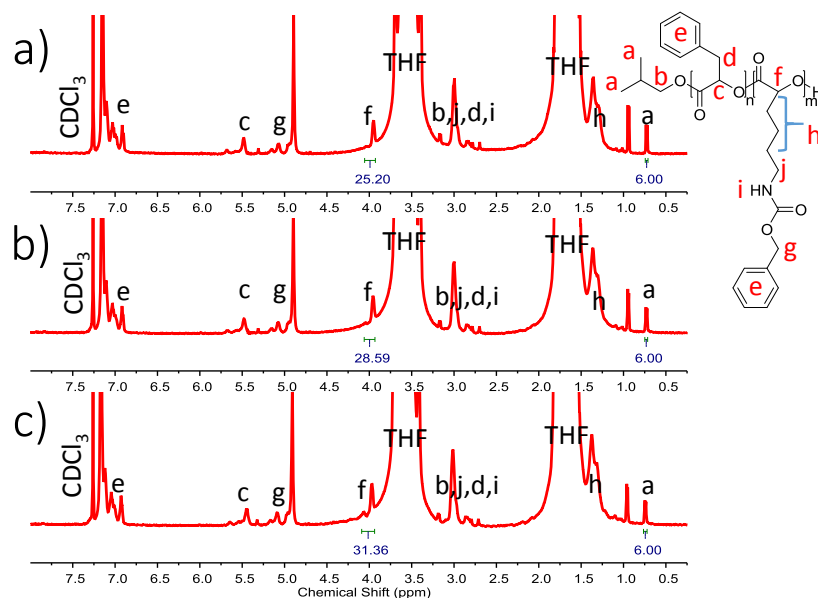


Figure 9.3. ¹H NMR spectra revealing the progress of the poly(PheLA)-mediated ROP of Lys(Cbz) OCA, (a) at 24 hours, (b) after 48 hours, and (c) after 96 hours, revealing the complete conversion of the OCA monomer to give the diblock poly(ester) macromolecule.

The polymerisation of Glu(Bz) OCA was monitored by comparing the ¹H NMR integration value corresponding to the CH₃ protons of the initiator (*ca* 0.75 ppm) with the integration value of the CH₂ protons from the benzyl ester protecting groups (Figure 9.4). ¹H NMR spectroscopy revealed that *ca* 30.2 Glu(Bz) repeat units were grafted from the poly(PheLA) block to give the required diblock macromolecule (Figure 9.4 c). Overall, there was no significant difference in the time that was taken for either the Lys(Cbz) OCA or the Glu(Bz) OCA to be converted fully to poly(ester)s (Figure 9.2 b). ¹H NMR spectroscopy revealed that the OCA monomers were polymerised completely within 120 hours, thus leading to the formation of the required diblock poly(ester) architectures; poly[(PheLA)_{10.4}-*b*-(Lys(Cbz)LA)_{31.4}] and poly[(PheLA)_{10.4}-*b*-(Glu(Bz)LA)_{30.2}]. The formation of the respective poly(ester)s was also confirmed by analyses that were carried out using FTIR spectroscopy and GPC (Figure 9.5). FTIR spectroscopy revealed the presence of infrared peaks that are characteristic of the poly(ester) macromolecules which

were created. These include the C=O ester stretch (1739 cm^{-1}), the C=C aromatic stretch (1374 cm^{-1}) and the H-bonded OH stretch (*ca.* 3320 cm^{-1}). GPC analyses revealed the macromolecules formed possess reasonably narrow PDI values of 1.09 for poly[(PheLA) $_{10.4}$ -*b*-(Lys(Cbz)LA) $_{31.4}$] and 1.11 for poly[(PheLA) $_{10.4}$ -*b*-(Glu(Bz)LA) $_{30.2}$].

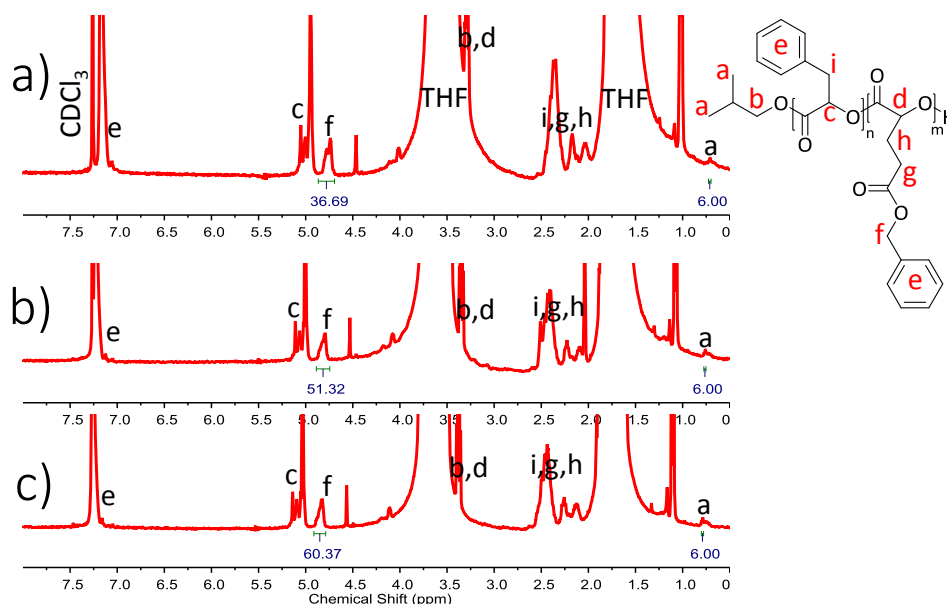


Figure 9.4. ^1H NMR spectra revealing the progress of poly(PheLA)-mediated ROP of Glu(bz) OCA, (a) at 24 hours, (b) after 48 hours, and (c) after 96 hours, revealing the complete conversion of the OCA monomer, to yield a diblock poly(ester) macromolecule.

Table 9.1. Polymer molecular weights and critical aggregation concentrations (CAC)s.

Poly(ester)	M_w (g/mol)	CAC ($\mu\text{g/mL}$)	CAC (Molar)
Poly[(PheLA) $_{10.4}$ - <i>b</i> -(Lys(Cbz)LA) $_{31.4}$]	9914.5 *	4.93	4.97×10^{-7} M
Poly[(PheLA) $_{10.4}$ - <i>b</i> -(LysLA) $_{31.4}$]	5702.8 *	6.32	1.11×10^{-6} M
Poly[(PheLA) $_{10.4}$ - <i>b</i> -(Glu(Bz)LA) $_{30.2}$]	8266.4 †	4.98	6.02×10^{-7} M
Poly[(PheLA) $_{10.4}$ - <i>b</i> -(GluLA) $_{30.2}$]	5544.8 †	5.81	1.05×10^{-6} M

Determined using ^1H NMR: * By comparing the integration value of CH_3 protons (*ca.* 0.75 ppm) of the initiator with the integration value of the aromatic protons of PheLA repeat groups (*ca.* 7.25 ppm) and with the integration value of the protons bonded to the alpha carbons of Lys(Cbz)LA repeat groups (*ca.* 4.05 ppm); † By comparing the integration value of CH_3 protons (*ca.* 0.75 ppm) of the initiator with the integration value of the aromatic protons of PheLA repeat groups (*ca.* 7.25 ppm) and with the integration value of the CH_2 protons of the Bz protecting groups (*ca.* 4.81 ppm)

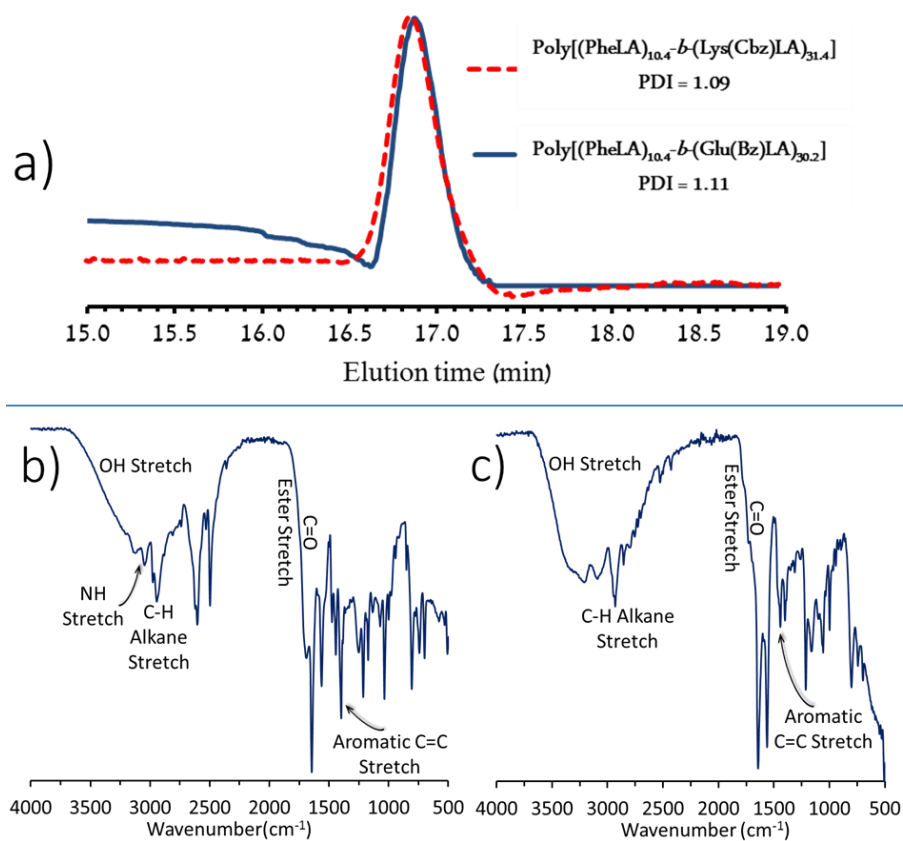


Figure 9.5. (a) GPC traces obtained from poly(ester) macromolecules (The instrument, GPC LC1260, was calibrated using poly(methyl methacrylate) standards, DMF + Libr (1 g/L) eluent, flow rate 1 mL/mL). FTIR spectroscopy spectra for (b) poly[(PheLA)_{10.4}-*b*-(Lys(Cbz)LA)_{31.4}] and (c) poly[(PheLA)_{10.4}-*b*-(Glu(Bz)LA)_{30.2}].

It was necessary to remove the Cbz protecting groups and the benzyl ester protecting groups from the macromolecules so as to generate amphiphilic architectures. Consequently, Pd/C-catalysed hydrogenolysis was used to cleave the protecting groups from the Lys(Cbz) and Glu(Bz) repeat units (Scheme 9.1 b). The ability of the deprotected poly[(PheLA)_{10.4}-*b*-(LysLA)_{31.4}] and the deprotected poly[(PheLA)_{10.4}-*b*-(GluLA)_{30.2}], to self-aggregate upon nanoprecipitation in aqueous media, was assessed by DLS and by SEM. In addition, the aggregation in aqueous medium of the protected poly[(PheLA)_{10.4}-*b*-(Lys(Cbz)LA)_{31.4}] and poly[(PheLA)_{10.4}-*b*-(Glu(Bz)LA)_{30.2}] was also assessed. Both, the protected macromolecules and the deprotected macromolecules were able to self-aggregate in aqueous solution at significantly low concentrations (Table 9.1), which are comparable to some values that have been reported [16-18]. Studies that were carried out using DLS revealed that poly[(PheLA)_{10.4}-*b*-(Lys(Cbz)LA)_{31.4}] and poly[(PheLA)_{10.4}-*b*-(Glu(Bz)LA)_{30.2}] self-aggregated into NPs that

possessed mean diameters of 80.5 nm and 79.0 nm, respectively (Figure 9.6 a, b; Table 9.2, Entry 1 & 3). There was a slight decrease in the particle size obtained after deprotection, as evidenced by the diameters, measuring 78.3 nm and 77.2 nm, for poly[(PheLA)_{10.4}-*b*-(LysLA)_{31.4}] and poly[(PheLA)_{10.4}-*b*-(Glu)LA)_{30.2}], respectively (Figure 9.6 c, d; Table 9.2, Entry 2 & Entry 4). The NPs that were formed possessed narrow PDIs (< 0.20). This is a desirable trait for NPs that are intended for applications *in vivo* [19-21]. Studies that were carried out using SEM confirmed the formation of NPs that possessed a spherical morphology and the hydrodynamic sizes were in agreement with the results from DLS analyses (Figure 9.6 e, f).

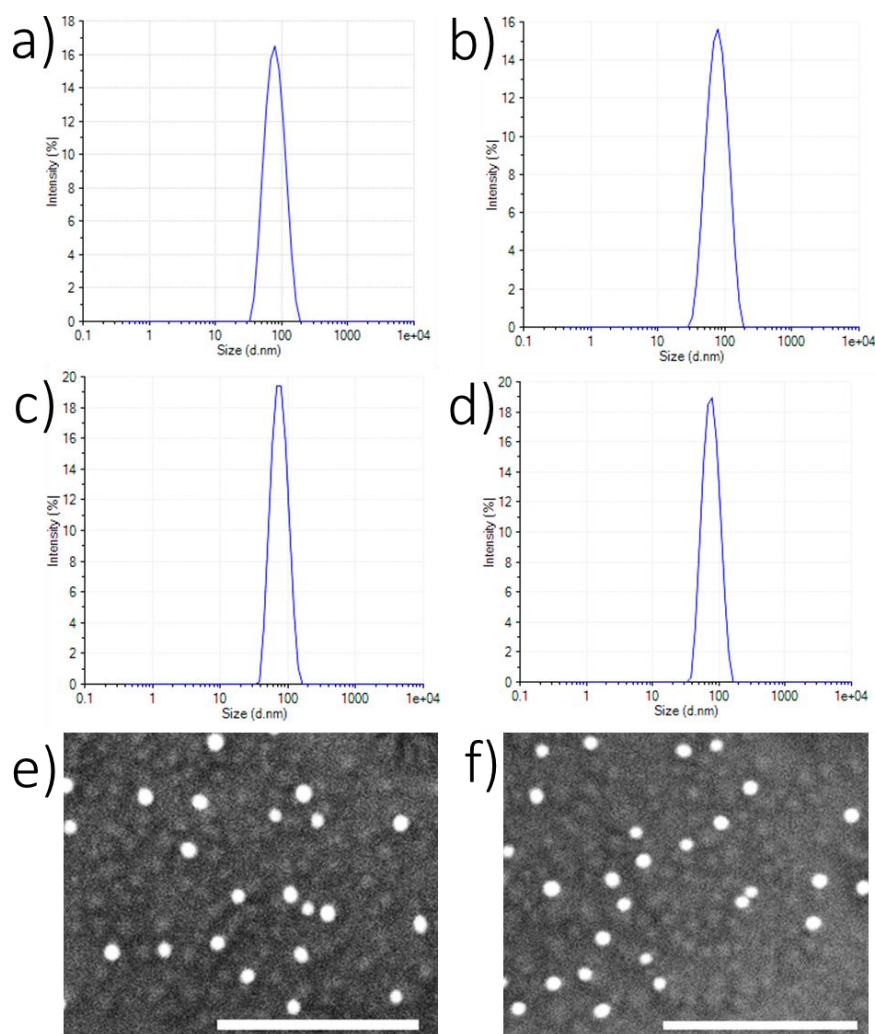


Figure 9.6. Graphical illustrations of self-aggregation of the poly(ester) macromolecules: DLS charts revealing the size distribution of poly[(PheLA)_{10.4}-*b*-(Glu(Bz)LA)_{30.2}] before (a) and after (c) the removal of benzyl ester protection groups and poly[(PheLA)_{10.4}-*b*-(Lys(Cbz)LA)_{31.4}] before (b) and after (d) the removal of Cbz protecting groups. SEM images of NPs formed by poly[(PheLA)_{10.4}-*b*-(Glu)LA)_{30.2}] (e) and formed by poly[(PheLA)_{10.4}-*b*-(LysLA)_{31.4}] (f). Scale bars represent 1 μ m.

Table 9.2. The critical aggregation concentrations, hydrodynamic sizes and polydispersity indices of NPs obtained from poly(ester) macromolecules.

Entry	Poly(ester)	Particle Size / (d.nm)	PDI
1	Poly[(PheLA) _{10.4} - <i>b</i> -(Lys(Cbz)LA) _{31.4}]	80.5 ± 31.6	0.17
2	Poly[(PheLA) _{10.4} - <i>b</i> -(LysLA) _{31.4}]	78.3 ± 31.8	0.17
3	Poly[(PheLA) _{10.4} - <i>b</i> -(Glu(Bz)LA) _{30.2}]	79.0 ± 33.5	0.19
4	Poly[(PheLA) _{10.4} - <i>b</i> -(GluLA) _{30.2}]	77.2 ± 33.6	0.19

It is envisaged that, due to its poly(cationic) nature, poly[(PheLA)_{10.4}-*b*-(LysLA)_{31.4}] may be exploited for antimicrobial applications [22-24] and gene delivery [25-27]. However, its poly(cationic) nature also dictates that this poly(ester) could pose cytotoxicity problems to healthy cells if it were to be used for drug delivery *in vivo* [28, 29]. As such, the NPs obtained from the protected macromolecule, i.e., poly[(PheLA)_{10.4}-*b*-(Lys(Cbz)LA)_{31.4}], and the NPs obtained from the deprotected poly[(PheLA)_{10.4}-*b*-(GluLA)_{30.2}], were used in the dox-encapsulation studies and in the subsequent drug release studies, *in vitro*.

Initially, dox hydrochloride was converted to its hydrophobic free-base by neutralisation using triethylamine [30], to optimise the encapsulation of the drug into the hydrophobic core of the nanoparticles. Drug encapsulation studies revealed that poly[(PheLA)_{10.4}-*b*-(GluLA)_{30.2}] NPs possessed an average drug encapsulation efficiency of 54.5% and a drug loading content of 3.19 wt. %. The poly[(PheLA)_{10.4}-*b*-(Lys(Cbz)LA)_{31.4}] NPs possess an average encapsulation efficiency of 45.3% and a drug loading content of 2.09 wt. % (Figure 9.7). The ability of the NPs to release the encapsulated drug, in response to the acidic pH hydrolysis of the poly(ester) backbone, was assessed using the dialysis method [31]. Studies were carried out at pH 5.0 to simulate the lysosomal pH conditions [32] and at pH 7.4 and 37 °C to simulate experimental conditions that are similar to the physiological fluid [33]. It was revealed that the *in vitro* release of dox from the NPs was greatest when the NPs were stored in acidic pH acetate buffer compared to the release of dox from the NPs that were stored in pH 7.4 PBS buffer solution.

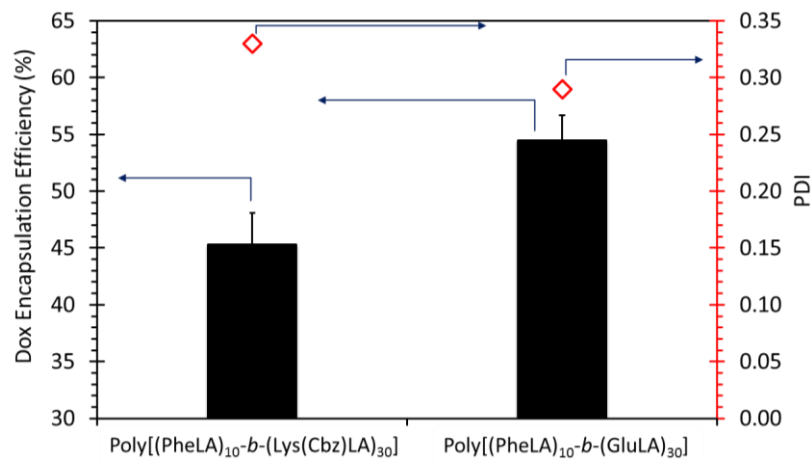


Figure 9.7. The encapsulation efficiency of dox into poly(ester) NPs (Data, $n = 3 \pm$ standard Error), and the polydispersity indices of the resulting dox-loaded NPs (\diamond).

In excess of 82% of the total dox was released from poly[(PheLA)_{10.4}-b-(GluLA)_{30.2}] NPs in response to acidic pH (5.0) stimulus, compared to less than 3% of the total dox that was released in response to incubation in pH 7.4 PBS buffer (Figure 9.8 a). In excess of 87% of the total dox was released from the poly[(PheLA)_{10.4}-b-(Lys(Cbz)LA)_{31.4}] NPs in response to an acidic pH (5.0) stimulus, while less than 4% of the total dox was released in response to incubation in a pH 7.4 PBS buffer (Figure 9.8 b).

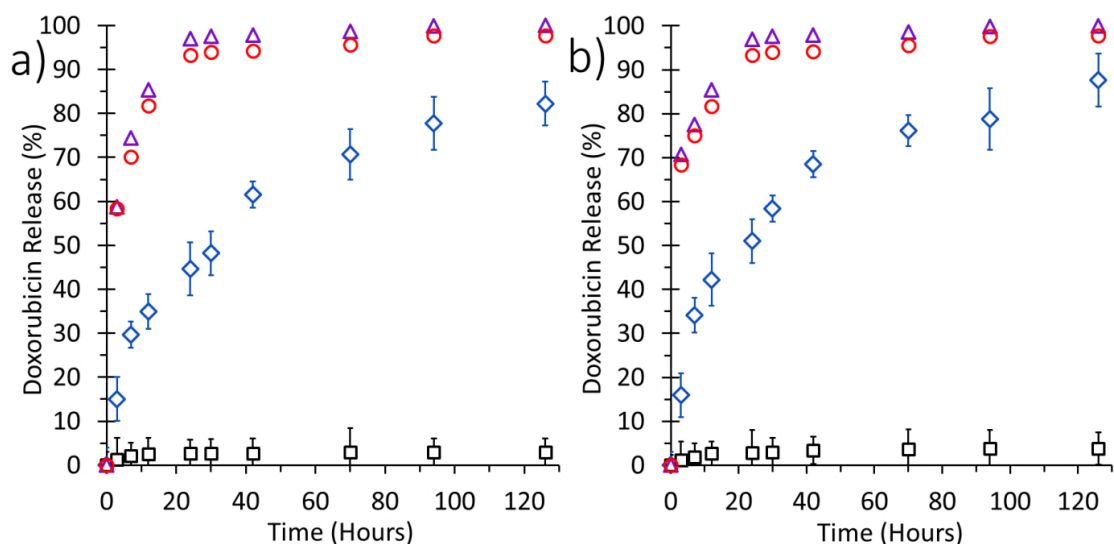


Figure 9.8. The release of dox from (a) poly[(PheLA)_{10.4}-b-(GluLA)_{30.2}] NPs and (b) poly[(PheLA)_{10.4}-b-(Lys(Cbz)LA)_{31.4}] NPs in response to incubation in acetate buffer maintained at pH 5.0 (\diamond) and PBS buffer maintained at pH 7.4 (\square). The release of free dox (un-encapsulated) from the dialysis tubing membrane in response to incubation at 37 °C in acetate buffer maintained at pH 5.0 (Δ) and PBS buffer maintained at pH 7.4 (\circ).

Additional control studies that were carried out using free dox revealed further that the encapsulated drug could be released in a controlled and sustained manner from both sets of nanoparticles. In contrast, the un-encapsulated (free) drug followed a rapid 'burst' release profile [34], at both pH 7.4 and pH 5.0, as characterised by the accelerated leaking of most of the drug out of the dialysis membrane in less than 30 hours (Figure 9.8 a,b). In both instances, more than 70% of free dox was released within 10 hours compared to the less than 35% of encapsulated dox. Close to 100% release of free dox was achieved within 30 hours.

The data that were obtained from the acidic pH-mediated release of dox from the NPs were fitted into the Korsmeyer-Peppas (KP) model (Chapter 2.22). The KP model states that the gradient, of a graphical plot of the logarithms of percentage drug release against the logarithms of time, is the release exponent (n). This can be used to predict the mechanism of drug release from the delivery vehicle [35]. A release exponent (n) equal to 0.43 was computed from the release of dox from poly[(PheLA)_{10.4}-*b*-(GluLA)_{30.2}] NPs, whilst a release exponent equal to 0.42 was computed from the release of dox from poly[(PheLA)_{10.4}-*b*-(Lys(Cbz)LA)_{31.4}] NPs (Figure 9.9).

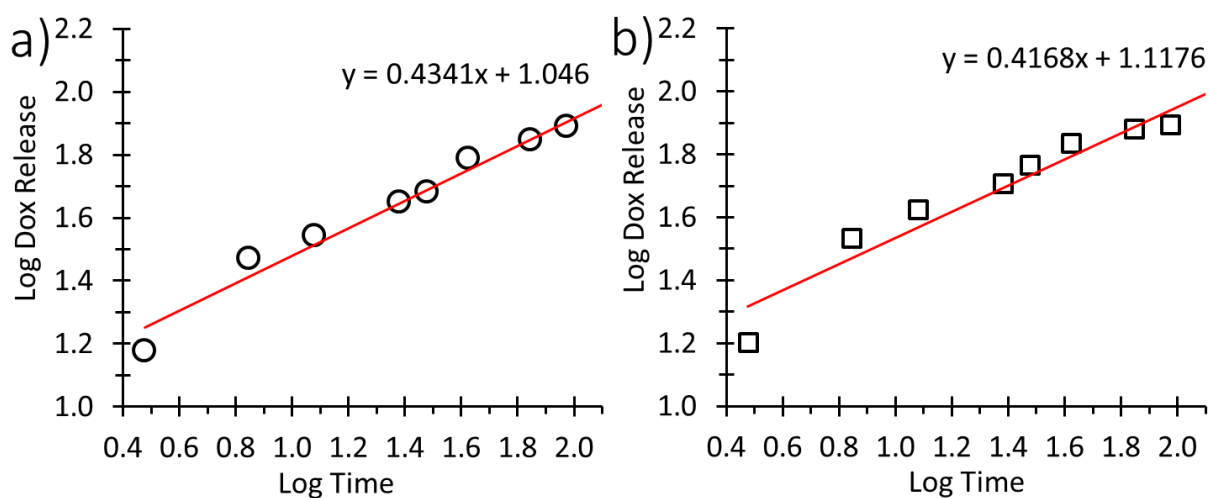


Figure 9.9. KP model plots of the release of dox from (a) poly[(PheLA)_{10.4}-*b*-(GluLA)_{30.2}] NPs and from (b) poly[(PheLA)_{10.4}-*b*-(Lys(Cbz)LA)_{31.4}] NPs in response to incubation in a pH 5.0 acetate buffer solution.

According to the KP model, values of $n \leq 0.45$ reveal that the release of drug molecules from spherical NPs follows the Fickian diffusion mechanism. As such, these findings suggest that the

acid-mediated release of dox molecules from poly[(PheLA)_{10.4}-*b*-(GluLA)_{30.2}] NPs and from poly[(PheLA)_{10.4}-*b*-(Lys(Cbz)LA)_{31.4}] NPs follows a Fickian diffusion mechanism.

9.4. Conclusion

Diblock poly(ester) macromolecules that were capable of self-assembling into monodisperse spherical NPs in aqueous media, were produced using OCA ROP. The NPs produced were proven to be capable of encapsulating and withholding significant a quantity (3.19 wt. %) of the chemotherapeutic dox before releasing it in a controlled manner, in response to hydrolysis by an acidic pH (5.0) stimulus. As such, these poly(ester) macromolecules offer an exciting prospect for the development of effective drug delivery compositions, for the release of cytotoxic chemotherapeutic molecules, especially dox.

9.5. References

1. Diana, I., Paolo, I., Fiorina, C., Pasquale, C., Michele Adolfo, T. and Maria Teresa Di, T. *Curr. Med. Chem.*, **2001**, 8, 1649-1660.
2. Curigliano, G., Cardinale, D., Suter, T., Plataniotis, G., de Azambuja, E., Sandri, M.T., Criscitiello, C., Goldhirsch, A., Cipolla, C. and Roila, F. *Ann. Oncol.*, **2012**, 23, vii155-vii166.
3. Chatterjee, K., Zhang, J., Honbo, N. and Karliner, J.S. *Cardiology*. **2010**, 115, 155-162.
4. Kumar, S., Marfatia, R., Tannenbaum, S., Yang, C. and Avelar, E. *Tex Heart Inst J.*, **2012**, 39, 424-427.
5. Steger, F., Hautmann, M.G. and Kölbl, O. *Radiat Oncol.*, **2012**, 7, 212-212.
6. Shek, T., Luk, I., Ma, L. and Cheung, K. *Arch Pathol Lab Med.*, **1996**, 120, 89-91.
7. Safra, T. *The Oncologist*. **2003**, 8, 17-24.
8. Bae, Y.H. and Park, K. *J. Control. Release*. **2011**, 153, 198-205.
9. Zhu, Q., Jia, L., Gao, Z., Wang, C., Jiang, H., Zhang, J. and Dong, L. *Mol. Pharm.*, **2014**, 11, 3269-3278.
10. Lv, S., Li, M., Tang, Z., Song, W., Sun, H., Liu, H. and Chen, X. *Acta Biomater.* **2013**, 9, 9330-9342.
11. Yi, H., Liu, P., Sheng, N., Gong, P., Ma, Y. and Cai, L. *Nanoscale*. **2016**, 8, 5985-5995.
12. Chaudhary, A., Dwivedi, C., Gupta, A. and Nandi, C.K. *RSC Adv.*, **2015**, 5, 97330-97334.
13. Qiu, J., Zhang, R., Li, J., Sang, Y., Tang, W., Rivera Gil, P. and Liu, H. *Int. J. Nanomedicine*. **2015**, 10, 6709-6724.
14. Manchun, S., Dass, C.R. and Sriamornsak, P. *Life Sci.*, **2012**, 90, 381-387.
15. Chen, X., Lai, H., Xiao, C., Tian, H., Chen, X., Tao, Y. and Wang, X. *Polym. Chem.* **2014**, 5, 6495-6502.
16. Jeong, J.H. and Park, T.G. *J. Control. Release*. **2002**, 82, 159-166.
17. Adams, M.L., Lavasanifar, A. and Kwon, G.S. *J. Pharm Pharm. Sci.*, **2003**, 92, 1343-1355.
18. Lee, S.C., Chang, Y., Yoon, J.-S., Kim, C., Kwon, I.C., Kim, Y.-H. and Jeong, S.Y. *Macromolecules*. **1999**, 32, 1847-1852.
19. Desai, M.P., Labhasetwar, V., Walter, E., Levy, R.J. and Amidon, G.L. *Pharm Res.*, **1997**, 14, 1568-1573.
20. Albanese, A. and Chan, W.C.W. *ACS Nano*. **2011**, 5, 5478-5489.
21. Mato, E., Puras, G., Bell, O., Agirre, M., Hernández, R., Igartua, M., Moreno, R., Gonzalez, G., de Leiva, A. and Pedraz, J. *J Nanomed Nanotechnol.*, **2015**, 6, p.1.
22. Carmona-Ribeiro, A.M. and de Melo Carrasco, L.D. *Int. J. Mol. Sci.*, **2013**, 14, 9906-9946.
23. Palermo, E.F., Lee, D.-K., Ramamoorthy, A. and Kuroda, K. *The Journal of Physical Chemistry B*. **2011**, 115, 366-375.
24. Mural, P.K.S., Kumar, B., Madras, G. and Bose, S. *ACS Sustain. Chem. Eng.*, **2016**, 4, 862-870.
25. Lv, H., Zhang, S., Wang, B., Cui, S. and Yan, J. *J. Control. Release*. **2006**, 114, 100-109.
26. Lee, H., Jeong, J.H. and Park, T.G. *J. Control. Release*. **2002**, 79, 283-291.
27. Askarian, S., Abnous, K., Darroudi, M., Oskuee, R.K. and Ramezani, M. *Biologicals*. **2016**, 44, 212-218.
28. Symonds, P., Murray, J.C., Hunter, A.C., Debska, G., Szweczyk, A. and Moghimi, S.M. *FEBS Letters*. **2005**, 579, 6191-6198.
29. Isaksson, K., Åkerberg, D., Posaric-Bauden, M., Andersson, R. and Tingstedt, B. *J. Mater. Sci. Mater. Med.*, **2014**, 25, 1293-1299.
30. Guo, S., Lv, L., Shen, Y., Hu, Z., He, Q. and Chen, X. *Sci. Rep.*, **2016**, 6, p.21459.
31. Hua, S. *Int J Nanomedicine*. **2014**, 9, 735-744.
32. Liu, Y., Wang, W., Yang, J., Zhou, C. and Sun, J. *Asian J. Pharmacol.*, **2013**, 8, 159-167.
33. Kayal, S. and Ramanujan, R.V. *Mater. Sci. Eng., C*. **2010**, 30, 484-490.
34. Kamba, S., Ismail, M., Hussein-Al-Ali, S., Ibrahim, T. and Zakaria, Z. *Molecules*. **2013**, 18, p.10580.
35. Fu, Y. and Kao, W.J. *Expert Opin Drug Deliv.*, **2010**, 7, 429-444.

Chapter 10. A Diblock Poly(Ester) for the Controlled Release of Hydrophobic Chemotherapeutics and for the pH-Induced Reversible Assembly in Nanobiotechnological Applications

Abstract

OCA ROP was used in the production of a diblock poly[(Lysine(Cbz)LA)_m-b-(Benzyl-Glutamic Acid)LA]_n] macromolecule. The poly(ester) produced aggregated in aqueous media to form spherical nanoparticles, which were capable of encapsulating and withholding doxorubicin (dox), before releasing it upon pH-mediated poly(ester) hydrolysis. In vitro cytotoxicity studies revealed that the poly(ester) is biocompatible. The dox-loaded NPs possessed anticancer potency against T47D and MCF-7 human breast cancer cells. Upon deprotection of the poly(ester) repeat units, a zwitterionic poly(ester) was generated, whose pH-dependent, reversible self-assembly was revealed by carrying out studies using DLS and SEM.

10.1. Introduction

Polymeric nanomaterials can be designed to be responsive to various stimuli that are applicable in the biomedicine. These include the enzymatic stimulation [1, 2], redox stimulation [3, 4], temperature stimulation [5, 6], light stimulation [7], electrical stimulation [8], magnetic stimulation [9, 10] and pH stimulation [11, 12]. Zwitterionic polymeric materials exhibit pH-induced self-assembly and dis-assembly at low pH levels and also at high pH levels. As such, these polymers are sometimes said to be 'schizophrenic' [13-16]. Zwitterionic polymeric materials are valuable in biomedicine because they can possess significant anti-fouling properties, due to their superior electrostatically-induced hydration [17-20]. These materials can be used in the development of anti-fouling payload delivery nanomaterials and as surface coatings in other medical applications [21-24].

Liu *et al.* [14] recently developed a zwitterionic lysine and hydrazine grafted poly(aspartamide) macromolecule that exhibited anti-protein-fouling properties. In addition, the macromolecule was able to encapsulate dox and, subsequently, released it after undergoing pH-induced disassembly. Chen *et al.* [25] have reported on an amphoteric, dendritic hybrid poly(amino acid), which exhibited reversible self-assembly into poly(glutamic acid)-core aggregates at an

acidic pH and into poly(lysine)-core aggregates at an alkaline pH. Rao *et al.* [26] initiated the ROP of Glu NCA, from monoamino-terminated poly(*N*-isopropylacrylamide), to produce a hybrid poly(*N*-isopropylacrylamide)-*b*-poly(L-glutamic acid) (PNIPAM-*b*-PLGA). The macromolecule showed potential use in biomedical applications by combining its thermo-responsiveness and its pH-responsiveness to give PNIPAM-core micelles, at alkaline pH and at elevated temperatures, and then PLGA-core micelles at acidic pH and ambient temperature. It has been reported that nanoparticles (NPs) that possess cationic surfaces are usually internalised easily by cells, because they can adsorb easily to the cell membranes [27, 28]. Yuan *et al.* [29] developed charge-switchable polymeric NPs, which were contained cysteamine repeat groups and 2-(mercaptoethyl)trimethylammonium repeat groups. The NPs were neutral at the physiological pH, but they assumed cationic charges when they were stimulated by the acidic pH environment, in the tumours. The cationic charge improved the uptake of the NPs by the tumours.

Poly(ethylene glycol) (PEG) is commonly used for antifouling purposes, to impart non-specific protein adsorption [30, 31]. Unfortunately, PEG can be susceptible to un-desirable oxidation in biological solutions. Also, its non-biodegradability can lead to long term storage diseases [32]. Unlike some PEGylated nanomaterials, which have been shown to induce the production of anti-PEG immunoglobulins, which results in premature clearance *in vivo* [32, 33], zwitterionic polymers can be used for passive targeting because they can avoid quick recognition by the immune system and thus afford longer circulation times [34]. Poly(ester)-based materials, which can be produced by the ROP of amino acid OCAs, provide the needed biodegradability, biocompatibility and side chain functional versatility from the various canonical amino acids that are at disposal. For the work presented in this chapter, the sequential ROP of N_ϵ -Carbobenzyloxy-L-Lysine (Lys(Cbz)) OCA and γ -benzyl-L-glutamic acid (Glu(Bz)) OCA was followed to produce a diblock poly(ester) macromolecule that self-aggregated in aqueous media, into NPs that were able to encapsulate and withhold dox, before releasing it in a controlled manner, in response to an environmental acidic pH stimulus. The subsequent poly(ester) deprotection unlocked the zwitterionic properties of the macromolecule, which exhibited then, the pH-dependent reversible assembly. Although a comparable system that is based on a diblock poly(amino acid) was reported previously by Rodríguez-Hernández and Lecommandoux [35],

the system described here presents a pH-responsive poly(ester) that is susceptible to acid-mediated degradation, and may be of value in drug delivery.

10.2. Experimental Details

10.2.1. Synthesis of Poly[(Lys(Cbz)LA)_m-*b*-(Glu(Bz)LA)_n]

Lys(Cbz) OCA (562 mg, 1.82 mmol) was dissolved in anhydrous DMF (10 mL), in a flame-dried and nitrogen-purged Schlenk tube that was equipped with a magnetic stirrer bar. 4-dimethylaminopyridine (DMAP) (22.3 mg, 0.18 mmol) was dissolved in anhydrous DMF (2 mL). The solution was injected into the Schlenk tube. Then, a solution of 2-methyl-1-propanol (4.50 mg, 0.06 mmol) in anhydrous DMF (5 mL) was added to initiate the reaction. The reaction medium was stirred at room temperature, for 120 hours under a nitrogen flow. Aliquots (0.1 mL) were extracted from the reaction medium at predetermined time intervals, added to 0.5 mL deuterated chloroform and analysed by ¹H NMR, to ascertain the degree of polymerisation. When the OCA monomer was polymerised fully, the poly(L-Lys(Cbz)LA)_m macromolecule was isolated by precipitation in cold diethyl ether and then centrifugation. The macromolecule was subsequently re-dissolved in anhydrous DMF (10 mL). The solution was injected into a flame-dried and nitrogen-purged Schlenk tube. DMAP (22.3 mg, 0.18 mmol) was dissolved in anhydrous DMF (2 mL) and added to the reaction medium. Then Glu(Bz) OCA (481.1 mg, 1.82 mmol) was dissolved in anhydrous DMF (5 mL) and injected gently into the reaction medium. The reaction medium was degassed and then stirred at room temperature, for a further 120 hours, after which the Glu(Bz) OCA had become fully polymerised. The reaction medium was diluted with distilled water (5 mL) and emptied into a dialysis tubing membrane (2000 Da, MWCO) and dialysed against distilled water for 96 hours, replenishing the dialysate every 12 hours. The diblock poly(ester) was eventually isolated by lyophilisation. Yield: 65 wt. %. ¹H NMR (500 MHz, CDCl₃, δ, ppm): 7.65 - 7.35 (C₆H₅), 5.24 - 5.09 (Ph-CH₂O), 4.98 (αCH(CO)O), 4.28 (NHCOO), 3.65 ((CH₃)₂CHCH₂), 3.49 - 3.05 (NHCH₂), 2.75 - 2.39 (CH₂)₂COO), 2.29 ((CH₃)₂CH), 2.11 - 1.01 (αCH(CH₂)₃), 0.88 (CH₃)₂. FTIR: ν_{max}/cm⁻¹ (solid): 690 - 800 cm⁻¹ (aromatic C-H bending), 1744 (C=O ester stretch), 2942 cm⁻¹ (C-H alkyl stretch).

10.2.2. Deprotection of Poly[(Lys(Cbz)LA)_m-*b*-(Glu(Bz)LA)_n]

Poly[(Lys(Cbz)LA)_m-*b*-(Glu(Bz)LA)_n] (320 mg) was dissolved in THF:methanol (1:1 v/v, 30 mL). The solution was injected into a sealed round bottomed flask, that was furnished with a 10% Pd/C (64 mg, 20 wt. % of poly(ester)). The reaction medium was purged several times using hydrogen, and then stirred under hydrogen flow for 72 hours, at room temperature. The Pd/C catalyst was isolated from the reaction medium by gravitational filtration. The filtrate was concentrated by rotary evaporation, yielding the crude deprotected poly(ester). The polymer was then dialysed against deionised water for 48 hours and then lyophilised. Yield: 185 mg, 57.8 wt %). ¹H NMR (500 MHz, D₂O, δ, ppm): 4.89 - 4.86 (αCH(CO)O), 4.35 - 4.28 (NHCOO), 3.74 - 3.65 ((CH₃)₂CHCH₂), 3.16- 3.07 (NHCH₂), 2.69 - 2.51 (CH₂)₂COO), 2.19 ((CH₃)₂CH), 2.01 - 1.21 (αCH(CH₂)₃, 0.81 (CH₃)₂). FTIR:ν_{max}/cm⁻¹ (solid): 1752 (C=O ester stretch), 2499 - 3300 cm⁻¹ (carboxylic acid OH stretch + C-H alkyl stretch).

10.2.3. Assessment of pH-Dependent Zwitterionic Behaviour

The poly(ester) solution (3 mg/mL) was prepared in anhydrous DMF and filtered through a 0.2 μm syringe filter. Then, aqueous buffer solutions, i.e., an acetate buffer (pH 4.5), a PBS buffer (pH 7.4) and a 4-(cyclohexylamino)-1-butanefulfonic acid (CABS) buffer (pH 11.2) were also filtered through 0.2 μm syringe filters. The filtered poly(ester) solution (1 mL) was added dropwise to the vigorously stirred pH 4.5, pH 7.4 and pH 11.2 aqueous buffer solutions (10 mL), respectively. The prepared samples were collected immediately into disposable poly(styrene)-based cuvettes, and the samples were analysed using DLS, at 37 °C, to ascertain polymer aggregation, aggregate sizes and zeta potential values, as described in Chapter 2.15. Samples were also collected immediately after nanoprecipitation, and deposited onto SEM stubs. These were air-dried, sputter-coated with gold and subsequently analysed using SEM (Chapter 2.17).

10.2.4. Dox-Loading and Release from Poly[(Lys(Cbz)LA)_m-*b*-(Glu(Bz)LA)_n] NPs

Dox-loaded poly[(Lys(Cbz)LA)_{26.6}-*b*-(Glu(Bz)LA)_{28.3}] NPs were prepared by the co-nanoprecipitation of the dox free-base and poly[(Lys(Cbz)LA)_{26.6}-*b*-(Glu(Bz)LA)_{28.3}] in a pH 7.4 PBS buffer. The NPs were then dialysed against the PBS buffer for 72 hours and subsequently lyophilised. Dox-loaded NPs were subsequently reconstituted in an acetate buffer (pH 4.5) only and in a PBS buffer (pH 7.4) only. The release profile of dox from the dispersions was assessed

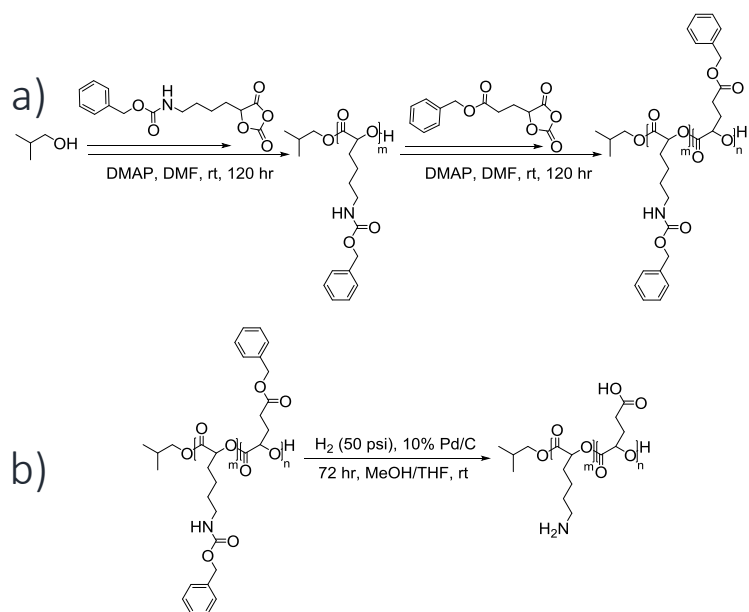
using the dialysis method. In addition, free dox was reconstituted in a acetate buffer (pH 4.5) only, and also in a PBS buffer (pH 7.4) only. The release profile of dox from the respective NPs was then assessed.

10.2.5. *In vitro* Cytotoxicity Assessment of Blank NPs and Dox-Loaded NPs

T47D and MCF-7 cells were supplied by the European Collection of Authenticated Cell Cultures (ECACC) and were cultured in DMEM (Invitrogen), supplemented with 10% (v/v) FCS (Sigma) at 37 °C in 5% CO₂. The cells were certified mycoplasma-free and were short tandem, repeat-profiled for verification. 1000 T47D cells and 2000 MCF-7 cells were plated in quadruplicate per well, in 96-well microplates. After 24 hours, the dox-loaded NPs were added to the cells at varying dox concentrations. In addition, equivalent loadings of blank NPs (polymer) only, and free dox only were added to cells in independent wells. The experimental sets-up were incubated for 72 hours, at 37 °C, in a humidified 5% CO₂-containing atmosphere. Then, the culture medium was replaced with an 0.5 mg/mL MTT-containing medium and the sets-up were incubated further for 3 hours, at 37 °C. The medium was replaced with DMSO. Then absorbance readings were recorded at 620 nm, using a Mithras LB 940 plate-reader. To obtain IC₅₀ values, data were fitted to the four-parameter log (inhibitor) versus response curve in GraphPad Prism (software version 7.02).

10.3. Results and Discussion

Glu(Bz) OCA and Lys(Cbz) OCA monomers were synthesised by following the procedures that are described in Chapter 3.3.11 and in Chapter 3.3.12, respectively. Isobutanol was then used to initiate the ROP of Lys(Cbz) OCA, in anhydrous DMF (Scheme 10.1 a). It was vital that the progress of the reaction was monitored to ascertain the point at which the cyclic monomer was fully polymerised, before Glu(Bz) OCA was added to the reaction. As such, the polymerisation was monitored using ¹H NMR spectroscopy (Figure 10.1), by comparing the integration value obtained from CH₃ protons (*ca* 0.75 ppm) of isobutanol initiator with the integration value obtained from the aromatic protons of the Lys(Cbz) repeat units (7.11 - 7.32 ppm). ¹H NMR spectroscopy revealed that 26.6 Lys(Cbz) repeat units were grafted from the isobutanol initiator, after 120 hours of polymerisation (Figure 10.1).



Scheme 10.1. (a) The sequential ROP of lys(Cbz) OCA and Glu(Bz) OCA, and (b) the deprotection of the lys(Cbz) and Glu(Bz) repeat units, using catalytic Pd/C hydrogenolysis.

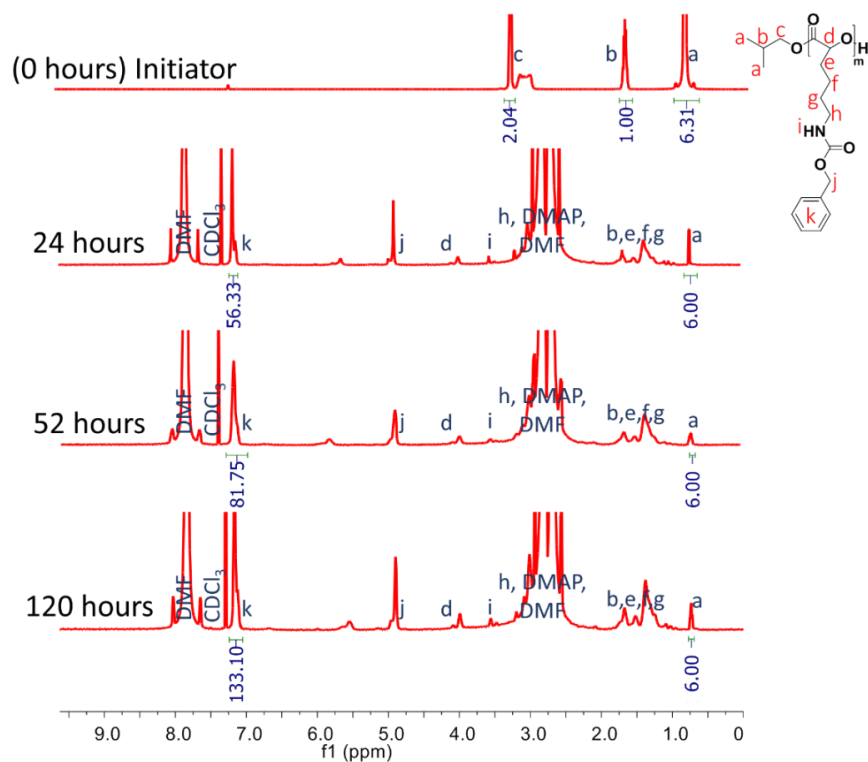


Figure 10.1. ^1H NMR spectra obtained from the analyses of reaction fractions that were extracted from the ROP of Lys(Cbz) OCA from an isobutanol molecule.

The poly(Lys(Cbz)LA) block was then isolated from any residual Lys(Cbz) OCA monomer, prior to the addition of the Glu(Bz) OCA to the reaction medium, by precipitation in cold diethyl

ether. The ROP of Glu(Bz) OCA from the terminal hydroxyl groups of poly(Lys(Cbz)LA) was then carried out for 120 hours. Analyses that were carried out using ^1H NMR spectroscopy helped to reveal that approximately 28.3 Glu(Bz) repeat units were grafted from the poly(Lys(Cbz)LA) block, yielding the required diblock poly(ester) architecture, poly[(Lys(Cbz)LA) $_{26.6}$ -*b*-(Glu(Bz)LA) $_{28.3}$] (Figure 10.2 a).

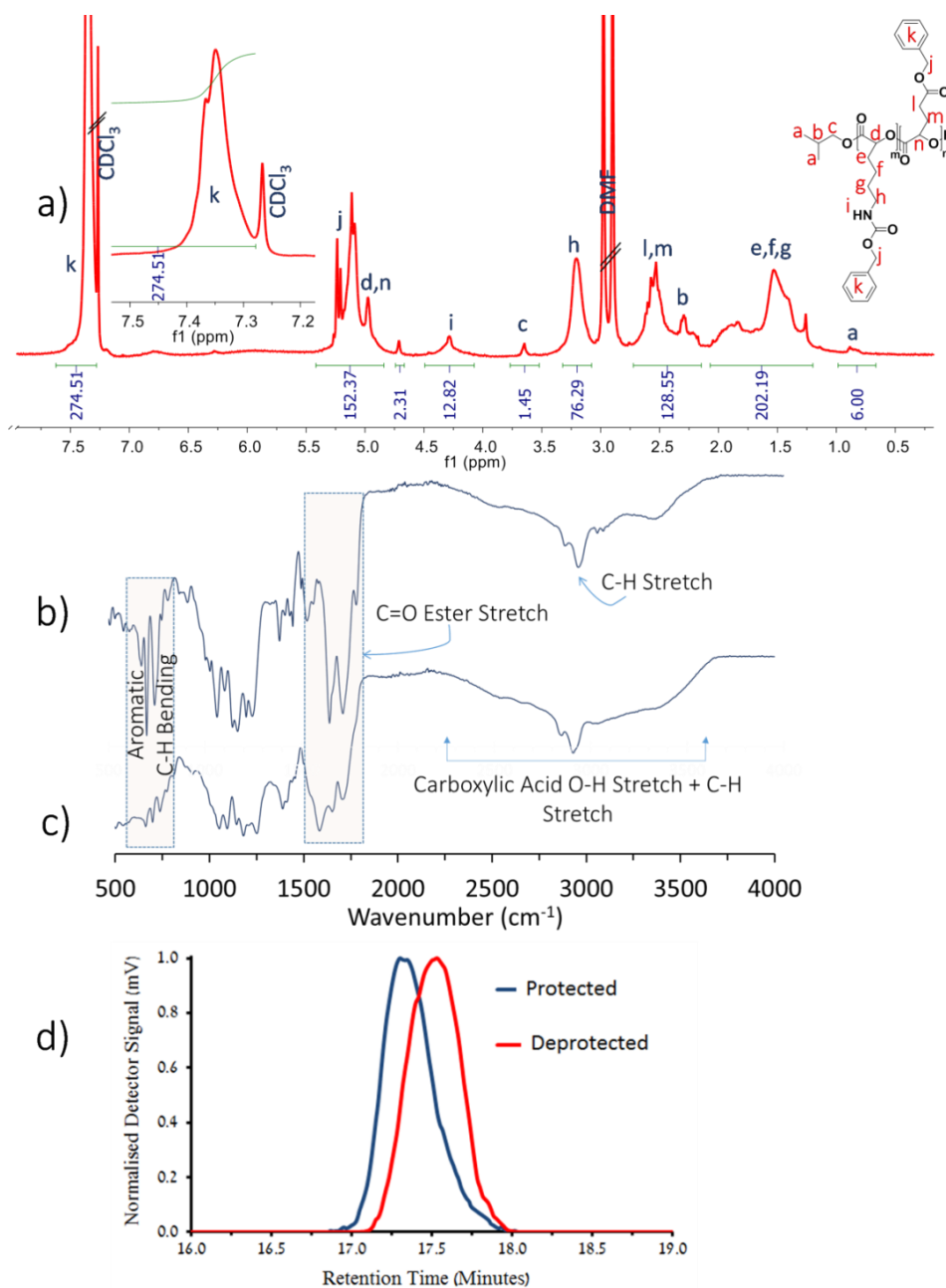


Figure 10.2. (a) ^1H NMR spectrum of poly[(Lys(Cbz)LA) $_{26.6}$ -*b*-(Glu(Bz)LA) $_{28.3}$], FTIR spectra of poly[(Lys(Cbz)LA) $_{26.6}$ -*b*-(Glu(Bz)LA) $_{28.3}$] before (b) and after poly(ester) deprotection (c), and (d) GPC chromatograms obtained from the analyses of poly[(Lys(Cbz)LA) $_m$ -*b*-(Glu(Bz)LA) $_n$] macromolecules before after poly(ester) deprotection and after poly(ester) deprotection.

FTIR spectroscopic evaluations revealed the presence of peaks emanating from the C-H alkyl stretch (2942 cm^{-1}) and from the C=O ester stretch from the poly(ester) backbone (1744 cm^{-1}) and aromatic C-H bending, from the Bz and Cbz protecting groups ($690 - 800\text{ cm}^{-1}$) (Figure 10.2 b). The protected macromolecule and the deprotected macromolecule possessed a unimodal distribution and narrow PDIs (1.07 and 1.08, respectively), as revealed by GPC (Figure 10.2 d).

NPs that have potential applications for the delivery of hydrophobic therapeutics can be obtained from hydrophobic poly(ester)s, such as poly(lactide-*co*-glycolide), poly(lactic acid) and poly(caprolactone) [36, 37]. Studies that were carried out using DLS revealed that the protected, and hence hydrophobic, poly[(Lys(Cbz)LA)_{26.6}-*b*-(Glu(Bz)LA)_{28.3}] is able to self-aggregate in aqueous media to form stable and monodisperse NPs at pH 4.5 (103.9 nm), at pH 7.4 (158.9 nm) and at pH 11.2 (80.1 nm), respectively (Figure 10.3 d,e,f). The correlation curves that were obtained from the respective NP dispersions displayed a smooth and single exponential decay (Figure 10.3 g,h,i), which is indicative of dispersions that contain mono-sized NPs [38]. The formation of the NPs was confirmed by carrying out analyses using SEM, which revealed the formation of spherical NPs, whose average hydrodynamic size were consistent with the findings from DLS analyses (Figure 10.3 a,b,c).

The use of hydrophobic polymers for the delivery of hydrophobic therapeutics is particularly desirable because these macromolecules absorb relatively less of the aqueous medium, compared to the hydrophilic polymers. This dictates that they are degraded much more slowly, thereby resulting in more sustained drug release [37]. Poly[(Lys(Cbz)LA)_{26.6}-*b*-(Glu(Bz)LA)_{28.3}] in particular is composed of a large number of aromatic groups, from the Bz and CBz protecting groups, which could enhance the physical encapsulation efficiency of dox *via* hydrophobic interactions and π - π interactions with dox molecules [14]. As such, the ability of poly[(Lys(Cbz)LA)_{26.6}-*b*-(Glu(Bz)LA)_{28.3}] NPs to encapsulate dox was evaluated.

The encapsulation of dox, at pH 7.4, resulted in an increase of the particle size from 158.9 nm to 168.4 nm (Figure 10.4), yielding NPs which had a drug-loading content of 2.73 wt. % and a drug-encapsulation efficiency of 39.7%. The dox-loaded NPs were subsequently assessed for their ability to release the encapsulated dox controllably in response to the environmental acid-mediated hydrolysis of the poly(ester) *in vitro*.

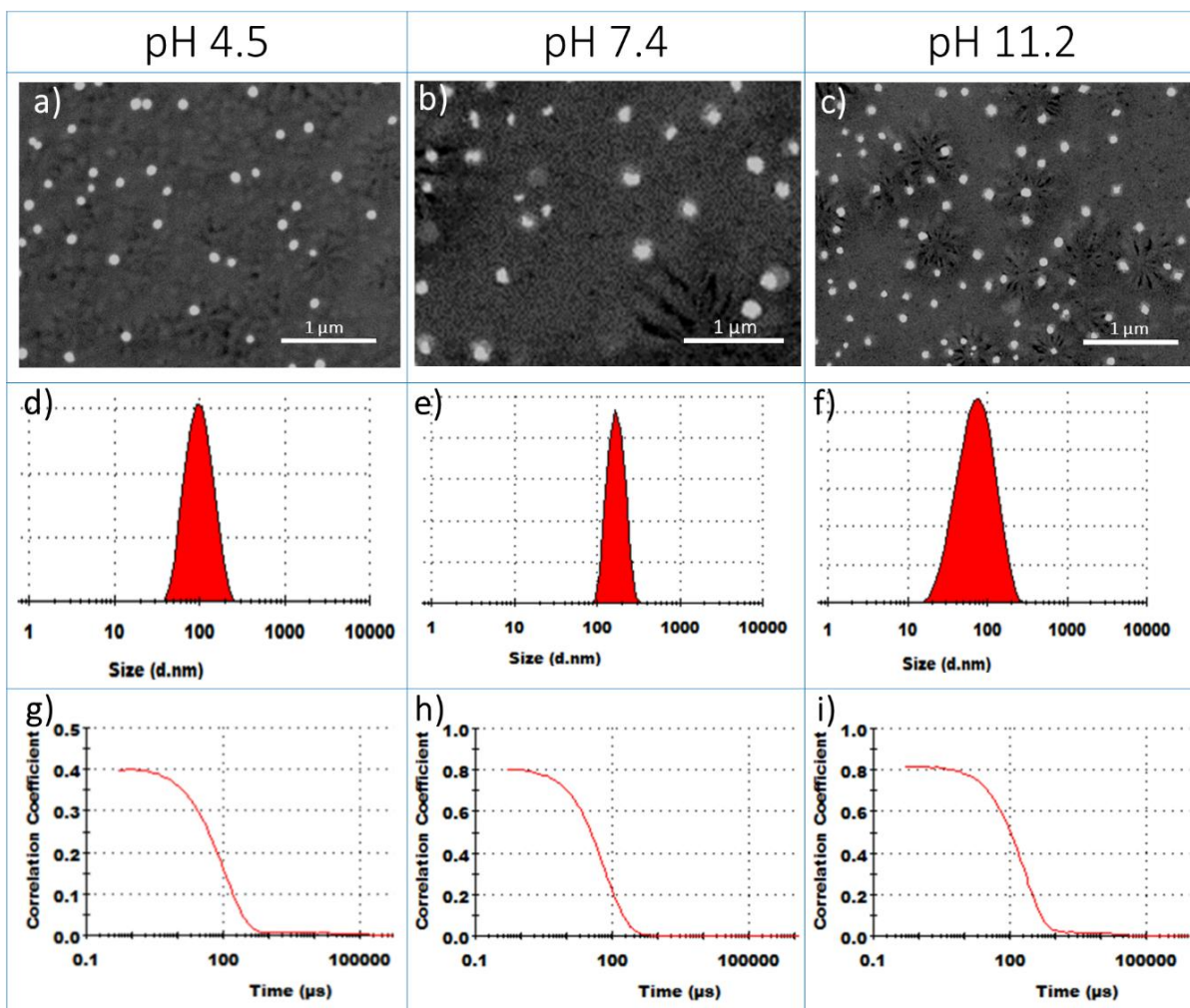


Figure 10.3. SEM images (a, b and c), DLS charts (d, e, f) and DLS correlation graphs (g, h, i) that were obtained after the self-assembly of poly[(Lys(Cbz)LA)_{26.6}-*b*-(Glu(Bz)LA)_{28.3}], in aqueous media maintained at pH 4.5, at pH 7.4 and at pH 11.2, respectively. Scale bars represent 1 μm .

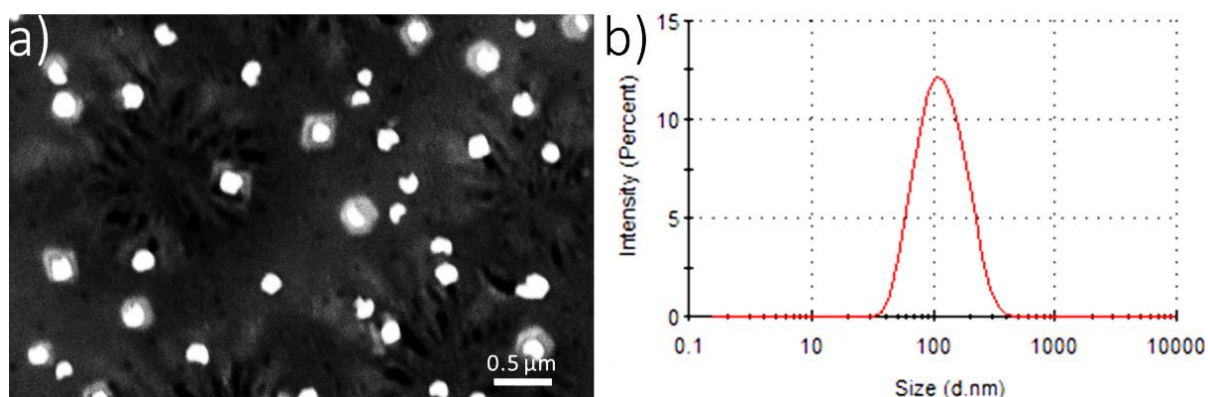


Figure 10.4. (a) SEM microphotograph and (b) DLS chart, revealing the size-distribution of dox-loaded poly[(Lys(Cbz)LA)_{26.6}-*b*-(Glu(Bz)LA)_{28.3}] NPs. Scale bar represents 0.5 μm .

The release of dox from poly[(Lys(Cbz)LA)_{26.6}-*b*-(Glu(Bz)LA)_{28.3}] NPs was greatest when the NPs were incubated in a pH 4.5 buffer acetate solution. More than 78% of the total dox was released from the NPs after 126 hours (Figure 10.5 a). Fitting the release data into the Korsmeyer-Peppas (KP) model [39] revealed a release exponent equal to 0.42 (Figure 10.5 b), suggesting that the release of dox follows a Fickian diffusion profile, upon polymer hydrolysis. In contrast, the NPs retained most of the encapsulated drug when they were incubated at pH 7.4. Less than 5% of the total dox was released, after 126 hours. In addition, the encapsulation of dox in the poly[(Lys(Cbz)LA)_{26.6}-*b*-(Glu(Bz)LA)_{28.3}] NPs resulted in the sustained and controlled release of the drug molecules, in contrast to the burst release profile that was observed in the release of the un-encapsulated drug. As such, poly[(Lys(Cbz)LA)_{26.6}-*b*-(Glu(Bz)LA)_{28.3}] NPs are a prospect for use in the development of effective delivery vehicles for hydrophobic chemotherapeutics.

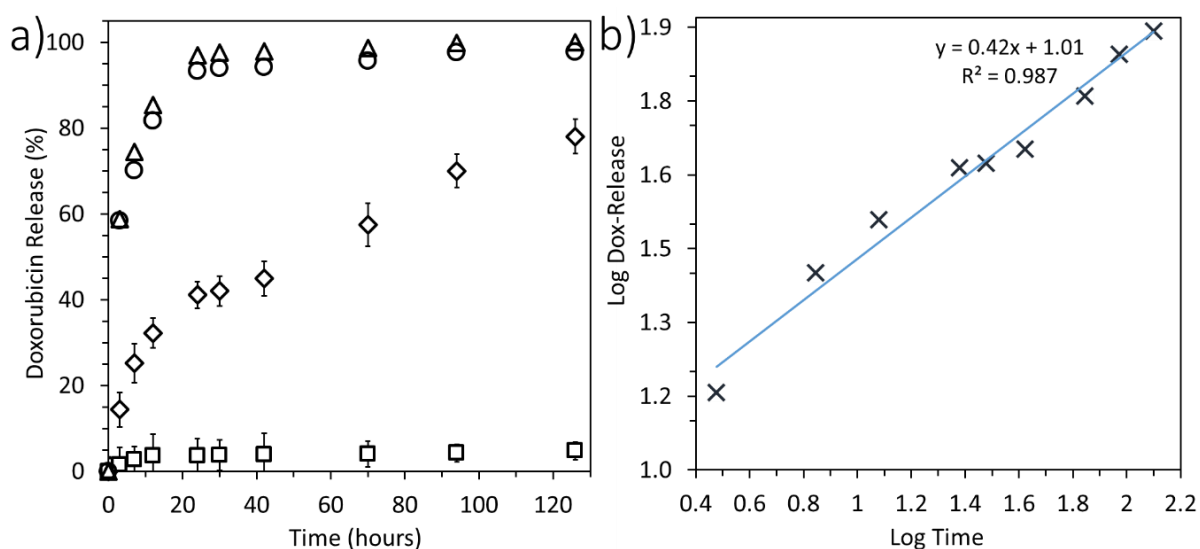


Figure 10.5. The release of dox from (a) poly[(Lys(Cbz)LA)_{26.6}-*b*-(Glu(Bz)LA)_{28.3}] NPs in response to incubation in pH 4.5 acetate buffer (◇) and pH 7.4 PBS buffer (□). The release of un-encapsulated dox from the dialysis tubing membrane in response to incubation in pH 4.5 acetate buffer (Δ) and pH 7.4 PBS buffer (○). (b) KP model plot for data (X) obtained from pH-mediated dox-release from poly[(Lys(Cbz)LA)_{26.6}-*b*-(Glu(Bz)LA)_{28.3}] NPs.

The *in vitro* cytotoxicity of poly[(Lys(Cbz)LA)_{26.6}-*b*-(Glu(Bz)LA)_{28.3}] NPs and dox-loaded poly[(Lys(Cbz)LA)_{26.6}-*b*-(Glu(Bz)LA)_{28.3}] NPs were evaluated by MTT assays on two human breast cancer cell lines, T47D [40] and MCF-7 [41]. Free dox was used as a control (Figure 10.6 a, b).

It was observed that the viability of the T47D cells and the MCF-7 cells remained significant for more than 72 hours when the cells were treated with blank NPs (> 95% viable at the highest concentration on T47D cells and > 60% viable at the highest concentration on MCF-7 cells). This is shown in representative images from the colorimetric MTT assays (Figure 10.6 c), which reveal an increased purple colouration for wells that contained cells that were treated with the blank NPs (the purple colouring indicates viable cells).

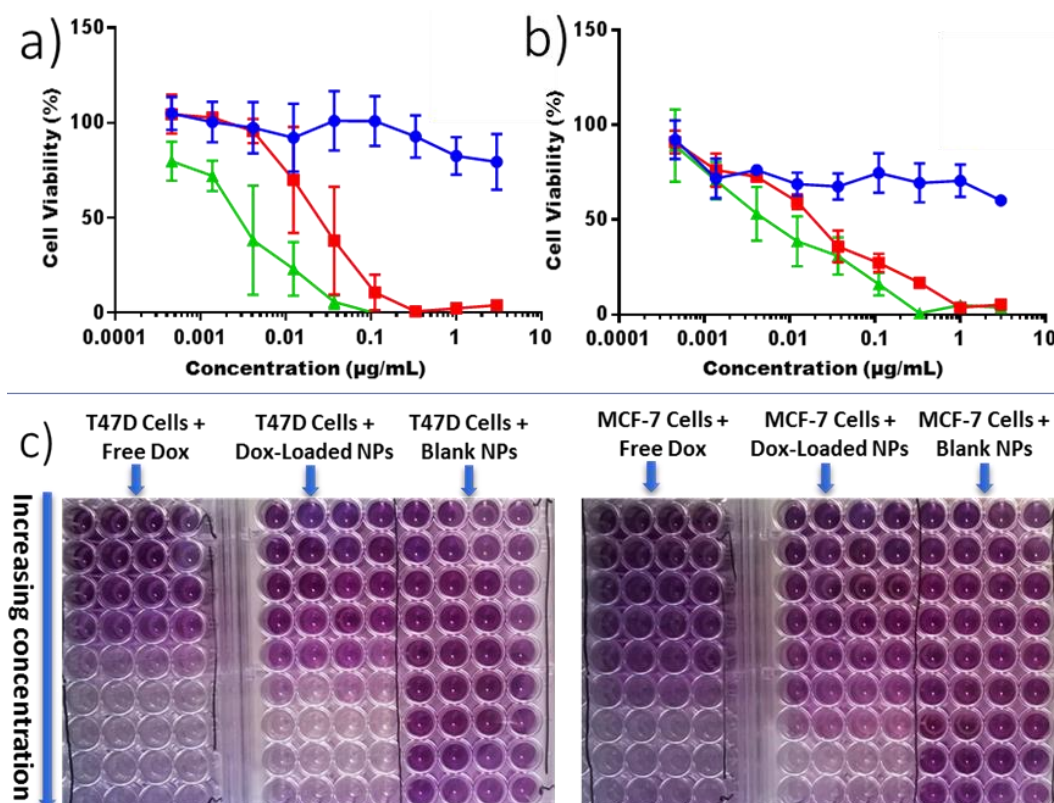


Figure 10.6. The effect of blank polymer NPs (●), dox-loaded polymer NPs (■) and free dox (▼) on the viability of (a) T47D human breast cancer cells and (b) MCF-7 human breast cancer cells. Data is presented as mean \pm SD (n = 4). (c) Representative macro images obtained from the colorimetric MTT assay in which the purple colouring indicates the presence of viable cells.

In contrast, dox-loaded NPs exhibited significant toxicity against the two cancer cell lines, as revealed by the rapid decrease in cell viability (visually observed by a reduction in the amount of formazan crystals in the MTT-containing medium (Figure 10.6 c)) and subsequent complete loss of viability of the cells after 72 hours, at dox concentrations ≥ 1 µg/mL. There was no significant difference in the effect of the dox-loaded NPs on T47D cells and MCF-7 cells. The IC_{50} of dox-loaded NPs was 0.0217 µg/mL on T47D cells, and was 0.0220 µg/mL on MCF-7 cells.

The IC₅₀ values of the free dox on the respective cell lines (T47D = 0.0040 µg/mL and MCF-7 = 0.0019 µg/mL) were lower than the values recorded for dox-loaded NPs, which could be attributed to the different cell response and cell internalisation pathways of free dox and dox-load NPs [42].

It is hoped that the encapsulation of dox in poly[(Lys(Cbz)LA)_{26.6}-*b*-(Glu(Bz)LA)_{28.3}] NPs could enhance drug accumulation in the tumour due to the enhanced permeability and retention effect (EPR) effect [43]. Also, the lowered pH environment of the tumour versus normal tissues (apart from the stomach) could promote drug release exclusively at targeted, cancerous, sites. Drug-encapsulation could also afford a greater maximum tolerated dose than the free drug can afford in a single dose *in vivo*, and induce tumour destruction after a reduced number of doses [44]. Although there remains a need to carry out further biological studies, the anticancer potency that was exhibited by dox-loaded poly[(Lys(Cbz)LA)_{26.6}-*b*-(Glu(Bz)LA)_{28.3}] NPs dictates that they could provide effective delivery vehicles.

The choice of the lys(Cbz) monomer OCA and the Glu(Bz) OCA monomer, in the design of poly[(Lys(Cbz)LA)_{26.6}-*b*-(Glu(Bz)LA)_{28.3}], was influenced by the desire to create a macromolecule that could exhibit zwitterionic properties upon poly(ester) deprotection. As such, catalytic hydrogenolysis was used to cleave the Cbz groups and the Bz groups from the poly(ester), to unlock the zwitterionic properties of the macromolecule (Scheme 10.1 b). The successful removal of Cbz and Bz protecting groups was confirmed by carrying out ¹H NMR spectroscopic analyses, that revealed the disappearance of peaks (7.21 - 7.39 ppm) that belonged to the aromatic protons (Figure 10.7). Poly(ester) deprotection was also confirmed further by carrying out FTIR spectroscopic analyses, that revealed the disappearance of the aromatic C-H bends (690 - 800 cm⁻¹) and the emergence of a carboxylic acid OH stretch (2499 - 3300 cm⁻¹), which emanated from the deprotected glutamic acid repeat units (Figure 10.2c).

The zwitterionic behaviour of the deprotected poly[(LysLA)_{26.6}-*b*-(GluLA)_{28.3}] was then assessed by carrying out studies of poly(ester) aggregation at an acidic pH, at normal physiological pH value and at an alkaline pH, using DLS and SEM. DLS revealed the pH-dependent aggregation of poly[(LysLA)_{26.6}-*b*-(GluLA)_{28.3}]. For example, the poly(ester) aggregated in aqueous solution of an acidic pH (pH 4.5) into monodisperse NPs that averaged 97.4 nm in size (Figure 10.8 b). However, no polymer aggregation was detected when the pH of the dispersion was switched

to the physiological pH value (pH 7.4). This was revealed by the absence of a size distribution DLS trace (Figure 10.8 d), the absence of a coherent correlation curve, which normally follows an exponential decay profile for the dispersions that contain NPs (Figure 10.8 e), and the 'expert advice' provided by the DLS software suggested that the polymer dispersion did not contain NPs (Figure 10.8 c).

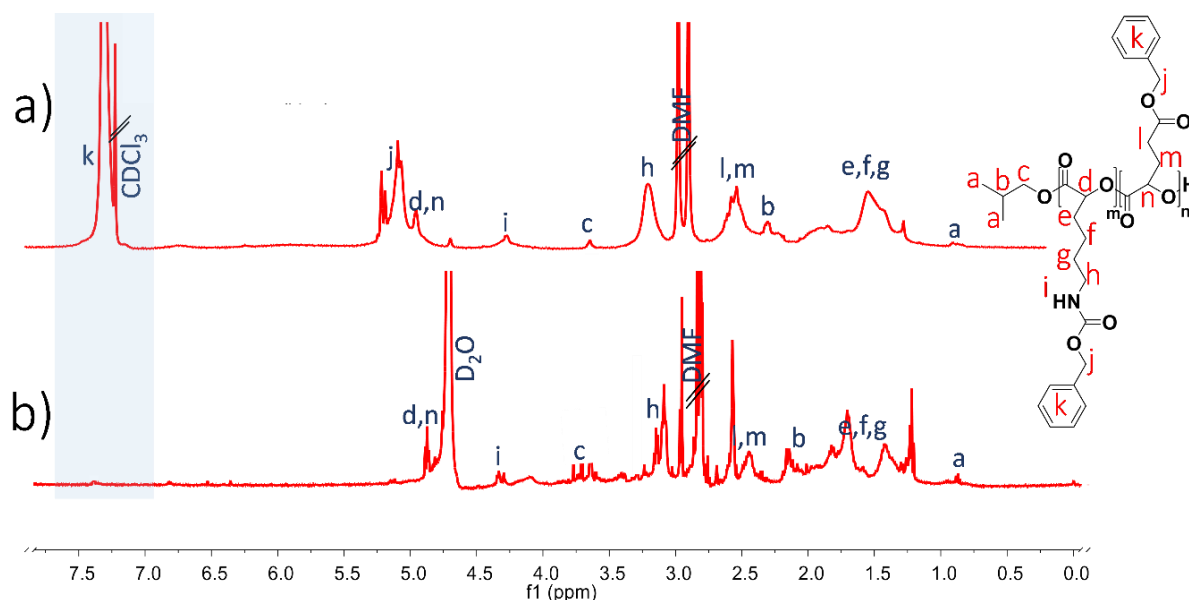


Figure 10.7. ¹H NMR spectra of (a) poly[(Lys(Cbz)LA)_m-b-(Glu(Bz)LA)_n] prior to carrying out deprotection and (b) the deprotected poly[(LysLA)_m-b-(GluLA)_n], revealing the absence of Cbz and Bz ester-protecting groups, which were removed by Pd/C catalytic hydrogenolysis.

Remarkably, the reformation of monodisperse particles, that averaged 103.7 nm in size, was detected when the pH of the dispersion was adjusted to a pH of 11.2 (Figure 10.8 g). The pH-dependent self-assembly was confirmed by studies which were carried out using SEM. The SEM studies revealed the formation of monodisperse NPs, at an pH acidic and at an alkaline pH, which possessed a spherical morphology (Figure 10.8 a and Figure 10.8 f, respectively).

It can be hypothesised that the lysine repeat units and the glutamic acid repeat units are protonated at an acidic pH to yield cationic (NH₃⁺) amino groups and the uncharged glutamic acid groups, respectively. As such, poly[(LysLA)_{26.6}-b-(GluLA)_{28.3}] would be able to aggregate at the acidic pH 4.5 into particles that are composed of a cationic, thus hydrophilic poly(lysLA) shell, and an uncharged, thus hydrophobic poly(GluLA) core (Figure 10.9 a). In contrast, the lysine repeat units and the glutamic acid repeat units would be expected to be deprotonated

at an alkaline pH, resulting in the formation of uncharged amino repeat groups and anionic (COO⁻) glutamic acid groups, respectively [35]. As such, the aggregates are also formed at an alkaline pH, which would consist of a charged, thus water-soluble poly(GluLA) shell and an uncharged, thus hydrophobic insoluble poly(LysLA) core (Figure 10.9 a). The presence of both the cationic lysine repeat units and the anionic glutamic acid repeat units at the physiological pH 7.4, dictates that the poly(ester) chains would exist as water-soluble unimers. This would explain the maintained absence of aggregation at a pH of 7.4.

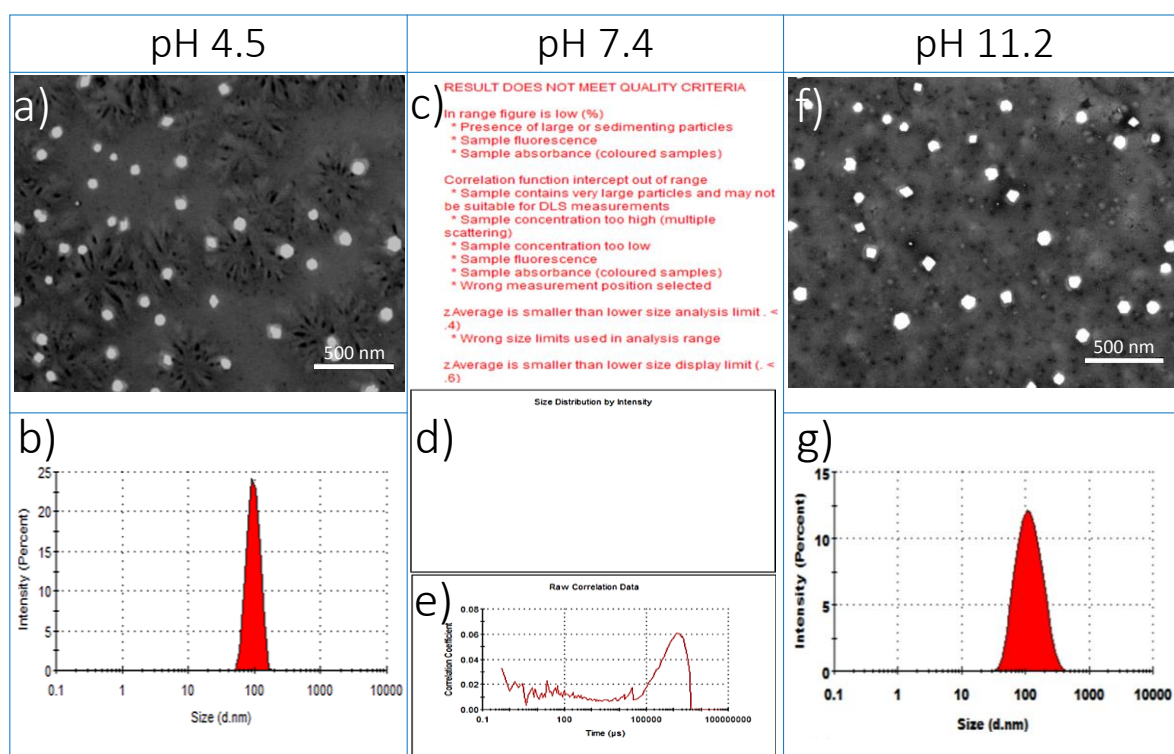


Figure 10.8. Determination of the zwitterionic behaviour of poly[(LysLA)_{26.6}-*b*-(GluLA)_{28.3}]. SEM images (a, f) and DLS charts (b, d, g) that were obtained from the pH-dependent assembly of poly[(LysLA)_{26.6}-*b*-(GluLA)_{28.3}]. A copy of the 'expert advice' obtained from DLS (c) and the DLS correlation curve (e) that were obtained from poly[(LysLA)_{26.6}-*b*-(GluLA)_{28.3}], at pH 7.4. Scale bars represent 0.5 µm.

The zwitterionic behaviour of the polymers formed was confirmed further by carrying out zeta potential analyses of poly(ester) dispersions at pH 4.5, pH 7.4 and pH 11.2, respectively (Figure 10.9 b). A positive zeta potential value (+11.3±7.34 mV) was recorded at a pH of 4.5, thus underlining the previous assertion that the poly(ester) aggregates that are formed at an acidic pH consist of a cationic poly(lysLA) shell. A zeta potential value of 0.02 mV was recorded at a pH of 7.4, which is suggestive of a neutral macromolecule at this pH value. However, a negative

zeta potential value (-17.4 ± 2.86 mV) was recorded at a pH of 11.2, thus supporting the previous assertion that the poly(ester) aggregates that are formed at alkaline pH consist of an anionic poly(GluLA) shell.

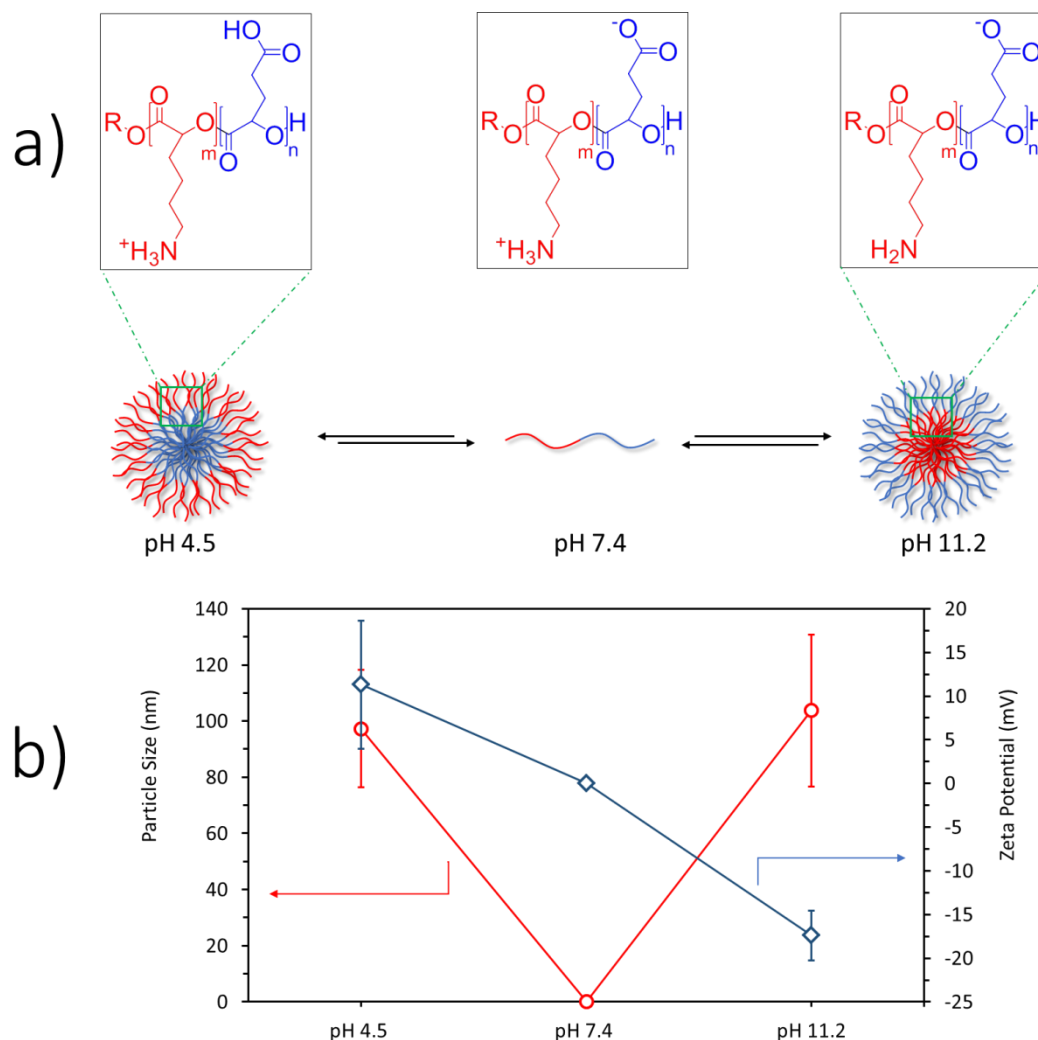


Figure 10.9. (a) Graphical illustration of the zwitterionic behaviour of poly[(LysLA)_{26.6}-*b*-(GluLA)_{28.3}] at pH 4.5, at pH 7.4 and at pH 11.2. (b) Chart illustrating the reversible-assembly, zwitterionic behaviour of poly[(LysLA)_{26.6}-*b*-(GluLA)_{28.3}], as evidenced by the pH-dependent polymer aggregation (○) and pH-dependent surface zeta potential (◇).

Poly[(LysLA)_{26.6}-*b*-(GluLA)_{28.3}] dispersions were then stored at pH 4.5 and at pH 11.2 for a prolonged time whilst monitoring the dispersions using DLS. Rapid aggregation behaviour was detected in the dispersion that was stored at pH 4.5, which resulted in the formation of aggregates that were greater than 3.5 μm , after 25 hours (Figure 10.10 a). In addition, the PDI

of the dispersion was equal to one, thus suggesting further that the dispersion was highly aggregated and sedimented.

In contrast, nominal aggregation behaviour and sedimentation behaviour were detected in the dispersion that was stored at a pH 11.2 (Figure 10.10 b). The rapid aggregation and sedimentation at pH 4.5 could have been caused by the breakdown of the poly(ester) upon hydrolysis by an acidic pH. Habraken *et al.* [45] revealed that polymer degradation can lead to the formation of larger aggregates in the nanoparticle dispersion. The nominal increase in size of aggregates at pH 11.2 could be due to the swelling of the particles and/or progressive sedimentation, as evidenced by the fluctuating size and PDI of aggregates.

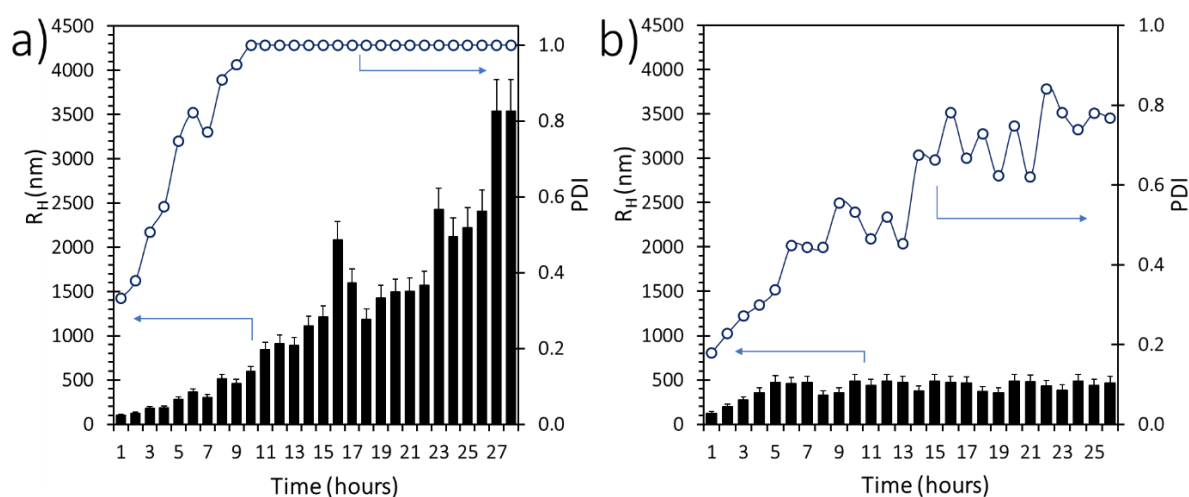


Figure 10.10. The evolution of the size of aggregates and the PDIs of poly[(LysLA)_{26.6}-*b*-(GluLA)_{28.3}] NPs that were incubated at (a) pH 4.5, at 37 °C and at (b) pH 11.2, at 37 °C.

These observations support further the previous findings from studies of the pH-mediated dox release that the poly(ester) backbone undergoes hydrolysis in solutions of acidic pH. This zwitterionic system needs to be investigated further for potential use in pH-induced encapsulation and subsequent pH-mediated delivery of sensitive drugs and proteins. The reported poly(ester) macromolecule is dependent on the availability of an acidic pH environment for self-assembly into NPs that possess a cationic surface. As such, this polymer could be triggered by an acidic extracellular tumour environment to yield NPs with a cationic surface, that could, subsequently leak into tumours by the EPR effect and be degraded by the prevailing acidic environment [29].

10.4. Conclusion

OCA ROP was used to produce a novel, versatile diblock poly[(Lys(Cbz)LA)_{26.6}-*b*-(Glu(Bz)LA)_{28.3}] macromolecule. The poly(ester) self-aggregated into monodisperse NPs in aqueous media, aided by the abundant Bz and Cbz protecting groups which afforded hydrophobic interactions and π - π stacking. The NPs produced were able to encapsulate and withhold dox, yielding particles with a drug-loading of at least 2.73 wt %. Acidic pH-mediated poly(ester) hydrolysis resulted in a controlled release of the drug. Thus, at least 78% of the drug was released after 126 hours, compared to less than 5% of drug that was released in response to the incubation at an environmental pH that was equal to the physiological pH (7.4). *In vitro* MTT assay cytotoxicity studies revealed that the dox-loaded NPs possess anticancer potency, against human breast cancer cells (T47D and MCF-7). The blank NPs had nominal cytotoxicity against T47D cells and MCF-7 cells.

Upon poly(ester) deprotection, poly[(LysLA)_{26.6}-*b*-(GluLA)_{28.3}], a poly(zwitterionic) macromolecule was produced. This exhibited pH-dependent reversible-assembly, as revealed by studies that were carried out using DLS and SEM. As such, this versatile macromolecule could provide a platform for the development of effective delivery vehicles for hydrophobic chemotherapeutics and zwitterionic NPs with potential biotechnological applications.

10.5. References

1. Thornton, P.D., Mart, R.J., Webb, S.J. and Ulijn, R.V. *Soft Matter*. **2008**, 4, 821-827.
2. Ke, W., Li, J., Zhao, K., Zha, Z., Han, Y., Wang, Y., Yin, W., Zhang, P. and Ge, Z. *Biomacromolecules*. **2016**, 17, 3268-3276.
3. Delplace, V. and Nicolas, J. *Nat Chem*. **2015**, 7, 771-784.
4. Zheng, N., Song, Z., Liu, Y., Zhang, R., Zhang, R., Yao, C., Uckun, F.M., Yin, L. and Cheng, J. *J. Controlled Release.*, **2015**, 205, 231-239.
5. Cheng, Y., He, C., Xiao, C., Ding, J., Zhuang, X. and Chen, X. *Polym. Chem.*, **2011**, 2, 2627-2634.
6. Fu, X., Ma, Y., Sun, J. and Li, Z. *RSC Adv.*, **2016**, 6, 70243-70250.
7. Yin, L., Tang, H., Kim, K.H., Zheng, N., Song, Z., Gabrielson, N.P., Lu, H. and Cheng, J. *Angew. Chem. Int. Ed.*, **2013**, 52, 9182-9186.
8. Mura, S., Nicolas, J. and Couvreur, P. *Nat Mater*. **2013**, 12, 991-1003.
9. Huang, J. and Heise, A. *Chem. Soc. Revs.*, **2013**, 42, 7373-7390.
10. Wang, J., Gong, C., Wang, Y. and Wu, G. *RSC Adv.*, **2014**, 4, 15856-15862.
11. Ge, C., Zhao, L., Ling, Y. and Tang, H. *Polym. Chem.*, **2017**.
12. Yang, H.Y., Jang, M.-S., Gao, G.H., Lee, J.H. and Lee, D.S. *Nanoscale*. **2016**, 8, 12588-12598.
13. Fujii, S., Kido, M., Sato, M., Higaki, Y., Hirai, T., Ohta, N., Kojio, K. and Takahara, A. *Polym. Chem.*, **2015**, 6, 7053-7059.
14. Liu, N., Han, J., Zhang, X., Yang, Y., Liu, Y., Wang, Y. and Wu, G. *Colloids and Surfaces B: Biointerfaces*. **2016**, 145, 401-409.
15. Yang, J., Chen, H., Xiao, S., Shen, M., Chen, F., Fan, P., Zhong, M. and Zheng, J. *Langmuir*. **2015**, 31, 9125-9133.
16. Wu, L., Ni, C., Zhang, L. and Shi, G. *J Biomater Sci. Polym Ed.*, **2016**, 27, 643-656.
17. Kwon, H.J., Lee, Y., Park, K.M. and Park, K.D. *Frontiers in Bioengineering and Biotechnology*.
18. Chang, Y., Chang, W.-J., Shih, Y.-J., Wei, T.-C. and Hsiue, G.-H. *ACS Appl. Mater. Interfaces.*, **2011**, 3, 1228-1237.
19. Shih, Y., Venault, A., Tayo, L.L., Chen, S.-H., Higuchi, A., Deratani, A., Chinnathambi, A., Alharbi, S.A., Quemener, D. and Chang, Y. *Langmuir*. **2017**, 33, 1914-1926.
20. Jiang, S. and Cao, Z. *Adv. Mater.*, **2010**, 22, 920-932.
21. Chen, S., Li, L., Zhao, C. and Zheng, J. *Polymer*. **2010**, 51, 5283-5293.
22. Zhang, H. and Chiao, M. *J. Med. Biol. Eng.*, **2015**, 35, 143-155.
23. Cao, Z., Yu, Q., Xue, H., Cheng, G. and Jiang, S. *Angew. Chem. Int. Ed.*, **2010**, 49, 3771-3776.
24. Keefe, A.J. and Jiang, S. *Nat Chem*. **2012**, 4, 59-63.
25. Chen, L., Chen, T., Fang, W., Wen, Y., Lin, S., Lin, J. and Cai, C. *Biomacromolecules*. **2013**, 14, 4320-4330.
26. Rao, J., Luo, Z., Ge, Z., Liu, H. and Liu, S. *Biomacromolecules*. **2007**, 8, 3871-3878.
27. Mukherjee, S., Sobhani, H., Lassiter, J.B., Bardhan, R., Nordlander, P. and Halas, N.J. *Nano Letters*. **2010**, 10, 2694-2701.
28. Cho, E.C., Xie, J., Wurm, P.A. and Xia, Y. *Nano Letters*. **2009**, 9, 1080-1084.
29. Yuan, Y.-Y., Mao, C.-Q., Du, X.-J., Du, J.-Z., Wang, F. and Wang, J. *Adv. Mater.*, **2012**, 24, 5476-5480.
30. Harris, J.M. and Chess, R.B. *Nat. Rev. Drug. Discov.*, **2003**, 2, 214-221.
31. Otsuka, H., Nagasaki, Y. and Kataoka, K. *Adv. Drug Deliv. Rev.*, **2003**, 55, 403-419.

32. Knop, K., Hoogenboom, R., Fischer, D. and Schubert, U.S. *Angew. Chem. Int. Ed.*, **2010**, 49, 6288-6308.
33. Mishra, S., Webster, P. and Davis, M.E. *Eur J Cell Biol.*, **2004**, 83, 97-111.
34. Bader, R.A., Silvers, A.L. and Zhang, N. *Biomacromolecules*. **2011**, 12, 314-320.
35. Rodríguez-Hernández, J. and Lecommandoux, S. *J. Am. Chem. Soc.*, **2005**, 127, 2026-2027.
36. Ashwanikumar, N., Kumar, N.A., Asha Nair, S. and Vinod Kumar, G.S. *Acta Biomaterialia*. **2014**, 10, 4685-4694.
37. Makadia, H.K. and Siegel, S.J. *Polymers*. **2011**, 3, 1377-1397.
38. Hoffmann, I., Michel, R., Sharp, M., Holderer, O., Appavou, M.-S., Polzer, F., Farago, B. and Gradzielski, M. *Nanoscale*. **2014**, 6, 6945-6952.
39. Kashyap, S., Singh, N., Surnar, B. and Jayakannan, M. *Biomacromolecules*. **2016**, 17, 384-398.
40. Fernandez, P., Wilson, C., Hoivik, D. and Safe, S.H. *Cell Biol. Int.*, **1998**, 22, 623-633.
41. COMŞA, Ş., CÎMPEAN, A.M. and RAICA, M. *Anticancer Res.*, **2015**, 35, 3147-3154.
42. Tomankova, K., Polakova, K., Pizova, K., Binder, S., Havrdova, M., Kolarova, M., Kriegova, E., Zapletalova, J., Malina, L., Horakova, J., Malohlava, J., Kolokithas-Ntoukas, A., Bakandritsos, A., Kolarova, H. and Zboril, R. *Int. J. Nanomedicine*. **2015**, 10, 949-961.
43. Nakamura, Y., Mochida, A., Choyke, P.L. and Kobayashi, H. *Bioconjugate Chem.*, **2016**, 27, 2225-2238.
44. Andrew MacKay, J., Chen, M., McDaniel, J.R., Liu, W., Simnick, A.J. and Chilkoti, A. *Nat Mater*. **2009**, 8, 993-999.
45. Habraken, G.J., Peeters, M., Thornton, P.D., Koning, C.E. and Heise, A. *Biomacromolecules*. **2011**, 12, 3761-3769.

Chapter 11. Proof-of-Concept Studies in the Development of Poly(Amino Acid)-Silver(I)-N-Heterocyclic Carbene Anticancer Therapeutics

Abstract

Five silver(I)-NHC complexes were generated as part of a collaborative research undertaking. The complexes exhibited anticancer potency against Panc 10.05 cancerous cells. They also exhibited the selectivity at distinguishing between healthy (ARPE-19) cells and cancerous Panc 10.05 cells, in comparison to cisplatin. Three approaches were then followed in proof-of-concept studies to encapsulate the complexes in poly(amino acid)s. The first approach involved the physical encapsulation of hydrophobic complexes in an amphiphilic mPEG₅₀₀₀-b-poly(Phe)₂₄ polymer, to obtain complex-loaded spherical particles (with diameters of 100 nm and 221.8 nm). In the second approach, complexes that furnish carboxylate ions in aqueous media, were encapsulated in mPEG₅₀₀₀-b-poly(Lys)_n copolymers, by an envisaged charge-driven coordination to the cationic repeat units of the poly(Lys)_n block. DLS and SEM studies revealed the formation of monodisperse spherical particles (with diameters ranging between 100 nm and 221.8 nm). Lastly, a covalent grafting approach was followed, in which a complex that was designed to contain hydroxyl groups was covalently attached to the carboxylic acid groups of poly(Glu)₄₂, using Steglich esterification. MTT assays revealed that the encapsulation of the complexes in polymers resulted in the formation of particles that exhibited superior anticancer potency, compared to the potency exhibited by the un-encapsulated complexes. These preliminary results suggest that the encapsulation of silver(I)-NHC complexes in poly(amino acid)s could provide a platform for developing effective polymer-metal-based anticancer therapeutics.

11.1. Introduction

11.1.1. Overview of Metal-N-Heterocyclic Carbenes in Anticancer Therapy

Metal complexes have been and are widely researched for their medicinal applications [1, 2]. When used in chemotherapeutics, metal atoms act by forming intrastrand and also interstrand DNA crosslinks. This induces the bending and unwinding of DNA which ultimately causes purine bases to destack, causing cell death [3]. This effect is enhanced in cancerous cells because they replicate faster than do non-diseased cells. A typical metal complex chemotherapeutic is

cisplatin, which was discovered in 1965 and has since been the 'gold' standard for metallo-based cancer chemotherapeutics [4]. Unfortunately, cisplatin has several disadvantages, such as its lack of selectivity, which makes it cytotoxic to healthy cells. Furthermore, certain tumours develop resistance to cisplatin and other platinum-based drugs because DNA repair mechanisms can reverse platinum-based damage [5].

This discovery led to continued research into alternative metallo-based chemotherapeutics. Metal-*N*-heterocyclic carbenes (NHCs), in particular, are now widely researched because of their promising anti-cancer activity and selectivity [6]. Examples include complexes that are based on compounds of platinum [7, 8], gold [9-17], ruthenium [18-22], palladium [23, 24], copper [25] and, more recently, those that are based on silver complexes [26].

Barnard *et al.* [27] have reported that bis gold (I)-NHC complexes can induce Ca²⁺ sensitive mitochondrial membrane permeation (MMP), causing mitochondrial swelling and subsequent cell death. Baker and co-workers [28] have reported cationic bis gold (I)-NHCs that also cause mitochondrial swelling, and they correlated this antitumor activity to the lipophilicity of the complexes. Hickey *et al.* [29] studied several cationic gold (I)-NHC complexes that target the mitochondria by selectively binding to selenol-containing proteins over thiol-containing proteins.

Skander *et al.* [7] developed several *trans*-configured, square planar platinum(II)-NHC-amine complexes. These complexes reportedly possess comparable anticancer potency to that provided by cisplatin, and also exhibit anticancer activity against some cisplatin-resistant cancer cell lines. Cyclometalated platinum complexes, that can accumulate in the cytoplasm and that are said to exhibit a high affinity to cancerous cells, have also been reported [8]. Other platinum-based complexes, including *bis*-amino platinum(II)-NHCs are claimed to be more potent than either cisplatin [30] or caffeine-based platinum(II)-NHCs [31].

Palladium(II)-NHC complexes, that are claimed to be more potent than cisplatin, have also been reported [32]. Haque *et al.* [33] researched two palladium(II)-NHC complexes and established that those with a *trans* geometry were viable against the human colorectal cancer cells. The interaction between DNA and a Ruthenium(III)-NHC complex was studied by Gallori and co-workers [18], who concluded that the new anti-tumour metastasis inhibitor (NAMI-A) possesses

anticancer potency. Malina *et al.* [19] and several other researchers [21, 22, 34, 35] have reported on ruthenium complexes, to ascertain their potential to be used as effective anticancer therapeutics. Copper-NHC complexes and their saturated imidazole analogues, which exhibited anticancer potency that is comparable to that of cisplatin, were reported [36].

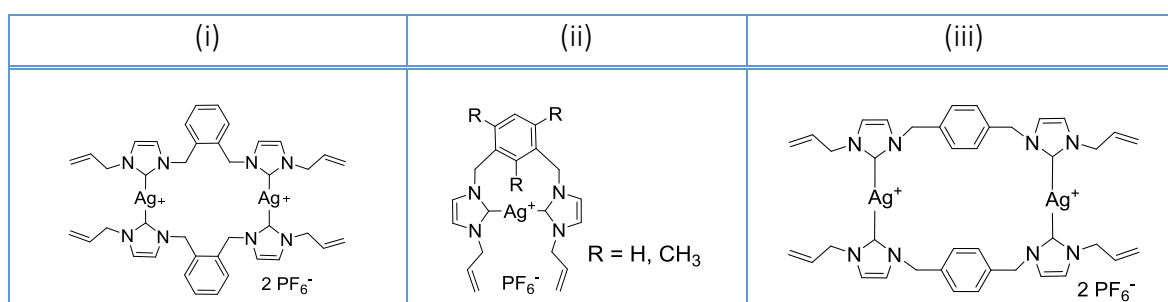
11.1.2. Silver-NHC Therapeutics

Silver compounds have a significant historical background in medicine, including in antimicrobial therapy, in water purification and in the cure of various ailments [37-41]. Historically, silver nitrate had wide-ranging applications from antibiotic therapy for burn wounds to the treatment of conjunctivitis in children. This was replaced by the more effective and safer silver sulfadiazine. However, these non-bulky structures accelerated the leakage of silver, which limited their antimicrobial potency. The realisation that the bioavailability of silver could be enhanced by the use of compounds that could efficiently trap silver ions and release them in a slow and prolonged manner [42], led to extensive research into silver-NHC complexes, for antimicrobial therapy [43-48].

There has been a steady increase in the amount of research into silver-NHC complexes for anticancer therapy. For example, mono-nuclear and binuclear silver-NHC complexes (Table 11.1) with different xylyl spacers have been reported [49]. The anticancer activity of some of these complexes is reportedly comparable to that of than 5-fluorouracil [49]. Silver-NHC complexes have also been reported whose anti-cancer efficacies against lung cancer (H460) cell lines were similar to that of cisplatin [50].

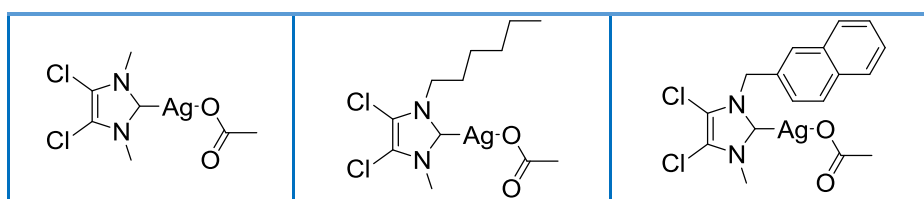
Significant success against various human cancer cell lines has also been reported using complex (i) (Table 11.1). This exhibited superior chemotherapeutic activity relative to cisplatin against oral carcinoma (KB), against promyelocytic leukaemia (HL60), against the resistant HL60 (HL60R), against MCF-7 breast cancer cell line, against the resistant MCF-7 (MCF-7R) and against T47D breast cancer cell line. Further studies revealed that the cytotoxicity of silver-NHC complexes can be enhanced by increasing the stability of the ligand, either by increasing the steric hindrance around the central metal atom or by decreasing the saturation on the ligand. Furthermore, increasing the size of the substituent on the imidazole ring has been reported to enhance the cytotoxicity of the metal complex [36].

Table 11.1. Silver-NHC anticancer complexes bearing different xylyl spacers [49].



Silver acetate-NHC-based complexes, including those shown in Table 11.2 [46], are said to exhibit anticancer activity against breast cancer (MB157) and against ovarian cancer (OVCAR-3) cell lines [51]. Monteiro *et al.* [52] recently synthesised a series of monodentate, bidentate and macrocyclic cationic silver-NHC complexes. These were subsequently tested against human breast adenocarcinoma (MCF7) and colon adenocarcinoma (DLD1). It was established that the stability and potency of the complexes increases from monocyclic to macrocyclic, due to the chelating effect which results in a more sustained release of silver atoms. The importance of silver-ligand complexes in anticancer activity was confirmed by the superior anticancer potency of the complexes, when they were compared to simple silver salts (AgBr, AgBF₄) and to imidazolium salt precursors that lacked silver [52].

Table 11.2. Examples of silver acetate-NHC-based complexes that exhibit anticancer potency against breast cancer (MB157) and ovarian cancer (OVCAR-3) cell lines [51].



It has also been reported that certain silver-NHC complexes possess anticancer potency that is comparable to those of gold-based complexes and platinum-based complexes, sometimes with greater anticancer potency than that of established chemotherapeutics, such as 5-fluorouracil [49-53]. The mode of action against cancerous cells, of some silver-NHC complexes, has been reported. For example, some silver-NHC complexes tend to accumulate in the mitochondria and depolarise its membrane. This induces apoptosis from within the mitochondria by damaging the endoplasmic reticulum and cytosolic translocation of the apoptotic inducing

factor (AIF) [54]. There have also been reports of another class of silver-NHC complexes that strongly inhibits the activity of thioredoxin reductase [55].

This chapter is based on ongoing research work. Several poly(amino acid)s and silver(I)-N-heterocyclic carbene complexes were synthesised and characterised. The anticancer activity of silver(I)-NHC complexes was demonstrated against an pancreatic adenocarcinoma cell line (Panc. 10.05). Cytotoxicity studies were also carried out against non-disease cells, the human retinal pigment epithelium cells (ARPE-19), to ascertain the extent to which the complexes can discriminate between cancer cells and non-disease cells. Proof-of-concept studies were then undertaken to develop polymer-metal complex anticancer therapeutics by following three approaches to the encapsulation of silver(I)-NHC complexes in polymeric substrate. These are, physical encapsulation by nanoprecipitation of an amphiphilic polymer in the presence of silver(I)-NHC complexes in aqueous medium, covalent conjugation of silver(I)-NHC complexes to polymer chains using an esterification reaction and charge-driven coordination interactions between the charged polymer and the charged silver(I)-NHC complex in aqueous medium.

11.2. Experimental Details

11.2.1. Synthesis of Poly(Glu(Bz))_n

Glu(Bz) NCA (1.29 g; 4.89 mmol) was dissolved in anhydrous DMF (20 mL). The solution was injected into a flame-dried and nitrogen-purged Schlenk tube. Benzylamine (10.5 mg; 0.095 mmol) was dissolved in anhydrous DMF (10 mL) and the solution was added to NCA solution. The reaction medium was degassed and then stirred at room temperature, under a nitrogen flow, for 96 hours. The polymer produced was precipitated in cold diethyl ether (1:5 v/v), centrifuged and dried *in vacuo*. Yield: 963.4 mg, 75.3%. ¹H NMR (500 MHz, TFA-d, δ, ppm): 8.49 (s, NH), 7.38 (m, Ph (benzylamine & benzyl ester)), 5.44 - 5.08 (m, Ar-CH₂), 4.83 - 4.80 (m, αCH), 2.78 - 2.15 (m, Ar-CH₂-COO), 2.15 - 60 (m, αCH-CH₂). FTIR: ν_{max}/cm⁻¹ (solid): 3276 (NH), 2582 - 3069 (COOH), 1672 (C=O amide), 1520 (C=C aromatic), 1411 (CH), 1250 (C-O benzyl ester).

11.2.2. Syntheses of mPEG₅₀₀₀-*b*-Poly(Lys(Cbz))_n Macromolecules

A representative procedure is given. This concerns a monomer-initiator molar feed ratio of 40. Briefly, Lys(Cbz) NCA (380.2 mg, 1.24 mmol) was dissolved in anhydrous DCM (10 mL). The

solution was injected into a flame-dried and nitrogen-purged Schlenk tube. Amine-terminated mPEG₅₀₀₀ (155 mg, 0.031 mmol) was dissolved in anhydrous DCM (10 mL). The solution was injected into the reaction medium. Further steps were carried out as described for the synthesis of poly(Glu(Bz))_n. Yield: [M/I] = 20: 88.3%; [M/I] = 40: 96.2%; [M/I] = 75: 94.6%. ¹H NMR (500 MHz, TFA-d, δ, ppm): 8.49 (s, CONH), 7.43 (m, *J* = 35.8 Hz, Ph (Cbz)), 5.26 (s, Ar-CH₂), 4.67 (s, αCHNH), 4.20 – 3.77 (m, methoxy-PEG₅₀₀₀), 3.30 (d, *J* = 12.0 Hz, CH₂NHCOO), 2.16 – 1.75 (m, αCHCH₂), 1.75 -1.15 (m, CH₂CH₂CH₂NH). FTIR: ν_{max}/cm⁻¹ (solid): 3710-3283 (NH, amide & amine), 2892 (C-H), 1652 (C=O amide), 1537 (NH), 1343 (C-H), 1114 (PEG), 1774 (Bz ester), 1686 (Ar C=C), 917 (Ar C-H).

11.2.3. Synthesis of mPEG₅₀₀₀-*b*-Poly(Phe)_n

A similar procedure to that described for the syntheses of mPEG₅₀₀₀-*b*-Poly(Lys(Cbz))_n macromolecules (11.2.2) was used for the synthesis of mPEG₅₀₀₀-*b*-Poly(Phe)_n. Yield: 532 mg, 44.6%. ¹H NMR (500 MHz, TFA-d, δ, ppm): 8.35 (s, αCHCONH), 7.10 - 6.88 (m, Phenyl), 4.02 (s, αCHCONH), 4.02 - 3.31 (m, mPEG₅₀₀₀), 2.96 - 2.81 (m, Ar-CH₂). FTIR: ν_{max}/cm⁻¹ (solid): 3287 (NH), 2882 (C-H), 1632 (CO amide), 1537 (NH), 1342 (Ar C=C), 1094 (PEG), 697 - 958 (Ar C-H).

11.2.4. Deprotection of Macromolecules

mPEG₅₀₀₀-*b*-Poly(Lys(Cbz))_n macromolecules were dissolved in TFA (7 mL). HBr in acetic acid (33 wt. %, 7 mL) was added to the polymer solutions. The solutions were stirred at room temperature, for 96 hours. The products were precipitated in cold diethyl ether, isolated by centrifugation, dialysed against distilled water and lyophilised. A similar procedure was used for the deprotection of poly(Glu(Bz))_n. mPEG₅₀₀₀-*b*-poly(Lys): [M/I] = 20: 73.8 wt.%; [M/I] = 40: 77.1 wt.%; [M/I] = 75: 88.4 wt. %. ¹H NMR (500 MHz, TFA-d, δ, ppm): 7.94 (d, *J* = 83.5 Hz, CONH), 4.25 (s, αCHNH), 3.72 - 3.34 (m, mPEG₅₀₀₀), 2.71 (d, *J* = 59.5 Hz, CH₂NH₂), 1.78 - 1.40 (m, αCHCH₂NH), 1.39 - 1.22 (d, *J* = 50.6 Hz, CH₂CH₂CH₂NH). FTIR: ν_{max}/cm⁻¹ (solid): 3509-3033 (NH, NH₂), 2892 (C-H), 1652 (CO amide), 1537 (NH), 1343 (C-H), 1114 (PEG). Poly(Glu)_n: 495.2 mg, 75.3%. ¹H NMR (500 MHz, TFA-d, δ, ppm): 8.04 - 7.86 (m, CONH), 7.56 - 7.39 (m, Ph (benzylamine)), 4.56 - 4.27 (m, αCHNH), 2.17 - 1.49 (m, CH₂COOH), 1.49 - 0.84 (m, αCHCH₂). FTIR: ν_{max}/cm⁻¹ (solid): 3276 (NH), 2582-3069 (COOH), 1672 (C=O amide), 1520 (C=C aromatic (initiator)), 1411 (CH), 1165 (C-O).

11.2.5. Syntheses of Silver (I)-NHC Complexes

11.2.5.1. Preparation of the Ligand (L01) of Complex C01

1-Methyl imidazole (1.84 mL, 24.4 mmol) and 2-chloro ethanol (1.63 mL, 24.4 mmol) were heated at 100 °C in a sealed ampoule for 72 hours. Diethyl ether (3 x 10 mL) was added and precipitation of the product was aided by sonication. The product was subsequently dried, *in vacuo*, to yield a brown oil. Yield: 3 g; 97%. ¹H NMR (300 MHz, D₂O, δ): 8.81 (s, 1H, NCHN), 7.57 (s, 1H, C=CH), 7.51 (s, 1H, C=CH), 4.37 (t, *J* = 9 Hz, 2H, CH₂), 3.98 (t, *J* = 9 Hz, 2H, CH₂), 3.96 (s, 3H, CH₃). ¹³C NMR (75 MHz, D₂O, δ): 136.2 (NCHN), 123.6 (C=C), 122.1 (C=C), 59.8 (CH₂), 51.6 (CH₂), 35.9 (CH₃). HRMS (ESI⁺): Calculated for C₆H₁₁N₂O [M - Cl]⁺: 127.087. Found: 127.087.

11.2.5.2. Preparation of Complex C01

L01 (0.80 g, 6.30 mmol) was dissolved in methanol (30 mL) and silver oxide (0.87 g, 3.80 mmol) was added. The mixture was refluxed for 8 hours and then filtered through celite. The filtrate was concentrated *in vacuo*, to yield a brown solid. This was recrystallised from methanol/diethyl ether, yielding a yellow solid. Yield: 220 mg; 22 %. ¹H NMR (300 MHz, DMSO-d₆, δ): 7.40 (s, 1H, C=CH), 7.36 (s, 1H, C=CH), 4.07 (t, *J* = 12 Hz, 2H, CH₂), 3.66 (t, *J* = 12 Hz, 2H, CH₂), 3.13 (s, 3H, CH₃). ¹³C NMR (125 MHz, DMSO-d₆, δ): 122.0, 121.8 (HC=CH), 61.5 (CH₂), 54.0 (CH₂), 37.8 (CH₃). ESI-MS (*m/z*): Calcd. for C₁₂H₂₁AgN₄O₂ [M - Cl]⁺ Calcd: 360.07; Found: 360.17. Anal. Calcd for C₁₂H₂₀AgClN₄O₂: C, 36.43; H, 5.10; N, 14.16. Found: C, 36.90; H, 5.30; N, 13.60.

11.2.5.3. Preparation of the Ligand (L02) of Complex C02

9-(chloromethyl) anthracene (0.5 g, 2.2 mmol) was dissolved in acetonitrile (30 mL) and transferred to an ampoule. 1-(2-hydroxyethyl) imidazole (0.21 mL, 2.2 mmol) was added and the mixture was heated at 90 °C for 24 hours. Excess diethyl ether was added to the then orange solution to yield the product as an orange precipitate, which was dried *in vacuo*. Yield: 710 mg; 95%. ¹H NMR (300 MHz, CDCl₃, δ): 10.23 (s, 1H, NCHN), 8.61 (s, 1H, aromatic), 8.39 (d, 2H, *J* = 6 Hz, aromatic), 8.08 (d, 2H, *J* = 6 Hz, aromatic), 7.66 (t, 2H, *J* = 9 Hz, aromatic), 7.53 (t, 2H, *J* = 9 Hz, aromatic), 7.14 (s, 1H, C=CH), 6.77 (s, 1H, HC=C), 6.55 (s, 2H, CH₂), 4.41 (t, 2H, *J* = 6 Hz, CH₂), 4.04 (t, 2H, *J* = 6 Hz, CH₂). ¹³C NMR (75 MHz, CDCl₃, δ): 137.5 (C), 131.4 (C), 131.1 (C), 130.7 (CH), 129.5 (CH), 128.5 (CH), 125.7 (CH), 122.9 (CH), 122.0 (CH), 121.0 (CH), 59.9 (CH₂), 52.9 (CH₂), 46.0 (CH₂). HRMS (ESI⁺): Calculated for C₂₀H₁₉N₂O [M-Cl]⁺: 303.149. Found: 303.148. FTIR

ν_{max}/cm^{-1} : 3233 (OH), 1548-1402 (C-C arom). Anal. Calculated for $\text{C}_{20}\text{H}_{19}\text{ClN}_2\text{O}_4 \cdot 3/4 \text{H}_2\text{O}$: C, 66.20; H, 6.02; N, 7.72; Found: C, 66.25; H, 5.90; N, 8.40.

11.2.5.4. Preparation of Complex C02

L02 (0.3 g, 0.89 mmol) and silver oxide (0.12 g, 0.53 mmol) were added to a pre-dried Schlenk tube containing molecular sieves (4Å). Anhydrous acetonitrile (20 mL) and methanol (14 mL) were added to the Schlenk tube. The reaction was stirred at room temperature, under nitrogen, for 18 hours. The reaction mass was then filtered through celite and the filtrate was dried, *in vacuo*, to yield a yellow solid. Yield: 90 mg; 23%. ^1H NMR (300 MHz, CDCl_3 , δ): 8.53 (s, 1H, aromatic), 8.32 (d, 2H, $J = 9$ Hz, aromatic), 8.05 (d, 2H, $J = 9$ Hz, aromatic), 7.54-7.44 (m, 4H, aromatic), 6.89 (s, 1H, C=CH), 6.50 (s, 1H, HC=C), 6.24 (s, 2H, CH_2), 4.33 (m, 2H, CH_2), 3.94 (m, 2H, CH_2). ^{13}C NMR (75 MHz, CDCl_3 , δ): 134.1 (C), 131.4 (C), 131.0 (C), 129.7 (CH), 129.5 (CH), 129.5 (CH), 127.6 (CH), 122.9 (CH), 125.5 (CH), 123.3 (CH), 121.7 (CH), 61.6 (CH_2), 55.0 (CH_2), 47.6 (CH_2). ESI-MS (m/z): Calcd for $\text{C}_{40}\text{H}_{36}\text{AgN}_4\text{O}_2 [\text{M}-\text{Cl}]^+$, Calcd: 711.188, Found: 711.188. Anal. Calcd for $\text{C}_{40}\text{H}_{36}\text{AgClN}_4\text{O}_2 \cdot 2\text{H}_2\text{O}$: C, 61.27; H, 5.14; N, 7.15, Found: C, 60.70; H, 5.00; N, 7.50.

11.2.5.5. Preparation of the Ligand (L03) of Complex C03

1,1'-methylene-bis-1H-imidazole (0.3 g, 2.03 mmol) was dissolved in anhydrous acetonitrile (5 mL). Then, *tert*-butyl chloroacetate (0.58 mL, 4.05 mmol) was added. The mixture was heated at 90 °C in a sealed ampoule for 72 hours and then filtered, followed by the addition of excess diethyl ether to the filtrate to yield a yellow solid. Recrystallisation from acetonitrile/diethyl ether yielded a white hygroscopic solid. Yield: 0.60 g (62%). ^1H NMR (300 MHz, CD_3CN , δ): 10.65 (s, 2H, NCHN), 8.72 (s, 2H, C=CH), 7.51 (s, 2H, HC=C), 7.39 (s, 2H, N- CH_2 -N), 5.02 (s, 4H, N- CH_2 -C=O), 1.48 (s, 18H, CH_3 (carbocation)). ^{13}C NMR (125 MHz, CD_3CN , δ): 165.9 (C=O), 140.5 (NCHN), 125.0 (C=C), 123.6 (C=C), 84.9 (C-(CH_3)₃ (carbocation)), 58.4 (N- CH_2 -N), 51.9 (N- CH_2 -C=O), 28.2 (C-(CH_3)₃ (carbocation)). HRMS (ESI⁺): Calcd for $\text{C}_{11}\text{H}_{14}\text{N}_4\text{O}_4 [\text{M}-2\text{Cl}]^{2+}$: 133.050. Found: 133.053. FTIR ν_{max}/cm^{-1} : 3598, 3358, 3080, 2977, 2930, 1740, 1153, 749, 615. Anal. Calcd for $\text{C}_{11}\text{H}_{14}\text{Cl}_2\text{N}_4\text{O}_4 \cdot 2\text{Et}_2\text{O}$: C, 47.01; H, 7.06; N, 11.54; Found: C, 46.30; H, 7.30; N, 12.40.

11.2.5.6. Preparation of Complex C03

L03 (0.2 g, 0.42 mmol) and silver oxide (0.19 g, 0.84 mmol) were added to activated molecular sieves (4Å) in a Schlenk tube and dried, *in vacuo*, degassed and nitrogen-purged. Anhydrous acetonitrile (10 mL) and anhydrous methanol (10 mL) were added to the Schlenk tube and

mixture was stirred at room temperature for 24 hours. The mixture, which had turned grey, was then filtered through celite. The solvent was removed under vacuum to yield the product as a white solid. Yield: 75 mg; 37%. ^1H NMR (300 MHz, MeOD, δ): 7.60 (s, 4H, C=CH), 7.33 (s, 4H, HC=C), 7.24 (s, 4H, N-CH₂-N), 6.48 (broad s, 6H, OH), 4.60 (s, 8H, N-CH₂-C=O). ^{13}C NMR (125 MHz, MeOD, δ): 124.1 (C=O), 121.3, 120.4 (C=C), 55.5, 51.8 (CH₂). ESI-MS (m/z): Calculated for C₂₃H₂₉Ag₂N₈NaO₉ [M-2OH+Na +MeOH]²⁺, Calculated: 399.498, Found: 399.561. FTIR ν_{max} /cm⁻¹: 3366, 3099, 2966, 1742 (ester), 1602, 1368, 1170, 727. Anal. Calculated for C₂₂H₃₀Ag₂N₈O₁₀.CH₃OH: C, 34.88; H, 4.15; N, 13.56. Found: C, 35.20; H, 3.90; N, 13.50.

11.2.5.7. Preparation of the Ligand (L04) of Complex C04

1H-imidazole (0.20 g, 2.94 mmol), potassium carbonate (0.66 g, 4.78 mmol) and chloroacetic acid (0.56 g, 5.88 mmol) were added to an ampoule. Acetonitrile (30 mL) was added to the mixture and the reaction was heated at 90 °C for 48 hours. The mixture was filtered. The residue was washed with DCM (3 x 30 mL) and then methanol (3 x 30 mL). The filtrate was dried *in vacuo* to yield a white solid. Yield: 460 mg; 70%. ^1H NMR (300 MHz, MeOD, δ): 9.04 (s, 1H, NCHN), 8.44 (s, 2H, HC=CH), 7.43 (broad s, 4H, CH₂). ^{13}C NMR (125 MHz, MeOD, δ): 179.4, 174.9, 171.7, 124.0. HRMS (ESI⁺): Calcd for C₇H₉N₂O₄ [M + H]⁺: 185.055. Found: 185.065.

11.2.5.8. Preparation of Complex C04

L04 (0.10 g, 0.45 mmol) and silver oxide (0.11 g, 0.45 mmol) were added to an ampoule containing molecular sieves (4Å), dried, *in vacuo*, degassed and then argon-purged. Anhydrous DCM (12 mL) and methanol (15 mL) were added to the ampoule. The mixture was stirred at room temperature for 24 hours. The reaction medium was filtered. The filtrate was dried *in vacuo* to yield a white solid. Yield: 70 mg, 30%. ^1H NMR (300 MHz, CDCl₃, δ): 5.28 - 5.24 (m, 2H, HC=CH), 4.12 - 4.08 (m, 2H, CH₂), 3.79 - 3.75 (m, 2H, CH₂), 3.68 - 3.64 (m, 1H, CHN).

11.2.5.9. Preparation of the Intermediate (P05) of Ligand L05 [56]

1H-imidazole (0.20 g, 2.94 mmol), potassium hydroxide (0.33 g, 5.88 mmol) and 9-chloromethyl anthracene (0.66 g, 2.94 mmol) were added into an ampoule. Acetonitrile (30 mL) was added. The mixture was heated at 90 °C, for 24 hours. The solution was then concentrated under vacuum, washed in distilled water (50 mL) and extracted with diethyl ether (3 x 50 mL) and DCM (3 x 50 mL). The combined organic layers were dried, *in vacuo*, to yield a brown solid. Yield: 700 mg; 92%. ^1H NMR (300 MHz, CDCl₃, δ): 8.52 (s, 1H, NCHN), 8.17 (d, 2H, *J* = 6 Hz, aromatic), 8.03

(d, 2H, $J = 6$ Hz, aromatic), 7.56-7.44 (m, 5H, aromatic), 6.96 (s, 2H, CH₂). HRMS (ESI⁺): Calculated for C₁₈H₁₄N₂ [M + H]⁺: 259.12, Found: 259.12.

11.2.5.10. Preparation of Ligand (L05) of Complex C05

P04 (0.15 g, 0.58 mmol) and chloroacetic acid (0.06 g, 0.58 mmol) were dissolved in acetonitrile (30 mL). The mixture was heated at 90 °C in a sealed ampoule, for 24 hours. The reaction medium was filtered. Diethyl ether was added to the filtrate (300 mL). The resulting yellow precipitate was filtered and dried, *in vacuo*. Yield: 90 mg; 46%. ¹H NMR (300 MHz, DMSO-d₆, δ): 8.70 (d, $J = 9$ Hz 1H, NCHN), 8.36 (d, $J = 9$ Hz, 2H, aromatic), 8.07 (d, $J = 9$ Hz, 2H, Ar), 7.60 - 7.47 (m, 5H, Ar) 6.41 (s, 2H, CH₂), 4.80 (s, 4H, CH₂). ¹³C NMR (75 MHz, DMSO-d₆, δ): 129.9, 129.1, 129.0, 127.5, 127.0, 125.3, 125.1, 123.7, 123.4, 123.1, 122.3, 121.9, 49.9 (CH₂), 44.8(CH₂). HRMS (ESI⁺): Calculated for C₂₀H₁₇N₂O₂ [M - Cl]⁺: 317.1285. Found: 317.13.

11.2.5.11. Preparation of Complex C05

L05 (0.05 g, 0.14 mmol) and silver oxide (0.42 g, 1.81 mmol) were added to an ampoule that contained molecular sieves (4Å), dried *in vacuo*, degassed and argon-purged. Anhydrous DCM (7 mL) and methanol (7 mL) were added to the reaction medium. The mixture was stirred at room temperature, for 24 hours. The reaction mass was filtered through celite. The filtrate was dried under vacuum to yield a red solid. Yield: 10 mg; 7%. ¹H-NMR (300MHz, MeOD, δ): 8.34 (m, 4H, aromatic), 8.20 (m, 4H, Ar), 7.77 - 7.25 (m, 10H, Ar), 6.46 (s, 4H, CH₂), 6.11 (s, 4H, CH₂). HRMS (ESI⁺): Calculated for C₄₀H₃₂AgN₄O₄ [M - Cl]⁺ Calculated : 741.15; found: 741.15.

11.2.6. Charge-Driven (Electrostatic) Coordination of Polymers with Complexes

An mPEG₅₀₀₀-*b*-poly(Lys)_n solution (10 mg/mL) in DMF, was passed through a 0.2 μm PTFE syringe filter. Likewise, complex solutions (10 mg/mL), prepared in DMF, were passed through 0.2 μm PTFE syringe filters. Then, the polymer solution (200 μL) and the complex solution (200 μL) were added to separate, independent PBS buffer solutions (pH 7.4, 2 mL). The respective dispersions were filtered (0.2 μm PTFE) and then analysed using DLS. The two dispersions were then mixed simultaneously, under vigorous stirring, and stored for subsequent analyses.

11.2.7. Physical Encapsulation of Complexes in Amphiphilic Polymers

A representative procedure is given using the encapsulation of C02 in mPEG₅₀₀₀-*b*-poly(Lys)_n macromolecules. Briefly, an mPEG₅₀₀₀-*b*-poly(Phe)_n solution (10 mg/mL) was prepared in DMF

and filtered (0.2 μm PTFE). A CO2 solution (10 mg/mL) was prepared in DMF and filtered (0.2 μm PTFE). Co-nanoprecipitation was then carried out by adding the polymer solution (200 μL) and the complex solution (200 μL) simultaneously to a vigorously stirred PBS buffer solution (pH 7.4, 4 mL).

11.2.8. Covalent-Linking of Silver (I)-NHC Complexes to Polymers

Poly(Glu)_n (50 mg) was dissolved in anhydrous DMF (10 mL) and injected into a sealed Schlenk tube. CO1 (242 mg, 0.46 mmol) and DMAP (2.6 mg, 0.02 mmol) were dissolved in anhydrous DMF (5 mL) and the solution was injected into the polymer solution. The reaction was degassed, purged with nitrogen and cooled to 0 °C. DCC (44 mg, 0.21 mmol) was dissolved in anhydrous DMF (5 mL). The solution was injected into the cooled reaction mass. The reaction was stirred at 0 °C, for 30 minutes, and then stirred at room temperature, for 12 hours. The solution was filtered and the filtrate was dried under vacuum. Yield: 50.3%. ¹H NMR (300 MHz, DMSO-d₆, δ): 8.04 - 7.86 (m, CONH), 7.56 - 7.39 (m, aromatic-H, CH=CH), 4.56 - 4.27 (m, α CH), 4.23 (dd, J = 10.8, 5.2 Hz, CH₂OCO), 3.73 (t, J = 5.2 Hz, CHCN), 3.31 - 2.80 (m, NCH₂), 2.70 - 2.52 (m, NCH₃), 2.17 - 1.49 (m, CH₂COO), 1.49 - 0.84 (m, α CHCH₂). FTIR: $\nu_{\text{max}}/\text{cm}^{-1}$ (solid): 3500-2983 (NH, OH), 2924, 2847 (sp³ CH), 1690 (C=O broad, ester+amide), 1068 (C-O ester) (COOH absent).

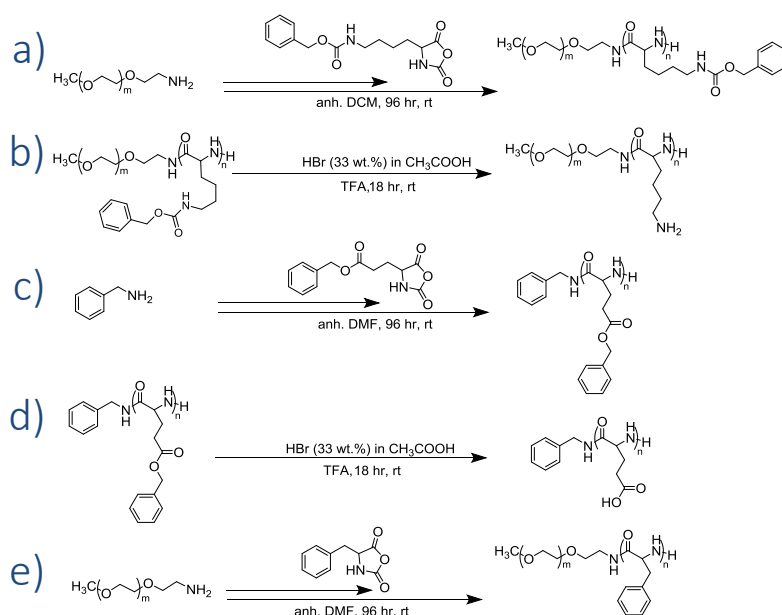
11.2.9. Biological Analyses

Cytotoxicity studies were carried by culturing cells (2 x 10³ per well of a 96-well microplate, in 200 μL of the cell culture medium) in the presence of varying concentrations (25 μM to 0.049 μM) of silver (I)-NHC compounds, polymer-silver complex compounds and cisplatin, in triplicate. Triplicate wells, containing cells cultured in cell culture medium only, were used as controls. An MTT assay was subsequently carried out to determine the viability of the cells in the respective plated wells. Then, the percentage cell survival in the respective experiments was determined by comparing the viability of cells cultured in the presence of an anticancer compound with the viability of cells cultured in control wells. The concentration required to kill 50% of cells (IC₅₀) was subsequently determined by comparison of percentage survival with the concentration of the compound that was used to treat the cells.

11.3. Results and Discussions

11.3.1. Poly(Amino Acid) Syntheses

NCA ROP was used in the synthesis of the required poly(amino acid)s (Scheme 11.1 a, c, e), which were obtained in reasonable yields (Table 11.3). In order to exploit the biocompatibility and the stealth behaviour of PEG [57], the amine-terminated mPEG₅₀₀₀ macroinitiator was used to initiate the ROP of Lys(Cbz) NCA and also to initiate the ROP of Phe NCA, respectively. Then, Cbz protecting groups and the Bz protecting groups were cleaved from the poly(amino acid) repeat units by hydrolysis in hydrobromic acid solution (Scheme 11 b, d). The successful removal of the protecting groups was confirmed by carrying out analyses using ¹H NMR spectroscopy and FTIR spectroscopy.



Scheme 11.1. (a) Synthesis of mPEG₅₀₀₀-b-Poly(Lys(Cbz)), (b) deprotection of mPEG₅₀₀₀-b-Poly(Lys(Cbz)), (c) synthesis of poly(Glu(Bz))_n, (d) deprotection of poly(Glu(Bz))_n, (e) synthesis of poly(Phe)_n.

¹H NMR spectroscopy revealed the disappearance of peaks that corresponded to the Cbz groups (7.15 - 7.40 ppm for aromatic protons and ca 5.20 ppm for CH₂ protons) from the ¹H NMR spectrum of mPEG₅₀₀₀-b-poly(Lys(Cbz))_n (Figure 11.1 b, c). ¹H NMR spectroscopy revealed the disappearance of peaks that belonged to the CH₂ groups of the benzyl ester protecting groups (4.98 ppm) when poly(Glu(Bz)) was deprotected (Figure 11.2 b, c). In addition, ¹H NMR spectroscopy revealed a reduction in the integration value for the aromatic protons (7.25

ppm), while the integral value of the remaining protons equated to those from the benzylamine initiator.

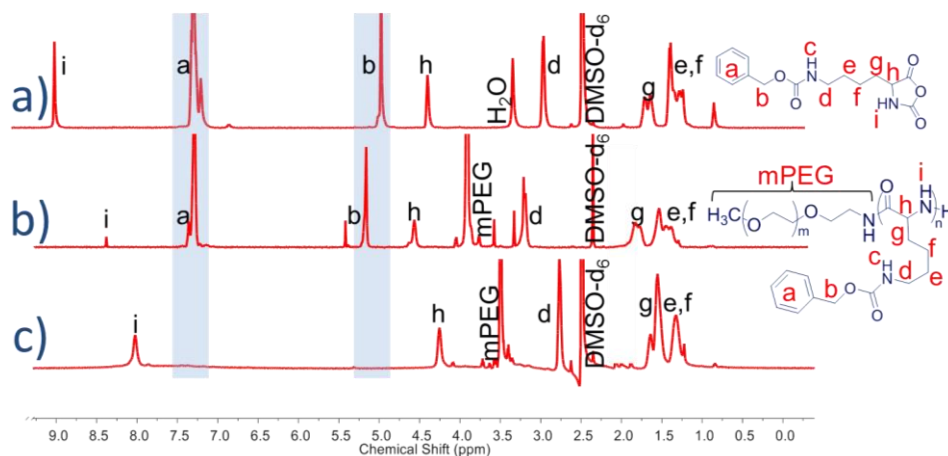


Figure 11.1. ¹H NMR spectra of (a) Lys(Cbz) NCA, (b) mPEG₅₀₀₀-b-poly(Lys(Cbz)) and (c) the mPEG₅₀₀₀-b-poly(Lys) macromolecule obtained after poly(amino acid) deprotection.

Lys(Cbz) NCA was chosen for the creation of hybrid mPEG-poly(amino acid)s because, upon deprotection, the lysine repeat units are able to furnish cationic side groups that can be exploited for electrostatic coordination to anticancer metal complexes, in aqueous media. The composition of the mPEG-*b*-poly(Lys)_{*n*} macromolecules was determined by comparing the integration value of mPEG protons (*ca.* 3.25 - 3.75 ppm) with the integration value of the protons, bonded to the alpha carbon of the amino acid repeat units (*ca.* 4.15 - 4.41 ppm). Approximately 39, 50 and 140 monomer units were shown to have grafted from the mPEG macroinitiator to yield three hybrid mPEG-poly(amino acid) copolymers (Entry 1-3, Table 11.3).

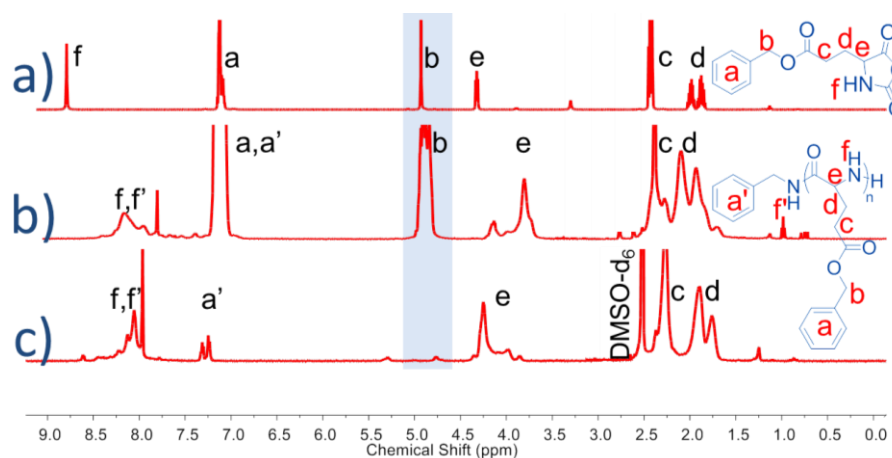


Figure 11.2. ¹H NMR spectra of (a) Glu(Bz) NCA, (b) poly(Glu(Bz)) and (c) poly(Glu).

Poly(Glu)_n was required for the current study because its deprotected amino acid repeat units possess pendant carboxyl groups that may be exploited for the post-polymerisation modification with hydroxyl group-containing silver(I)-NHC complexes using esterification reactions. Comparisons between the ¹H NMR integration value corresponding to the CH₂ protons of the benzyl protecting group (*ca* 4.65 - 5.19 ppm) with the integration value of protons that are bonded to the alpha carbon of the amino acid repeat units (*ca* 3.95 - 4.50 ppm), revealed that a total of 42 glutamic acid monomer units were grafted from the benzylamine initiator, to yield poly(Glu)₄₂ (Entry 4, Table 11.3).

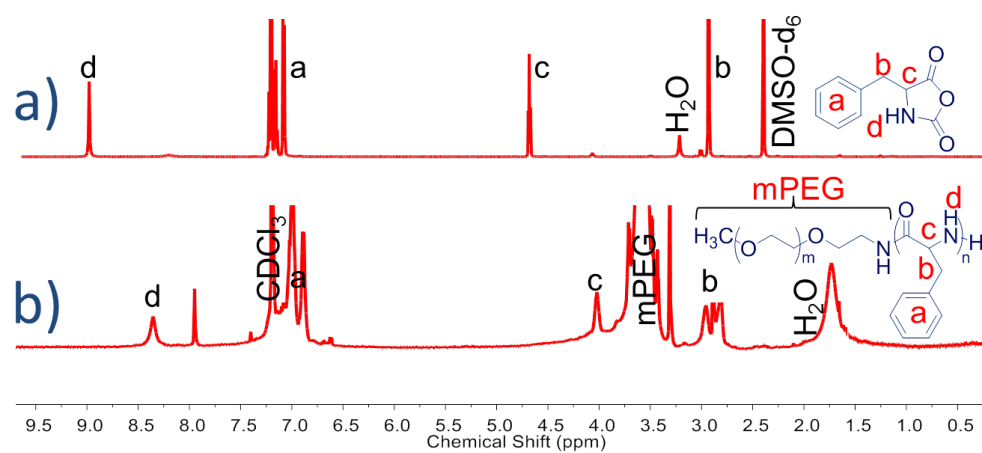


Figure 11.3. ¹H NMR spectra of Phe NCA (a) and mPEG₅₀₀₀-b-poly(Phe) (b).

Table 11.3. The various poly(amino acids) that were synthesised by NCA ROP

Entry	Polymer	[M/I]	Yield	Theoretical M _w ⁺ /(g/mol)	Actual M _w [*] /(g/mol)
1	mPEG ₅₀₀₀ -b-poly(Lys) ₃₉	20	88.3%	7564	9999
2	mPEG ₅₀₀₀ -b-poly(Lys) ₅₀	40	96.2%	10128	11410
3	mPEG ₅₀₀₀ -b-poly(Lys) ₁₄₀	75	94.6%	14614	22947
4	Poly(Glu) ₄₂	50	75.3%	6563	5530
5	mPEG ₅₀₀₀ -b-poly(Phe) ₂₄	20	44.6%	7944	8533

⁺ Calculated from the monomer-to-initiator molar feed ratios; ^{*} Computed using ¹H NMR Spectroscopy.

It was envisaged that the phenyl groups of the Phe amino acid would enable poly(amino acid) self-assembly to occur *via* π - π stacking and hydrophobic interactions, in aqueous media [58, 59]. Comparisons between the integration value of mPEG protons and the integration value of protons that are bonded to the alpha carbon of Phe repeat units, revealed that a total of 24 monomer units were grafted from the mPEG macroinitiator, to yield the desired hybrid macromolecule (Entry 5, Table 11.3).

11.3.2. Silver(I)-*N*-Heterocyclic Carbene (NHC) Complexes

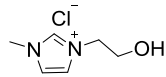
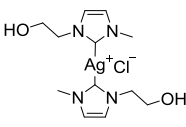
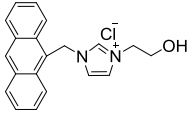
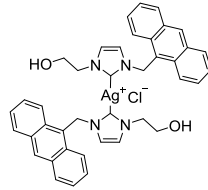
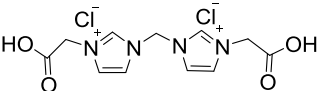
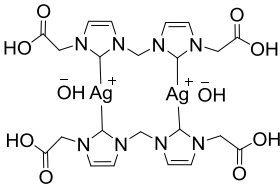
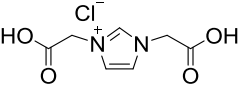
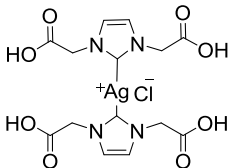
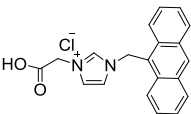
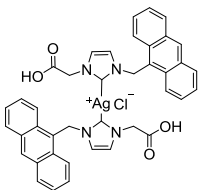
Firstly, five *N*-heterocyclic carbene ligands were synthesised for use as intermediates of the desired silver(I)-NHC complexes. These were subsequently chelated to metallic silver to furnish the desired silver(I)-NHC complexes (Table 11.4). Of the complexes that were synthesised, C01 has been reported in literature [60]. However, its encapsulation in polymers and its controlled release from polymeric nanocarriers has yet to be reported. C02, C03, C04 and C05 were synthesised as novel silver(I)-NHC complexes. The cytotoxicity of the complexes was evaluated against two contrasting cell lines; Panc 10.05 (cancerous cells) and ARPE-19 cells (non-diseased cells). In addition, the activity of cisplatin was also evaluated against Panc 10.05 cells and ARPE-19 cells to provide cytotoxicity data and, subsequently, to provide a comparison of the anticancer effectiveness of these silver(I) NHC complexes with this established drug (Figure 11.4, Table A11.1 (*Appendix 11*)).

The IC₅₀ value can be used to gauge the potency of anticancer therapeutics. Ideally, the IC₅₀ value obtained from an anticancer agent should be greatest (less toxic) against healthy cells and minimal (highly toxic) against cancerous cells. One of the disadvantages of cisplatin is that it lacks significant selectivity between cancerous cells and healthy cells. This renders it highly toxic to healthy cells [5]. This was evident when cisplatin was tested against Panc 10.05 cells and against ARPE-19 cells. There was no significant difference between the effect of the drug against the healthy cells (ARPE-19, IC₅₀ = 6.41 μ M) and against the cancerous cells (Panc 10.05, IC₅₀ = 1.71 μ M). This gave the lowest selectivity ratio (*ca.* 1.27) against this particular pair of cell lines (Figure 11.4).

In contrast, the synthesised silver(I)-NHC complexes (C01, C02, C03 and C05) were relatively less inhibitory to the healthy cells, as evidenced by the IC₅₀ values that ranged from 68 to above

100. Furthermore, the silver(I)-NHC complexes demonstrated superior selectivity, as evidenced by the selectivity ratios that are almost double (C01, C02, C05), and those that are more than double (C03), the selectivity ratio of cisplatin. As such, these preliminary results suggest that the silver(I)-NHC complexes possess anticancer properties. Thus, they are a serious prospect for use in effective chemotherapy.

Table 11.4. Structure of NHC ligands and their respective silver(I)-NHC complexes

Ligand	Complex	In-text Reference
		C01
		C02
		C03
		C04
		C05

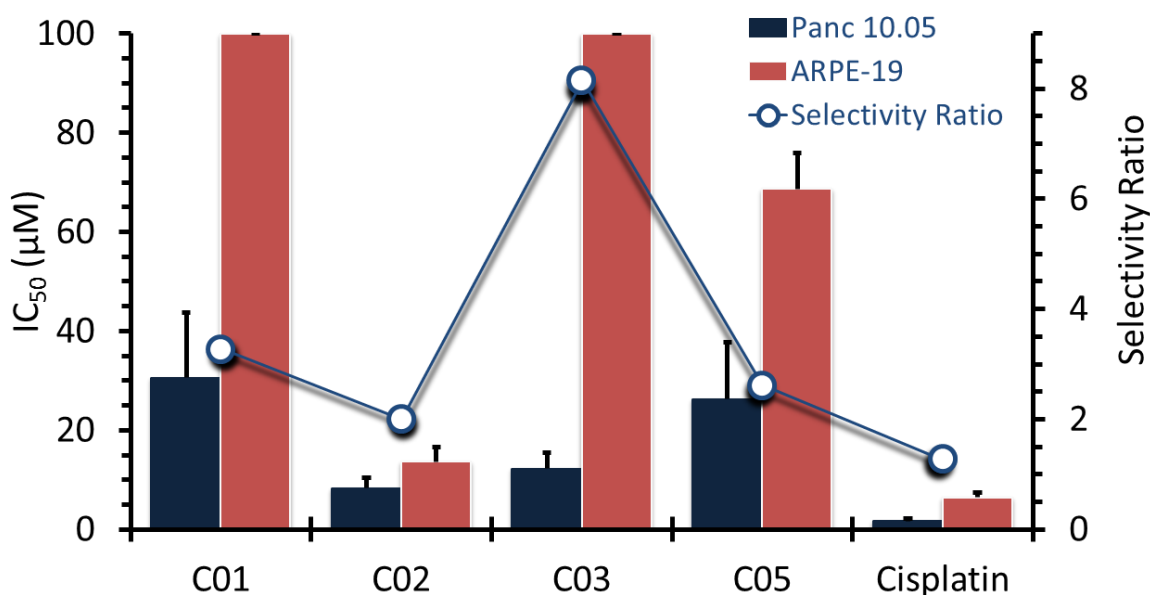


Figure 11.4. Evaluation of anticancer potencies of silver(I)-NHC complexes and cisplatin, against Panc. 10.05 cells and against ARPE-19 cells.

11.3.3. Physical Encapsulation of Complexes in an Amphiphilic Polymer

A supramolecular-driven assembly was exploited to encapsulate physically a chosen silver (I)-NHC complex in an amphiphilic copolymer, mPEG₅₀₀₀-*b*-poly(Phe)₂₄. Initially, the self-aggregation of the polymer in an aqueous medium was confirmed by observing the formation of spherical particles. These measured 121.4 nm in diameter (Figure A11.1) and possessed a PDI of 0.26. Then, the physical encapsulation of C01 complexes and of C02 complexes in amphiphilic mPEG₅₀₀₀-*b*-poly(Phe)₂₄ was attempted by allowing the polymer to self-aggregate in the presence of the complex. It can be hypothesised at this point that, upon self-aggregation in an aqueous medium, by directing the hydrophilic mPEG block towards water and shielding the hydrophobic poly(Phe)₂₄, the polymer may simultaneously encapsulate the silver complex molecules, whose solubility in aqueous medium is limited (Figure 11.5, *top*).

According to the results obtained from DLS analyses, the envisaged encapsulation of C01 complexes and of C02 complexes in mPEG₅₀₀₀-*b*-poly(Phe)₂₄ resulted in the formation of particles that possessed average hydrodynamic diameters of 151.7 nm and 139.4 nm, respectively (Figure 11.5 a, c). As such, in both instances, the encapsulation of silver complexes had caused an increase in the size of the particles from an initial size of 121.4 nm. SEM analysis

revealed that both sets of the silver(I)-NHC complex-loaded particles possessed a spherical morphology (Figure 11.5 b, d).

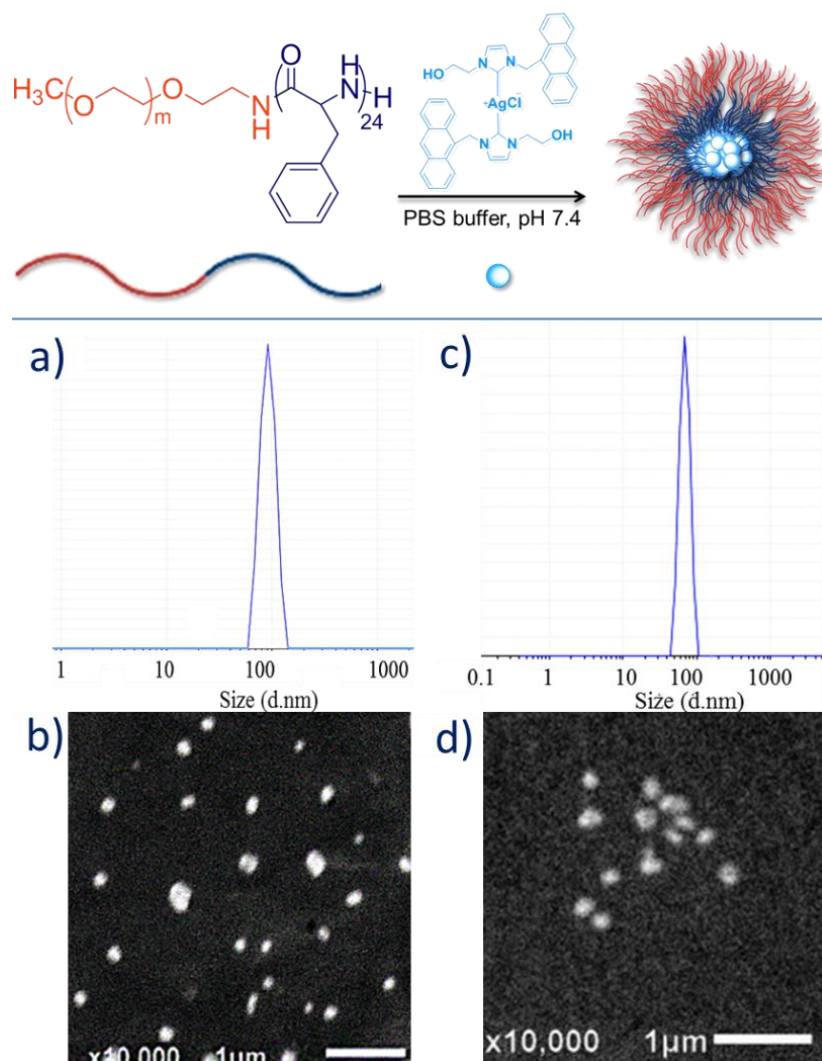


Figure 11.5. The envisaged self-aggregation of mPEG₅₀₀₀-b-poly(Phe)₂₄ into particles that entrapped physically the silver (I)-NHC complexes (top). DLS charts revealing the size distribution of C01-loaded particles (a) and C02-loaded particles (c). SEM microphotographs for C01-loaded particles (b) and C02-loaded particles (d). Scale bars represent 1 μm.

Energy-dispersive x-ray (EDX) spectroscopy was then used to map the area within the individual particles to provide an elemental map that could be used to ascertain if the silver atoms were contained in the particles. EDX spectroscopy revealed the presence of clusters of the silver-based element that were located in the area in and around the discrete particles (Figure 11.6

b). This point was also confirmed by the EDX spectrum corresponding to the map (Figure 11.6 c).

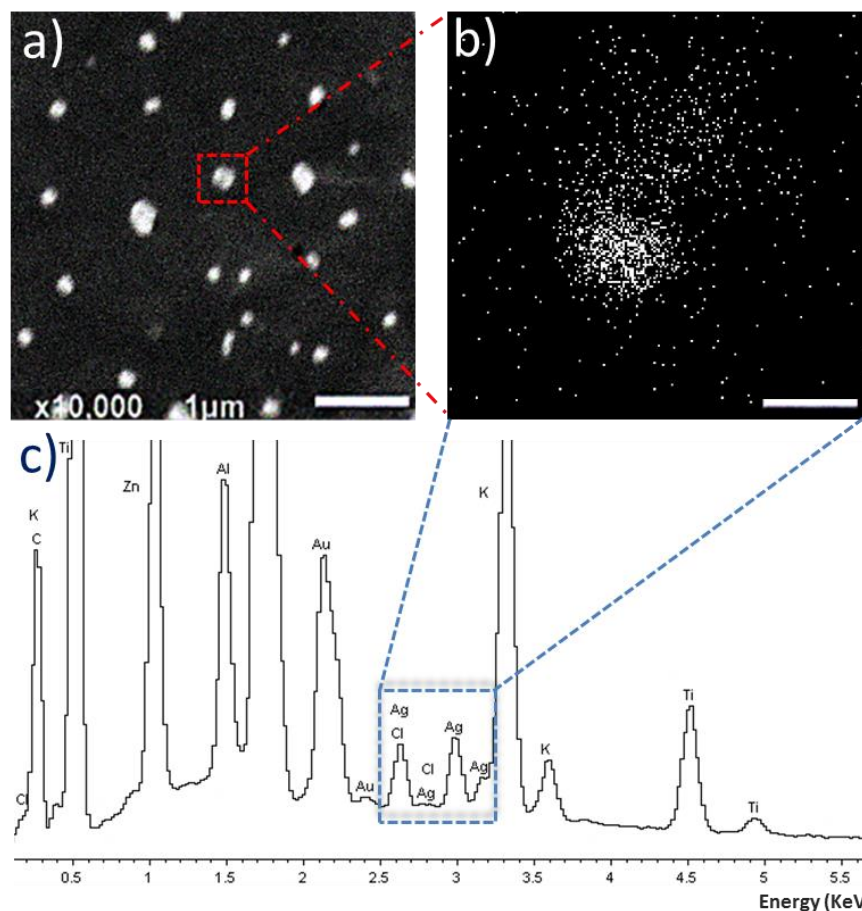


Figure 11.6. (a) SEM image of CO₂-loaded mPEG₅₀₀₀-b-poly(Phe)₂₄ particles, (b) the EDX map corresponding to an area that is located within a CO₂-loaded particle and (c) the EDX spectrum corresponding to an area that is located within a CO₂-loaded particle, showing the silver elements. The rest of the elements that appear on the spectrum emanated from the composition of the SEM glass cover slide and from the gold-coating. Scale bars represent 1 μm.

To emphasise further the encapsulation of silver(I)-NHC complexes in the particles, the intrinsic fluorescence property of the complex CO₂ was exploited to map the location of the complexes in the particles. Confocal laser scanning microscopy was used to image the CO₂-loaded particles. Imaging was carried out under visible light to map the polymeric shell (Figure 11.7 a) and under fluorescence to map the inherently fluorescent silver(I)-NHC complexes (Figure 11.7 b). These images were overlaid (Figure 11.7 c) and resolved further to reveal clearly the two distinct regions in the particles (Figure 11.7 d). The discrete clusters that fluoresced, and were thus assumed to be the silver (I)-NHC complex, occupy positions that coincide with the

positions that are occupied the dark spots (i.e., assumed to be the discrete polymeric particles) (Figure 11.7 c, d). As such, it can surmised that the silver(I)-NHC complexes either become adsorbed onto the polymeric particles or are encapsulated within the polymeric particles. The latter possibility seems more plausible because of the intrinsic hydrophobicity of the metal complex.

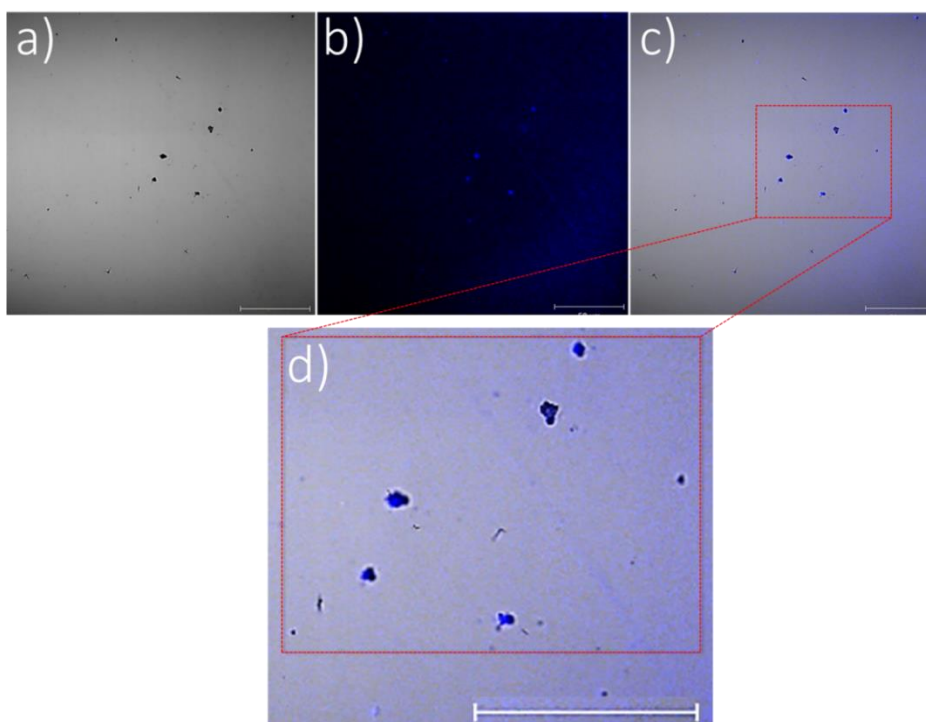


Figure 11.7. Confocal microscopy images obtained from CO₂-loaded mPEG₅₀₀₀-b-poly(Phe)₂₄ particles under visible light (a), under fluorescence (b), an overlay of the two images (c) and highly resolved image (d) that reveals clearly that the blue fluorescent spots (i.e., assumed to be the molecules of the encapsulated complexes) occupy the same positions as the black clusters (which are assumed to be the polymeric shell). Scale bars represent 1 μ m.

Apart from the limited solubility of the reported silver(I)-NHC complexes in aqueous media, the encapsulation of the complexes could also be enhanced by hydrophobic interactions, between the complex and the polymer. In the example of the encapsulation of CO₂, it is possible that self-organisation is reinforced by interactions between the anthracenyl groups of the complex and the phenyl groups of the amphiphilic poly(amino acid). This could suggest the likelihood of enhancing the encapsulation and the subsequent delivery of silver (I)-NHC complexes species by tuning the composition of the delivery vehicles.

11.3.4. Charge-Driven (Electrostatic) Coordination of Complexes with Polymers

Complexes CO3, CO4 and CO4 were chosen for this proof-of-concept study because they contain carboxyl groups that can deprotonate in aqueous media to present anionic groups (COO^-). These may bind *via* electrostatic interactions to the cationic (NH_3^+) repeat units of mPEG-*b*-poly(Lys)_n macromolecules. Initially, the polymer solutions and metal complex solutions were filtered through 0.2 μm PTFE syringe filters to eliminate any undissolved matter prior to the chelation step. Relative to this point, DLS confirmed the absence of particles in the polymer solutions and in the metal complex solution, by revealing blank DLS charts (Figure 11.8 a). When the respective polymer solutions were mixed with silver(I)-NHC complex solutions (1:1 v/v), studies that were carried out using DLS confirmed the formation of particles, by revealing the emergence of size distribution traces that were initially not present in either the independent polymer solutions or in the complex solutions (Figure 11.8 b, Table 11.5).

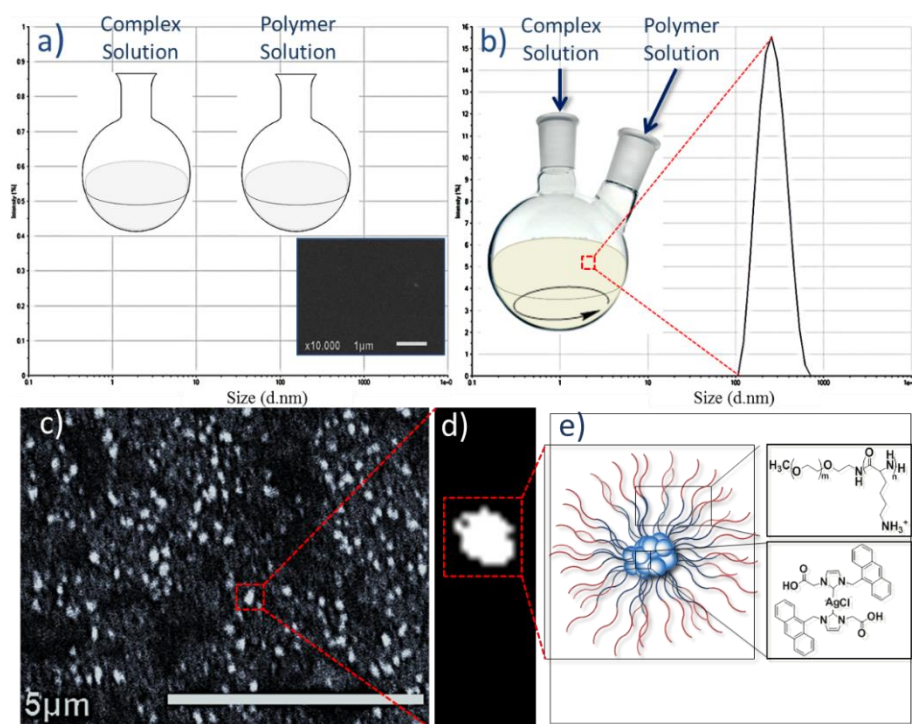
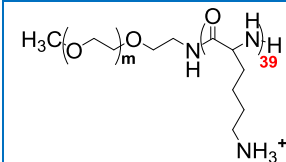
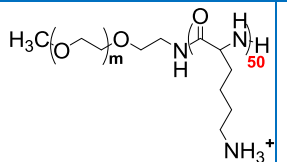
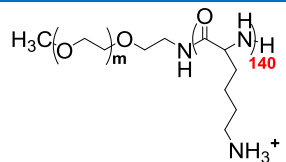
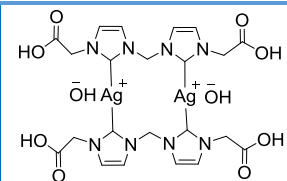
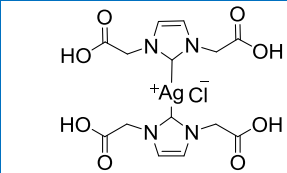
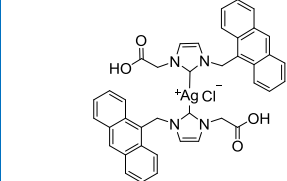


Figure 11.8. (a) No aggregates were detected when either mPEG-*b*-poly(L-lys)_n solutions or silver(I)-NHC complex solutions were assessed by DLS and SEM (inset). (b) Aggregates were subsequently formed and detected upon mixing the polymer solutions and the complex solutions, as evidenced by the emergence of DLS size distribution traces (b) and spherical aggregates (c). The particles clearly possess a spherical morphology (d) and it is envisaged that the copolymer forms the core-shell which encapsulates the complexes (e).

mPEG-*b*-poly(Lys)₃₉ coordinated with CO₃, with CO₄ and with CO₄, to form particles whose diameters averaged 101.1 nm, 159.7 nm and 160.8 nm, respectively (Figure 11.9 a-c, Table 11.5). mPEG-*b*-poly(Lys)₅₀ coordinated with CO₃, with CO₄ and with CO₄, to form particles whose diameters averaged 175.6 nm, 178.2 nm and 219.1 nm, respectively (Figure 11.10 a-c, Table 11.5). mPEG-*b*-poly(Lys)₁₄₀ coordinated with CO₃, with CO₄ and with CO₄, to form particles whose diameters averaged 176.5 nm, 199.5 nm and 221.8 nm, respectively (Figure 11.11 a-c, Table 11.5). The mPEG-*b*-poly(Lys)_n macromolecules were assembled with poly(Lys) blocks of varying molecular weights, with the intention that this would result in variable loadings of complexes. This factor could be the reason for the observed minor increase in the size of the aggregates, which tended to increase in proportion to the increase in the molecular weight for all polymers. SEM revealed that the charge-coordinated polymer-metal complex particles possessed a spherical morphology, as revealed by the representative microphotograph (Figure 11.8 c, d). It is envisaged that these particles could consist of a PEG shell that encapsulates those silver(I)-NHC complexes that are coordinated to the cationic lysine repeat units, thereby forming the core of the particles (Figure 11.8 e).

Table 11.5. Polymer-metal complex-based particles created by electrostatic coordination of silver(I)-NHC complexes complexes to mPEG-*b*-poly(Lys)_n polymers in aqueous medium.

			
	159.7 nm PDI: 0.19	175.6 nm PDI: 0.17	176.5 nm PDI: 0.15
	101.1 nm PDI: 0.77	178.2 nm PDI: 0.28	199.5 nm PDI: 0.38
	160.8 nm PDI: 0.25	219.1 nm PDI: 0.21	221.8 nm PDI: 0.14

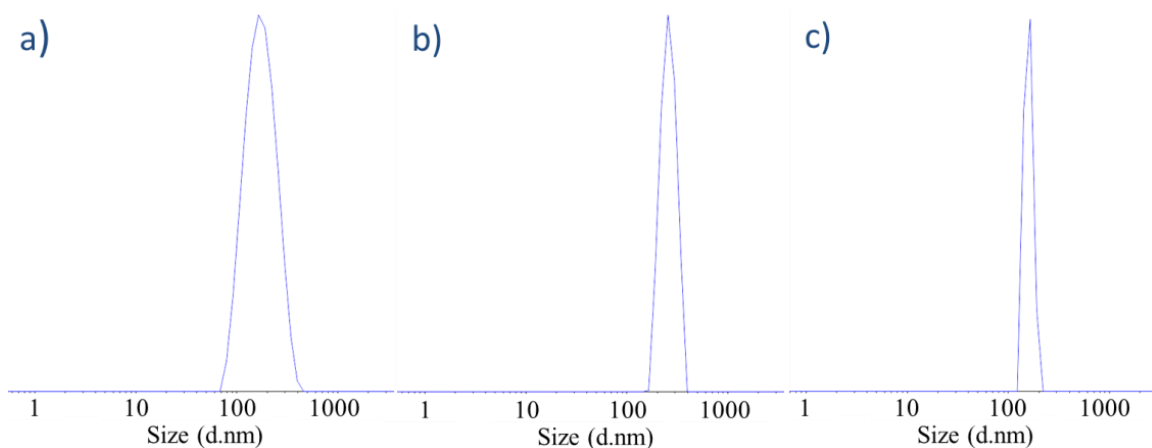


Figure 11.9. DLS charts obtained from mPEG₅₀₀₀-*b*-Poly(L-lys)₃₉-C03 particles (a), mPEG₅₀₀₀-*b*-Poly(L-lys)₅₀-C03 particles (b) and mPEG₅₀₀₀-*b*-Poly(L-lys)₁₄₀-C03 particles (c).

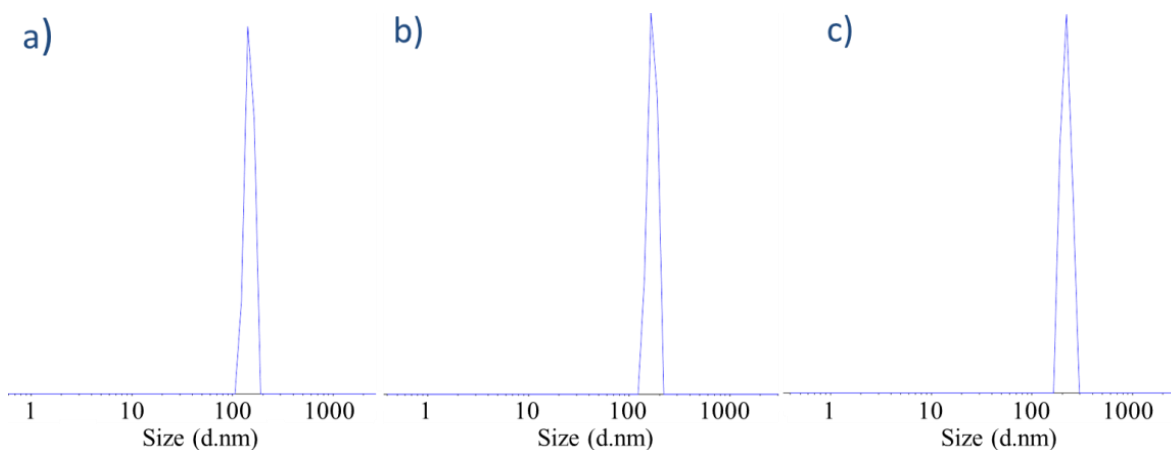


Figure 11.10. DLS traces obtained from mPEG₅₀₀₀-*b*-Poly(L-lys)₃₉-C04 particles (a), mPEG₅₀₀₀-*b*-Poly(L-lys)₅₀-C04 particles (b) and mPEG₅₀₀₀-*b*-Poly(L-lys)₁₄₀-C04 particles (c).

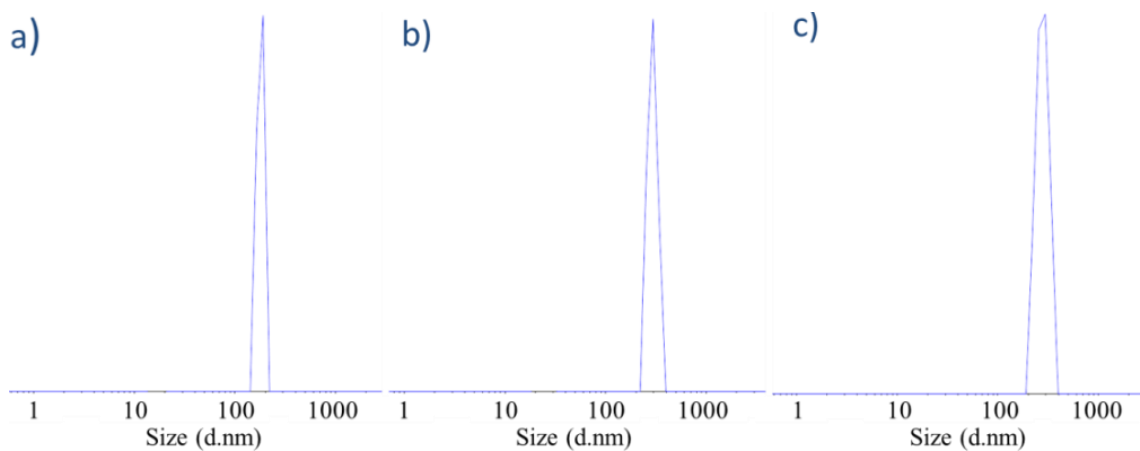


Figure 11.11. DLS traces obtained from mPEG₅₀₀₀-*b*-Poly(L-lys)₃₉-C05 particles (a), mPEG₅₀₀₀-*b*-Poly(L-lys)₅₀-C05 particles (b) and mPEG₅₀₀₀-*b*-Poly(L-lys)₁₄₀-C05 particles (c).

Biological studies were carried out to evaluate the anticancer potency of the free silver(I)-NHC complexes and of the polymer-metal complex particles. C04 complex and the C04-loaded mPEG-*b*-poly(Lys)_n particles were not analysed because the IC₅₀ for C04 was not determined. Instead, C03-loaded mPEG-*b*-poly(Lys)₅₀ particles (PLC03) and mPEG-*b*-poly(Lys)₁₄₀-C05 particles (PLC05), which possessed narrow PDIs, were progressed towards proof-of-concept biological studies. Their respective anticancer potencies were subsequently compared with the anticancer potency of the corresponding free complexes (C03 and C05). MTT assays revealed that the metal complex-loaded mPEG-*b*-poly(Lys)_n particles possess superior anticancer potency against Panc. 10.05 cells in comparison to free complexes. For example, C03-loaded mPEG-*b*-poly(Lys)₅₀ particles had an IC₅₀ value that is approximately 35.2% less than the IC₅₀ value of the free C03 complex (Figure 11.12). C05-loaded mPEG-*b*-poly(Lys)₁₄₀ particles had an IC₅₀ value that is approximately 43.4% less than that of the free C05 complex (Figure 11.12). Thus, the coordination of silver (I)-NHC complexes to the polymeric carriers appears to improve their anticancer efficacy, *in vitro*. This effect is possibly due to the enrichment of their uptake and their retention (EPR effect) [61] by the mammalian carcinoma. The anticancer efficacy of the complex-loaded particles could perhaps be improved if these delivery systems were to be optimised.

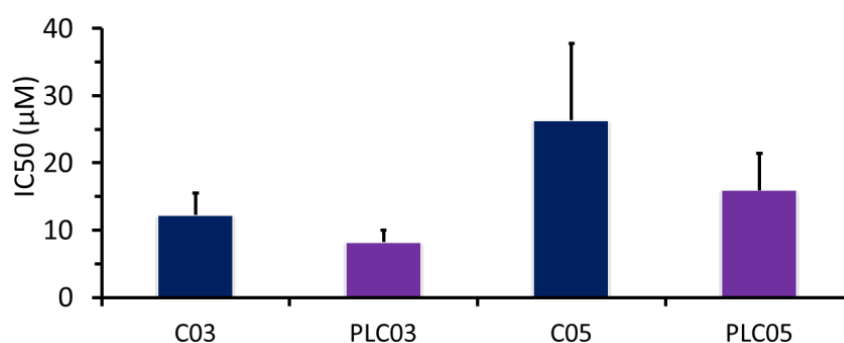
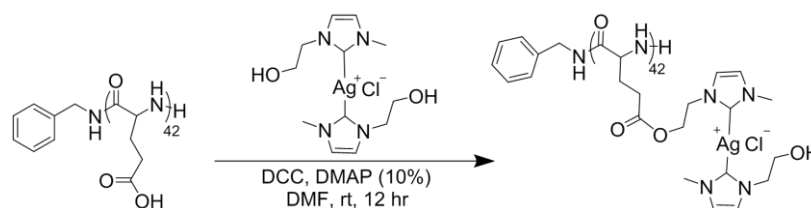


Figure 11.12. The anticancer potencies of C03-loaded mPEG-*b*-poly(Lys)₅₀ particles (PLC03) and mPEG-*b*-poly(Lys)₁₄₀-C05 particles (PLC05), against Panc. 10.05 cells. The anticancer potencies of the free (un-encapsulated) complexes, C03 and C05, against Panc. 10.05 cells. (Data, n = 3, mean ± SD).

11.3.5. Covalent Conjugation of Silver(I)-NHC Complexes to Poly(Amino Acid)s

Poly(Glu)₄₂ and C01 were chosen for this proof-of-concept study. This was because this poly(amino acid) possesses pendant carboxyl groups that could be reacted with the hydroxyl groups of the silver (I)-NHC complex to form degradable ester linkages (Scheme 11.2).



Scheme 11.2. The formation of a poly[(Glu)₂₄-silver(I)-C01] (PGC01) anticancer conjugate.

Initially, a Fischer esterification reaction was attempted to attached C01 complexes covalently to the repeat units of the poly(amino acid). However, studies that were carried out using ¹H NMR spectroscopy, FTIR spectroscopy and ESI-MS revealed that this method did not yield the desired polymer-silver (I)-NHC conjugate. This could be because the prevailing acidic conditions that are employed in the procedure might have induced the acidic pH hydrolysis of the ester linkages that are formed between the polymer and complex. Thus, Steglich esterification, utilising a DCC coupling reagent and a DMAP catalyst, was used (Scheme 11.2). This approach resulted in the formation of the desired poly[(Glu)₄₂-silver(I)-C01] (PGC01) conjugate. Studies that were carried out using ¹H NMR spectroscopy confirmed the formation of PGC01 by revealing the presence of additional proton peaks (*ca.* 2.72 - 4.10 ppm) that are characteristic of the proton peaks from C01 (Figure 11.13).

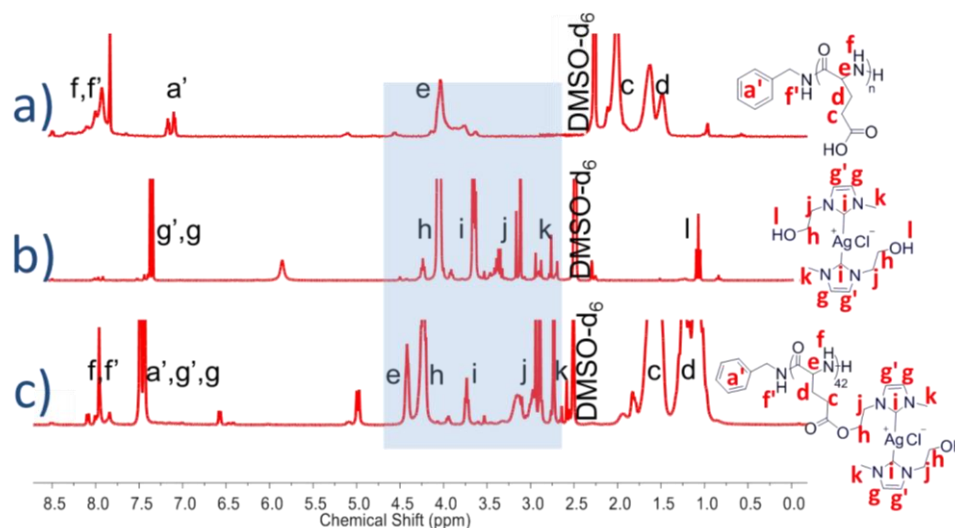


Figure 11.13. ¹H NMR spectra of (a) poly(Glu)₂₄ (a), (b) C01 silver(I)-NHC complex and (c) poly[(Glu)₂₄-silver(I)-NHC] (PGC01) obtained after carrying out Steglich esterification.

The formation of PGC01 was assessed further using FTIR spectroscopy (Figure 11.14). The formation of the characteristic ester linkages (1720 cm⁻¹) was revealed by FTIR spectroscopy (Figure 11.14 c), thus suggesting that the silver(I)-NHC molecules could be linked to the

carboxylic acid repeat units. In addition, FTIR spectroscopy revealed the emergence of an sp^3 C-H stretch (2848 cm^{-1}), associated with ester linkages, thus asserting further the presence of ester linkages in the PGC01 product.

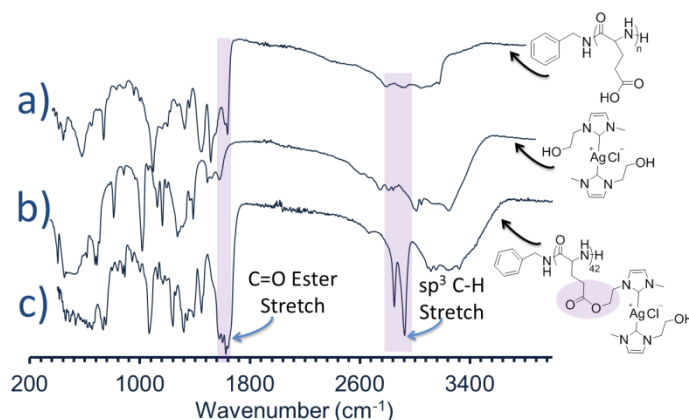


Figure 11.14. FTIR spectra of (a) poly(Glu)₂₄ (PG), (b) C01 and (c) poly[(Glu)₂₄-silver(I)-C01] (PGC01) revealing the emergence of C=O ester stretch and sp^3 C-H stretch signals.

An MTT assay was carried out to assess the anticancer potency of poly[(Glu)-silver(I)-C01] and of the corresponding free complex C01, against Panc. 10.05 cells. The poly[(Glu)-silver(I)-C01] conjugate exhibited a superior anticancer activity in comparison to that of the free complex. For example, conjugation of the complex molecules to the poly(amino acid) repeat units resulted in an approximately 58.7% improvement in the anticancer potency (Figure 11.15 b).

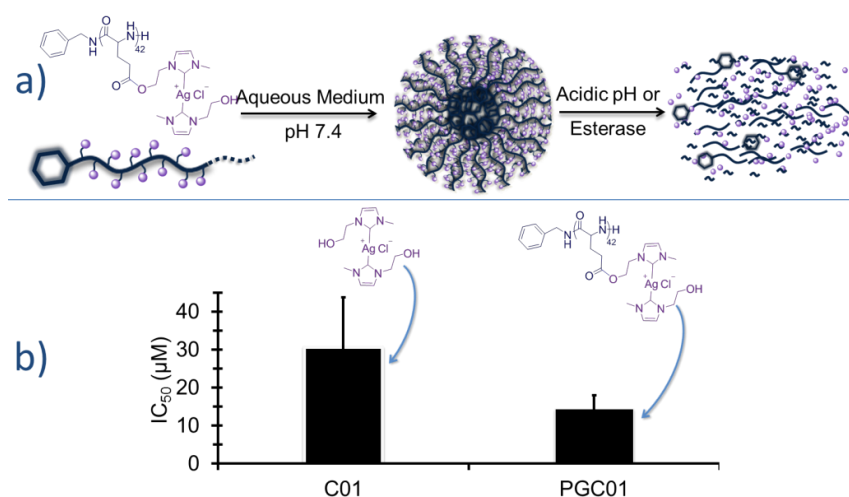


Figure 11.15. The envisaged self-organisation of PGC01 conjugates in aqueous media to generate drug-loaded particles, which could be targeted towards acidic pH or esterase enzymes to cleave the ester linkages and to release the silver complexes (a). (b) Comparison of the anticancer potency of PGC01 and of free C01, against Panc. 10.05 cells (Data: $n = 3$, mean \pm SD).

The acidic pH-catalysed degradation of polymeric carrier vehicles, for the targeted delivery of therapeutic molecules is a well-researched approach that exploits the presence of an acidic tumour pH as a trigger stimulus [62, 63]. As such, poly(amino acid)-silver(I)-NHC conjugates, that are designed to comprise of acid pH-susceptible ester linkers, could offer significant promise in the development of effective anticancer therapeutics. Furthermore, the covalent linking of silver(I)-NHC complexes to individual repeat units of poly(amino acid)s could furnish particles that possess greater drug loadings (Figure 11.15 a). This could lead to a reduction in the material wastage that is usually associated with conventional drug-loading procedures. Subsequent cleavage of ester linkages, to release the conjugated metal complex molecules, can only be possible in the presence of the relevant trigger stimuli (e.g., acidic pH or esterase enzyme), thus negating the toxicity of chemotherapeutics against non-diseased tissues which is usually associated with premature drug release and dose dumping *in vivo* [64, 65].

11.4. Conclusion

This research has resulted in the generation of five silver(I)-*N*-heterocyclic carbene complexes. These exhibited anticancer potency against Panc 10.05 cells and also possessed better selectivity at distinguishing between healthy cells and cancerous cells, in comparison to cisplatin. Three approaches were then followed in proof-of-concept studies to encapsulate silver(I)-NHC complexes in poly(amino acid)s. Initially, the hydrophobic C01 complexes and C02 complexes were encapsulated physically in an amphiphilic mPEG₅₀₀₀-*b*-poly(Phe)₂₄ polymer to give complex-loaded spherical particles, whose diameters were equal to 151.7 nm and 139.4 nm, respectively. In the second approach, C03 complexes, C04 complexes and C05 complexes, that contain carboxyl groups in their design, were encapsulated in mPEG₅₀₀₀-*b*-poly(Lys)_n copolymers, by an envisaged charge-driven coordination to the cationic repeat units of the poly(Lys)_n block. DLS and SEM studies revealed the formation of monodisperse spherical particles that ranged in diameter between 100 nm and 221.8 nm. Lastly, a covalent grafting approach was followed in which C01 complex, designed to contain hydroxyl groups, could form ester bonds with the carboxylic acid groups of poly(Glu)₄₂, when the Steglich esterification protocol was employed. This approach resulted in the formation of a poly[(Glu)-C01] conjugate. The MTT assays revealed that the encapsulation of C01, C03 and C05 in poly(amino acid)s resulted in poly(amino acid)-metal complex particles that exhibited superior anticancer

potency compared to the potency of the un-encapsulated metal complexes. The anticancer potency of the various polymer-silver(I)-NHC conjugates improved by significant margins, ranging between 35% and 58% of the anticancer potencies of their corresponding free complexes. These preliminary findings suggest that the encapsulation of silver(I)-NHC complexes in poly(amino acid)s could provide a platform for the development of effective anticancer therapeutics.

11.5. References

1. Bruijninx, P.C.A. and Sadler, P.J. *Curr. Opin. Chem. Biol.*, **2008**, 12, 197-206.
2. Che, C.-M. and Siu, F.-M. *Curr. Opin. Chem. Biol.*, **2010**, 14, 255-261.
3. Dasari, S. and Tchounwou, P.B. *Eur. J. Pharmacol.*, **2014**, 740, 364-378.
4. Rahman, A.-u. and Choudhary, M.I. *Frontiers in anti-cancer drug discovery*. **2010**, Vol. 1, Bentham Science Publishers
5. Housman, G., Byler, S., Heerboth, S., Lapinska, K., Longacre, M., Snyder, N. and Sarkar, S. *Cancers*. **2014**, 6, 1769-1792.
6. Aher, S.B., Muskawar, P.N., Thenmozhi, K. and Bhagat, P.R. *Eur. J. Med. Chem.*, **2014**, 81, 408-419.
7. Skander, M., Retailleau, P., Bourrie, B., Schio, L., Mailliet, P. and Marinetti, A. *J. Med. Chem.*, **2010**, 53, 2146-2154.
8. Sun, R.W.-Y., Chow, A.L.-F., Li, X.-H., Yan, J.J., Chui, S.S.-Y. and Che, C.-M. *Chem. Sci.*, **2011**, 2, 728-736.
9. Rubbiani, R., Kitanovic, I., Alborzina, H., Can, S., Kitanovic, A., Onambele, L.A., Stefanopoulou, M., Geldmacher, Y., Sheldrick, W.S., Wolber, G., Prokop, A., Woelfl, S. and Ott, I. *J. Med. Chem.*, **2010**, 53, 8608-8618.
10. Rubbiani, R., Can, S., Kitanovic, I., Alborzina, H., Stefanopoulou, M., Kokoschka, M., Moenchgesang, S., Sheldrick, W.S., Woelfl, S. and Ott, I. *J. Med. Chem.*, **2011**, 54, 8646-8657.
11. Liu, W., Bendorf, K., Proetto, M., Abram, U., Hagenbach, A. and Gust, R. *J. Med. Chem.*, **2011**, 54, 8605-8615.
12. Liu, W., Bendorf, K., Proetto, M., Hagenbach, A., Abram, U. and Gust, R. *J. Med. Chem.*, **2012**, 55, 3713-3724.
13. Kunz, P.C., Wetzell, C., Koegel, S., Kassack, M.U. and Spingler, B. *Dalton Trans.*, **2011**, 40, 35-37.
14. Weaver, J., Gaillard, S., Toye, C., Macpherson, S., Nolan, S.P. and Riches, A. *Chem. Eur. J.*, **2011**, 17, 6620-6624.
15. Sivaram, H., Tan, J. and Han Vinh, H. *Dalton Trans.*, **2013**, 42, 12421-12428.
16. Schuh, E., Pflueger, C., Citta, A., Folda, A., Rigobello, M.P., Bindoli, A., Casini, A. and Mohr, F. *J. Med. Chem.*, **2012**, 55, 5518-5528.
17. Kaps, L., Biersack, B., Mueller-Bunz, H., Mahal, K., Muenzner, J., Tacke, M., Mueller, T. and Schobert, R. *J. Inorg. Biochem.*, **2012**, 106, 52-58.
18. Gallori, E., Vettori, C., Alessio, E., Vilchez, F.G., Vilaplana, R., Orioli, P., Casini, A. and Messori, L. *Arch. Biochem. Biophys.*, **2000**, 376, 156-162.
19. Malina, J., Novakova, O., Keppler, B.K., Alessio, E. and Brabec, V. *J. Biol. Inorg. Chem.*, **2001**, 6, 435-445.
20. Cetinbas, N., Webb, M.I., Dubland, J.A. and Walsby, C.J. *J. Biol. Inorg. Chem.*, **2010**, 15, 131-145.
21. Tan, C., Hu, S., Liu, J. and Ji, L. *Eur. J. Med. Chem.*, **2011**, 46, 1555-1563.
22. Oehninger, L., Stefanopoulou, M., Alborzina, H., Schur, J., Ludewig, S., Namikawa, K., Munoz-Castro, A., Koester, R.W., Baumann, K., Woelfl, S., Sheldrick, W.S. and Ott, I. *Dalton Trans.*, **2013**, 42, 1657-1666.
23. Wang, C.-H., Shih, W.-C., Chang, H.C., Kuo, Y.-Y., Hung, W.-C., Ong, T.-G. and Li, W.-S. *J. Med. Chem.*, **2011**, 54, 5245-5249.
24. Budagumpi, S., Haque, R.A. and Salman, A.W. *Coord. Chem. Rev.*, **2012**, 256, 1787-1830.

25. Hackenberg, F. and Tacke, M. *Dalton Trans.*, **2014**, 43, 8144-8153.
26. Mohamed, H.A. and Willans, C.E., *J. Organomet. Chem.*, **2014**, 39, 26-50.
27. Barnard, P.J., Baker, M.V., Berners-Price, S.J. and Day, D.A. *J. Inorg. Biochem.*, **2004**, 98, 1642-1647.
28. Baker, M.V., Barnard, P.J., Berners-Price, S.J., Brayshaw, S.K., Hickey, J.L., Skelton, B.W. and White, A.H. *Dalton Trans.*, **2006**, 3708-3715.
29. Hickey, J.L., Ruhayel, R.A., Barnard, P.J., Baker, M.V., Berners-Price, S.J. and Filipovska, A. *J.A.C.S.*, **2008**, 130, 12570-+.
30. Chtchigrovsky, M., Eloy, L., Jullien, H., Saker, L., Segal-Bendirdjian, E., Poupon, J., Bombard, S., Cresteil, T., Retailleau, P. and Marinetti, A. *J. Med. Chem.*, **2013**, 56, 2074-2086.
31. Gautier, A. and Cisnetti, F. *Metallomics*. **2011**, 4, 23-32.
32. Ray, S., Mohan, R., Singh, J.K., Samantaray, M.K., Shaikh, M.M., Panda, D. and Ghosh, P. *J.A.C.S.*, **2007**, 129, 15042-15053.
33. Haque, R.A., Salman, A.W., Budagumpi, S., Abdullah, A.A.-A. and Majid, A.M.S.A. *Metallomics*. **2013**, 5, 760-769.
34. Sava, G., Zorzet, S., Turrin, C., Vita, F., Soranzo, M., Zabucchi, G., Cocchietto, M., Bergamo, A., DiGiovine, S., Pezzoni, G., Sartor, L. and Garbisa, S. *Clin. Cancer Res.*, **2003**, 9, 1898-1905.
35. Vock, C.A., Scolaro, C., Phillips, A.D., Scopelliti, R., Sava, G. and Dyson, P.J. *J. Med. Chem.*, **2006**, 49, 5552-5561.
36. Teyssot, M.-L., Jarrousse, A.-S., Manin, M., Chevry, A., Roche, S., Norre, F., Beaudoin, C., Morel, L., Boyer, D., Mahiou, R. and Gautier, A. *Dalton Trans.*, **2009**, 6894-6902.
37. Lansdown, A.B.G. and Williams, A. *J. wound care*. **2004**, 13, 131-6.
38. Klasen, H.J. *Burns*. **2000**, 26, 117-130.
39. Lansdown, A.B.G. *J. wound care*. **2002**, 11, 125-30.
40. Melaiye, A. and Youngs, W.J. *Expert. Opin. Ther. Pat.*, **2005**, 15, 125-130.
41. Kascatan-Nebioglu, A., Panzner, M.J., Tessier, C.A., Cannon, C.L. and Youngs, W.J. *Coord. Chem. Rev.*, **2007**, 251, 884-895.
42. Garrison, J.C. and Youngs, W.J. *Chem. Revs.*, **2005**, 105, 3978-4008.
43. Melaiye, A., Sun, Z.H., Hindi, K., Milsted, A., Ely, D., Reneker, D.H., Tessier, C.A. and Youngs, W.J. *J.A.C.S.*, **2005**, 127, 2285-2291.
44. Hindi, K.M., Ditto, A.J., Panzner, M.J., Medvetz, D.A., Han, D.S., Hovis, C.E., Hilliard, J.K., Taylor, J.B., Yun, Y.H., Cannon, C.L. and Youngs, W.J. *Biomaterials*. **2009**, 30, 3771-3779.
45. Kascatan-Nebioglu, A., Melaiye, A., Hindi, K., Durmus, S., Panzner, M.J., Hogue, L.A., Mallett, R.J., Hovis, C.E., Coughenour, M., Crosby, S.D., Milsted, A., Ely, D.L., Tessier, C.A., Cannon, C.L. and Youngs, W.J. *J. Med. Chem.*, **2006**, 49, 6811-6818.
46. Hindi, K.M., Siciliano, T.J., Durmus, S., Panzner, M.J., Medvetz, D.A., Reddy, D.V., Hogue, L.A., Hovis, C.E., Hilliard, J.K., Mallet, R.J., Tessier, C.A., Cannon, C.L. and Youngs, W.J. *J. Med. Chem.*, **2008**, 51, 1577-1583.
47. Hackenberg, F., Lally, G., Mueller-Bunz, H., Paradisi, F., Quaglia, D., Streciwilk, W. and Tacke, M. *J. Organomet. Chem.*, **2012**, 717, 123-134.
48. Roland, S., Jolival, C., Cresteil, T., Eloy, L., Bouhours, P., Hequet, A., Mansuy, V., Vanucci, C. and Paris, J.-M. *Chem. Eur. J.*, **2011**, 17, 1442-1446.
49. Haque, R.A., Ghdayeb, M.Z., Salman, A.W., Budagumpi, S., Ahamed, M.B.K. and Majid, A.M.S.A. *Inorg. Chem. Commun.*, **2012**, 22, 113-119.

50. Siciliano, T.J., Deblock, M.C., Hindi, K.M., Durmus, S., Panzner, M.J., Tessier, C.A. and Youngs, W.J. *J. Organomet. Chem.*, **2011**, 696, 1066-1071.
51. Medvetz, D.A., Hindi, K.M., Panzner, M.J., Ditto, A.J., Yun, Y.H. and Youngs, W.J. *Met. Based Drugs*, **2008**, 2008.
52. Monteiro, D.C.F., Phillips, R.M., Crossley, B.D., Fielden, J. and Willans, C.E. *Dalton Trans.*, **2012**, 41, 3720-3725.
53. Oehninger, L., Rubbiani, R. and Ott, I. *Dalton Trans.*, **2013**, 42, 3269-3284.
54. Eloy, L., Jarrousse, A.-S., Teysot, M.-L., Gautier, A., Morel, L., Jolival, C., Cresteil, T. and Roland, S. *Chemmedchem*. **2012**, 7, 805-814.
55. Pellei, M., Gandin, V., Marinelli, M., Marzano, C., Yousufuddin, M., Dias, H.V.R. and Santini, C. *Inorg. Chem.*, **2012**, 51, 9873-9882.
56. Liu, Q.X., Xu, F.B., Li, Q.S., Zeng, X.S., Leng, X.B., Chou, Y.L. and Zhang, Z.Z. *Organometallics*. **2003**, 22, 309-314.
57. Knop, K., Hoogenboom, R., Fischer, D. and Schubert, U.S. *Angew. Chem. Int. Ed.*, **2010**, 49, 6288-6308.
58. Castelletto, V. and Hamley, I.W. *Biophys. Chem.*, **2009**, 141, 169-174.
59. Carlsen, A. and Lecommandoux, S. *Curr. Opin. Colloid Interface Sci.*, **2009**, 14, 329-339.
60. Hameury, S., de Fremont, P., Breuil, P.A., Olivier-Bourbigou, H. and Braunstein, P. *Dalton Trans.* **2014**, 43, 4700-10.
61. Greish, K. Enhanced Permeability and Retention (EPR) Effect for Anticancer Nanomedicine Drug Targeting. In: Grobmyer, R.S. and Moudgil, M.B. eds. *Cancer Nanotechnol.*, Totowa, NJ: Humana Press, 2010, pp.25-37.
62. Colley, H.E., Hearnden, V., Avila-Olias, M., Cecchin, D., Canton, I., Madsen, J., MacNeil, S., Warren, N., Hu, K., McKeating, J.A., Armes, S.P., Murdoch, C., Thornhill, M.H. and Battaglia, G. *Mol. Pharm.*, **2014**, 11, 1176-1188.
63. Schmaljohann, D. *Adv. Drug Deliv. Rev.*, **2006**, 58, 1655-1670.
64. Malewar, N., Avachat, M., Pokharkar, V. and Kulkarni, S. *AAPS pharmscitech*. **2013**, 14, 1178-1189.
65. Jedinger, N., Khinast, J. and Roblegg, E. *Eur. J. Pharm. Biopharm.*, **2014**, 87, 217-226.

Concluding Remarks and Future Work

This PhD thesis has demonstrated how the ROP of NCA monomers and the ROP of OCA monomers, may be exploited to create a variety of stimuli-responsive, biodegradable polymeric materials. These could be of practical use in various biomedical settings, and are also of academic value. Novel materials, including pH-responsive vegetable oil-based organogels, redox-responsive chemical hydrogels, enzymatically-responsive nanoparticles, pH-responsive nanoparticles and a poly(ester) that exhibits pH-dependent reversible self-assembly behaviour, were all reported. However, there is scope for developing further some of the research work that has been detailed.

In chapter 3, NCA ROP was initiated successfully from a model therapeutic molecule, dopamine. Future undertakings can be focused on replacing dopamine, by initiating NCA ROP from hydrophobic chemotherapeutics, such as doxorubicin. Chapters 8, 9 and 10 reported on the use of OCA ROP to create a library of acidic pH-responsive poly(ester) macromolecules that could be used to develop effective delivery vehicles for chemotherapeutics. In the future, attempts could be made to initiate OCA ROP directly from chemotherapeutic molecules, so as to attempt to furnish polymeric drugs that negate the conventional drug-loading procedures. Further research has to be carried out to assess the biocompatibility of the poly(ester) nanoparticles and cell viability of dox-loaded nanoparticles. Further studies may also be carried out to ascertain the antimicrobial potency of poly[(PheLA)_{10.4}-*b*-(LysLA)_{31.4}] nanoparticles.

OCA ROP may be exploited further to create scaffolds for tissue engineering. The use of OCA ROP affords the creation of macromolecules that boast of a variety of side chain functionalities because of the various canonical amino acids that are at disposal. As such, post-polymerisation modifications to attach carbohydrate moieties, and/or the design of OCA monomers that contain carbohydrate moieties, could be exploited to enable the creation of hybrid poly(ester)s which boast cell-binding groups, e.g., galactose.

Proof-of-concept studies in the creation of polymer-silver(I) NHC anticancer therapeutics were reported in Chapter 11. This research work is ongoing and can be developed further by carrying out exhaustive biological studies *in vitro*. Furthermore, there remains a long term need to carry

out research into the mechanism of release of silver(I) NHC complexes from the poly(amino acid) nanocarriers. The outcomes of *in vitro* studies will have an influence on whether the research is progressed to further research *in vivo* (long term). Finally, the research can be widened to exploit poly(ester)s which are created using OCA ROP for the development of effective poly(ester)-silver(I) NHC anticancer therapeutics, which would be susceptible to degradation by acidic pH and esterase enzymes to release chemotherapeutics, on demand.

List of Publications

Khuphe M.; Kazlaucius A.; Huscroft M.; Thornton P. D., The formation of biodegradable micelles from a therapeutic initiator for enzyme-mediated drug delivery, *Chemical Communications*, 2015, 51, 1520 - 1523. <http://dx.doi.org/10.1039/c4cc08387c>

Khuphe M.; Mukonoweshuro B.; Kazlaucius A.; Thornton P. D., A vegetable oil-based organogel for use in pH-mediated drug delivery, *Soft Matter*, 2015, 11, 9160 - 9167. <http://dx.doi.org/10.1039/c5sm02176f>

Khuphe M.; Mahon C. S.; Thornton P.D., Glucose-bearing biodegradable poly(amino acid) and poly(amino acid)-poly(ester) conjugates for controlled payload release, *Biomaterials Science*, 2016, 4, 1792-1801 <http://dx.doi.org/10.1039/c6bm00535g>

McAvan B.S.*; Khuphe M.*; Thornton, P.D., Polymer hydrogels for glutathione-mediated protein release, *European Polymer Journal*, 2017, 87, 468-477. <http://dx.doi.org/10.1016/j.eurpolymj.2016.09.032> (*Authors contributed equally to the research).

Appendix 3

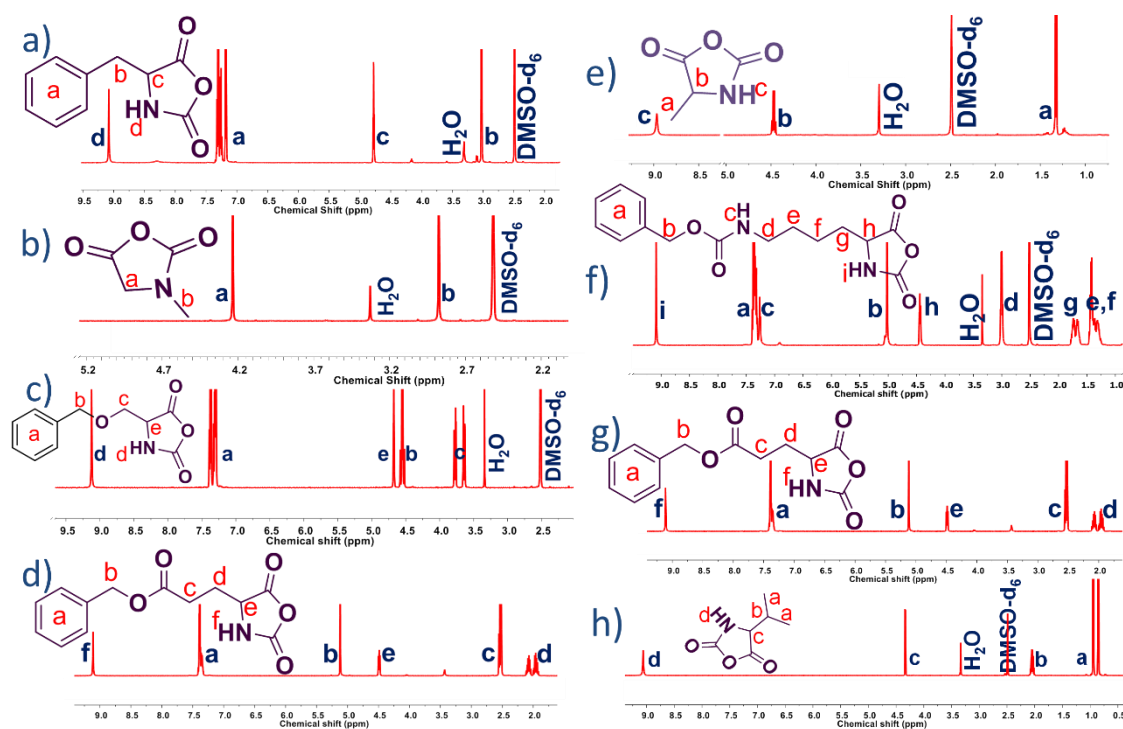


Figure A3.1 ^1H NMR spectra of (a) Phe NCA, (b) Sar *N*-NCA, (c) Ser(OBz) NCA, (d) Glu(Bz) NCA, (e) Ala NCA, (f) Lys(Cbz) NCA, (g) Asp(Bz) NCA and (h) Val NCA.

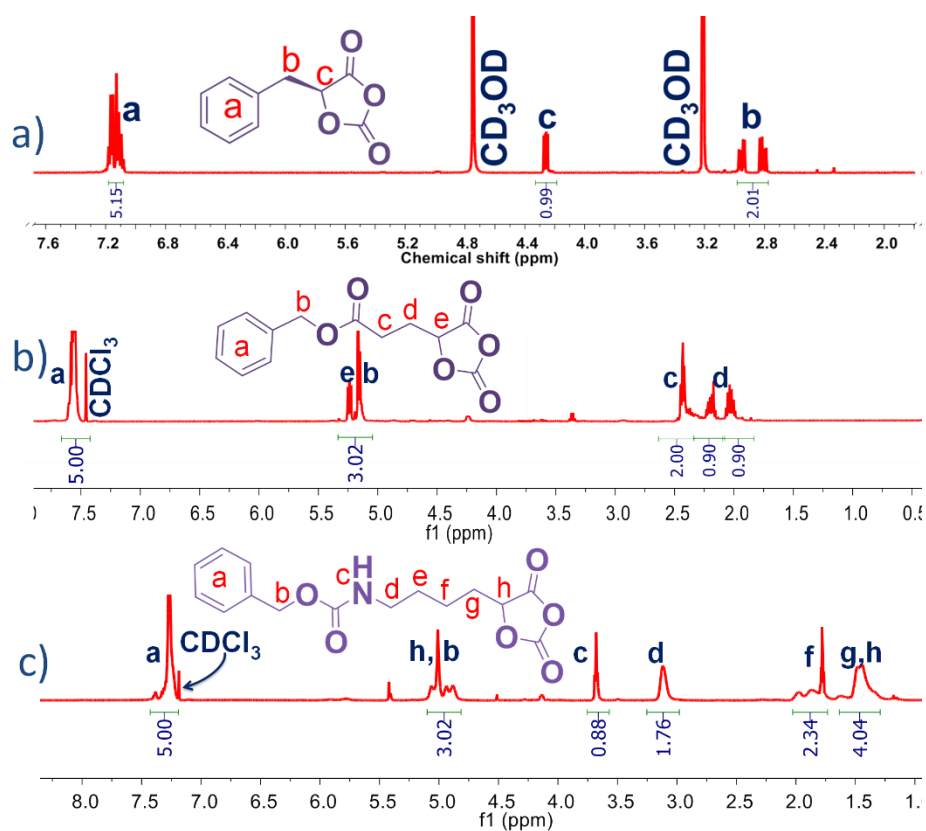


Figure A3.2 ^1H NMR spectra of Phe OCA (a), Glu(Bz) OCA (b) and Lys(Cbz) OCA (c).

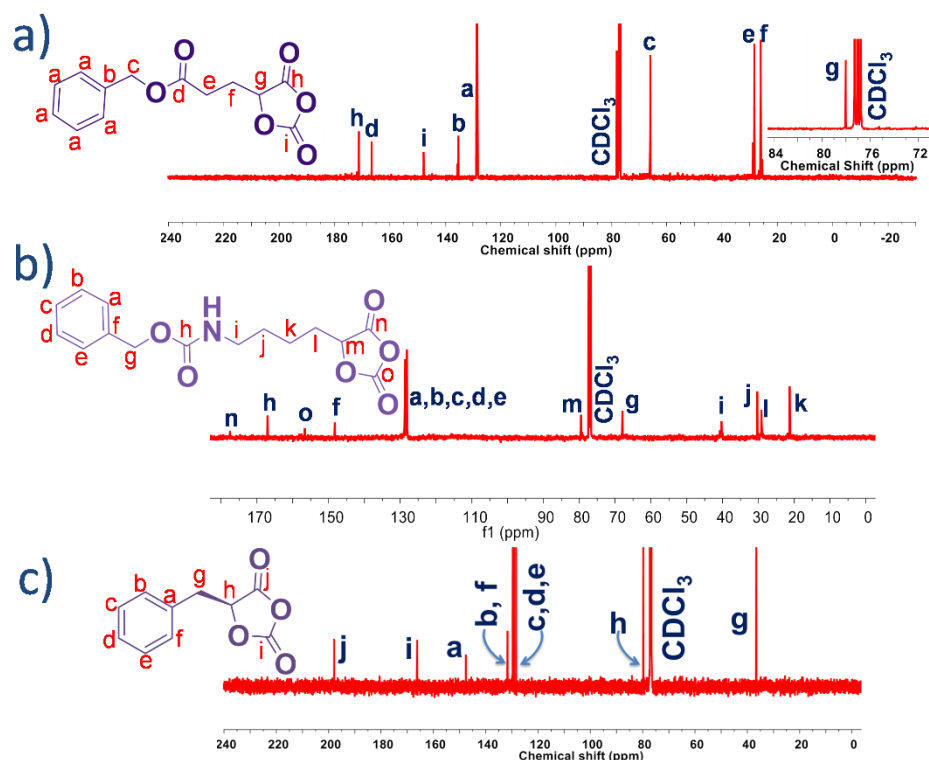


Figure A3.2 ^{13}C NMR spectra of Glu(Bz) OCA (a), Lys(Cbz) OCA (b) and Phe OCA (c).

Appendix 4

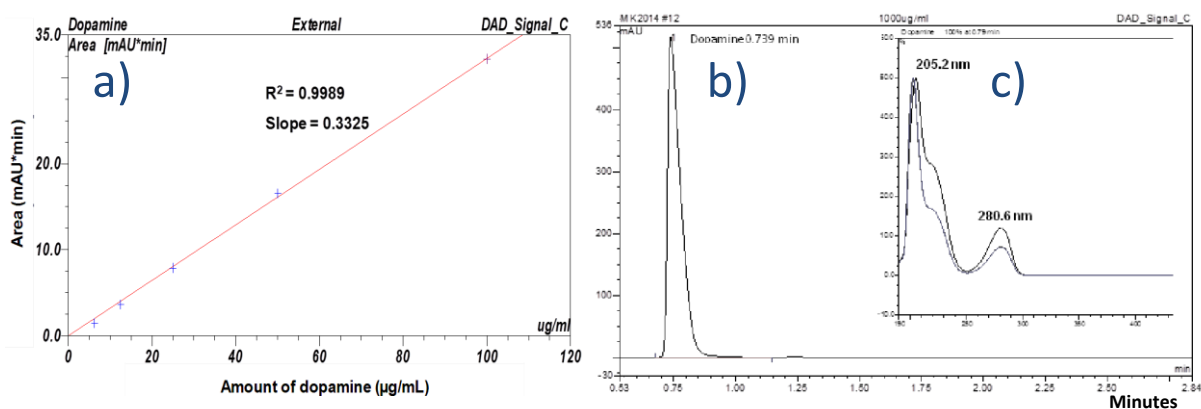


Figure A4.1. (a) The calibration graph used for the assessment of dopamine release by HPLC from dop-(peptide)-(peptoid) particles. The chromatogram of free dopamine (b) and inset (b) is an overlay of UV absorption spectra from several dopamine runs showing the two absorption maxima (205.2 nm for the amine group and 280.6 nm for the phenolic group).

Computing Dopamine Loading Within Particles

Data obtained from HPLC experiments was used to determine the percentage of dopamine that was released from the particles upon enzymatic activity. The maximum possible dopamine loading per unit volume of particles was calculated from ^1H NMR spectra of the dopamine-terminated macromolecules produced. The spectra were normalised to the dopamine aromatic peak and the concentration of dopamine in each sample calculated as detailed below. The respective dopamine concentrations were used as references (relative to the results

obtained from the HPLC studies) to determine the percentage of dopamine released during the individual enzyme-mediated release experiments.

Dop-(Ala)₅-(Sar)₁₅:

¹H NMR compositional ratios; Dopamine : Alanine: Sarcosine = 1 : 5 : 15

Dopamine loading by mass = (152) / (1*152 + 5*71 + 15*71) = 9.6692%

Concentration of polymer in nanoparticle sample = 0.1 mg/mL

Therefore, maximum dopamine loading = (9.6692/100) * 0.1 mg/mL = 9.67 µg/mL

Dop-(Phe)₄-(Sar)₁₈:

¹H NMR compositional ratios; Dopamine: Phenylalanine: Sarcosine = 1 : 4 : 18

Dopamine loading = (152) / (1*152 + 4*147 + 18*71) = 7.5322%

Concentration of polymer in nanoparticle sample = 0.1 mg/mL

Therefore, maximum dopamine loading = (7.5322/100) * 0.1 mg/mL = 7.53 µg/mL

Appendix 5

$$\text{Grafting Efficiency} = \left[\frac{\text{Carbon Content of PSOA Measured After Poly(Ser) Modification}}{\text{Theoretical Carbon Content of PSOA}} \right] * 100\% \quad (\text{A6.1})$$

$$= (69.4/71.3)*100 \%$$

$$= \underline{97.3 \%}$$

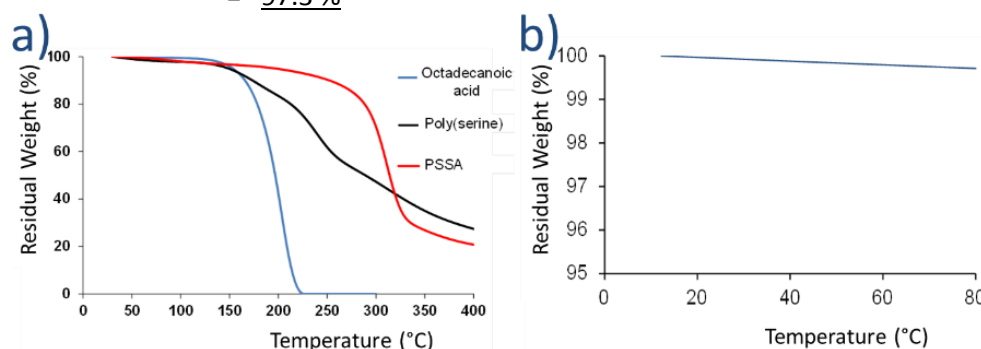


Figure A5.1. (a) The TGA thermograms of octadecanoic acid, the unmodified oligo(Ser) and the PSOA gelator. (b) The TGA thermogram of a 2w. % organogel.

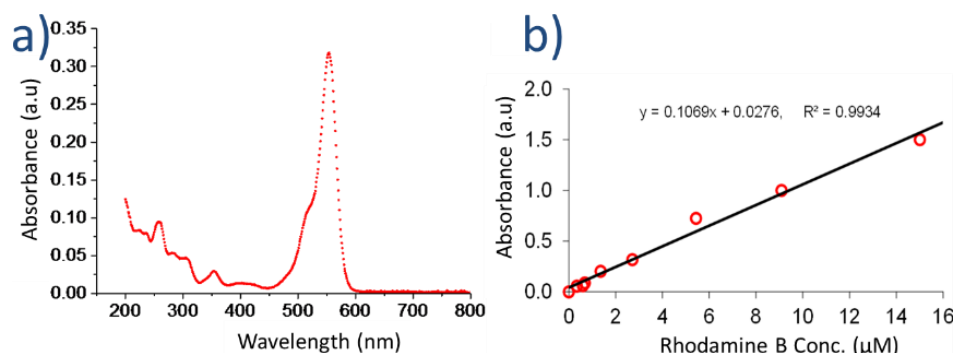


Figure A5.2. (a) The UV-Vis spectrum of the released rhodamine B ($\lambda_{\text{max}} = 554 \text{ nm}$). (b) The calibration graph used to quantify Rhodamine B release from PSOA-safflower oil organogels.

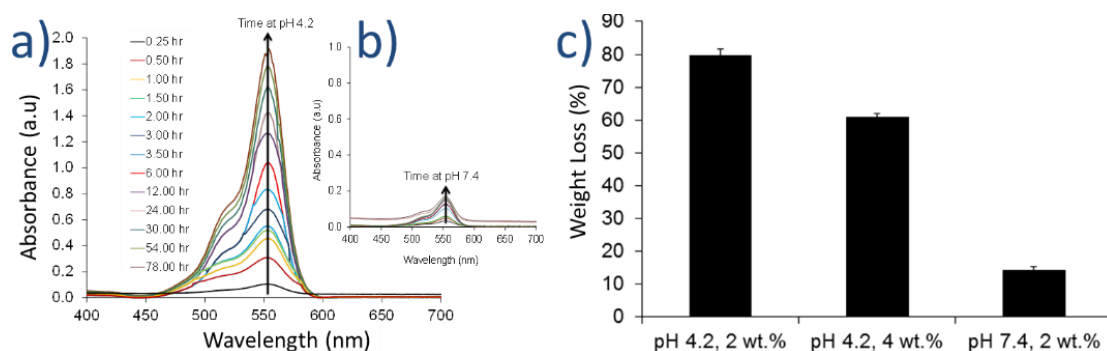


Figure A5.3. (a) UV-Vis spectra for the time-dependent release of rhodamine B from the 2 wt. % organogel, into PBS maintained at pH 4.2 and (b) at pH 7.4 (*inset*). (c) The extent of degradation of organogels, as indicated by total weight lost after 78 hours of incubation at respective pH media.

Appendix 6

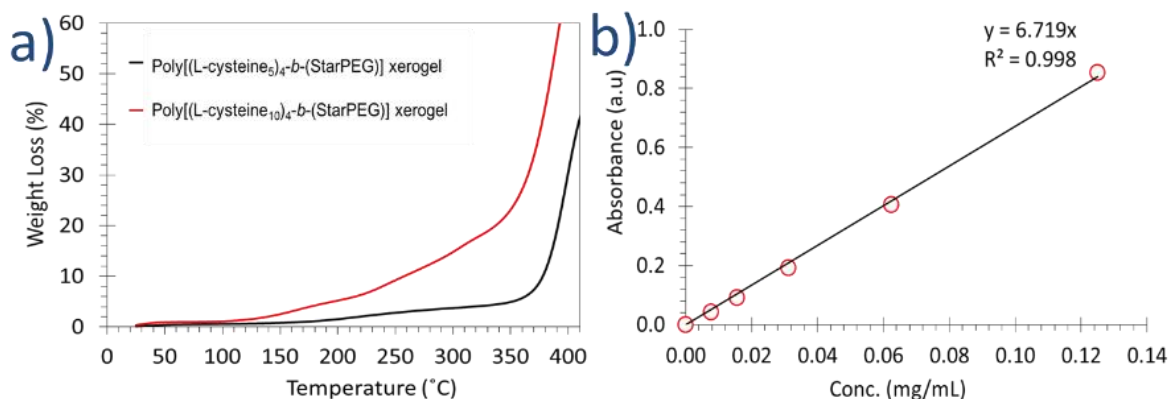


Figure A6.1. (a) Comparison of the thermal stability of the poly[(L-Cysteine₅)₄-b-(StarPEG_{10k})] hydrogel and of the poly[(L-Cysteine₁₀)₄-b-(StarPEG_{10k})] hydrogel. (b) Calibration curve used to quantify the release of FITC-albumin from the hydrogels.

Disulfide Reduction

Concentration of GSH used in experiments = 5 mM

Moles of GSH available in 10 mL GSH release media = 0.05 mmol

a) Poly[(L-Cysteine₅)₄-b-(StarPEG_{10k})] = 66.1% water and 33.9% polymer

Mass of hydrogel used = 29.5 mg; Mass of polymer within the hydrogel = $0.339 \times 29.5 \text{ mg} = 10 \text{ mg}$

Molecular weight of peptide blocks grafted from the 4 arms of StarPEG = $20 \times 103.15 = 2063 \text{ g/mol}$

Molecular weight of poly[(L-Cysteine₅)₄-b-(StarPEG_{10k})] = 12063 g/mol

As such, $[2063/12063 \times 100] = 17.1\%$ of total polymer is the cross-linkable (peptide component)

Mass of cysteine within the copolymer = $17.1\% \times 10 \text{ mg} = 0.17 \times 0.01 \text{ g} = 0.00171 \text{ g}$
 Moles of cysteine within the copolymer = $0.00171 / 2063 = 8.3 \times 10^{-7} \text{ moles} = 8.3 \times 10^{-4} \text{ mmol}$
 Multiply by 20 to take into account 20 cysteine repeat units = $8.3 \times 10^{-4} \text{ mmol} \times 20 = 0.0166 \text{ mmol}$

Two cysteine units form a single disulphide bond, therefore $0.0166 / 2 \text{ mmol}$ of glutathione are required to break all the crosslinks = 0.0083 mmol .

As such, the amount of GSH provided is in excess, and thus sufficient to cleave all crosslinks in the hydrogel.

b) Poly[(L-Cysteine)₁₀]-b-(StarPEG_{10k}) = 46.5% water and 53.5% polymer

Mass of hydrogel used = 18.7 mg; Mass of polymer within the hydrogel = $0.465 \times 18.7 = 10 \text{ mg}$

Mw of peptide blocks grafted from the 4 arms of StarPEG = $40 \times 103.15 = 4126 \text{ g/mol}$

Molecular weight of poly[(L-Cysteine)₅]-b-(StarPEG_{10k}) = 14126 g/mol

As such, $[4126/14126 \times 100] = 29.2\%$ of total polymer is the cross-linkable (peptide component)

Mass of cysteine within the copolymer = $29.2\% \times 10 \text{ mg} = 0.292 \times 0.01 \text{ g} = 0.00292 \text{ g}$

Moles of cysteine within the copolymer = $0.00292 / 4126 = 7.08 \times 10^{-7} \text{ moles} = 7.08 \times 10^{-4} \text{ mmol}$

Multiply by 40 to take into account 40 Cys repeat units = $7.08 \times 10^{-4} \text{ mmol} \times 40 = 0.0283 \text{ mmol}$

Two cysteine units form a single disulphide bond, therefore $0.0283 / 2 \text{ mmol}$ of glutathione are required to break all the crosslinks = 0.0142 mmol .

As such, the amount of GSH provided is in excess, and thus sufficient to cleave all crosslinks in the hydrogel.

Appendix 7

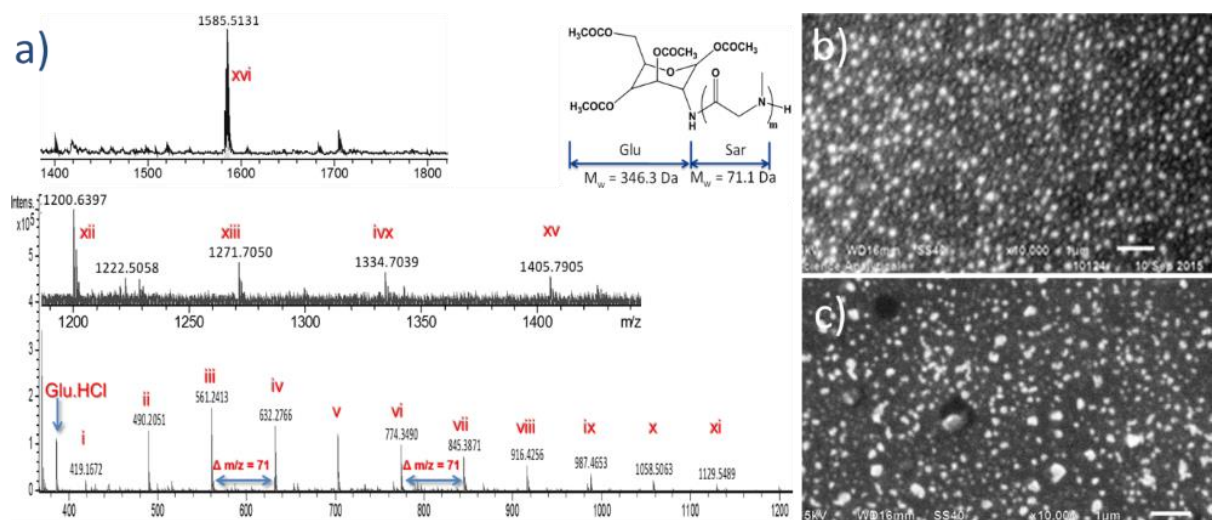


Figure A7.1. (a) ESI MS analysis of reaction media, to ascertain the feasibility of ROP of Sar NCA from a GluAm molecule, confirming the presence of Glu-(Sar) macromolecules. The various peaks have been assigned as; i: Glu-(Sar)₁, ii: Glu-(Sar)₂, iii: Glu-(Sar)₃, iv: Glu-(Sar)₄, v: Glu-(Sar)₅, vi: Glu-(Sar)₆, vii: Glu-(Sar)₇, viii: Glu-(Sar)₈, ix: Glu-(Sar)₉, x: Glu-(Sar)₁₀, xi: Glu-(Sar)₁₁, xii: Glu-(Sar)₁₂, xiii: Glu-(Sar)₁₃, ivx: Glu-(Sar)₁₄, xv: Glu-(Sar)₁₅, xvi: Glu-(Sar)₁₇. SEM microphotographs of NPs formed from Glu-poly[(Sar)_m-b-(PheLA)_n] (b) and from Glu-poly[(Sar)_m-b-(Phe)_n] (c).

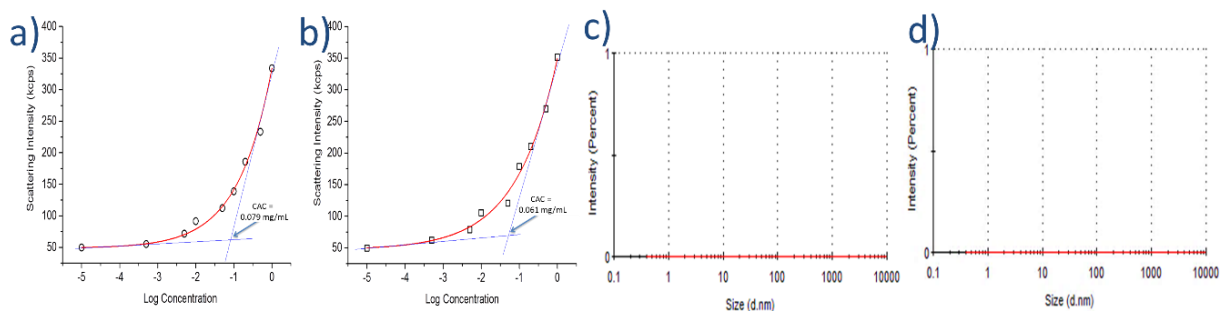


Figure A7.2. Determination of the critical aggregation concentration (CAC) of Glu-poly[(Sar)_m-b-(Phe)_n] (a) and of Glu-poly[(Sar)_m-b-(PheLA)_n] (b), using the Malvern Instruments' method for the determination of CAC, using DLS [Reference 21, Chapter 7]. DLS result obtained from aqueous solution of (c) RCA₁₂₀ lectin and (d) from a solution of Con A lectin, revealing the absence of aggregates, prior to carrying out lectin binding studies on the NPs.

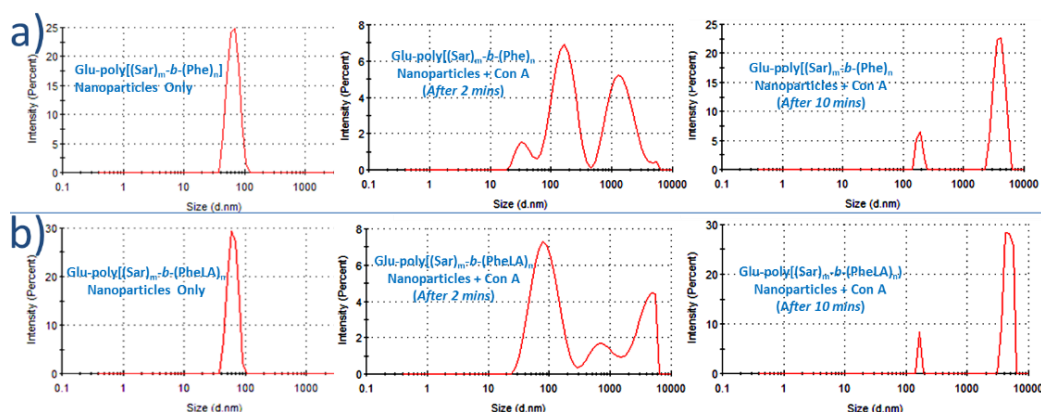


Figure A7.3. DLS traces obtained at different time intervals, from the agglutination studies of Glu-poly[(Sar)_m-b-(Phe)_n] NPs (a) and of Glu-poly[(Sar)_m-b-(PheLA)_n] NPs (b), with Con A, respectively, showing clearly the gradual complexing into large aggregates.

Appendix 8

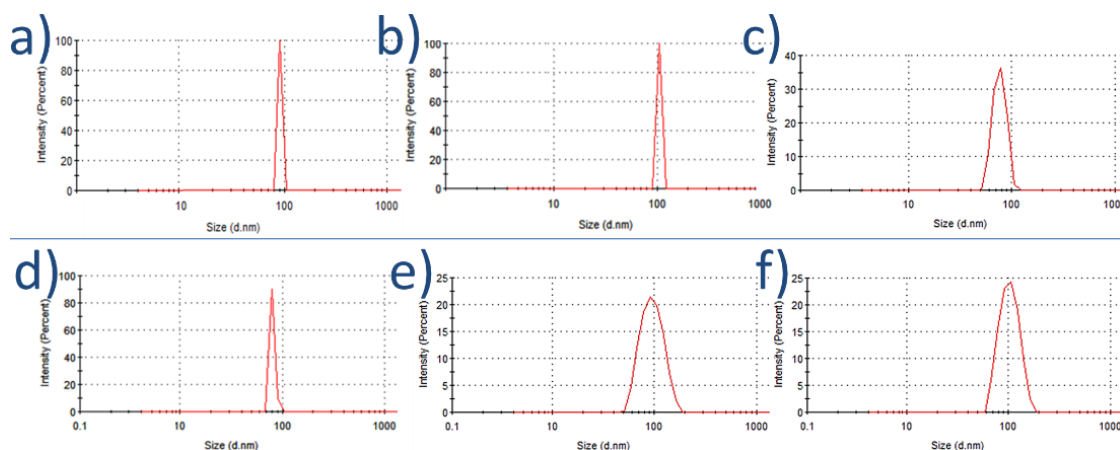


Figure A8.1. DLS traces, depicting the size distribution of NPs that were produced from (a) poly[(Ser)_{19.6}-g-(Phe AHA)₆], (b) poly[(Ser)_{19.6}-g-(Phe AHA)_{3.1}], (c) poly[(Ser)_{18.7}-g-(Phe AHA)_{3.0}], (d) poly[(Ser)_{18.7}-g-(Phe AHA)_{3.0}], (e) poly[(Ser)_{9.6}-g-(Phe AHA)_{5.2}] and (f) poly[(Ser)_{9.6}-g-(Phe AHA)_{1.8}].

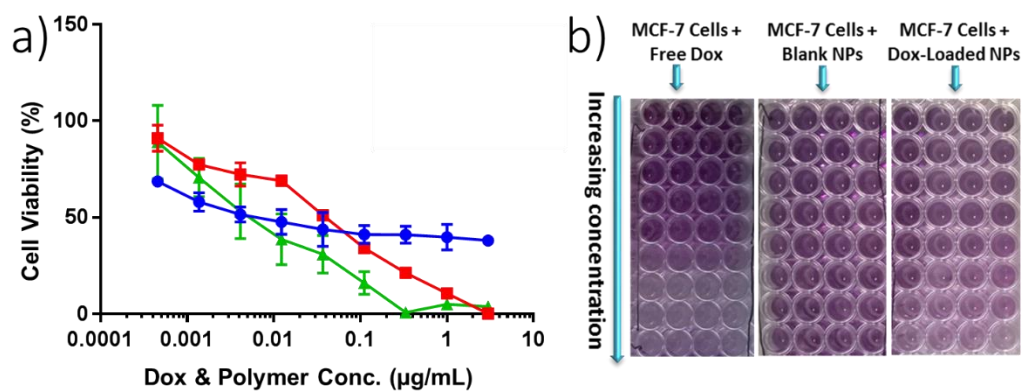


Figure A8.2 (a) The effect of blank poly[(Ser)_{19.6}-g-(Phe AHA)₆] NPs (●), dox-loaded poly[(Ser)_{19.6}-g-(Phe AHA)₆] NPs (■) and free dox (▼) on the viability of MCF-7 (human breast cancer) cells. Data: mean ± SD (n = 4). (b) Representative macro images obtained from the colorimetric MTT assays in which the purple colouring indicates viable cells and discolouration indicates absence of viable cells.

Appendix 11

Table A11.1. The anticancer potencies of silver(I)-NHC complexes and of cisplatin, against Panc 10.05 cells and against ARPE-19 cells

Silver(I)-NHC Complex	Cell Line & IC ₅₀ Values		Selectivity Ratio
	Panc 10.05	ARPE-19	
C01	30.6 ± 13.2	>100	3.27
C03	12.3 ± 3.20	>100	8.15
C05	26.3 ± 11.5	68.7 ± 7.16	2.61
C02	8.27 ± 2.06	13.65 ± 2.91	2.00
C04	<i>No cytotoxicity results yet</i>		
Cisplatin	1.71 ± 0.41	6.41 ± 0.95	1.27

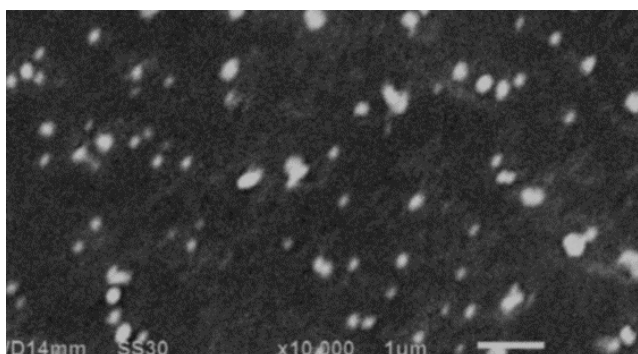


Figure A11.1. SEM image of mPEG₅₀₀₀-b-poly(Phe)₂₄ particles in a PBS buffer solution, at pH 7.4, prior to the encapsulation of the silver (I)-NHC complexes. Scale bar represents 1 µm.